INFORMATION TO USERS

This manuscript has been reproduced from the microfilm master. UMI films the text directly from the original or copy submitted. Thus, some thesis and dissertation copies are in typewriter face, while others may be from any type of computer printer.

The quality of this reproduction is dependent upon the quality of the copy submitted. Broken or indistinct print, colored or poor quality illustrations and photographs, print bleedthrough, substandard margins, and improper alignment can adversely affect reproduction.

In the unlikely event that the author did not send UMI a complete manuscript and there are missing pages, these will be noted. Also, if unauthorized copyright material had to be removed, a note will indicate the deletion.

Oversize materials (e.g., maps, drawings, charts) are reproduced by sectioning the original, beginning at the upper left-hand corner and continuing from left to right in equal sections with small overlaps. Each original is also photographed in one exposure and is included in reduced form at the back of the book.

Photographs included in the original manuscript have been reproduced xerographically in this copy. Higher quality 6" x 9" black and white photographic prints are available for any photographs or illustrations appearing in this copy for an additional charge. Contact UMI directly to order.

U·M·I

University Microfilms International
A Bell & Howell Information Company
300 North Zeeb Road, Ann Arbor, MI 48106-1346 USA
313/761-4700 800/521-0600

Order Number 9417512

Molecular orbital studies of hydrogen-bond directed aggregation and crystal formation

Turi, László, Ph.D.

City University of New York, 1994

Copyright ©1994 by Turi, László. All rights reserved.

U·M·I
300 N. Zeeb Rd.
Ann Arbor, MI 48106

MOLECULAR ORBITAL STUDIES OF HYDROGEN-BOND DIRECTED AGGREGATION AND CRYSTAL FORMATION

by

László Turi

A dissertation submitted to the Graduate Faculty in Chemistry in partial fulfillment of the requirements for the degree of Doctor of Philosophy, The City University of New York

1994

© 1994

LÁSZLÓ TURI

All Rights Reserved

This manuscript has been read and accepted for the Graduate Faculty in Chemistry in satisfaction of the dissertation requirement for the degree of Doctor of Philosophy.

28 December 1993

Date

Chair of Examining Committee

Jan 4, 1994

Date

Executive Officer

Supervisory Committee

THE CITY UNIVERSITY OF NEW YORK

ABSTRACT

MOLECULAR ORBITAL STUDIES OF HYDROGEN-BOND DIRECTED AGGREGATION AND CRYSTAL FORMATION

by

László Turi

Adviser: Professor Joseph J. Dannenberg

Ab initio and semiempirical molecular orbital calculations have been performed for the crystal formation of four molecules: 1,3-cyclohexanedione, acetic acid, *para*-nitroaniline and *meta*-nitroaniline. Hydrogen bonding interactions are shown to be the primary structure determinants in these crystals via a) strong hydrogen bonding cooperativity and b) C-H...O interactions. Hydrogen bonding cooperativity explains not only the significant geometry changes of the individual molecules within the crystal lattice compared to the gas or liquid phase structures but often dictates the H-bonding network of the crystalline phase, as for 1,3-cyclohexanedione. All the examined cases illustrate the importance of C-H...O hydrogen bonds in determining the crystal structure. This influence is especially important in the stacking phenomenon of acetic acid and *m*-nitroaniline crystals. In the latter case, C-H...O H-bonds provide the extra stabilization necessary to overcome the unfavorable electrostatic effects of the head-to-head chain orientation that leads to non-centrosymmetric crystal structure and nonlinear optical properties. High level

ab initio calculations on small molecular complexes of HCN and H_2C_2 with water, formaldehyde and ozone also support the existence and significance of C-H...O interactions.

I found very good correlation between the calculated and experimental crystal structures. The semiempirical AM1 method proved to be especially impressive for estimating heat of sublimation values, reproducing experimental geometries or unit cell parameters.

It was concluded that empirical potential functions based on two-body interactions are not very likely to be useful for studying crystal formation, biological systems or any related problem where strong cooperative (non-additive) effects might arise.

For ab initio calculations on molecular complexes containing more than two molecules, a simple counterpoise procedure for correcting the basis set superposition error is examined and proposed.

ACKNOWLEDGEMENT

First of all, I should like to express my deepest gratitude to Professor J. J. Dannenberg, my thesis adviser, for his guidance, advises and critical comments through my Ph.D study.

I should like to thank the Thesis Advisory Committee, Professors Max Diem, Richard Frank and Jerome Schulman (Queens College), for their thorough attention toward my Thesis, their valuable remarks and sometime troubling questions pointing sharply to overlooked details.

I am especially thankful to Professor Mihály Mezei (Mount Sinai School of Medicine) for his critical observations and suggestions about this manuscript.

Many other people also contributed to this work with their invaluable advises. Among them, I should like to mention Professor Margaret Etter (University of Minnesota) without whose pioneer work on the field of molecular recognition and crystal engineering I would probably have never started this project.

Drága Feleségemnek

TABLE OF CONTENTS

LIST OF TABLES

CHAPTER II

CHAPTER IV

CHAPTER VI

CHAPTER VII

LIST OF FIGURES

CHAPTER II

CHAPTER IV

CHAPTER V

CHAPTER VI

CHAPTER VII

I. INTRODUCTION

Crystal formation. Many scientists are fascinated by this process and its result, the order that the known crystal structures exhibit. However, it is still one of those fields where the knowledge of today's science is surprisingly limited. The clear answers are curiously still missing for the most important questions: What are the compelling forces for the molecules to aggregate and form highly structured crystals? How do the molecules 'know' where to interact with another molecules? How do they 'recognize' certain geometric and energetic patterns during the aggregation? And once they aggregate what leads to the striking differences between the geometric parameters of the gas or liquid state structures and those of the crystals?

These questions, lying at the very heart of crystal formation can lead to many exciting research areas. It is easy to see the kinetic and statistical aspects (in addition to those of thermodynamics) of these questions. The implications for the so-called molecular recognition are of high interest in biochemical processes like the DNA reproduction or protein synthesis in living systems. Another interesting biochemical appearance of this problem is the inhibition of the active site of certain enzymes. The chemistry of inclusion complexes has also gone through an explosive development in the last decade. The need for designing different inclusion complexes alongside many other useful solid materials also evoked the concept of molecular recognition. It offers wide horizons, for instance, in the quest for new non-linear optical materials, often in the form of cocrystals.

Beyond the practical applications of crystal formation, the theoretical possibilities

are also appealing. Simple crystal structures can serve as case studies for testing the available theoretical methods and models. The simpler model systems also can be the prototypes for theoretical examinations of the more complex, interconnected networks of intermolecular interactions - often called packing interactions - characteristic of the crystal structures.

My dissertation primarily concentrates on the theoretical facet of the crystal formation of simple molecules. I undertake the molecular orbital (MO) examination of the crystal formation of three groups of simple organic molecules: 1,3-diones, acetic acid and various nitroanilines. The aggregation (and eventually the crystallization) of these molecules is controlled by hydrogen-bond formation. The hydrogen-bond directed crystallization is simpler than other crystal formation processes, in having a strong dominant interaction leading to comparatively simpler orientation patterns. Another important advantage of examining H-bond directed crystallization is the opportunity to explore hydrogen-bonding cooperativity that plays a crucial role in aggregation processes. The hydrogen-bonding cooperativity is stronger, therefore easier to recognize and characterize than other cooperative effects inherent in intramolecular interactions. The simpler molecular orientation patterns of H-bonded systems and the cooperativity dictate the final crystal structures in the cases I shall focus on. The common thread between the orientation and cooperativity is the natural tendency of every system to reach the state of lowest possible energy suggesting that MO treatment might be a useful tool in examining the molecular aggregation processes.

The aims of this Dissertation can be summarized in the following (in thematic

order): 1) To explore cooperative effects (in all three dimensions), its features and its effect(s) on the aggregation processes. 2) To completely map and characterize all the interactions in the examined three crystal structures. 3) To predict thermodynamic (heat of sublimation) and crystallographic properties (unit cell dimensions) of these crystals and compare them to those measured experimentally. 4) To examine the correlation between the crystal structures of nitroanilines and their nonlinear optical properties.

The basic structure of this work reflects these outlined goals. After the Introduction, in Chapter II, I examine the MO methods employed during my work, their reasonable applications, their limitations and the problems arising with their use for larger aggregates. The counterpoise (CP) correction for the basis set superposition error (BSSE) will be discussed in more detail. In particular, I describe a CP procedure that avoids certain ambiguities that arise when correcting for aggregates containing more than two molecules. Before investigating the properties of our model systems in detail, I devote the next two chapters (Chapters III and IV) to two important phenomena central to understanding the peculiar features of the H-bond directed crystal formations: the cooperative effect and the C-H..O interactions. Chapter III deals with the cooperativity, examine its origin, its impact on aggregation processes. This Chapter also provides a *qualitative* illustration of the origin of the cooperativity by using traditional second and third-order Rayleigh-Schroedinger perturbation theory. Chapter IV gives a detailed description of the characteristic properties of the C-H..O H-bonds. Various MO calculations for small C-H..O hydrogen-bonded model systems are presented here to gain insight into the characteristics of this interaction. Chapters V-VII contain the results of

the MO calculations for the H-bonding cooperativity and crystal formation of acetic acid, 1,3-cyclohexanedione and *meta*- and *para*-nitroanilines. The interactions in one-, two-, and three-dimensional aggregates are explored. The good agreement between the calculated and experimentally measured properties for three-dimensional microcrystals demonstrates the applicability of MO methods for such complex problems as crystal formation. In addition to reproducing the experimentally measured properties of two different nitroanilines reasonably well, I present calculations that shed light on the relationship between the crystal structure of the nitroanilines and their nonlinear optical properties. For all these crystals the reader will be continuously reminded of the importance of C-H...O interactions in determining the structure of the solid phase.

II. METHODS

I have indicated in the Introduction that the focus of my Dissertation is the examination of H-bond directed crystal nucleation and the association of several simple organic molecules by the means of molecular orbital (MO) theory. The topic requires a brief overview of MO theory, the applied methods, their approximations and applicability for the problem under examination. In this chapter, however, instead of going into details of the basics of the theory of molecular orbital calculations, I wish to emphasize more the practical issues arising during the actual execution and interpretation of the calculations for H-bonded systems. They include, for example, a discussion about the performance of various ab initio methods, the effect of basis sets, electron correlation and different types of corrections to the interaction energy and comparison between the ab initio and semiempirical techniques.

1. Molecular Orbital Theory: A Simple Overview[1]

The fundamentals of the molecular orbital theory were laid down in the second half of the 20th century by the rapid development of the quantum theory. The application of the quantum theory for chemical problems is called quantum chemistry. The ultimate goal of quantum chemical methods is to find the solution of the time-independent Schroedinger equation.

$$\hat{H}\psi = E\psi \qquad \text{(II.1)}$$

where Ψ and E denote the eigenfunctions and eigenvalues of $\hat{H}$, the Hamiltonian operator of the system. The exact analytical solution of this second-order partial differential equation exists only in few very simple cases like for the problem of a particle moving in a potential well, or under a central force (hydrogen atom) and for the harmonic oscillator. The mathematical treatment for such a very simple system as the helium atom requires the application of approximations. The two major approximative methods in quantum mechanics are the variational and the perturbational theory. When increasing the size of the investigated systems, even the approximative procedures become more and more tedious leading to insurmountable mathematical difficulties. In practice, the following three additional approximations are usually employed to make the quantum chemical problems tractable: a) In the Born-Oppenheimer approximation the nuclear and electronic motions are assumed to be independent for polyatomic molecules. As a result, the original time-independent Schroedinger-equation separates into nuclear and electronic equations. For most practical problems (for example, the ground electronic states of molecules) it is sufficiently accurate to treat the electronic part of these two equations and solve it for fixed molecular positions. The sum of the electronic and nuclear energies gives the total energy, where this latter is simply calculated classically for the fixed nuclear positions. According to this approximation, the term Schroedinger-equation will refer to the electronic equation in the future. b) The wavefunction (Ψ) of a chemical system is approximated as the anti-symmetrized product (Slater determinant) of one-electron functions, molecular orbitals (MO). c) The molecular orbitals are expressed as finite linear combinations of mathematical functions (LCAO: linear combination of atomic

orbitals), the so-called basis functions.

These three approximations combined with the variational method result in the iterative Hartree-Fock-Roothaan[2] (or simply Hartree-Fock) equations. In the well-known matrix form:

$$\mathbf{F}\mathbf{c}_i = \varepsilon_i \mathbf{S}\mathbf{c}_i \qquad \text{(II.2)}$$

where, F and S denote the Fock and overlap matrices, c column vector contains the expansion coefficients of the i-th MO for a given basis set, while ε is the orbital energy. The eigenfunctions (c vectors) and the eigenvalues (ε-s) of the Hartree-Fock equations give the canonical (one-electron) molecular orbitals and their orbital energy. This formalism also provides an expression for the total energy of the system. The Hartree-Fock method based on equation II.2 provides a computationally simple iteration technique for solving the Schroedinger equation. This computational simplicity is the main reason of the Hartree-Fock method's popularity and explains why this method became the prototype of all self-consistent-field molecular orbital (SCF-MO) or simply MO methods.

The mathematical treatment of the Hartree-Fock equation separates the two mainstreams of quantum chemical techniques. The ab initio methods evaluate all integrals (either analytically or numerically) during the solution of the Hartree-Fock equations without using additional simplifications. This means that in the ab initio methods one solves the eigenvalue equation of the Hamiltonian defined by the Born-Oppenheimer approximation and the choice of the basis set (see the three approximations above). In the semiempirical methods, on the other hand, the Hamiltonian of the system is further simplified employing different integral estimation schemes. In this formalism one neglects

certain two-electron integrals, while some other integrals are replaced by either purely empirical equations or equations based on simple physical models. The former equations usually contain adjustable parameters, while the parameters in the latter are very often in close correlation with experimental measurements (for example, spectroscopic parameters). The main practical and philosophical differences between the ab initio and semiempirical techniques warrant their separate analysis.

2. Ab Initio Calculations for Hydrogen Bonded Systems I.: The Electron Correlation and Basis Sets[1]

As the corrections for the Born-Oppenheimer approximation are negligible compared to the effect of the other two approximations (MO-s and LCAO), I shall investigate only the latter two in more detail. An important consequence of the use of the anti-symmetrized Slater-determinant leading to the Hartree-Fock equations is that the electrons move in and feel an average potential of all the other electrons of the system. In the original Hartree-Fock treatment (restricted Hartree-Fock method, RHF),[2] where two electrons with different spin can occupy the same spatial orbital, the motion of the electrons is not correlated. It means that RHF neglects the natural tendency of the electrons to be farthest from each other. In RHF, for example, the probability of finding two electrons with opposite spins in an infinitesimally small (neglecting the volume of the electrons) dV volume element around the same position at the same time is not zero. A more illustrative example is that of the probability distribution of two electrons with

opposite spins on a *p* atomic orbital (with its well-known two lobes). According to non-correlated methods, the probability of finding both particles in the same lobe of a *p* orbital is exactly the same as finding the electrons in different lobes. This artifact is clearly in contrast with expectations based on electrostatic Coulomb repulsion. On the other hand, because of the Pauli principle, the probability of finding two electrons with identical spin states within the same infinitesimally small volume element at the same time is zero. Although the RHF contains this latter correlation effect, the difference between the RHF and the exact non-relativistic energies is by definition called correlation energy.

The role of electron-correlation is crucial in predicting energetics, molecular geometry and conformational preference, as exemplified recently by studies on hydroxamic acids.[3] Formohydroxamic acid can exist in two tautomeric forms, keto or iminol. In addition, both forms can be present in either *E* or *Z* orientation about the C-N bond (Figure 1). The 2.5 - 2.9 kcal/mol energetic difference between the two most stable forms, the non-planar (*E*)-keto and planar (*Z*)-keto conformers, calculated at various Hartree-Fock levels essentially disappears upon the application of methods

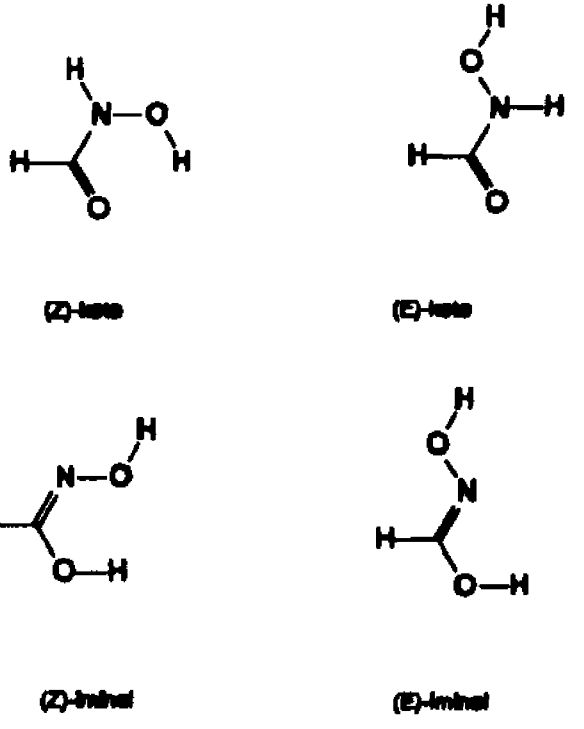

Figure 1. Formohydroxamic acid tautomers and conformers.

including electron-correlation. Moreover, the planar (*Z*)-iminol form becomes more stable approaching the stability of the keto forms.

The effects of electron correlation on the properties of hydrogen-bonded molecules can be illustrated by the water dimer. The influence of electron correlation on the potential surface is well documented in the vast literature of water dimer calculations.[4] Not only do these works give slightly different interaction energies depending upon the applied methods (and the extent of electron correlation), but some of them predict a very flat potential surface. On this flat surface different techniques can favor different orientations, predict different local and global minima and consequently, different molecular properties such as dipole moments or vibrational frequencies. These studies also showed that even the best Hartree-Fock calculations cannot account for -0.372 hartrees correlation energy for the water monomer that is significant on a practicing chemist's energy scale (about 200 kcal/mol). Dewar et al. illustrated that the magnitude of the error in molecular energies is comparable to the corresponding heats of atomization.[5] This large error introduces significant uncertainty in the calculation of interaction energies. The conclusions of the forementioned papers with the calculations presented later in this work provide ample evidence that the Hartree-Fock method is not satisfactory for most H-bonded systems. Nevertheless, being the simplest of all ab initio calculations, I shall use the Hartree-Fock method extensively in my studies. These calculations also can carry crucial (in most cases qualitative) information about different chemical problems.

The introduction of different spatial functions for all the one-electron orbitals leads to the unrestricted Hartree-Fock (UHF) method.[6] The UHF method becomes important

in applications for systems with open electron shells. As my studies do not deal with such molecules, I shall not apply the UHF method in the following investigations.

The so-called post Hartree-Fock methods center on including the electron correlation in the energy calculations. I summarize the general features of these methods very briefly on the examples of the two most popular post HF techniques, the CI and MP*n* methods. Instead of using a single determinant (configuration) for the representation of the wavefunction, one can employ a linear combination of the ground state (Hartree-Fock determinant, ψ_0) and various excited state determinants (ψ_i-s).

$$\Psi = \sum_{i=0} c_i \Psi_i \qquad \text{(II.3)}$$

This technique is called configuration interaction (CI).[7] In the CI method, similarly to the single-determinant Hartree-Fock methods, an iterative matrix eigenvalue equation is the direct result of the application of the variational theorem. While the variational solutions have the distinctive advantage that the calculated energies provide an upper limit for the ground state (and in appropriate form for any excited state) energy, the CI methods suffer from the so-called size-consistency error. A molecular orbital method is size-consistent (for example Hartree-Fock method), if the energies of two individual molecules is the same as the energy of a system containing these two molecules at infinite intermolecular separation. Unfortunately, this trivial requirement does not hold for the CI and other related correlated methods, therefore, their use for estimating hydrogen-bonding energies is not practical.[4] (Note: The full CI method using all possible configurations is size-consistent. The truncated CI methods used in practice

are, however, not. See the book of Szabo and Ostlund for more discussion.[1])

The second major approximative technique, the perturbational theory, forms the basis for the best known and most frequently used perturbational method, the Møller-Plesset method.[8] The Møller-Pleaset method is based on the standard Rayleigh-Schroedinger perturbational procedure. It uses the Fock operator as the zeroth order Hamiltonian and the HF wavefunction as the zeroth order wavefunction (see Chapter III for an example on the application of the perturbational theory). The Møller-Plesset methods calculate the energy and wavefunction corrections up to various orders and are denoted by MP2, MP3, MP4 and so on, corresponding to the highest order of applied energy correction. Although MP*n* and other perturbational methods do not provide upper limit to the energy of the system, they are becoming very popular for hydrogen-bonded systems. Beside the impressive development of new generations of powerful computers that makes the every-day use of MP*n* methods possible, the main reason for this popularity lies in the size-consistency of the MP*n* methods.[1]

After having considered the general characteristics (size-consistency, upper limit for the energy, inclusion of correlation energy) of different ab initio techniques for hydrogen-bonded systems, the second part of this section deals with the practical issues concerning the choice of the appropriate basis sets. According to the third approximation mentioned at the beginning of this Chapter, the MO-s are approximated as finite linear combinations of basis functions. A basis set is a collection of mathematical functions employed to expand the MO-s (and the wavefunction) of a given chemical system. In the last three decades, during the explosive advance of MO theory, many different basis sets

of various mathematical form have been developed. Examples include Slater-type AO-s (STO-s),[9] Gaussian-type AO-s (GTO-s),[10] Gaussian lobe functions[11] and various bond centered functions.[12] Among these, the Gaussian exponential type AO-s proved to be the most popular and durable. Unlike the Slater functions whose exponential part depends on the first power of r, the electron-nucleus distance, the Gaussian orbitals contain r^2, in the exponential (equation II.4). The Cartesian Gaussians are defined as

$$\chi_{klmn} = N x^k y^m z^n \exp(-\xi r^2) \qquad \text{(II.4)}$$

The functions with constant L=k+m+n are usually called s (L=0), p (L=1), d (L=2), etc. sets. The product of two Gaussian functions located on different centers can be expressed as a linear combination of Gaussians from a third, common center. Thus, the integral evaluation of three- and four-center integrals in polyatomic molecules using Gaussians is extremely simple compared to other basis functions, especially STO-s, where the above mentioned transformation cannot be performed analytically. On the other hand, the description of the correct form of Ψ at the atomic centers (cusp) and at very large distances (tail) suffer from serious deficiencies in the Gaussian AO representation. The GTO-s are not able to reproduce the discontinuity of the wavefunction at the nucleus and their decay rate is wrong at larger distances (Figure 2). In practice, linear combinations of Gaussian orbitals are used to enhance the properties of Ψ. Consequently, the number of GTO-s required to describe the correct behavior of the wavefunction is larger than that of more expensive STO-s. Instead of using individual GTO-s (primitive functions, usually denoted by parentheses) one can use their fixed linear combinations (contracted Gaussian type functions, usually denoted by brackets) with different exponents.[13] This technique

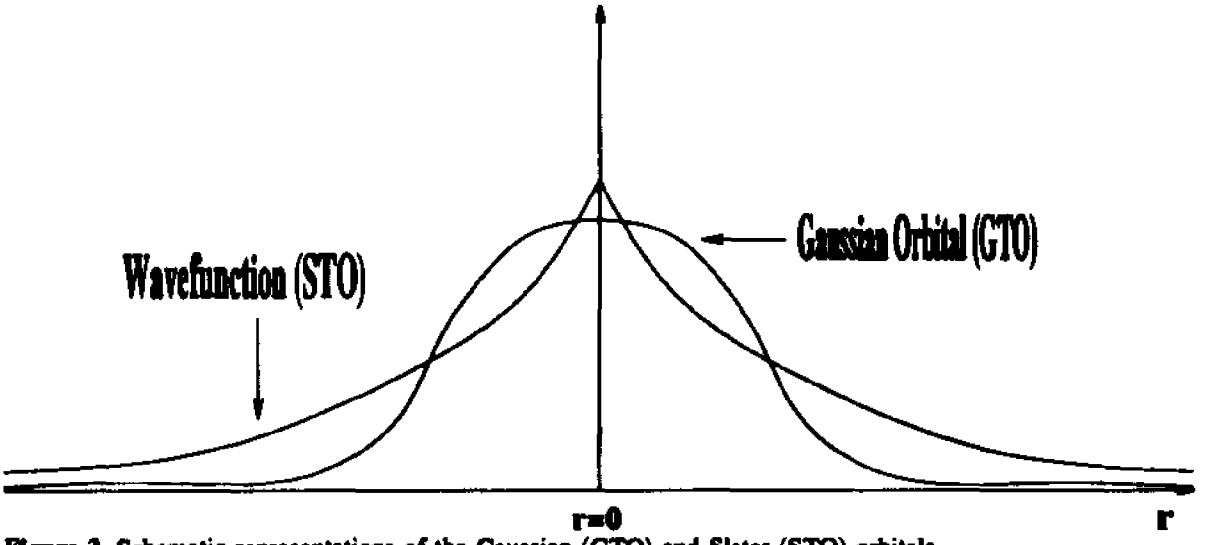

Figure 2. Schematic representations of the Gaussian (GTO) and Slater (STO) orbitals.

can significantly improve the shape of the wavefunction and, at the same time, decrease the computational costs.

In practical applications, one very often optimizes the linear coefficients and exponents of a given contracted basis set by minimizing the energy of individual atoms. In the next step, the optimized (contracted) basis functions (AO-s) are transferred and applied to molecular calculations. At this point it is necessary to mention few of the most popular basis sets. The Pople split valence shell basis sets[14] are widely used because of their easy accessibility. The 6-31G set contains a contracted function (linear combination of six primitive Gaussians) for the inner shell orbitals. In this set two contracted Gaussians (double-zeta sets), linear combinations of three and one (!) primitive(s) describe the valence shell AO-s. These functions can be augmented with polarization and diffuse functions. The polarization functions[15] are basis functions of higher angular quantum number than the highest occupied orbitals in the corresponding free atom (for example *p*, *d*, ... functions for hydrogen, *d*, *f*, ... function for the second-row atoms, like carbon).

The corresponding letters in parentheses following the symbol of the parent basis set indicate the presence of polarization functions. The diffuse sets[16] contain functions with lower angular quantum number and small orbital exponents. They are denoted by + or ++ depending on whether they are applied only on heavy atoms or all atoms including hydrogens. A good example is the 6-31G++(2d,2p) set where the parent 6-31G set is supplemented with two sets of *d* polarization functions on heavy atoms, two sets of *p* functions on hydrogens and diffuse functions on both the heavy and hydrogen atoms. It is worth mentioning that while a *p* set (L=1 in equation II.4) consists only three GTO-s, a set of *d* functions (L=2) includes six functions, one of which is an *s* function. Another example of a popular basis set is the Dunning-Huzinaga D95 double-zeta set.[17] In this set the original (9*s*5*p*) primitive set is contracted to a [4*s*2*p*] basis set. Since it employs more primitive (9 functions) and contracted (2 functions) functions to represent the core orbitals of the first row heavy atoms, the description of the cusp is more reliable than with the Pople sets. We shall see an important consequence of this property later in Chapter IV.

According to the variational theorem, application of larger basis sets results in lower energy.[18] The use of a sufficiently large basis set can result an energy value so low, that cannot be improved by more than a very small threshold value by only increasing the size of the basis set. It is common practice to call this energy value the Hartree-Fock limit, the basis set saturated. The use of saturated basis sets suppresses the so-called basis set superposition error (BSSE), that can cause serious problems in the calculations of weakly bonded complexes. This topic will be further pursued in the next

sections. On the other hand an increase in the number of basis functions leads to rapidly increasing computational costs limiting the application of larger basis sets for larger molecules. In Hartree-Fock methods, for example, the number of integrals is proportional to the fourth power of the number of Gaussian primitives. Other steps depend on the number of contracted functions. A Hartree-Fock integral transformation goes as $(n+N)^5K^5$, MP2 as nN^4K^4, MP3 as $n^2N^4K^4$, where n is the number of doubly occupied orbitals (contracted Gaussians), N is the number of unoccupied orbitals in each of K identical atoms of a hypothetical molecule. In addition to the number of integral evaluation and transformation steps (time factor), the physical storage of the calculated information might become difficult (hardware factor). Therefore, the choice of the computational technique and basis set, on one hand, must be based on intelligent considerations of the required accuracy and computational resources, on the other hand. A review of Davidson and Feller gives a thorough inspection of this problem.[19]

In summary: The properties of different computational techniques such as whether they include electron-correlation, provide an upper limit for the energy of the examined systems or are size-consistent, determine their reasonable applications for hydrogen-bonded systems. Weighing additional factors, as the size of basis set and molecule, I decided to use the standard Hartree-Fock calculations with geometry optimizations. For taking the correlation energy into account I also used the second-order Møller-Plesset method, where the size of the examined problem allowed it. The basis sets extended from the simplest 3-21G set through 6-31G and 6-311G++(d,p) to the double-zeta quality D95++(d,p) basis set. Using the usual notations, where the method and the basis set

characterize the computational technique, the examinations spanned from HF/3-21G to MP2/D95++(d,p).

3. Ab Initio Calculations for Hydrogen-Bonded Systems II.: Interaction Energy and Thermochemical Properties[30]

According to the first law of thermodynamics and the results of statistical mechanics the change in the internal energy of an equilibrium system composed of molecules A and B undergoing the association reaction

$$A+B \rightarrow A\ldots B \tag{II.5}$$

is the difference between the energy of the composite system, A...B, and those of the separate subsystems, A and B.

$$\Delta E^{A\ldots B} = E^{A\ldots B} - E^{A} - E^{B} \tag{II.6}$$

Assuming ideal gas behavior between the particles of macroscopic systems, the original Schroedinger equation of an *N*-particle system breaks down to *N* one-particle Schroedinger equations. The ideal gas behavior (and consequently, the simplification of the Schroedinger equation) combined with the application of Boltzmann statistics (through the introduction of one-particle partition functions) allows one to calculate the energy of a macroscopic system as the sum of one-particle contributions. As a primary approximation for evaluating the one-particle energies one assumes, that the translation of a molecule is independent of its internal motion. Similarly the rotations and the

vibrations of a molecule are assumed to be independent. These idealizations lead to the separation of the Schroedinger equation into independent equations for the translation, rotations and vibrations of the molecule. In this approximation the total energy of a molecule is

$$E_{total} = E_{nucl} + E_{el} + E_{vibr} + E_{rot} + E_{trans} \qquad \text{(II.7)}$$

which contains the nuclear, electronic, vibrational, rotational and translational energy, respectively. A schematic representation for the energy levels of the internal motion of a molecule can be seen on Figure 3. In the calculation of interaction energies the first term denotes the additive term of the nuclear repulsion in the Born-Oppenheimer approximation. Note that equation II.7 does not contain the contribution from the nuclear spin (not affected in chemical changes). The other factors, however, need more attention.

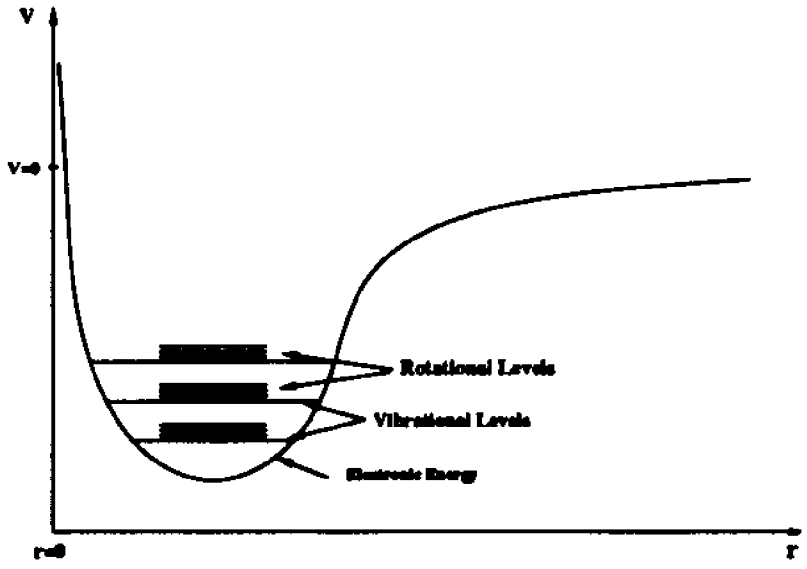

Figure 3. A schematic representation of the hierarchy of electronic, vibrational and rotational energy levels.

From equations II.6 and II.7, the electronic part of the interaction energy is the difference between the electronic energy of A...B and the sum of the energies of A and B. Although the solution of the electronic Schroedinger equation furnishes the necessary

energies, a serious difficulty arises at the calculation of the interaction energy: the basis set superposition error (BSSE). The BSSE originates from the use of finite or truncated basis sets. According to the variational theory, the energies of monomers, A and B become lower in the supermolecule, AB, as the unoccupied molecular orbitals of one of the monomers become available for the other and vice versa, causing non-physical energy lowering of the supermolecule. Many attempts have been made to eliminate this artificial energy term. Since I have also made intensive research in this field, I shall devote the next section to a more detailed discussion of the BSSE problem.

The third term of equation II.7 concerns the calculation of vibrational energies. In the Born-Oppenheimer approximation, the solution of the nuclear Schroedinger equation provides the frame for the vibrational analysis.[21] If the Taylor-series expansion of the potential energy operator of the nuclear Schroedinger equation (the electronic energy for that particular nuclear arrangement) about the equilibrium nuclear position is terminated after the quadratic term, one can talk about harmonic approximation. For a molecule composed of N atoms centered at $\mathbf{r}_1$, $\mathbf{r}_2$,...,etc., the Taylor-series takes the following form:

$$V(r_1...r_N)-V(r_1^0...r_N^0)+\sum_{i-1}\frac{\delta E}{\delta r_i}\Delta r_i+\frac{1}{2}\sum_{ij-1}\frac{\delta^2 E}{\delta r_i \delta r_j}\Delta r_i \Delta r_j+... \qquad \text{(II.8)}$$

The first term of equation II.8 depends only on the choice of zero potential energy level, therefore, can be set to be equal to zero. The second term is zero at the bottom of the potential well (Figure 3). The second order expansion coefficients, the second derivatives of the electronic energy correspond to the classical force constants. After

performing a coordinate transformation of the displacements of the Cartesian coordinates to internal coordinates (bond stretches, bond angle bends, torsional coordinates, etc.) and then to the so-called normal coordinates, the originally coupled differential equations separate to 3N-6 (3N-5 for linear molecules) independent, one-variable harmonic oscillator equations, where N is the number of the nuclei of the molecule. The normal coordinates - linear combinations of the internal coordinates - are perfectly analogous to the vibrations of a diatomic molecule. The modern ab initio program packages usually employ the harmonic approximation in combination with Pulay's gradient method, that revolutionized the calculation of the quadratic force constants (from the energy gradient) and consequently the harmonic vibrational frequencies.[22] With the vibrational frequencies, the vibrational energy of a molecule can be written as

$$E_{vib} = \sum_{i=1}^{3N-6} \frac{1}{2}h\nu_i + \frac{h\nu_i}{e^{h\nu_i/kT}-1} \qquad \text{(II.9)}$$

where ν_i denotes the vibrational frequency of the i-th vibration, h, k and T are the Planck constant, Boltzmann constant and temperature in K, respectively. The summation runs from 1 to 3N-5 for linear molecules. The first, temperature-independent part of the energy expression is the zero-point vibrational energy (ZPVE), a consequence of the application of quantum theory to the harmonic oscillator problem. The vibrational energy contributes significantly to the interaction energy for H-bonded molecules, since the association of two molecules to form a H-bonded complex generally creates six new intermolecular vibrations. Although these vibrations are usually weaker than most of the intramolecular ones, they result in destabilizing energy contribution to the internal energy (Figure 3).

The most significant errors of the vibrational analysis stem from the harmonic approximation and the inadequate description of the electronic potential surface. In a recent review of ab initio calculations of vibrational spectra Zahradnik et al. suggest that the accuracy of a frequency analysis is affected more by the quality of the calculated potential than by the neglect of anharmonicity.[23] Although this might be true for the intramolecular vibrations of hydrogen-bonded species, the anharmonicity of the weak intermolecular vibrational modes (shallow potential, Figure 3) can be a source of significant errors. In addition to the sensitivity of the potential surface of simple molecules for electron-correlation and the quality of basis sets, the potential hypersurface of H-bonded complexes also can be distorted seriously by the basis set superposition error. A recent study of Boutellier and Behrouz illustrated that the ν_{HF} and $\nu_{F...N}$ stretching frequencies calculated on the BSSE corrected potential surface of the HCN..HF complex reproduce the experimentally determined frequencies significantly better than those calculated on the uncorrected surface.[24]

For the calculation of translational and rotational energies one usually applies the Boltzmann statistics on the quantum mechanical translational and rotational problem. In the classical limit, the translational energy is described by equations 10.

$$E_{trans} = \frac{3}{2}NkT \qquad \text{(II.10)}$$

The expressions are similar for molecular rotation:

$$E_{rot} = \frac{3}{2}NkT \qquad \text{(II.11)}$$

and

$$E_{rot} = NkT \qquad \text{(II.12)}$$

for non-linear and linear molecules, respectively, where N is the number of molecules. As a result, the contributions to the interaction energy for the association of *n* moles of individual molecules to one mole H-bonded complex are 3/2(1-*n*)RT kcal/mol for both the translational and the rotational energy (for non-linear molecules).

To avoid the forbidding task of solving the Schroedinger equation for a macroscopic system, one is forced to employ many simplifications, idealizations concerning the chemical systems under discussion. Thus, we must realize the limitations of our approximations. The most consequential simplification is the conjecture of the ideal gas behavior, which means that there is no interaction between the molecules in the examined systems. Beside this crude approximation, the factorization of the molecular Schroedinger equation to independent electronic, vibrational, etc. equations is also a necessary step to simplify our approach. Nevertheless coupling between vibrations and rotational motions can cause significant errors. The treatment of internal rotations as vibrations (good approximation at low temperatures) is erroneous at higher temperatures, where the internal rotations can become unhindered. Fortunately, many of the errors stemming from our simplifications cancel during the interaction energy calculations, as the effect of the assumptions is approximately the same in both the individual molecules and the composite interacting system.

Beside the calculation of the internal energies one also may need to consider the enthalpy change following a formation of one mole H-bonded molecule from n moles of constituent molecules. Using classical thermodynamical results for ideal gases, the corresponding enthalpy change is

$$\Delta H = \Delta E + \Delta(pV) = \Delta E + (1-n)RT \qquad \text{(II.13)}$$

where p and V are the pressure and volume of the equilibrium system.

Although during this work I shall not go beyond the use of internal energy and enthalpy, I feel necessary to note here, that the calculation of other thermochemical quantities would follow similar procedure. The knowledge of all the internal energy levels with the appropriate multiplicities allows one to construct the appropriate partition functions, the entropy, the Gibbs free energy and other useful thermodynamical properties.[20] One, however, must be very cautious using these latter quantities. The problem originates from the fact that a minimum on the internal energy surface does not necessarily correspond to a minimum on the enthalpy or free energy surface. Consequently, the experimentally determined enthalpy or Gibbs free energy values corresponding to the appropriate equilibrium systems and minima on the potential surfaces will differ from those determined at the internal energy minimum.

In summary, the usual scheme of my computations followed the next five steps:

1. Calculation of electronic energies of the interacting molecules separately and that of the composite H-bonded system by solving the electronic Schroedinger equation. The interaction energy calculated from equation II.6, must then be corrected for BSSE.

2. Vibrational analysis. The difference in the ZPVE-s and the corrected electronic

interaction energy gives the internal energy change at 0 K for the formation of the H-bonded complex.

3. In the next step the temperature dependent parts of the internal energy are considered; the vibrational (second term on the right side of equation II.9), the translational (equation II.10) and the rotational energy (equations II.11 and II.12). This step results in the internal energy change at a given T temperature.

4. The calculation of the enthalpy change at T temperature from equation II.13.

5. The calculation of other thermochemical properties: partition function, entropy, Gibbs free energy and others.

4. Ab initio Calculation for Hydrogen Bonded Systems III.: The Basis Set Superposition Error and Its Correction for Aggregates Containing More than Two Interacting Molecules[25]

Introduction: The BSSE Problem

The calculation of energies of association using ab initio techniques with basis sets below the Hartree-Fock limit (saturated basis set) is subject to the basis set superposition error (BSSE). The origin of this error, as was briefly mentioned in the previous sections, lies in the possibility that the unused basis functions of the second unit in the associated complex may augment the basis set of the first unit, thus lowering its energy compared to a calculation of this unit alone. The first unit will cause a similar error on the second. This energy lowering is the consequence of the variational theory and of the use of basis

sets of different size in the monomer and the supermolecule calculations. The effects of BSSE are manifold. First, it distorts the potential surface: lowers the interaction energies and changes the positions of various minima. Consequently, the geometries corresponding to stationary points (global and local minima), to transition states on the potential surface and different properties at these points (for example, the dipole moment) can suffer from serious errors. Errors in calculated force constant and vibrational frequencies will appear as another result of the distorted potential surface. (See Section II.3 and Chapter IV for examples.)[24]

Thus, the correction for the BSSE is a major concern for quantum chemists from both the theoretical and practical viewpoints. In the former category, it is challenging to correct an error that is a consequence of one of the fundamental approximations (application of finite basis sets) of quantum chemistry. These investigations may give additional insight into the nature of variational theory and can lead to alternative computational techniques. In applications, to make reliable predictions of interaction energies, vibrational frequencies, etc., one must have a reliable theoretical procedure to do so.

Several approaches for correcting the BSSE have been proposed in the literature.[26,27] The basic principle behind most of the proposed techniques is the attempt to make the basis sets of the monomer and supermolecule calculations consistent with each other. For example, Mayer et al.[26a] attempted to 'a priori' adjust the supermolecule basis set to the monomer calculations by modifying the non-block diagonal matrix elements of the Fock-operator of the supermolecule. This procedure (Chemical

Hamiltonian Approach, CHA) employs projection operators to confine the molecular functions into the subspace of the same molecule. The practical difficulties in the application of the CHA approach for everyday routine problems prevented this method from being used widely. A similar principle led Sadlej with his constrained dimer function (CDF) approach.[26b] He imposed algebraic constraints on the wavefunction of the supermolecule, requiring that the monomers behave in the supermolecule as if they were the solutions of the monomeric Hartree-Fock equations. The inconsistencies of the CDF method have been sharply criticized by Mayer.[26c]

Boys and Bernardi, on the other hand, 'a posteriori' extended the monomer basis sets and made them consistent with the supermolecule basis set.[27] Although, it has its advocates[28] and critics,[29] this latter procedure, the counterpoise (CP) correction, has become the most popular means of correcting for BSSE. The CP method calculates each of the interacting units with the basis functions of the other (without the nuclei or electrons), using so-called 'ghost orbitals'. It is worth noting that the most often mentioned defect of the CP method is its tendency to overcorrect.[26a,29]

It is curious that the precise procedure for calculating the CP for aggregates in which the individual units and the aggregate have been separately optimized has not been clearly described in the literature.[30] The Boys-Bernardi procedure requires five individual calculations for a dimer (monomers A and B with ghost orbitals, in addition to the three calculations for the interaction energy: dimer, monomers A and B), with the CP given by equation II.14, where A^* and B^*, indicate calculations with ghost orbitals. Extending this procedure to supermolecules where the monomers and the dimers have been individually

optimized requires two additional calculations (monomers A and B without ghosts, must be calculated in both their optimized geometries as well as in those they assume in the dimer), for a total of seven individual calculations. The CP is given by equation II.15, where A' and B' represent A and B frozen in their dimer geometries. While I have used the seven calculation method in my work, recent discussions have indicated that the use of the five calculation method may have been used by others, as indicated by a recent communication by Mayer and Surján that emphasizes this point.[31]

$$CP-(E_A-E_{A^*})+(E_B-E_{B^*}) \qquad \text{(II.14)}$$

$$CP-(E_{A'}-E_{A^*})+(E_{B'}-E_{B^*}) \qquad \text{(II.15)}$$

The extension of the CP correction for associated complexes containing three or more units has been attempted by Wells et al.[32] They investigated helium trimers and suggested the so-called pairwise additive function counterpoise (PAFC) and the site-site function counterpoise procedures (SSFC). They concluded similarly to my observations during my work on associations of more than two molecules that, when more than two molecules are involved, the magnitude of the CP correction depends upon the way it is calculated. In this section I shall use hydrogen fluoride to illustrate this point.

Methods

H-bonding aggregates from dimers to pentamers of HF have been calculated using the 6-31G, 6-31G(d), and 6-31G(d,p) basis sets at the Hartree-Fock and MP2 levels. Rather than use the experimental[33] or completely optimized[29b] geometries for the global

minimum, the HF aggregates were kept linear for simplicity. The aggregates were calculated in two different ways: a) both the intra- and intermolecular distances in the aggregates were kept at the HF/6-31G optimized geometry for the monomer (intramolecular H-F, 0.9209 Å) and dimer (intermolecular F..H, 1.8024 Å) and b) the aggregates were completely optimized (with the linear constraint). These two approaches allow us to separate the pure CP correction (due solely to the basis set interaction) from the coupled effect of the varied geometries of the different sized aggregates.

For the fixed geometries, the counterpoise correction is calculated by equation II.14. For cases where the monomers and aggregates are optimized, equation II.15 must be used.

Results and Discussion

While calculating the CP for the association of two HF molecules is fairly unambiguous, calculating this correction for the formation of a third HF with the dimer is not. One can see from Table I, that the CP is different for the two possible reactions

$$HF+(HF)_n \rightarrow HF\cdots(HF)_n \qquad \text{(II.16)}$$

$$(HF)_n+HF \rightarrow (HF)_n\cdots HF \qquad \text{(II.17)}$$

II.16 and II.17, where the third HF is added to the two different ends (F or H) of the dimer. Using these procedures would lead to different association energies for adding the third HF to the different ends of the dimer, in clear violation of the first law of thermodynamics. The calculations were performed both with the H-F intramolecular and

the F...H intermolecular (H-bonding) distances fixed and completely optimized. The calculated CP's are collected in Table I.

Fixed Geometries

Adding HF molecules to the H-end of the growing chain (method 1 in Table I) produces a constant CP for all levels of calculation (after a slight reduction in CP on going from dimer to trimer). However, adding HF's to the F-end of the growing chain (method 2) results in larger CP's, which increase in magnitude as the chain grows. While they will presumably reach an asymptotic limit, they have not yet done so at the pentamer level.

$$CP_{(HF)_n} = \sum_{(i=1,n)} (E_{HF_i} - E_{HF_i^{**}}) \qquad \text{(II.18)}$$

A third way (method 3) to calculate the CP for adding a HF unit to a growing aggregate is to calculate the full CP of each aggregate (before and after the HF is added) as described (for fixed geometries) in equation II.18 (where HF_i^{**} denotes the i-th HF molecule calculated with ghost orbitals for all the other (n-1) molecules; then, obtain the difference in the two CP's. Using equation II.18 requires that each HF in each aggregate be individually calculated with the ghost orbitals of all the other the HF's in that aggregate. Thus, for a trimer, all three component HF's (which have different ghost orbitals) must be individually calculated. This method is preferable, as it removes any ambiguity about which end of the aggregate should be used to attach the next unit of HF. I note here that this procedure is equivalent to Wells' SSFC procedure.[32] Using this method, the CP decreases slightly upon going from dimer to trimer, then remains constant

Table I. Calculated Counterpoise Correction for Linear Aggregation of HF Molecules[a]

	$(HF)_n + HF \rightarrow (HF)_{n+1}$ (kcal/mol)					
	fixed geom. (method)			optimized geom. (method)		
n	1	2	3	1	2	3
			HF/6-31G			
1	0.954	0.954	0.954	0.949	0.949	0.949
2	0.944	1.029	0.938	0.984	1.071	1.014
3	0.944	1.056	0.938	0.997	1.134	1.044
4	0.943	1.065	0.938	1.003	1.164	1.064
			HF/6-31G(d)			
1	0.875	0.875	0.875	0.780	0.780	0.780
2	0.870	0.951	0.868	0.839	0.897	0.883
3	0.871	0.975	0.869	0.855	0.940	0.915
4	0.870	0.981	0.868	0.861	0.958	0.932
			HF/6-31G(d,p)			
1	0.951	0.951	0.951	0.832	0.832	0.832
2	0.938	1.041	0.941	0.906	0.973	0.971
3	0.936	1.068	0.940	0.931	1.029	1.035
4	0.935	1.077	0.940	0.942	1.054	1.067
			MP2/6-31G			
1	1.398	1.398	1.398	1.312	1.312	1.312
2	1.375	1.510	1.376	1.395	1.524	1.469
3	1.373	1.549	1.375	1.426	1.627	1.543
4	1.372	1.562	1.375	1.438	1.677	1.587
			MP2/6-31G(d)			
1	1.521	1.521	1.521	1.383	1.383	1.383
2	1.508	1.633	1.511	1.494	1.588	1.584
3	1.506	1.665	1.511	1.532	1.672	1.675
4	1.505	1.676	1.511	1.547	1.710	1.721
			MP2/6-31G(d,p)			
1	1.573	1.573	1.573	1.445	1.445	1.445
2	1.547	1.697	1.557	1.596	1.698	1.727
3	1.545	1.737	1.558	1.652	1.806	1.865
4	1.544	1.748	1.555	1.677	1.858	1.941

[a]Methods 1 and 2 refer to adding the next HF to the H-end and F-end, respectively, of the growing aggregate. Method 3 involves calculating the CP for each aggregate from the monomeric units, then taking the difference in CP's between $(HF)_n$ and $(HF)_{n+1}$.

for all ab initio methods used. Curiously, the third method sometimes gives values that are less than either of those obtained by the first two (HF/6-31G, HF/6-31G*).

While the energetic differences in the calculated CP corrections are small for the fixed geometry calculations, it is somewhat disconcerting that the CP's tend to decrease as HF molecules are added to the H-end, but increase as they are added the F-end. For each basis set used, the increase in the CP observed for method 2 is entirely due to the $(HF)_n$ component when n is 2 or more (the CP for the HF being added is constant to 0.001 kcal/mol).

Optimized Geometries

When each aggregate is fully optimized, changes in the CP can be due to the differences in the distances and orientations of the ghost orbitals with respect to the individual HF units as their geometries relax. Thus, the intramolecular H-F distances increase while the intermolecular distance decreases as the aggregate becomes larger (see Table II). One might expect the CP's to increase in the growing aggregates since, as the intermolecular distances decrease, the ghost orbitals move closer to the atomic centers of the molecule. The CP corrections for the optimized aggregates are also included in Table I. The results indicate that the CP's are generally larger in all cases. The CP's should not reach an asymptotic limit until the geometries also do so. This has not yet happened at the pentamer level. As in the fixed geometry series, method 2 (adding monomer to the F-end of the aggregate) consistently results in a higher CP than method 1. However, method 3 (the extension of SSFC for optimized geometries) produces CP's similar to (and

Table II. Optimized H-F (Intramolecular) and F...H (Intermolecular) Distances in $(HF)_n$ Aggregates[a]

	Intramolecular H-F distances (Å)					Intermolecular F..H distances (Å)			
n	1	2	3	4	5	1-2	2-3	3-4	4-5
					HF/6-31G				
1	0.9209								
2	0.9218	0.9242				1.8024			
3	0.9226	0.9283	0.9267			1.7162	1.7381		
4	0.9229	0.9305	0.9324	0.9278		1.6877	1.6462	1.7159	
5	0.9231	0.9315	0.9354	0.9343	0.9283	1.6759	1.6151	1.6215	1.7065
					HF/6-31G(d)				
1	0.9110								
2	0.9130	0.9132				1.9297			
3	0.9138	0.9166	0.9144			1.8474	1.8682		
4	0.9141	0.9180	0.9185	0.9150		1.8258	1.7885	1.8498	
5	0.9142	0.9186	0.9202	0.9194	0.9152	1.8170	1.7642	1.7692	1.8428
					HF/6-31G(d,p)				
1	0.9006								
2	0.9018	0.9030				1.9181			
3	0.9024	0.9057	0.9043			1.8408	1.8614		
4	0.9027	0.9069	0.9077	0.9049		1.8184	1.7790	1.8433	
5	0.9029	0.9074	0.9091	0.9084	0.9051	1.8083	1.7541	1.7595	1.8352
					MP2/6-31G				
1	0.9470								
2	0.9463	0.9490				1.8174			
3	0.9466	0.9516	0.9514			1.7254	1.7506		
4	0.9467	0.9533	0.9557	0.9524		1.6949	1.6528	1.7272	
5	0.9469	0.9542	0.9584	0.9578	0.9530	1.6821	1.6187	1.6261	1.7172
					MP2/6-31G(d)				
1	0.9340								
2	0.9357	0.9360				1.8737			
3	0.9366	0.9398	0.9377			1.7926	1.8168		
4	0.9367	0.9412	0.9421	0.9382		1.7671	1.7304	1.7967	
5	0.9369	0.9419	0.9442	0.9433	0.9385	1.7566	1.7022	1.7087	1.7885
					MP2/6-31G(d,p)				
1	0.9213								
2	0.9225	0.9238				1.8618			
3	0.9228	0.9266	0.9253			1.7773	1.8024		
4	0.9230	0.9279	0.9291	0.9259		1.7493	1.7109	1.7813	
5	0.9232	0.9286	0.9311	0.9304	0.9263	1.7367	1.6789	1.6866	1.7718

[a]The intramolecular H-F and intermolecular F...H distances are listed going from left to right in the linear $(HF)_n$ aggregates.

Table III. Calculated CP Correction for Each Individual HF Molecules (Going from Left to Right within the Chain) of a Pentamer Aggregate, $(HF)_5$, at Different Levels of Theory

	1 (H-end)	2	3	4	5 (F-end)
HF/6-31G	0.674	1.029	1.031	0.984	0.353
HF/6-31G(d)	0.658	0.885	0.901	0.865	0.202
HF/6-31G(d,p)	0.839	0.994	1.013	0.944	0.115
MP2/6-31G	1.111	1.497	1.516	1.433	0.355
MP2/6-31G(d)	1.220	1.614	1.644	1.555	0.329
MP2/6-31G(d,p)	1.418	1.781	1.820	1.685	0.275

often larger than) method 2. To use method 3 for cases where aggregates and monomers are individually optimized, the monomers frozen in their aggregate geometries, HF', must be used as in equation II.19.

$$CP_{(HF)_n} = \sum_{(i=1,n)} (E_{HF_i'} - E_{HF_i''}) \qquad \text{(II.19)}$$

All three methods predict the CP to increase as the aggregate grows, but the energetic differences between them also increases, approaching 0.3 kcal/mol at the pentamer level, where the geometries have not yet reached their limiting values. One can expect these energetic differences to increase as the aggregate grows further.

When method 3 is used, the contributions of the individual HF molecules to the CP of the aggregate are largest for those in the center. The values are significantly lower for the molecule on the F-end than for that on the H-end. Table III illustrates several examples of the individual contributions for method 3.

The fact that the three methods for calculating the CP give different results

emphasizes the arbitrariness (and non-additivity) inherent in the CP method. However, until a better and more practical approach to correcting the BSSE arises, it is important that a choice be made between the several ways of calculating the CP. Unfortunately, I have no acceptable means of deciding which method gives the more correct BSSE. However, only method 3 is independent of the means in which the aggregate is constructed. Thus, I recommend that method 3 be generally applied to aggregates containing several monomeric units. This suggestion is similar to that of Wells and Wilson.[32]

5. Semiempirical Calculations for Hydrogen Bonded Systems

Beside the ab initio calculations, the second large group of molecular orbital techniques consists of the semiempirical methods. The semiempirical and the ab initio methods depart from the same theoretical frame, their common goal being the solution of the iterative Hartree-Fock-Roothaan equations. The way they approach this aim distinguishes them from each other. Contrary to the ab initio methods that do not use any new approximation beyond those leading to the Hartree-Fock equations, the semiempirical calculations further simplify the solution of the Hartree-Fock equations by introducing parametrized integral evaluation schemes from either physical models or purely empirical approximations. While, the integrals based upon physical models usually contain parameters related to experimentally measurable properties, the empirical equations have adjustable parameters and other simplifications (neglect of certain integrals) mostly in the

difficult and time consuming three- and four-center integral evaluation.

The purpose of this simplification is two-fold. First, the parametrization of the difficult integrals can speed up the computational procedure astoundingly; a factor of 100 or more is commonplace in comparison with the most primitive ab initio methods.[34] The second reason is rather philosophical than economical. Calculations for water monomer and dimers exemplify[4] that even the best ab initio calculations including electron correlation can suffer from an error of 10 kcal/mol magnitude in the total energy. This fact indicates that calculations of sufficient accuracy for even small chemical systems will not likely be feasible soon. However, the problem of accuracy can be circumvented without using these highly expensive techniques.

Thus, one can introduce empirical or semiempirical parameters in the integral evaluation within the proper theoretical frame and optimize these parameters in a way that one or more experimentally measurable properties of a representative sample of compounds be reproduced as accurately as possible. Successive calculations on other compounds can justify the use of these approximations and parameters or refute the theory. The consequences (speed and reliability) of this approach make the application of semiempirical methods for large molecules, biological systems favorable over that of the ab initio techniques. Nevertheless, the two methods can be used in tandem as this Dissertation will illustrate. The (at least theoretically) more developed ab initio calculations on smaller systems, which can model the interacting parts of larger systems (for example, active center and substrate interaction of an enzyme) can be compared to the results of semiempirical calculations. The comparison can mutually reinforce the

results of both methods and lead to credible, though empirical relations between the two techniques.

In my work I used the three most popular semiempirical methods, AM1[35], MNDO-PM3[36] (or PM3) and SAM1.[37] These three methods evolved from a series of failures and successes of attempts to develop a reliable and yet fast technique. The common feature of these and other earlier methods is that they treat only the valence electrons in the Hartree-Fock equations. The inner shell electrons with the nuclei form the core. While earlier attempts concentrated only on the π-electrons (π-electron methods, for example Huckel methods,[38] Pariser-Parr-Pople method[39]), later the all valence electron methods gradually replaced them. The first generation of the all valence electron methods used crude approximations, like ZDO (zero differential overlap). The ZDO approximation neglects all two-electron integrals in which the charge density of two different atomic orbitals occurs:

$$\int \chi_\lambda(1)\chi_\mu(1)\frac{1}{r_{12}}\chi_\nu(2)\chi_\rho(2)dr_1dr_2 = \delta_{\lambda\mu}\delta_{\nu\rho}\gamma_{\lambda\nu} \qquad \text{(II.20)}$$

The deviation from the ZDO approximation characterizes the different all valence electron methods. CNDO[40] (complete neglect of differential overlap) employs the ZDO completely, INDO[41] (intermediate NDO) keeps the atomic exchange integrals, while NDDO[42] (neglect of diatomic differential overlap) neglect only those integrals that contain differential overlaps belonging to different atoms. The MINDO[43] (modified INDO) method marks the birth of the second generation of the all valence electron methods. Its distinguishing feature from the earlier methods that its purpose is not the

reproduction of ab initio results anymore (as in CNDO, INDO and NDDO), but to reproduce experimentally measurable properties, most importantly the heat of formation of molecules. MINDO uses the INDO approximations but most of the expressions (even the nuclear-nuclear repulsion) are parametrized. Further progress led to the MNDO[44] (modified NDO) method. MNDO retains the integrals of NDDO and attempts to reproduce not only the heat of formation of molecules, but molecular geometries, dipole moments, ionization potentials, etc. This evolution of methods resulted in more and more reliable techniques. However, even the most sophisticated of them, the MNDO method, is not able to model hydrogen bonding systems satisfactorily. This is the main reason I turned my attention toward the methods of the third generation that were developed with the purpose of reliable description of the hydrogen-bonded systems.

All three methods employed in my work are based on the MNDO approximation. AM1 contains a simple modification compared to MNDO: the core repulsion function (CRF), that is also parametrized in MNDO, is replaced by a new expression containing additional Gaussian functions. These extra functions compensate for the excessive repulsion at large interatomic separations. The remaining expressions are similar to those in MNDO. This means that in addition to seven optimized parameters (for example U_{ss}, U_{pp} one-center one-electron energies; β_s and β_p in the expression for the one-electron two-center resonance integrals; etc.) and five parameters estimated from spectroscopic measurements (for example, g_{ss}, Coulomb integrals; h_{sp}, exchange integrals), twelve new parameters were introduced in the CRF function. All parameters were completely reoptimized using a selective grid search for the minimum of the sum of the squares of

the weighed errors for the calculated properties. This minimization procedure leads to the final form of the method. AM1 proved to be very successful at describing a wide variety of chemical problems. A recent review of Dannenberg and Evleth examines the description of hydrogen-bonded systems using AM1 method.[45] They compare more than one hundred calculated H-bonding enthalpies with experimental values and conclude that, though AM1 tends to underestimate the interaction energies, the agreement is reasonable. They also question the often cited statement that the tendency of AM1 for multicentered hydrogen bonds would be a big shortcoming of the method. Many other examples will be mentioned in this work later, where the AM1 method is superior over other semiempirical calculations. Beside AM1's success on hydrogen-bonded systems,[46] its reasonable predictions on chemical reactions,[47] molecular geometry[35] and other molecular properties[48] serve as the main reason that the method endured almost ten years without losing its popularity.

The MNDO-PM3 (parametrization method 3) method is a completely reparametrized version of AM1. This method breaks with every theoretical development of its parameters.[49] While, the five parameters evaluated from spectroscopic measurements in AM1 (and MNDO) have certain physical meaning, they are replaced by numerical values to give the best possible fit in the PM3 optimization procedure. The advantage of this method is that it undoubtedly gives a better description for most of the properties of the compounds that are part of the optimization sample. However, the price of losing the physical interpretation of the parameters is that this approach can lead to physically meaningless results for compounds and reactions outside the circle of the

representative compounds. A recent paper by Jurema and Shields who compare the PM3 method with AM1, mentions such an example.[50] The authors indicate that the ammonia dimer is held together by + 0.19 kcal/mol (!) interaction enthalpy. Another serious error of PM3 is that it predicts almost free internal rotation around the CN bond in formamide.[37] It also fails to reproduce monotonically changing tendencies along a given row (going from C to F) of the periodic table, such as properties strongly related to electronegativity.[37] Most of these errors involve the nitrogen atom indicating distortion in its parameter set. Other examples for peculiar PM3 results include the interaction between two molecules of methane.[51] Despite these failures I extensively used the PM3 method in comparison with other semiempirical and ab initio methods. During my examinations I also found a suspicious complex between acetylene and ozone, whose PM3 description, similarly to those mentioned above, is hard to reconcile with any reasonable physical model (see later in Chapter IV).

The most recent semiempirical method is SAM1 (semi-ab initio method). The major difference between SAM1 and AM1 involves the calculation of the repulsion integrals. These are calculated using a STO-3G basis set and then scaled to account for electron correlation. Being the newest method, SAM1 results are scarce in the literature. In parts of my work I used SAM1 for experimental purposes, to compare its capability to those of AM1 and PM3.

6. Computational Facilities

I used the RS/6000 version of the GAUSSIAN90 and GAUSSIAN92[52] program packages to perform ab initio calculations on both Hartree-Fock and second-order Møller-Plesset level. The basis sets included the standard 3-21G, 6-31G, 6-31G(d), 6-31G(d,p), 6-31G++(d,p), 6-311G(d,p), 6-311G++(d,p) and D95++(d,p) sets.

I also performed semiempirical AM1, PM3 and SAM1 calculations using the AMPAC 2.1 (AM1)[53] and AMPAC 4.5 (SAM1 and PM3)[54] programs. The IBM PC and RISC/6000 versions of the PCMODEL[55] and MOTECC-90[56] programs were used to generate the input and visualize the final structures.

The calculations were performed on IBM RISC/6000 and Ulysses Systems 386/486 workstations.

7. References

1. See any basic quantum chemistry books. Examples: a) Levine, I. N. *Quantum Chemistry, 3d ed.*; Allen and Bacon: Boston, 1983. b) Szabo, A.; Ostlund, N. S.; *Modern Quantum Chemistry*; McGraw-Hill: New York, 1989. c) Sutcliffe, B. T., Fundamentals of computational quantum chemistry in *Computational Techniques in Quantum Chemistry*; Diercksen, G. H. F.; Sutcliffe, B. T.; Veillard, A., editors; Reidel: Boston, 1975.

2. Roothaan, C. C. J. *Rev. Mod. Phys.*, **1951**, *23*, 69.

3. Turi, L.; Dannenberg, J. J.; Rama, J. B.; Ventura, O. N. *J. Phys. Chem.*, **1992**, *96*, 3709. Ventura, O. N.; Rama, J. B.; Turi, L.; Dannenberg, J. J. *J. Am. Chem. Soc.*, **1993**, *115*, 5754.

4. a) Chakravorty, S. J.; Davidson, E. R. *J. Phys. Chem.*, **1993**, *97*, 6373. Kim, K. S.; Mhin, B. J.; Choi, U-S.; Lee, K. *J. Chem. Phys.*, **1992**, *97*, 6649. van Duijneveldt-van de Rijdt, J. G. C. M.; van Duijneveldt, F. B. *J. Chem. Phys.*, **1992**, *97*, 5019. Dannenberg,

J. J.; Mezei, M. *J. Phys. Chem.*, **1991**, *95*, 6396. Muguet, F. F.; Robinson, G. W.; Bassez-Muguet, M. P. *Int. J. Quantum Chem.*, **1991**, *39*, 449. Dannenberg, J. J. *J. Phys. Chem.*, **1988**, *92*, 6869. b) Racine, S. C.; Davidson, E. R. *J. Phys. Chem.*, **1993**, *97*, 6367.

5. a) Dewar, M. J. S.; Ford, G. P. *J. Am. Chem. Soc.*, **1979**, *101*, 5558. b) Dewar, M. J. S.; Storch, D. M. *J. Am. Chem. Soc.*, **1985**, *107*, 3898.

6. Pople, J. A.; Nesbet, R. K. *J. Chem. Phys.*, **1959**, *22*, 571.

7. Foresman, J. B.; Head-Gordon, M.; Pople, J. A.; Frisch, M. J. *J. Phys. Chem.*, **1992**, *96*, 135. Pople, J. A.; Binkley, J. S.; Seeger, R. *Int. J. Quant. Chem. Symp.*, **1976**, *10*, 1.

8. Møller, C.; Plesset, M. S. *Phys. Rev.*, **1934**, *46*, 618.

9. see for example: Clementi, E.; Raimondi, D. L. *J. Chem. Phys.*, **1963**, *38*, 2686.

10. Boys, S. F. *Proc. R. Soc. London A*, **1950**, *200*, 542.

11. Preuss, H. *Z. Naturforsch.*, **1956**, *11*, 823.

12. Rothenberg, S.; Schaefer III, H. F. *J. Chem. Phys.*, **1971**, *54*, 2765.

13. Clementi, E. *IBM J. Res. and Dev.*, **1965**, *9*, 2. Whitten, J. L. *J. Chem. Phys.*, **1966**, *44*, 359.

14. 3-21G: Binkley, J. S.; Pople, J. A.; Hehre, W. J. *J. Am. Chem. Soc.*, **1980**, *102*, 939. 6-31G. Hehre, W. J.; Ditchfield, R.; Pople, J. A. *J. Chem. Phys.*, **1972**, *56*, 2257.

15. Hariharan, P. C.; Pople, J. A. *Theor. Chim. Acta*, **1973**, *28*, 213. Gordon, M. S. *Chem. Phys. Lett.*, **1980**, *76*, 163.

16. Clark, T.; Chandrasekhar, J.; Spitznagel, G. W.; Schleyer, P. v. R. *J. Comput. Chem.*, **1983**, *4*, 294.

17. Dunning, T. H.; Hay, P. J. *Modern Theoretical Chemistry*, Plenum: New York, 1976.

18. Note, that this, however, does not necessarily mean better variational wavefunction (the word 'better' means any wavefunction whose overlap with the exact Ψ is closer to 1) and consequently molecular properties, as the Eckart inequality is only valid at the proximity of the exact wavefunction.[1]

19. Davidson, E. R.; Feller, D. *Chem. Rev.*, **1986**, *86*, 681.

20. Details about the standard expressions of the thermochemical properties for ideal gases in the canonical ensemble can be found in many textbooks. Examples: Benson, S. W. *Thermochemical Kinetics*, Wiley and Sons: New York, 1968. Andrews; F. C.

Equilibrium Statistical Mechanics, Wiley and Sons: New York, 1975.

21. See for example: Levine, I. N. *Molecular Spectroscopy*, Wiley and Sons: New York, 1975.

22. Pulay, P. In *Modern Theoretical Chemistry*, Schaefer, H. F., III, Ed.; Vol. 4, Plenum: New York, 1977. Pulay, P. *Mol. Phys.*, **1969**, *17*, 197.

23. Hess, B. A.; Schaad, L. J.; Carsky, P.; Zahradnik, R. *Chem. Rev.*, **1986**, *86*, 709.

24. Boutellier, Y.; Behrouz, H. *J. Chem. Phys.*, **1992**, *96*, 6033.

25. The content of this section is based on the following article: Turi, L.; Dannenberg, J. J. *J. Phys. Chem.*, **1993**, *97*, 2488.

26. For example a) Mayer, I., Surján, P. R. *Int. J. Quant. Chem.*, **1989**, *36*, 225. Mayer, I.; Turi, L. *J. Mol. Str. (THEOCHEM)*, **1991**, *227*, 43. b) Sadlej, A. J. *J. Chem. Phys.*, **1991**, *95*, 6705. c) Mayer I. *J. Chem. Phys.*, **1992**, *97*, 5257. Sadlej, A. J. *J. Chem. Phys.*, **1992**, *97*, 5259.

27. Boys, S. F.; Bernardi, F., *Mol. Phys.*, **1970**, *19*, 553.

28. a) Szalewicz, K.; Cole, S. J.; Kolos, W.; Bartlett, R. J. *J. Chem. Phys.*, **1988**, *89*, 3662. b) Gutowski, M.; van Duijneveldt, F. B.; Chalasinski, G.; Piela, L. *Mol. Phys.*, **1987**, *61*, 233. Gutowski, M.; van Duijneveldt-van de Rijdt, J. G. C. M.; van Lenthe, J. H.; van Duijneveldt, F. B. *J. Chem. Phys.*, **1993**, *98*, 4728.

29. a) Schwenke, D. W.; Truhlar, D. G. *J. Chem. Phys.*, **1984**, *82*, 2418. b) Frisch, M. J.; Del Bene, J. E.; Binkley, J. S.; Schaefer, H. F. III *J. Chem. Phys.*, **1986**, *84*, 2279.

30. Despite the fact that the following references correctly describe the procedure, they are rarely referenced in the current literature: a) Emsley, J.; Hoyte, O. P. A.; Overill, R. E. *J. Am. Chem. Soc.*, **1978**, *100*, 3303. b) Leclercq, J. M.; Allavena, M.; Bouteiller, Y. *J. Chem. Phys.*, **1983**, *78*, 4606.

31. Mayer, I.; Surján, P. R. *Chem. Phys. Lett.*, **1992**, *191*, 497.

32. Wells, B. H.; Wilson, S. *Chem. Phys. Lett.*, **1983**, *101*, 429.

33. a) (gas phase) Bauer, S. H.; Beach, J. Y.; Simons, J. H. *J. Am. Chem. Soc.*, **1939**, *61*, 19. b) (crystal structure) Atoji, M.; Lipscomb, W. N. *Acta Crystallogr.*, **1954**, *7*, 173.

34. See reference 5b for a simple qualitative discussion.

35. Dewar, M. J. S.; Zoebisch, E. G.; Healy, E. F.; Stewart, J. J. P. *J. Am. Chem. Soc.*, **1985**, *107*, 3902.

36. Stewart, J. J. P. *J. Comput. Chem.*, **1989**, *10*, 209.

37. Dewar, M. J. S.; Jie, C.; Yu, J. *Tetrahedron*, **1993**, *49*, 5003.

38. For a discussion of the original Huckel theory see Levine (reference 1) pages 466-492.

39. Pariser, R. D.; Parr, R. G. *J. Chem. Phys.*, **1953**, *21*, 466 and 767. Pople, J. A. *Trans. Faraday Soc.*, **1953**, *49*, 1375.

40. Pople, J. A.; Segal, G. A. *J. Chem. Phys.*, **1965**, *43*, S136. Pople, J. A.; Segal, G. A. *J. Chem. Phys.*, **1966**, *44*, 3289.

41. Pople, J. A.; Beveridge, D. L.; Dobosh, P. A. *J. Chem. Phys.*, **1967**, *47*, 2026.

42. Pople, J. A.; Santry, D. P.; Segal, G. A. *J. Chem. Phys.*, **1965**, *43*, S129.

43. The last of the MINDO series of programs, is the MINDO/3: Bingham, R. C.; Dewar, M. J. S.; Lo, D. H. *J. Am. Chem. Soc.*, **1975**, *97*, 1285.

44. Dewar, M. J. S.; Thiel, W. *J. Am. Chem. Soc.*, **1977**, *99*, 4899.

45. Dannenberg, J. J.; Evleth, E. M. *Int. J. Quant. Chem.*, **1992**, *44*, 869.

46. Dannenberg, J. J.; Vinson, L. K. *J. Phys. Chem.*, **1988**, *92*, 5635. Dannenberg, J. J. *J. Phys. Chem.*, **1988**, *92*, 6869. Vinson, L. K.; Dannenberg, J. J. *J. Am. Chem. Soc.*, **1989**, *111*, 2777. Dannenberg, J. J. *Materials*, **1990**, *2*, 635.

47. Dewar M. J. S.; Jie, C. *Acc. Chem. Res.*, **1992**, *25*, 537. Huang, X. L.; Dannenberg, J. J. *J. Org. Chem.*, **1991**, *56*, 6367. Kaila, N. ; Franck, R. W.; Dannenberg, J. J. *J. Org. Chem.*, **1989**, *54*, 4206. Sodupe, M.; Oliva, A.; Bertran, J.; Dannenberg, J. J. *J. Org. Chem.*, **1989**, *54*, 2488. Dannenberg, J. J.; Baer, B. *J. Am. Chem. Soc.*, **1987**, *109*, 292.

48. An example on AM1 capability on non-linear optical properties (second-order hyperpolarizibilities): Yusukawa, T.; Kimura, T. *Chem. Phys. Lett.*, **1990**, *169*, 259.

49. The criticism of this procedure can be found in the following papers: Dewar, M. J. S. *Int. J. Quant. Chem. Symp.*, **1988**, *22*, 557 and reference 37.

50. Jurema, M. W.; Shields, G. C. *J. Comput. Chem.*, **1993**, *14*, 89.

51. Messinger, J.; Heuser, N. *QCPE Bull.*, **1991**, *11(1)*.

52. *Gaussian92*, Frisch, M. J.; Trucks, G. W.; Head-Gordon, M.; Gill, P. M. W.; Wong, M. W.; Foresman, J. B.; Johnson, B. G.; Schlegel, H. B.; Robb, M. A.; Replogle, E. S.; Gomperts, R.; Andres, J. L.; Raghavachari, K.; Binkley, J. S.; Gonzalez, C.; Martin, R. L.; Fox, D. J.; Defrees, D. J.; Baker, J.; Stewart, J. J. P.; Pople, J. A.; Gaussian, Inc.,

Pittsburgh, PA, 15213, 1992. *Gaussian90*, Frisch, M. J.; Head-Gordon, M.; Foresman, J. B.; Trucks, G. W.; Raghavachari, K.; Schlegel, H. B.; Robb, M. A.; Binkley, J. S.; Gonzalez, C.; Defrees, D. J.; Fox, D. J.; Whiteside, R. A.; Seeger, R.; Melius, C. F.; Baker, J.; Kahn, L. R.; Stewart, J. J. P.; Fluder, E. M.; Topiol, S.; Pople, J. A.; Gaussian, Inc., Pittsburgh, PA, 15213, 1990.

53. A copy of AMPAC 2.1 (which was adapted for RS/6000 by J. J. Dannenberg) was graciously furnished by M. J. S. Dewar and E. Healy.

54. Copyright 1992 Semichem, 12715 W. 66th Terrace, Shawnee, KS 66216.

55. Serena Software, Bloomington, Indiana.

56. Copyright 1989, 1990 IBM Corporation. Center for Scientific and Engineering Computations. Department 48B/428, Neighborhood Road, Kingston, NY 12401.

III. COOPERATIVITY

1. Cooperativity: What Is It?

The concept of non-additivity in molecular interactions appeared in the literature relatively early, in the 1930's.[1] Approximately 25 years later, Frank and Wen postulated that the formation of H-bonds in water is cooperative[2] suggesting strengthened H-bonds in larger H-bonded clusters. Since then, many qualitative and quantitative observations demonstrated the cooperative phenomenon. For example, the concept is of central importance to understanding why consecutive ligands bind to a macromolecule with different affinities. Biological examples include a study on the binding of oxygen to hemoglobin.[3] The analysis of the positive or negative cooperativity in biological systems is based upon graphical methods, the Scatchard plot[4] and the Hill plot.[5] An account from Dahlquist summarizes the correlation between these plots and the cooperative effects for a number of interesting cases.[6]

The complex relations between molecular structure and cooperative phenomena are manifest in relatively simpler non-biological systems, too.[7] An example is the neutron diffraction study on the crystal structure of β-cyclodextryn-ethanol-octahydrate by Saenger et al.[7b] The well-ordered hydrogen-bonding network of the water molecules in the crystal structure, where all the hydrogens point in the same direction (homodromic arrangements), was attributed to strong cooperative effects. The relation between cooperativity, orientation and crystal structure exemplified the undoubtedly great

importance of cooperativity in the crystal formation process. The cooperativity also has a profound effect on the vibrational spectra of H-bonded species. The effect of aggregation on the shift of various X-H streching vibrations was recently investigated by the means of matrix-isolation FT-IR spectroscopy.[7a] These studies found a quantitative relationship between the relative X-H frequency shifts and the fortification of the H-bonding strength upon increasing the number of interacting molecules. They characterized this relationship by developing so-called cooperativity factors. This latter study exemplifies the merits and limitations of most of these experimental studies. First, these experiments usually provides indirect and/or specific proofs. Second, their mostly phenomenological approach limits them to empirical correlations between the observations and the observed phenomenon. Thus, it is imperative to study cooperative effects on strictly theoretical base, too. The results of theoretical studies on small model systems combined with experimental observations can furnish the most satisfying explanation for the origin of cooperative effects.

In fact, many MO studies[8,9] have been performed on multi-hydrogen-bonded systems. They pointed out that, for example, the strength of the second H-bond depends not only on the strength of the first bond but on the orientation of the second interaction, as well. The studies on water trimers predicted minima with both stronger and weaker H-bonding interactions than found in the appropriate dimers.[8] It is widely accepted in these studies to ascribe the cooperative phenomenon to the non-additive part of the molecular interactions. The deviation from the expected interaction energies based on pairwise contributions is called non-additivity arising from three-body (or generally many-body)

interactions. Cooperativity manifests itself not only in energetic but in structural changes as well, suggesting that the origin of the phenomenon arises from the change in the electron distribution of the interacting molecules. I shall illustrate this point later.

Since the use of MO methods is limited to smaller systems, empirical intermolecular potential functions are extremely important in simulations for larger clusters or biological systems. Potentials containing only pairwise interactions such as the Lennard-Jones potential or the exponential-six potentials widely used in simulations cannot account for non-additive effects. On the contrary, functions based on the classical multipole expansion of specific interactions (for example, water-water potential) include cooperative effects in the form of interactions between polarizable charge distributions.[10] These latter studies defined cooperativity as the part of non-additivity that arises from the cooperative reinforcements of the electric fields.[10] The difference between this definition and that of the MO studies (as I mentioned earlier, most of the MO studies identify cooperativity with non-additivity) indicates certain arbitrariness in where to draw the line between cooperativity and non-additivity.

In a slightly different theoretical approach of the next section, I should like to illustrate the origin of non-additivity in molecular interactions by using traditional Rayleigh-Schroedinger perturbation theory. I have to emphasize that the following treatment is only *illustrative*, lacking strict mathematical rigor.

2. A Qualitative Illustration of Cooperativity with Rayleigh-Schroedinger Perturbation Theory.

Another possibility to investigate cooperative effects is to make use of perturbation theory. Perturbation theory for both a) the long range intermolecular forces[10,11] and b) the forces in the small orbital overlap region[12] has long been developed for two interacting species. As the treatment of the long range forces is much simpler in terms of mathematical details I directed my attention to the cooperativity of long range molecular interactions.

Dimers

Let us consider molecules A and B. Let φ_0^A, φ_1^A, φ_2^A, ..., and φ_0^B, φ_1^B, φ_2^B, ... be the orthonormalized, non-degenerate eigenfunctions of $\hat{H}^A$ and $\hat{H}^B$, the Hamiltonians of A and B, where $\hat{H}^A$, for example, is

$$\hat{H}^A = -\frac{1}{2}\sum_i \nabla_i^2 - \sum_{i,P}\frac{Z_P}{r_{iP}} + \sum_{i>i'}\frac{1}{r_{ii'}} + \sum_{P>P'}\frac{Z_P Z_{P'}}{r_{PP'}} \qquad \text{(III.1)}$$

where i and i' denotes electron, P and P' mean nuclei belonging to system A with Z_P and $Z_{P'}$ nuclear charges. In equation III.1 and later in the text atomic units are used.

The starting point of the usual Rayleigh-Schroedinger perturbation theory is the determination of the Hamiltonian $\hat{H}^{AB}$ of the interacting system, AB. $\hat{H}^{AB}$ consists of $\hat{H}^A$, $\hat{H}^B$ (the Hamiltonians of the separate subsystems) and V^{AB}, the perturbation. The zeroth order Hamiltonian of the system AB can be written in the following form:

$$\hat{H}^{AB(0)} = \hat{H}^{A} + \hat{H}^{B} \qquad \text{(III.2)}$$

The interaction between these two molecules can be treated as a perturbation, V^{AB}.

$$V^{AB} = \sum_{i,j} \frac{1}{r_{ij}} - \sum_{i,Q} \frac{Z_Q}{r_{iQ}} - \sum_{j,P} \frac{Z_P}{r_{jP}} + \sum_{P,Q} \frac{Z_P Z_Q}{R_{PQ}} \qquad \text{(III.3)}$$

Here again i and P denote electrons and nuclei of system A, while j and Q refer to the electrons and nuclei of system B, respectively.

For long range forces (at distances where there is virtually no overlap of the interacting systems) we can neglect the electron-exchange between the interacting systems by assigning the set of electrons i to molecule A, j to B. Therefore, the ground state zeroth-order wavefunction may be written as, $\varphi_0^A(i) \times \varphi_0^B(j)$, the product of the correct ground state wavefunctions of systems A and B. In the region of small orbital overlap one has to deal with electron-exchange, therefore the zeroth-order function becomes $\hat{A}\varphi_0^A \times \varphi_0^B$, where $\hat{A}$ is the antisymmetrizer which ensures the correct symmetry of the wavefunction.

The correct wavefunction of the system will be a linear combination of the ground state zeroth-order wavefunction and various products of excited states of molecules A and B. However, I shall not go into the details of the correct form of the wavefunction. Rather, I shall concentrate on the expansion of interaction energy.

The zeroth-order energy of the system is simply the sum of the energies of the separate subsystems.

$$E^{(0)} = \langle \varphi_0^A \varphi_0^B | \hat{H}^{AB(0)} | \varphi_0^A \varphi_0^B \rangle = \langle 0^A 0^B | \hat{H}^{AB(0)} | 0^A 0^B \rangle = E_0^A + E_0^B \qquad \text{(III.4)}$$

where, for the sake of simplicity, I changed the notation of the wavefunction φ_i^A to i^A.

According to equation III.4, every higher order energy correction can be viewed as a contribution to the interaction energy. The first-order energy correction has long been interpreted as the classical electrostatic interaction between two molecules.[4b]

$$E_{AB}^{(1)} = \langle 0^A 0^B | V^{AB} | 0^A 0^B \rangle \tag{III.5}$$

In the second-order perturbation theory of the long range forces the matrix elements corresponding to states $i^A 0^B$ or $0^A j^B$ of the perturbation matrix represent the induction forces [due to the (static) moment, the potential field of B induces in A and vice versa] and those belonging to states $i^A j^B$ express the dispersion (or London) forces [due to dynamic or momentary induction].[12b]

In the Rayleigh-Schroedinger perturbation theory the second- and third-order correction to the energy have the following form:

$$E_{AB}^{(2)} = \sum_{i \text{ or } j \neq 0} \frac{|\langle i^A j^B | V^{AB} | 0^A 0^B \rangle|^2}{(E_0^A - E_i^A) + (E_0^B - E_j^B)} \tag{III.6}$$

$$E_{AB}^{(3)} = \sum_{i \text{ or } j,\, p \text{ or } q \neq 0} \frac{\langle 0^A 0^B | V^{AB} | i^A j^B \rangle \langle i^A j^B | V^{AB} | p^A q^B \rangle \langle p^A q^B | V^{AB} | 0^A 0^B \rangle}{[(E_0^A - E_i^A) + (E_0^B - E_j^B)]\,[(E_0^A - E_p^A) + (E_0^B - E_q^B)]} -$$

$$- \sum_{i \text{ or } j \neq 0} \frac{\langle 0^A 0^B | V^{AB} | 0^A 0^B \rangle\, |\langle 0^A 0^B | V^{AB} | i^A j^B \rangle|^2}{[(E_0^A - E_i^A) + (E_0^B - E_j^B)]^2} \tag{III.7}$$

where i,j,p and q are the i-th, j-th ... excited states of molecules A and B.

Trimers

Now let us consider three interacting systems, A, B and C with the same orthonormalization and non-degeneracy conditions for their eigenfunctions as used for the

dimer. The Hamiltonian of this system is very similar to that for the dimer.

$$\hat{H}^{ABC} = \hat{H}^{A} + \hat{H}^{B} + \hat{H}^{C} + V^{ABC} \qquad \text{(III.8)}$$

The first three terms on the right side of equation III.8 serve as the zeroth-order Hamiltonian in this treatment. I shall employ the same approximation with respect to the electron exchange as I did for the dimer case. Thus, the zeroth-order wavefunction can be written as the product of the ground state wavefunctions of the separate systems. Further inspection indicates that the perturbation V^{ABC} in equation III.8 can be separated to three terms expressing the pairwise potentials of the molecules:

$$V^{ABC} = V^{AB} + V^{BC} + V^{AC} \qquad \text{(III.9)}$$

The potentials, V^{AB}, V^{BC} and V^{AC}, have exactly the same form, as V^{AB} in dimer AB (see equation III.3). In one of the special cases of trimer arrangements, in linear (or semi-linear in cases of complex internal molecular structure) geometry, we can very easily interpret this potential, V^{ABC}, as the sum of the two nearest-neighbor interactions (1,2-interaction), and a second-nearest-neighbor interaction (1,3-interaction).

Using the terms defined in this section, the energy expressions for the perturbation theory of trimeric interactions in zeroth- and first-order are the following:

$$E^{(0)}_{ABC} = \langle 0^A 0^B 0^C | \hat{H}^{ABC(0)} | 0^A 0^B 0^C \rangle = E_A + E_B + E_C \qquad \text{(III.10)}$$

$$E^{(1)}_{ABC} = \langle 0^A 0^B 0^C | V^{AB} + V^{BC} + V^{AC} | 0^A 0^B 0^C \rangle =$$

$$= \langle 0^A 0^B | V^{AB} | 0^A 0^B \rangle + \langle 0^B 0^C | V^{BC} | 0^B 0^C \rangle + \langle 0^A 0^C | V^{AC} | 0^A 0^C \rangle \qquad \text{(III.11)}$$

At this point of the discussion it seems to be worthwhile to compare these results

with the dimer energies. Equations III.10 and III.11 again indicate that the zeroth-order energy is simply the sum of the ground state energies of the components of the system. The first-order correction to the energy can be interpreted as the sum of the first-order energies of every pair of molecules (within every 'dimer' of the trimer). Thus, one can see that the long range forces are additive up to the first-order energy correction.

However, extending the examinations to the second-order corrections, I shall demonstrate that the additivity no longer holds.

$$E^{(2)}_{ABC} = \sum_{i\,or\,j\,or\,k \neq 0} \frac{|\langle i^A j^B k^C | V^{ABC} | 0^A 0^B 0^C \rangle|^2}{(E^A_0 - E^A_i) + (E^B_0 - E^B_j) + (E^C_0 - E^C_k)} -$$

$$- \sum_{i\,or\,j\,or\,k \neq 0} \frac{|\langle i^A j^B k^C | V^{AB} + V^{BC} + V^{AC} | 0^A 0^B 0^C \rangle|^2}{(E^A_0 - E^A_i) + (E^B_0 - E^B_j) + (E^C_0 - E^C_k)} \qquad \text{(III.12)}$$

After evaluating the square of the absolute value of a complex sum, the second-order energy correction becomes

$$E^{(2)}_{ABC} = \sum_{i\,or\,j \neq 0} \frac{|\langle i^A j^B | V^{AB} | 0^A 0^B \rangle|^2}{(E^A_0 - E^A_i) + (E^B_0 - E^B_j)} +$$

$$+ \sum_{j\,or\,k \neq 0} \frac{|\langle j^B k^C | V^{BC} | 0^B 0^C \rangle|^2}{(E^B_0 - E^B_i) + (E^C_0 - E^C_j)} + \sum_{i\,or\,k \neq 0} \frac{|\langle i^A k^C | V^{AC} | 0^A 0^C \rangle|^2}{(E^A_0 - E^A_i) + (E^C_0 - E^C_k)} + E^{(2)}_{\text{cross}}$$

(III.13)

The fourth term of the right side has three cross-product contributions.

$$E^{(2)}_{cross} = E^{(2)}_{AB,BC} + E^{(2)}_{AB,AC} + E^{(2)}_{AC,BC} \tag{III.14}$$

where, for example,

$$E^{(2)}_{AB,BC} = -\sum_{j\neq 0} \frac{\langle 0^A 0^B | V^{AB} | 0^A j^B \rangle \langle j^B 0^C | V^{BC} | 0^B 0^C \rangle + \langle 0^B 0^C | V^{BC} | j^B 0^C \rangle \langle 0^A j^B | V^{AB} | 0^A 0^B \rangle}{E_0^B - E_j^B}$$

$$= -\sum_{j\neq 0} \frac{2Re\langle 0^A j^B | V^{AB} | 0^A 0^B \rangle Re\langle j^B 0^C | V^{BC} | 0^B 0^C \rangle + 2Im\langle 0^A j^B | V^{AB} | 0^A 0^B \rangle Im\langle j^B 0^C | V^{BC} | 0^B 0^C \rangle}{E_0^B - E_j^B} \tag{III.15}$$

where Re(x) and Im(x) denote the real and the imaginary part of a complex number, x. All three contributions of the cross-energy are similar. One has to change only the appropriate indices and subscripts.

The first three terms of the second-order energy of the trimer are present in the second-order perturbational treatment of the appropriate dimers (AB, BC and AC), but the cross terms are not. These terms cannot appear in the higher-order corrections of dimers because they contain cross terms between two different dimer interactions. In fact, they are many-body interaction terms. This means that the long range intermolecular interactions are not additive in second-order perturbation theory.

Although I shall not express the third-order energy correction for trimers because of its lengthy derivation, its treatment is analogous to what I have shown for the second-order theory. The results can be expressed in the following equation.

$$E^{(3)}_{ABC} = E^{(3)}_{AB} + E^{(3)}_{BC} + E^{(3)}_{AC} + E^{(3)}_{cross} \tag{III.16}$$

where the three first terms on the right side represent the third-order correction of the

separate dimers. The last term embodies the third-order non-additivity that consists of more than 30 terms, with various integral cross-products and different summations due to orthonormality. While the second-oder cross terms contain only three-body interactions, the third-order cross terms consist of both three- and four-body contributions. None of the cross terms (even in higher order) contains two-body (or pairwise) interactions indicating their additivity. Algebraically it is easy to see that, for example, the second-order cross terms do not appear in any of the higher order cross terms, that is, the cross terms do not cancel each other. On the other hand, alternatively negative and positive corrections to the total energy at consecutive MP*n* levels would suggest the theoretical possibility that the non-additive cross terms can vanish numerically if considering higher and higher order perturbational corrections. However, the experimental and theoretical evidence for the existence of cooperative phenomenon support the assumption that the cross terms of the perturbational treatment indeed represent the non-additive part of the intermolecular interactions. Nevertheless, more thorough investigations are necessary in the future to prove the validity of this assumption and assess the relative importance of various cross terms to non-additivity.

3. Cooperativity and Incremental Interaction Energies

According to the results of the forementioned MO studies and the illustrative perturbational treatment above, the intermolecular interaction between three molecules can be expressed generally in the following simple equation:[13]

$$\Delta E_{ABC} = \Delta E_{AB} + \Delta E_{BC} + \Delta E_{AC} + \Delta E_{non\text{-}add.} \qquad \text{(III.17)}$$

ΔE_{ABC} is the total interaction energy of the trimer, ΔE_{AB}, ΔE_{BC} and ΔE_{AC} are the interactions of the appropriate dimers. The term, $\Delta E_{non\text{-}add.}$, refers to the non-additivity (or many-body interactions).

If we build, for example, a H-bonded homotrimer step by step, taking dimer A...B, adding the third molecule, C to this dimer forming a H-bond between B and C (III.18),

$$A...B + C = A...B...C \qquad \text{(III.18)}$$

then the interaction energy of the first step is ΔE_{AB}; and that of the second step (incremental interaction energy) is

$$\Delta E^{inc.} = \Delta E_{BC} + \Delta E_{AC} + \Delta E_{non\text{-}add.} \qquad \text{(III.19)}$$

The change in the strength of the second interaction compared to that of the first one is the sum of a 1,3-interaction and the non-additive term. This crucial point is expressed in the following equation:

$$\Delta E^{(coop.)} = \Delta E_{AC} + \Delta E_{non\text{-}add.} \qquad \text{(III.20)}$$

This expression is different from those seen in the first section as definitions for cooperativity. However, my investigations will primarily concentrate on H-bonding homopolymers and changes in their incremental interactions when building an aggregate step by step. Thus, the quantity embodied by equation III.20 appears to be more descriptive for my examinations than the single non-additive part. Therefore, the term cooperativity will be arbitrarily used according to III.20, as the change (strengthening or

weakening) in incremental intermolecular interactions.

After having recognized the general non-additivity in intermolecular interactions, the question arises how the two-body potential energy operators originated from classical mechanics lead to many-body terms or many-body interactions in quantum mechanics. A qualitative explanation is based upon the non-rigidity and internal structure of molecules (and atoms). The original electron-distribution of a molecule in an intermolecular associate is disturbed and changed by the potential of the other molecule even for fixed intramolecular geometries. This does not cause any problem in the case of two interacting molecules, giving the first interaction energy. However, as the third molecule appears on the scene, it changes the electron distribution of the dimer. The changing electron distribution results in changing the potential energy terms (repulsions and attractions), as the interacting electron distributions will be definitely different in the trimer from those of the separate dimers in the trimer arrangement. Therefore, the potential energy contributions in trimers become different from those in dimers. This difference (the effect of perturbation) will manifest itself through three-body terms, as the two-body potential energy contributions being the same in dimers and trimers are not able to express this. And, although, the additivity is still valid for charged particles without internal structure in fixed position, this is not the case for interacting molecules.

These considerations will naturally become more complex for non-rigid molecular geometries where in addition to pairwise and non-additive contributions one also has to consider certain relaxation effects. The most convenient way to deal with this problem is to include relaxations into the non-additive effects (as I shall demonstrate later).

4. Cooperativity and Crystal Formation

The mechanism of nucleation is an important consideration in crystal formation. Presumably the crystal must start as a dimer, become a trimer (or tetramer by coalescing two dimers), and continue to add individual units or small aggregates until it has acquired enough three dimensional supermolecular structure to be considered a crystal. For this process to occur, it seems necessary that positive cooperativity (strengthening) in the change of the Gibbs free energy play an important role in the interaction of adding individual units to the growing aggregate. One might expect that the entropic component of ΔG does not exhibit cooperative effect as ΔS would be essentially the same for the association of a monomer and a smaller aggregate as for the same monomer and a larger cluster (the same number of degrees of freedom is lost in both processes). Thus, the interaction energy between two individual molecules must be less enthalpically stabilizing than between an aggregate and an individual molecule. If this were not true, many small aggregates (dimers, trimers, etc.) would form, rather than fewer larger crystals. Also, the enthalpic component must be negative and larger in size than the entropic part to insure the start of the nucleation process (from thermodynamical viewpoint). The role of temperature is of central importance in this balance. Furthermore, one should expect the extent of the cooperativity to increase as the aggregate grows, eventually asymptotically reaching the interaction energy of a single unit with an established crystal. In principle, this kind of behavior should obtain for growth in all three crystal directions, however it is possible (even likely) that one or two directions of growth might dominate the other(s).

It can be seen from equations II.13, II.7, II.9-II.11 that the source of enthalpic cooperativity is the cooperative effect originating from the change in the electronic energy of the interacting molecules. This is so, because neither the $\Delta(pV)$ component of ΔH nor the translational, rotational or vibrational contributions to ΔE exhibit cooperativity.[14] Thus, MO examinations on the cooperative phenomenon that provide electronic energies containing the many-body effects are extremely important to explore the forces behind the nucleation and crystal formation processes.

5. References

1. a) London, F. *Z. Phys. Chem.(B)*, **1930**, *11*, 222. London, F. *Trans. Faraday Soc.*, **1937**, *33*, 8. b) Pauling, L.; Wilson, E. B. *Introduction to Quantum Mechanics*, McGrew-Hill: New York, 1935. c) Margenau, H. *Rev. Mod. Phys.*, **1936**, *11*, 1. d) Axilrod, B. M.; Teller E. *J. Chem. Phys.*, **1943**, *11*, 299.

2. Frank, H. S.; Wen, W.-Y. *Discuss. Faraday Soc.*, **1957**, *24*, 133.

3. Imai, K. *J. Biol. Chem.*, **1974**, *249*, 7606.

4. Scatchard, G. *Ann. N. Y. Acad. Sci.*, **1949**, *51*, 660.

5. Hill, A. V. *J. Physiol. (London)*, **1910**, *90*, iv-vii.

6. Dahlquist, F. W. *Methods in Enzymology*, **1978**, *48*, 270.

7. a) Maes, G.; Smets, J. *J. Phys. Chem.*, **1993**, *97*, 1818. Kleeberg, H.; Klein, D.; Luck, W. A. *J. Phys. Chem.*, **1987**, *91*, 3200. b) Steiner, T.; Saenger, W. *J. Am. Chem. Soc.*, **1992**, *114*, 7123. Steiner, T.; Mason, S. A.; Saenger, W. *J. Am. Chem. Soc.*, **1990**, *112*, 6184. c) Jeffrey, G. A.; Gress, M. E.; Takagi, S. *J. Am. Chem. Soc.*, **1977**, *99*, 609.

8. Mo, O.; Yanez, M.; Elguero, J. *J. Chem. Phys.*, **1992**, *97*, 6628. Lentz, B. R.; Scheraga, H. A. *J. Chem. Phys.*, **1973**, *58*, 5296. Hankins, D.; Moskowitz, J. W.; Stillinger, F. H. *J. Chem. Phys.*, **1970**, *53*, 4544.

9. Guo, H.; Karplus, H. *J. Phys. Chem.*, **1992**, *96*, 7273. Hodoscek, M.; Kocjan, D.; Hadzi, D. *J. Mol. Struct. (THEOCHEM)*, **1988**, *42*, 115. Koehler, J. E. H.; Saenger, W.;

Lesyng, B. *J. Comput. Chem.*, **1987**, *8*, 1090. Remko, M. *Z. Phys. Chem. (Munich)*, **1983**, *138*, 223; Del Bene, J. E. *J. Chem. Phys.*, **1980**, *72*, 3423. Karpfen, A.; Ladik, J.; Russegger, P.; Schuster, P.; Suhai, S. *Theor. Chim. Acta*, **1974**, *34*, 115.

10. a) Campbell, E. S.; Mezei, M. *J. Chem. Phys.*, **1977**, *67*, 2338. Campbell, E. S.; Mezei, M. *Mol. Phys.*, **1980**, *41*, 883. b) Belford, D.; Campbell, E. S. *J. Chem. Phys.*, **1983**, *80*, 3288.

11. Eisenshitz, R.; London, F. *Zeits. f. Physik*, **1930**, *60*, 491. London, F. *Zeits. f. Physik*, **1930**, *63*, 245.

12. Daudey, J., P.; Claverie, P.; Malrieu P. *Int. J. Quantum Chem.*, **1974**, *8*, 1. Murrell, J. N.; Shaw, G. *J. Chem. Phys.*, **1967**, *46*, 1768. b) Murrell, J. N.; Randić, M.; Williams, D. R. *Proc. Roy. Soc. (London)*, **1965**, *284*, 566.

13. Smit, P. H.; Derissen, J. L.; van Duijneveldt, F. B. *Molec. Phys.*, **1979**, *37*, 501.

14. This statement is not exactly true for the vibrational part, but it can be shown that in all the examined cases the incremental change in the vibrational energy contribution was significantly smaller than that of the electronic energy.

IV. C-H..O (HYDROGEN-BONDING) INTERACTIONS.[1]

1. Introduction: The Hydrogen-Bond and the C-H..O Interaction.

Beside the cooperative effects, the second factor of special importance in the crystal formation of my examined systems is the existence of the C-H..O interactions. As we shall see later (Chapters V-VII), C-H..O interactions, though much weaker than the primary O-H..O hydrogen-bonds, can stabilize one-dimensional chains, two-dimensional layers (for example with C-H..O interactions between the one-dimensional chains) and three-dimensional crystal-like aggregates. Ultimately, C-H..O interactions in combination with cooperative effects can discriminate between competing orientation patterns and dictate the final form of the crystal structure. This gives the special significance of their careful examinations.

Stabilizing interactions between C-H bonds and electronegative atoms (X=N, O, F, but particularly oxygen) are well-known features of many crystal structures. These interactions are usually called C-H hydrogen bonds. Despite the relatively early experimental proposal,[2] the concept of C-H hydrogen bonds only recently became accepted. The final evidence came from Taylor and Kennard who analyzed 113 neutron diffraction structures[3] and found that the C-H..X (X=O, N, Cl) interactions are abundant in crystal structures. Both their geometric orientations and their abundance lead these authors to conclude that "...(the C-H..X interactions) can reasonably be described as hydrogen bonds". Since then the analysis of the Cambridge Structural Database[4] proved

to be the most useful tool in providing additional evidence illustrated by recent papers.[5] Although, the practice of crystal structure determinations is well developed, we run into obvious experimental difficulties when examining C-H hydrogen-bonded complexes in gas phase. The C-H hydrogen bonds are certainly weaker than the more conventional O-H or N-H hydrogen bonds, therefore direct measurement of their associated binding energies in the gas phase would be very difficult. Nevertheless, their apparent influence upon the way molecules aggregate and crystallize dictates the need to better understand the nature of these interactions. The application of various theoretical methods proved to be extremely useful in this sense. The results of different theoretical examinations (for example, the non-bonding distances between the hydrogen atom and the electronegative acceptor, the directionality of the interactions and the binding energies) compared to available experimental data can provide valuable information about the character of the C-H interactions.

From analyses of the Cambridge Structural Database, Glusker has defined scatterplots that indicate the general directional tendencies of H-bonds to specific groups of compounds in the database.[6] In particular, she has found that H-bonds to carbonyl groups tend to have H...O=C angles clustered near 120°, while H-bonds to ethers form both in the COC plane, as well as above and below it.

Among the recent experimental reports, one indicates that HCN bonds to O_3 with a three-centered hydrogen-bond in an argon matrix.[7] Others report the IR and/or rotational spectra of the H_2CO/HCN;[8] $H_2O/HCCH$;[9,10,11] and H_2O/HCN[12,13] complexes. In the last few years several molecular orbital (MO) studies on different, small

C-H..O hydrogen-bonded complexes have also been reported.[14]

The purpose of this chapter is to summarize the results of both ab initio and semiempirical MO calculations on complexes of the C-H donors, HCCH and HCN; with the acceptors, H_2O, H_2CO, and O_3. I chose these complexes because a) HCN and HCCH should be reasonably good H-donors; b) $H_2C{=}O$ and H_2O are prototypes of the carbonyl and ether moieties that have different H-bonding patterns in crystals; and, c) the HCN/O_3 complex has been experimentally observed to have a 3-center H-bond in an inert matrix. This last complex is a rare experimental example of multicentered H-bonds, common in crystal structures,[15] in isolated dimers. I compare the results of the MO calculations with experimental structural and spectroscopic data, as well as, with data from previous MO studies.

2. Computational Methods

Molecular orbital calculations on all the C-H..O H-bonded complexes considered above were performed using the semiempirical AM1, PM3 and SAM1 techniques and ab initio Hartree-Fock and second-order Møller-Plesset (MP2) methods with 6-31G(d,p) and D95++(d,p) basis sets. These basis sets will be denoted by I and II, respectively, in the tables. All species were completely optimized in all internal coordinates, at *each level of calculation*. The vibrational frequencies were individually calculated at *each level of calculation* to verify the optimizations, as well as, provide zero point vibrational energy corrections (ZPVE), enthalpies at 298 K, and comparisons with experimentally observed

Table I. Total Energies (hartrees)

complex		HF/6-31G(d,p)	HF/D95++(d,p)	MP2/6-31G(d,p)	MP2/D95++(d,p)
HCN		-92.8771381	-92.8931254	-93.1743655	-93.2100120
H_2C_2		-76.8218374	-76.8340689	-77.0914579	-77.1199087
H_2O		-76.0236150	-76.0498335	-76.2224486	-76.2640590
H_2CO		-113.8697432	-113.8979009	-114.1910157	-114.2408314
O_3		-224.2614365	-224.3284397	-224.8767539	-224.9795896
HCN/H_2O[a]	p	-168.9106799	-168.9518861	-169.4078044	-169.4839841
	np			-169.4080032	
H_2C_2/H_2O[a]	p	-152.8505746	-152.8887151	-153.3204205	-153.3902319
	np	-152.8507154		-153.3211121	-153.3902643
HCN/H_2CO		-206.7550180	-206.7985421	-207.3745732	-207.4587586
H_2C_2/H_2CO		-190.6960518	-190.7358171	-191.2890371	-191.3664352
HCN/O_3[b]	s	-317.1422004	-317.2238171	-318.0573838	-318.1930819
	ns		-317.2239688		-318.1931654
H_2C_2/O_3[b]	s	-301.0854548	-301.1638140	-301.9729684	-302.1022976
	ns		-301.1638158		-302.1023579

[a]p: planar structure; np: non-planar structure (see text). [b]s: symmetrical complex; ns: non-symmetrical complex (see text).

vibrations. The CP correction for the basis set superposition error (BSSE) for each monomer was calculated as the difference between the energy of the monomer in the complexed geometry with the basis set of the whole complex and that of the same monomer without ghost orbitals.

3. Results and Discussion

The total energies (hartrees) for all the ab initio calculations are presented in Table

I, while all the interaction energies (kcal/mol) calculated by the semiempirical methods are collected in Table II. As the ab initio interaction energies must be corrected for BSSE, ZPVE, and enthalpy at 298 K before they can be properly compared with the semiempirical results, the data for the interactions with H_2O, H_2CO and O_3 are reported in separate tables. The structure and energetics of each set of interaction will be discussed first, followed by an analysis of the vibrational data.

3a. Interactions with Water

HCN

The interaction with HCN, is considerably stronger than that of HCCH, as expected from its greater acidity. Tables II and III contain the interaction energies and enthalpies of these complexes. The MP2 calculations give a fully corrected interaction enthalpy of -3.89 and -3.79 (-4.76 at the planar geometry, see below) kcal/mol with the 6-31G(d,p) and D95++(d,p) basis sets, respectively. The corresponding HF results are -4.46 and -4.03 kcal/mol. The AM1 result, -3.12 kcal/mol, agrees well with the MP2 results, as does PM3 (-4.31) while the SAM1 result (-4.78) is somewhat than the others. The calculated geometries (Figure 1 and Table IV) indicate that AM1 agrees best

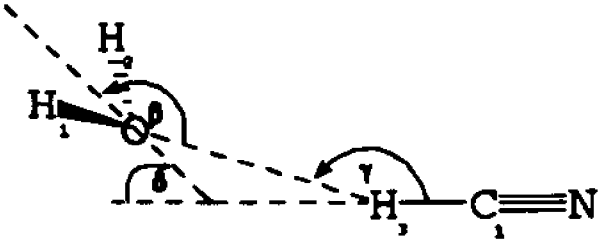

Figure 1. HCN/H_2O complex. Angles β and γ characterize the orientation of the molecule.

Table II. Semiempirical Interaction Enthalpies at 25 °C (kcal/mol)

complex		PM3[a]	AM1	SAM1[c]
HCN/H_2O[a]	p	-4.23	-3.12	-4.78
	np	-4.31		
H_2C_2/H_2O[a]	p	-0.92	-1.75	-3.10
	np	-0.95	-1.77	
HCN/H_2CO		-3.16	-2.68	-3.62
H_2C_2/H_2CO		-0.73	-1.38	-1.92
HCN/O_3[b]	s	-1.01	-1.13	
	ns	-1.04		-3.24
H_2C_2/O_3[b]	s	-0.28	-0.62	
	ns	-0.32 (+0.70)		-1.32

[a]p: planar structure; np: non-planar structure. [b]s: symmetrical complex; ns: non-symmetrical complex. [c]For SAM1, the H-bonds are not three-centered, while the PM3 result in parentheses corresponds to a 'repulsive' minimum.

with the MP2 geometries for the internal geometrical parameters of the individual molecules. It also agrees reasonably well with the MP2 calculations for the intermolecular coordinates. The O..H distances seem too short for both SAM1 (1.768 Å) and PM3 (1.797 Å).

All methods considered except MP2/6-31G(d,p) and PM3 predict the HCN to be coplanar with the H_2O. Upon recalculation with the constraint that it be planar, the MP2/6-31G(d,p) energy increases by only 0.12 kcal/mol. Moreover, upon correction for either ZPVE or CP, it becomes lower in energy than the uncorrected minimum. When fully corrected (enthalpy + CP) the planar structure is lower than the optimized structure by 0.87 kcal/mol.

Table III. Interaction Energies and Enthalpies (kcal/mol) of the HCN/H_2O and H_2C_2/H_2O Complexes at 298 K.

		HF/6-31G(d,p)		HF/D95++(d,p)		MP2/6-31G(d,p)		MP2/D95++(d,p)	
		corr.	energy	corr.	energy	corr.	energy	corr.	energy
					HCN/H_2O complex				
Energy[a]	p		-6.23		-5.60		-6.90		-6.22
	np						-7.02		
ZPVE	p	1.19	-5.04	1.24	-4.36	1.30	-5.60	1.15	-5.07
	np					1.64	-5.38		
CP	p	0.61	-5.62	0.43	-5.17	1.42	-5.48	1.27	-4.95
	np					1.76	-5.26		
CP+ZPVE	p	1.80	-4.43	1.67	-3.93	2.72	-4.18	2.42	-3.80
	np					2.40	-3.62		
Enthalpy	p	1.16	-5.07	1.14	-4.46	0.72	-6.18	1.16	-5.06
	np					1.37	-5.65		
Enthalpy + CP	p	1.77	-4.46	1.57	-4.03	2.14	-4.76	2.43	-3.79
	np					3.13	-3.89		
					H_2C_2/H_2O complex				
Energy	p		-3.21		-3.02		-4.09		-3.93
	np		-3.30				-4.52		-3.95
ZPVE	p	0.82	-2.39	0.97	-2.05	0.96	-3.13	0.95	-2.98
	np	1.11	-2.19			1.45	-3.07	1.17	-2.78
CP	p	0.51	-2.70	0.39	-2.63	1.21	-2.88	1.20	-2.73
	np	0.77	-2.54			2.10	-2.43	1.27	-2.68
CP+ZPVE	p	1.33	-1.88	1.36	-1.66	2.17	-1.92	2.15	-1.78
	np	1.88	-1.43			3.55	-0.98	2.44	-1.51
Enthalpy	p	0.47	-2.74	1.10	-1.92	0.55	-3.54	0.54	-3.39
	np	1.13	-2.17			1.28	-3.24	1.16	-2.79
Enthalpy + CP	p	0.98	-2.23	1.49	-1.53	1.76	-2.33	1.74	-2.19
	np	1.90	-1.41			3.38	-1.15	2.43	-1.52

[a] p: planar structure; np: non-planar structure.

Table IV. Optimized Geometries of HCN/H_2O Complex[a]

Geom. parameters[b]		PM3	AM1	SAM1	Hartree-Fock		MP2		exp.[15]
					I	II	I	II	
intramolecular geometry (H_2O)									
$O\text{-}H_1$	p	0.951	0.961	0.965	0.943	0.945	0.961	0.965	
	np	0.952					0.962		
$O\text{-}H_2$	p	0.951	0.961	0.965	0.943	0.945	0.961	0.965	
	np	0.952					0.962		
$H_1\text{-}O\text{-}H_2$	p	108.6	103.9	102.3	106.7	107.1	105.1	105.3	
	np	108.3					104.6		
intramolecular geometry (HCN)									
$H_3\text{-}C_1$	p	1.088	1.075	1.064	1.067	1.068	1.073	1.076	
	np	1.090					1.074		
$C_1\text{-}N$	p	1.156	1.161	1.141	1.134	1.136	1.177	1.182	1.155
	np	1.156					1.177		
intermolecular geometry									
$O..H_3$	p	1.799	2.161	1.768	2.076	2.113	2.009	2.051	
	np	1.797					2.020		
$O..C_1$	p	2.886	3.235	2.833	3.143	3.181	3.082	3.126	3.152
	np	2.886					3.092		
$H_1\text{-}O..H_3$	p	127.4	129.5	128.7	126.6	126.5	127.5	127.3	
	np	119.7					116.9		
β	p	178.3	179.1	179.9	180.0	179.4	180.0	180.0	
	np	147.6					137.6		
$O..H_3\text{-}C_1$ (γ)	p	179.9	178.5	179.8	180.0	179.6	180.0	180.0	
	np	177.8					177.0		

[a]Distances in Å, bond angles in degrees. Basis Sets: (I) 6-31G(d,p), (II) D95++(d,p). [b]p: planar structure; np: non-planar structure.

Gutowsky, et al recently reported rotational spectra of this complex.[13] The same report contains molecular mechanics for clusters (MMC)[16] calculations that predict the complex to be nonplanar. The complex was proposed to have a significantly bent geometry at the potential minimum with a zero point vibration above the planar transition state. However, a planar minimum is also consistent with this experimental report.[17]

HCCH

The results for HCCH/H_2O complex (Tables II, III, and V) parallel those for HCN/H_2O in many respects, although the binding energies are much smaller. The AM1 binding enthalpy is closest to all the (completely corrected) ab initio values. SAM1 predicts a stronger, while PM3 finds only a very weak interaction. The O...H distance (Table V) for AM1 agrees well with the ab initio and experimental values, while that of SAM1 is significantly shorter and PM3, longer. All of the methods I used initially predict a non-planar structure except SAM1 and HF/D95++(d,p). The orientations of the molecules are similar for AM1 and all other ab initio methods. The angle between the symmetry axis of H_2O and the H..O, characterizing the non-planarity (180 - β) is in the range of 0°-70.3°, suggesting that the surface might be very flat with respect to variation of this angle. This conclusion is supported by calculations on the planar transition states connecting the two equivalent minima. While all methods except HF/D95++(d,p) predict a nonplanar structure to be favored, this no longer holds after either ZPVE or CP correction (see Table III). At the highest level used, MP2/D95++(d,p), where the CP correction is small, the planar and completely optimized structures differ by only 0.02

Table V. Optimized Geometries of the H_2C_2/H_2O Complex[a]

Geom. parameters[b]		PM3	AM1	SAM1	Hartree-Fock		MP2		exp.[10]
					I	II	I	II	
intramolecular geometry (H_2O)									
O-H_1	p	0.951	0.961	0.965	0.943	0.945	0.961	0.964	
	np	0.951	0.961		0.943		0.962	0.965	
O-H_2	p	0.951	0.961	0.965	0.943	0.945	0.961	0.964	
	np	0.951	0.961		0.943		0.962	0.965	
H_1-O-H_2	p	107.9	103.8	102.2	106.6	107.0	104.8	105.2	
	np	107.8	103.8		106.3		104.2	105.0	
intramolecular geometry (H_2C_2)									
H_3-C_1	p	1.067	1.066	1.053	1.062	1.065	1.067	1.074	
	np	1.068	1.066		1.062		1.068	1.074	
C_1-C_2	p	1.190	1.196	1.231	1.187	1.192	1.218	1.227	
	np	1.190	1.196		1.187		1.218	1.227	
H_4-C_2	p	1.064	1.060	1.040	1.057	1.060	1.061	1.068	
	np	1.064	1.060		1.057		1.062	1.068	
intermolecular geometry									
O..H_3	p	2.527	2.223	1.802	2.250	2.297	2.153	2.191	2.229
	np	2.488	2.212		2.263		2.197	2.188	
O..C_1	p	3.592	3.288	2.854	3.311	3.361	3.220	3.264	
	np	3.542	3.266		3.315		3.256	3.262	
H_1-O..H_3	p	123.0	127.2	126.9	126.7	126.5	127.6	127.4	
	np	112.1	118.8		113.2		101.9	123.1	
β	p	176.9	179.1	178.0	180.0	180.0	180.0	180.0	
	np	132.8	142.3		132.4		109.7	154.2	
O..H_3-C_1	p	175.5	179.7	176.8	180.0	180.0	180.0	180.0	
(γ)	np	169.2	169.7		170.9		170.7	178.8	

[a]Distances in Å, bond angles in degrees. [b]p: planar structure; np: non-planar structure.

kcal/mol before any correction.

The literature on the HCCH/H_2O complex is somewhat confusing. Based upon gas phase radiofrequency and microwave spectra, Peterson and Klemperer[10] have reported the complex to be planar, with an H...O distance of 2.229 Å. Comparison of the dipole moments of the protiated and deuterated complexes led him to suggest that the surface be close to a harmonic oscillator (i.e., single minimum), although they did not rigorously exclude the possibility of a double well with a zero point vibration above the barrier. Engdahl and Nelander seem to suggest that there be an equilibrating double well based upon an infrared study of the complex in an argon matrix.[11] They claim to be in reasonable agreement with an early semiempirical (CNDO) study.[18] Early ab initio calculations were reported by Vishveshwara[14a] and Frisch, Pople and Del Bene.[14b] These were only optimized at the HF level. A molecular mechanics for clusters (MMC) treatment by Dykstra[19] predicts the complex to significantly deviate from planarity.

Miller et al. have reported MP2/6-31G(d,p) and MP2/D95(d,p) calculations on this complex.[9] Their reported total energy (-153.321112 hartrees) agrees exactly with my value (Table I) for the common calculation [MP2/6-31G(d,p)], however the reported geometry differs.[20] They characterize the complex as 'quasiplanar', with an angle between the plane of the HOH and the axis of the HCCH (δ in figure 1) of 35.1° (for MP2/6-31G(d,p)) in disagreement with the value of 79.6° reported here.

None of the previous ab initio studies considered the effect of BSSE on the position of the minimum. Rather, they explained the experimental reports with the suggestion that the low barrier to planarization would fall below the zero point vibrational

level. My calculations suggest that, after correction for BSSE, the true minimum should correspond to the planar geometry. This result agrees better with Klemperer's suggestion that the ratio of the dipole moments of the deuterated and protiated complexes are consistent with a harmonic oscillator[10] and Glusker's analysis of the crystallographic data.[6] However, both explanations remain possible.

3b. Interactions with Formaldehyde

HCN

Tables II and VI collect the interaction energies for the HCN/H_2CO and $HCCH/H_2CO$ complexes. The MP2/6-31G(d,p) and MP2/D95++(d,p) interaction enthalpies are very similar to the AM1 and PM3 values, while SAM1 predicts a stronger complex. The HF interactions are about 1 kcal/mol stronger than the MP2 values. All methods predict virtually planar complexes[21] (Figure 2 and Table VII). The C=O..H angle (β in Figure 2) varies from 117 to 158 degrees for the ab initio and from 130 to 177 degrees for the semiempirical calculations. Again the AM1 O...H distance (2.239 Å) agrees best with the ab initio values (2.087-2.165 Å). SAM1 and PM3 predict distances that are considerably shorter (1.835 Å and 1.810 Å).

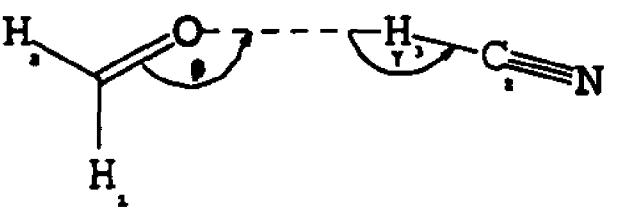

Figure 2. HCN/H_2CO complex with the intermolecular β and γ angles.

Table VI. H-Bonding Interaction Energies and Enthalpies (kcal/mol) at 298 K of Formaldehyde Complexes with HCN and Acetylene

	HF/6-31G(d,p)		HF/D95++(d,p)		MP2/6-31G(d,p)		MP2/D95++(d,p)	
	corr.	energy	corr.	energy	corr.	energy	corr.	energy
				HCN/H_2CO complex				
Energy		-5.10		-4.72		-5.77		-4.97
ZPVE	1.01	-4.09	0.79	-3.93	1.38	-4.39	1.02	-3.95
CP	0.67	-4.44	0.23	-4.48	1.90	-3.87	1.07	-3.90
CP+ZPVE	1.68	-3.43	1.02	-3.69	3.28	-2.49	2.09	-2.88
Enthalpy	1.16	-3.94	1.08	-3.64	1.38	-4.39	1.16	-3.81
Enthalpy + CP	1.83	-3.27	1.31	-3.41	3.28	-2.49	2.23	-2.74
				H_2C_2/H_2CO complex				
Energy		-2.81		-2.41		-4.12		-3.57
ZPVE	0.92	-1.88	0.72	-1.69	1.28	-2.84	1.00	-2.57
CP	0.87	-1.93	0.27	-2.14	2.02	-2.10	1.31	-2.26
CP+ZPVE	1.80	-1.10	0.99	-1.42	3.30	-0.82	2.31	-1.26
Enthalpy	1.11	-1.70	1.04	-1.37	1.26	-2.86	1.11	-2.46
Enthalpy + CP	1.98	-0.82	1.31	-1.10	2.28	-0.84	2.42	-1.15

HCCH

The data for the HCCH/H_2CO complex are collected in Tables II, VI and VII. The MP2/D95++(d,p) and AM1 (-1.15 and -1.38 kcal/mol) interaction enthalpies are in good agreement. The SAM1 value is greater and the PM3 smaller. The O...H distances are again computed to be similar by both ab initio and AM1. Both SAM1 and PM3 predict shorter distances. The ab initio structures are more bent (β = 99.0-134.2°, see Figure 2) than those obtained with the semiempirical methods (β = 125.9-148.7°). All ab initio methods find the complex to be planar, PM3 and SAM1 predict a slightly nonplanar,

Table VII. Optimized Intermolecular Geometries for the HCN/H_2CO and H_2C_2/H_2CO Complexes[a]

Geom. parameters	PM3	AM1	SAM1	Hartree-Fock		MP2		exp.[a]
				I	II	I	II	
intermolecular geometry (HCN/H_2CO)								
$O..H_3$	1.810	2.239	1.835	2.152	2.165	2.087	2.106	
$O..C_2$	2.901	3.311	2.899	3.214	3.230	3.153	3.176	3.271
C_1-$O..H_3$ (β)	130.1	177.0	142.0	136.2	157.8	117.3	127.8	138.1
$O..H_3$-C_2 (γ)	176.6	175.9	177.0	174.7	178.5	173.0	173.7	
H_1-C_1=$O..H_3$	-0.4	-107.1	-1.9	0.0	0.0	0.0	0.0	
C_1=$O..H_3$-C_2	-4.9	11.8	-12.7	0.0	0.6	0.0	0.0	
intermolecular geometry (H_2C_2/H_2CO)								
$O..H_3$	1.844	2.299	1.884	2.352	2.361	2.221	2.251	
$O..C_2$	2.925	3.363	2.936	3.327	3.418	3.216	3.229	
C_1-$O..H_3$ (β)	125.9	148.7	140.7	106.5	134.2	99.0	101.2	
$O..H_3$-C_2 (γ)	176.3	170.0	176.1	152.3	172.5	154.5	150.7	
H_1-C_1=$O..H_3$	-2.9	-21.7	0.3	0.0	0.0	0.0	0.0	
C_1=$O..H_3$-C_2	-11.6	-20.1	0.9	0.0	-0.1	0.0	0.0	

[a]Distances in Å, bond angles in degrees.

while AM1 predicts a distinctly nonplanar complex.

3c. Interactions with Ozone

HCN

Tables II, VIII and IX contain the data for the HCN/O_3 complex. Both MP2 and HF/6-31G(d,p), as well as, AM1 predict a symmetric 3-center hydrogen bond between

HCN and O_3, in apparent agreement with experiment.[7] MP2 and HF/D95++(d,p) predict HCN to form an unsymmetrical 3-center H-bond, with one O...H interaction 0.5-0.7 Å shorter than the other. All ab initio and AM1 calculation predict the HCN to be coplanar with O_3. PM3 predicts O...H distances similar to HF and MP2/D95++(d,p), but the HCN is no longer coplanar with the O_3. SAM1 predicts the HCN to interact with only one oxygen atom, with the HCN significantly out of the plane of the O_3. Constraining the two O..H distances to be equal causes the energy to be increased by only 0.08 and 0.04 kcal/mol for HF and MP2/D95++(d,p), respectively. After correcting for ZPVE and BSSE the symmetrical structures become more stable. The CP correction has a small effect, particularly on the HF calculation. However, the ZPVE correction clearly favors the symmetric structure. Whether the surface contains a symmetric single well or two shallow wells, the HCN/O_3 complex probably has a symmetric 3-center H-bond, as the barrier between the wells predicted by MP2/D95++(d,p) is below the zero point vibration.

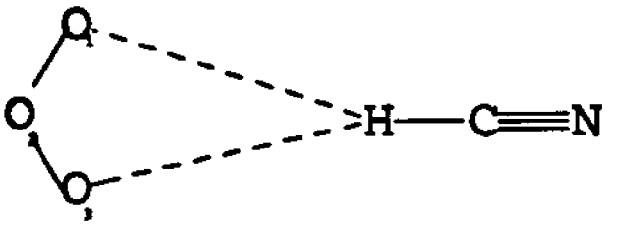

Figure 3. HCN/O_3 symmetric (C_{2v}), three-centered structure.

The AM1 and PM3 binding enthalpies, -1.13 and -1.04 kcal/mol, are close to the symmetric fully corrected D95++(d,p) values (-0.95 and -1.15 kcal/mol, for HF and MP2, respectively) while the -3.24 kcal/mol binding enthalpy of SAM1 is much greater.

Table VIII. Interaction Energies and Enthalpies (kcal/mol) at 298 K for Ozone Complexes with HCN and Acetylene

		HF/6-31G(d,p)		HF/D95++(d,p)		MP2/6-31G(d,p)		MP2/D95++(d,p)	
		corr.	energy	corr.	energy	corr.	energy	corr.	energy
					HCN/O_3 complex				
Energy[a]	s		-2.27		-1.43		-3.93		-2.18
	ns				-1.51				-2.24
ZPVE	s	0.60	-1.68	0.38	-1.05	0.90	-3.03	0.38	-1.80
	ns			0.50	-1.01			0.53	-1.71
CP	s	0.88	-1.40	0.14	-1.30	2.29	-1.64	0.70	-1.48
	ns			0.14	-1.37			0.76	-1.48
CP+ZPVE	s	1.48	-0.80	0.52	-0.91	3.19	-0.74	1.08	-1.10
	ns			0.64	-0.87			1.29	-0.95
Enthalpy	s	1.02	-1.26	0.34	-1.08	1.18	-3.03	0.33	-1.85
	ns			0.95	-0.56			0.95	-1.29
Enthalpy + CP	s	1.90	-0.37	0.48	-0.95	3.47	-0.46	1.03	-1.15
	ns			1.09	-0.42			1.71	-0.53
					H_2C_2/O_3 complex				
Energy	s		-1.37		-0.80		-2.98		-1.76
	ns				-0.82				-1.79
ZPVE	s	0.55	-0.82	0.37	-0.43	0.85	-2.13	0.39	-1.37
	ns			0.43	-0.39			0.54	-1.25
CP	s	0.82	-0.54	0.25	-0.54	2.17	-0.81	0.90	-0.85
	ns			0.24	-0.58			0.96	-0.84
CP+ZPVE	s	1.37	+0.00	0.62	-0.18	3.02	+0.04	1.29	-0.46
	ns			0.67	-0.15			1.50	-0.30
Enthalpy	s	1.02	-0.35	0.35	-0.45	1.18	-1.80	0.36	-1.40
	ns			0.95	+0.13			0.98	-0.81
Enthalpy + CP	s	1.84	+0.47	0.60	-0.20	3.35	+0.37	1.26	-0.49
	ns			1.19	+0.37			1.94	+0.14

[a]s: symmetrical H-bond; ns: non-symmetrical H-bond.

Table IX. Optimized Intermolecular Geometries of the HCN/O_3 Complexes[a]

Geom. parameters[b]		PM3	AM1	SAM1[c]	Hartree-Fock		MP2	
					I	II	I	II
$O_1..H_1$	s	2.814	2.450		2.704	2.834	2.524	2.680
	ns	2.615		1.875		2.539		2.443
$O_2..H_1$	s	3.305	2.812		3.111	3.252	2.957	3.132
	ns	3.468		2.894		3.313		3.164
$O_3..H_1$	s	2.839	2.451		2.704	2.835	2.524	2.680
	ns	3.380		3.432		3.265		2.989
$O_1..C_1$	s	3.808	3.456		3.706	3.842	3.513	3.682
	ns	3.678		2.924		3.596		3.510
$H_1..O_2-O_1$	s	56.2	60.1		59.4	59.4	58.1	58.0
	ns	38.1		26.9		41.7		45.8
$H_1..O_2-O_3$	s	57.4	60.2		59.4	59.4	58.1	58.0
	ns	75.7		105.2		77.2		70.3
$C_1-H_1..O_2$	s	170.7	179.9		180.0	180.0	180.0	180.0
	ns	169.9		163.8		168.6		163.5
$H_1..O_1-O_2-O_3$	s	-0.9	-0.1		0.0	0.0	0.0	0.0
	ns	-2.2		-61.5		0.0		0.0
$C_1-H_1..O_1-O_2$	s	-160.1	-179.9		180.0	180.0	179.9	180.0
	ns	-148.5		-113.8		180.0		180.0

[a]Distances in Å, bond angles in degrees.[b]s: symmetrical H-bond; ns: non-symmetrical H-bond. [c]Two-centered H-bonds in SAM1 non-symmetrical structures.

HCCH

The geometries of the $HCCH/O_3$ complex (Tables II, VIII and X) are somewhat similar to those of HCN/O_3 complex; however the energetics are quite different. Both MP2 methods initially predict bonding interactions of -2.98 [6-31G(d,p)] and -1.79 kcal/mol [D95++(d,p)]. Both ZPVE and CP corrections lower the stabilities of the complex. If all corrections (including enthalpy at 298 K) are applied, the complex is

Table X. Optimized Intermolecular Geometries of the H_2C_2/O_3 Complexes[a]

Geom. parameters[b]		PM3[c]	AM1	SAM1[d]	Hartree-Fock		MP2	
					I	II	I	II
$O_1..H_1$	s	3.018	2.472		2.888	3.064	2.628	2.798
	ns	2.771		1.905		2.792		2.520
		(1.885)						
$O_2..H_1$	s	3.513	2.832		3.307	3.459	3.071	3.259
	ns	3.673		2.917		3.531		3.356
		(2.918)						
$O_3..H_1$	s	3.033	2.472		2.888	3.064	2.628	2.798
	ns	3.632		3.619		3.421		3.279
		(3.142)						
$O_1..C_1$	s	4.019	3.471		3.893	4.077	3.620	3.804
	ns	3.834		2.951		3.837		3.544
		(2.952)						
$H_1..O_2$-O_1	s	56.6	60.3		59.5	59.5	58.2	58.1
	ns	38.6		27.5		44.1		40.8
		(25.0)						
$H_1..O_2$-O_3	s	57.3	60.3		59.5	59.5	58.2	58.1
	ns	78.5		115.2		74.9		75.4
		(89.0)						
C_1-$H_1..O_2$	s	171.9	179.0		180.0	179.9	180.0	180.0
	ns	166.9		161.1		174.4		179.9
		(170.1)						
$H_1..O_1$-O_2-O_3	s	-3.1	0.7		0.0	0.0	0.0	0.0
	ns	-3.4		-86.7		0.0		0.0
		(0.6)						
C_1-$H_1..O_1$-O_2	s	-160.3	177.5		180.0	180.0	180.0	180.0
	ns	-120.7		-85.6		180.0		180.0
		(177.2)						

[a]Distances in Å, bond angles in degrees. [b]s: symmetrical H-bond; ns: non-symmetrical H-bond. [c]The PM3 results in parentheses correspond to a 'repulsive' minimum. [d]Two-centered H-bonds in SAM1 non-symmetrical structures.

predicted to be repulsive by 0.37 and 0.14 kcal/mol, respectively. The HF results are analogous. Undoubtedly, the completely 'corrected' binding enthalpies must be in error. If the complex be repulsive, there would be no increase in ZPVE over that of the separated species. Thus, the application of both vibrational and CP corrections simultaneously must underestimate the bonding enthalpy.

As for HCN/O_3, the AM1 and 6-31G(d,p) (both MP2 and HF) predict a symmetrical 3-center interaction, while the D95++(d,p) calculations predict an unsymmetrical 3-center interaction before corrections, with the symmetrical 3-center H-bond becoming more stable upon correction for ZPVE and CP. The fully corrected D95++(d,p) calculations for the symmetrical structure predict stabilizing interactions of -0.20 and -0.49 kcal/mol (HF and MP2, respectively) while AM1 and SAM1 predict -0.62 and -1.32 kcal/mol. The 6-31G(d,p) calculations predict the interaction to be repulsive after corrections are applied. These values are overcorrected for the reasons stated previously.

Unlike the other methods PM3 predicts two different minima, a curious result that suggests that serious problems might exist in the methodology. For one minimum, the complex is 0.70 kcal/mol higher than the separated species. In this complex the HCCH is more closely bound to the O_3 than in the other calculations (Tables II and X, in parentheses). Force calculations demonstrate that the structure is a minimum upon the potential surface. For the second minimum (binding by 0.32 kcal/mol), the HCCH bent significantly out of the plane of the O_3, although the C-H..O distance is similar to the other calculations.

SAM1 also behaves differently from the other methods in predicting the HCCH to interact with only one oxygen and be roughly perpendicular to the plane of the O_3.

3d. Vibrational Calculations

Tables XI-XVII contain the unscaled calculated (harmonic) and experimental (where available) vibrational frequencies for the monomeric components (Table XI),[22,23,24,25,26,27,28,29,30,31,32,33,34,35,36,37] and each of the complexes studied. Table XVIII reports several statistical analyses of these results. One can easily note that the MP2 vibrations are generally lower than those for HF, indicating that scaling is unnecessary for MP2 vibrations. In fact, the vibrations calculated by MP2/6-31G(d,p) or MP2/D95++(d,p) are slightly lower than the experimentally derived harmonics. The frequencies for O_3 are particularly difficult to calculate,[38] but only the symmetrical stretch is grossly in error.

In Table XVIII the calculated vibrational frequencies are compared with the experimentally observed fundamentals and with the corresponding harmonic frequencies of the uncomplexed molecules. Statistical analyses are shown for both the ratios of the frequencies and the absolute errors. Where more than one set of experimental frequencies exist, I used the latest results for the statistical analyses. The data for O_3 were eliminated from the overall statistics due to the problems involved in modeling this compound. The superiority of the MP2 vibrations (over the HF) is clear from both the average errors and standard deviations. The MP2/D95++(d,p) are marginally better than the MP2/6-31G(d,p)

Table XI. Calculated and Experimental Frequencies (in cm^{-1}) for the Uncomplexed Molecules

	PM3	AM1	SAM1	Hartree-Fock		MP2		experiment[a]
				I	II	I	II	
HCN								
ν_2	859.4	946.7	1018.4	880.8	866.1	738.7	709.8	726.6[22], 727.0[23] (713.5)[24]
ν_2'	859.4	946.8	1018.4	880.8	866.1	738.7	709.8	726.6, 727.0 (713.5)
ν_1	2286.0	2379.7	2412.9	2435.4	2407.6	2045.0	2003.3	2131.8, 2129.1 (2096.7)
ν_3	3297.4	3385.7	3200.4	3652.9	3640.1	3533.3	3506.6	3438.3, 3442.3 (3311.5)
H_2C_2								
ν_4	854.7	803.8	544.6	800.1	775.2	459.0	526.9	624.8[25], 624.0[26] (612.9)[27]
ν_4'	854.9	804.1	544.6	800.1	775.2	459.0	526.9	624.8, 624.0 (612.9)
ν_5	897.6	928.8	999.0	877.9	860.9	755.6	731.8	763.8, 746.7 (730.3)
ν_5'	897.6	928.8	999.0	877.9	860.9	755.6	731.8	763.8, 746.7 (730.3)
ν_2	2138.9	2181.4	2378.9	2243.5	2207.5	2002.9	1957.1	1992.1, 2007.6 (1973.9)
ν_3	3318.3	3423.5	3177.1	3584.4	3573.8	3501.7	3460.6	3418.7, 3415.2 (3281.9)
ν_1	3394.4	3476.0	3292.4	3696.1	3683.9	3591.8	3555.1	3496.1, 3495.1 (3372.8)
H_2O								
ν_2	1742.6	1885.6	1815.5	1769.5	1729.4	1683.9	1624.8	1653.9[28],1648.5[29], 1648.9[30] (1594.6[29])
ν_1	3869.5	3505.8	3452.1	4148.0	4156.1	3894.8	3881.0	3825.3, 3832.2, 3832.0 (3656.7)
ν_3	3990.0	3584.8	3502.8	4265.0	4275.8	4033.3	4025.7	3935.6, 3942.5, 3942.5 (3755.8)

Table XI. Cont.

	PM3	AM1	SAM1	Hartree-Fock		MP2		experiment[a]
				I	II	I	II	
H_2CO								
ν_4	1068.7	1164.8	1132.9	1335.6	1335.1	1220.3	1206.8	1191.0[31], 1186.5[32], 1191.0[33], 1188[34] (1163.5[33], 1167.3[35], 1170.2[35])
ν_6	1095.2	1176.1	1143.3	1376.7	1362.6	1298.4	1272.3	1287.7, 1281.9, 1298.9, 1269 (1247.4, 1249.1, 1250.6)
ν_5	1288.3	1443.6	1359.8	1668.3	1654.4	1589.2	1564.9	1562.6, 1516.7, 1529.0, 1544 (1500.6, 1500.2, 1500.3)
ν_2	1987.3	2053.0	2057.8	2025.3	2006.3	1796.0	1763.8	1763.7, 1761.5, 1778.3, 1778 (1746.0, 1746.0, 1755.9)
ν_1	2999.0	3085.1	2795.3	3120.5	3143.5	3027.1	3035.2	2944.3, 2944.0, 2977.9, 2937 (2766.4, 2782.5, 2811.4)
ν_3	3021.2	3121.3	2812.0	3195.4	3219.2	3105.1	3117.1	3008.7, 3032.7, 2997.0, 3012 (2843.3, 2843.3, 2861.3)
O_3								
ν_2	742.9	923.0	806.3	849.3	844.7	728.1	730.2	716.0[37] (700.9[37])
ν_3	1593.2	1695.5	2116.5	1454.3	1437.9	1173.7	1181.0	1089.2 (1042.1)
ν_1	1600.5	1699.7	2370.2	1537.6	1543.7	2373.2	2435.6	1134.9 (1103.1)

[a]Experimental harmonic vibrations (fundamental frequencies in parentheses).

frequencies. Interestingly, all three semiempirical methods give better average frequencies than the HF calculations, but their standard deviations are much greater. Among the semiempirical methods, SAM1 had the best average ratio (1.05), and absolute error (in cm^{-1}). PM3 has the lowest standard deviation, while SAM1 has the highest. PM3 is

Table XII. Calculated Frequencies for HCN/H_2O (in cm^{-1})

vibration[a]		PM3	AM1	SAM1	Hartree-Fock		MP2	
					I	II	I	II
ν_1[b]	p	145.7i	48.6	55.8	50.4	94.0	136.9i	47.7
	np	101.1					123.1	
ν_2	p	94.3	53.2	78.8	104.5	106.5	113.7	98.3
	np	114.9					127.2	
ν_3	p	116.6	116.2	117.9	145.9	143.9	140.1	117.6
	np	216.3					166.7	
ν_4	p	280.2	150.3	228.9	155.0	175.3	166.4	150.5
	np	306.9					209.5	
ν_5	p	366.5	161.5	253.4	276.1	280.0	256.8	271.9
	np	373.7					294.5	
$\nu_6(\nu_2$ HCN)	p	892.2	960.0	1040.9	972.2	940.6	885.0	789.3
	np	904.5					904.3	
$\nu_7(\nu_2'$ HCN)	p	916.4	963.8	1060.6	1010.2	966.1	945.1	846.5
	np	927.2					960.2	
$\nu_8(\nu_2$ H_2O)	p	1731.4	1877.1	1800.8	1767.2	1751.2	1676.2	1654.0
	np	1731.9					1677.7	
$\nu_9(\nu_1$ HCN)	p	2310.7	2377.6	2390.1	2421.7	2393.5	2047.4	2003.6
	np	2308.9					2045.0	
$\nu_{10}(\nu_3$ HCN)	p	3252.3	3347.2	3087.6	3549.0	3545.1	3413.1	3395.6
	np	3227.0					3393.0	
$\nu_{11}(\nu_3$ H_2O)	p	3870.9	3502.0	3449.3	4147.9	4150.0	3899.7	3876.3
	np	3866.7					3889.3	
$\nu_{12}(\nu_1$ H_2O)	p	3995.5	3582.6	3498.1	4262.9	4265.4	4034.2	4016.4
	np	3991.5					4023.4	

[a]p: planar structure; np: non-planar structure. [b]i denotes the imaginary frequencies.

Table XIII. Calculated and Experimental Frequencies for H_2C_2/H_2O (in cm^{-1})

vibration[a]		PM3	AM1	SAM1	Hartree-Fock		MP2		Exp.[b]
					I	II	I	II	
ν_1	p	47.2i	35.3i	49.3	98.1i	69.6	156.3i	92.0i	
	np	30.4	46.7		77.2		94.4	77.9	
ν_2	p	21.7	38.9	66.5	67.9	73.3	77.1	72.9	
	np	37.0	53.4		82.1		101.4	85.2	
ν_3	p	58.0	81.2	109.6	108.3	109.3	110.6	102.3	
	np	82.4	115.9		115.1		131.8	126.0	
ν_4	p	86.0	120.4	212.8	114.3	127.0	131.9	123.7	
	np	97.1	132.9		178.9		216.5	148.3	
ν_5	p	91.5	127.4	217.4	202.2	218.7	185.5	224.7	
	np	113.1	144.1		231.2		244.9	235.8	
$\nu_6(\nu_4\ H_2C_2)$	p	837.7	813.0	592.9	810.3	790.4	483.0	554.1	
	np	839.0	814.4		814.6		512.9	557.9	
$\nu_7(\nu_4'\ H_2C_2)$	p	838.9	814.1	606.3	815.7	792.9	509.7	572.8	
	np	839.3	814.9		818.9		534.6	573.5	
$2\nu_8(\nu_5\ H_2C_2)$	p	902.6	938.7	1013.6	926.2	912.7	823.8	784.7	
	np	903.5	940.7		936.7		846.9	792.9	
$\nu_9(\nu_5'\ H_2C_2)$	p	903.4	940.7	1025.6	953.7	926.8	865.3	822.5	
	np	904.0	941.4		960.3		886.4	826.7	
$\nu_{10}(\nu_2\ H_2O)$	p	1739.2	1880.0	1801.6	1763.7	1743.9	1673.8	1646.8	
	np	1739.3	1880.1		1765.9		1678.6	1641.1	
$\nu_{11}(\nu_2\ H_2C_2)$	p	2138.3	2179.5	2366.3	2232.4	2197.0	1994.3	1948.5	
	np	2137.8	2179.4		2232.2		1993.2	1948.1	
$\nu_{12}(\nu_3\ H_2C_2)$	p	3305.1	3397.9	3113.7	3547.1	3535.4	3452.6	3409.2	3254.68
	np	3300.8	3393.9		3545.0		3442.3	3405.4	
$\nu_{13}(\nu_1\ H_2C_2)$	p	3387.5	3468.4	3260.3	3676.7	3663.8	3570.5	3533.6	
	np	3385.3	3467.0		3675.9		3568.1	3532.7	
$\nu_{14}(\nu_1\ H_2O)$	p	3870.8	3504.6	3448.7	4149.5	4153.7	3896.9	3876.3	3655.84
	np	3869.3	3504.3		4145.5		3882.6	3875.5	
$\nu_{15}(\nu_3\ H_2O)$	p	3992.2	3584.0	3497.3	4266.7	4271.7	4034.2	4019.5	3765.77
	np	3990.7	3583.8		4261.7		4019.1	4017.5	

[a] p, planar structure; np nonplanar structure. [b] i denotes the imaginary frequencies.

Table XIV. Calculated Frequencies for HCN/H_2CO (in cm^{-1})

vibration	PM3	AM1	SAM1	Hartree-Fock		MP2	
				I	II	I	II
ν_1	55.6	21.1	37.3	37.0	23.1	34.1	29.9
ν_2	97.0	30.0	56.5	86.6	57.9	117.9	91.4
ν_3	162.6	72.0	132.5	129.0	112.1	149.0	124.9
ν_4	176.6	84.8	147.5	143.9	120.0	170.3	142.9
ν_5	342.3	112.7	201.9	167.9	139.6	205.9	168.6
ν_6(ν_2 HCN)	925.7	959.0	1057.0	967.6	928.1	902.5	807.1
ν_7(ν_2'HCN)	926.5	960.7	1060.1	975.3	934.6	910.2	813.3
ν_8(ν_4 H_2CO)	1068.6	1168.1	1134.0	1343.9	1344.2	1224.8	1208.7
ν_9(ν_6 H_2CO)	1105.6	1176.3	1148.8	1376.3	1362.6	1298.0	1275.9
ν_{10}(ν_3 H_2CO)	1280.6	1442.4	1358.1	1666.4	1653.8	1584.9	1565.0
ν_{11}(ν_2 H_2CO)	1976.9	2050.4	2049.2	2013.5	1997.4	1786.2	1761.7
ν_{12}(ν_1 HCN)	2301.5	2377.4	2386.5	2425.2	2397.2	2045.9	2002.3
ν_{13}(ν_1 H_2CO)	3002.2	3088.7	2811.2	3142.8	3164.1	3055.2	3059.4
ν_{14}(ν_5 H_2CO)	3040.8	3121.9	2821.4	3228.8	3249.2	3148.4	3154.3
ν_{15}(ν_3 HCN)	3176.9	3353.7	3075.0	3577.0	3674.8	3426.7	3400.7

marginally better than AM1 for this sample. Not surprisingly, the calculated frequencies agree better with the experimentally derived harmonic rather than fundamental frequencies.

There is no reliable experimental data on the low frequency vibrations for most complexes studied here that involve the intermolecular degrees of freedom in the complexes. These vary substantially from one calculation to another. Lacking experimental data and compelling trends, it is difficult to reach sound conclusions with respect to these frequencies.

Table XV. Calculated Frequencies for H_2C_2/H_2CO (in cm^{-1})

vibration	PM3	AM1	SAM1	Hartree-Fock		MP2	
				I	II	I	II
ν_1	50.1	11.6	36.5	32.7	24.8	48.9	48.3
ν_2	79.2	68.8	51.5	91.7	71.5	103.5	87.9
ν_3	145.8	72.8	116.6	119.2	92.1	142.4	130.1
ν_4	150.0	93.1	123.7	136.5	111.1	163.5	146.8
ν_5	303.9	104.4	178.5	156.5	125.1	204.4	172.5
$\nu_6(\nu_4\ H_2C_2)$	853.3	812.1	600.3	816.1	787.9	512.4	555.0
$\nu_7(\nu_4'H_2C_2)$	854.1	812.8	602.1	817.9	788.9	529.4	559.8
$\nu_8(\nu_5\ H_2C_2)$	943.9	937.7	1024.6	924.5	900.5	828.2	775.9
$\nu_9(\nu_5'H_2C_2)$	944.9	938.8	1025.4	926.5	901.7	834.4	783.9
$\nu_{10}(\nu_4\ H_2CO)$	1069.0	1166.8	1134.4	1341.0	1341.4	1224.7	1209.3
$\nu_{11}(\nu_6\ H_2CO)$	1102.2	1176.8	1147.1	1378.2	1363.6	1299.3	1277.2
$\nu_{12}(\nu_3\ H_2CO)$	1281.9	1442.9	1357.9	1665.3	1654.3	1582.2	1563.2
$\nu_{13}(\nu_2\ H_2CO)$	1979.7	2051.8	2051.5	2015.4	2000.9	1783.0	1758.4
$\nu_{14}(\nu_2\ H_2C_2)$	2147.1	2179.4	2362.3	2234.4	2198.8	1994.5	1949.1
$\nu_{15}(\nu_1\ H_2CO)$	3001.2	3086.3	2806.3	3135.1	3155.0	3047.7	3050.2
$\nu_{16}(\nu_5\ H_2CO)$	3035.3	3120.9	2817.2	3228.8	3236.2	3137.4	3140.6
$\nu_{17}(\nu_3\ H_2C_2)$	3229.5	3401.1	3098.9	3557.9	3545.3	3456.1	3415.1
$\nu_{18}(\nu_1\ H_2C_2)$	3375.0	3468.7	3258.5	3680.6	3667.1	3570.4	3533.6

3e. General Observations

MP2 calculations consistently predict stronger interactions with shorter O...H interactions than HF calculations before the CP correction. The CP correction, consistently greater for the MP2 than for the HF cases, reverses this tendency for all HCN/H_2O and HCN/H_2CO calculations, as well as, for the $HCCH/H_2O$ 6-31G(d,p) results. While the

Table XVI. Calculated and Experimental Frequencies for HCN/O_3 (in cm^{-1})

vibration[a]		PM3	AM1	SAM1	Hartree-Fock		MP2		exp.[7]
					I	II	I	II	
ν_1	s	30.2i	33.0		28.2	47.3i	55.6	53.9i	
	ns	14.6		20.5		24.9		23.8	
ν_2	s	30.0	43.7		52.7	37.3	60.4	31.7	
	ns	26.3		40.9		45.1		41.7	
ν_3	s	35.2	48.2		55.4	39.1	69.4	34.8	
	ns	41.4		88.6		63.7		67.0	
ν_4	s	39.7	85.7		64.0	50.9	88.9	64.2	
	ns	72.9		115.8		72.3		80.2	
ν_5	s	99.7	122.8		149.9	128.5	165.2	125.8	
	ns	90.4		198.6		121.5		126.1	
$\nu_6(\nu_2\ O_3)$[b]	s	750.9	929.5		859.0	853.1	738.2	704.0	710.5
	ns	748.8		807.3		849.8		723.8	
$\nu_7(\nu_2\ HCN)$	s	860.4	952.9		907.2	869.5	789.4	736.4	745.0
	ns	862.4		1039.9		885.4		741.1	
$\nu_8(\nu_2{}^{13}HCN)$	s	866.1	962.0		932.5	884.2	868.6	736.9	749.8
	ns	864.3		1049.6		888.7		744.8	
$\nu_9(\nu_3\ O_3)$	s	1594.1	1689.1		1446.9	1432.5	1177.3	1186.3	1047.7
	ns	1584.9		2113.2		1423.7		1184.9	
$\nu_{10}(\nu_1\ O_3)$[c]	s	1597.4	1704.7		1538.7	1545.7	2386.0	2003.2	
	ns	1607.9		2361.3		1556.9		2434.1	
$\nu_{11}(\nu_1\ HCN)$[c]	s	2283.4	2379.2		2433.8	2405.4	2047.5	2435.6	
	ns	2284.4		2400.5		2404.4		2002.7	
$\nu_{12}(\nu_3\ HCN)$	s	3272.7	3363.2		3641.9	3626.6	3515.5	3483.4	3274.4
	ns	3277.0		3112.2		3619.5		3476.0	

[a]s: symmetrical H-bond; ns: non-symmetrical H-bond. [b]Strong coupling with ν_7 at MP2/D95++(d,p) level.

[c]Reverse order for ν_{10} and ν_{11} in MP2 calculations.

Table XVII. Calculated Frequencies for H_2C_2/O_3 (in cm^{-1})

vibration[a]		PM3	AM1	SAM1	Hartree-Fock		MP2	
					I	II	I	II
ν_1	s	25.8i	35.2		32.0	24.1i	46.3	31.8i
	ns	3.3		29.1		21.2		18.0
ν_2	s	15.8	44.7		41.2	36.1	50.2	22.5
	ns	13.8		48.4		42.3		50.0
ν_3	s	21.9	48.0		50.5	42.7	65.4	43.8
	ns	31.0		73.5		47.7		59.0
ν_4	s	25.3	84.4		58.7	49.5	75.4	51.8
	ns	41.9		100.6		57.1		73.8
ν_5	s	65.9	96.0		117.5	105.3	131.9	108.8
	ns	59.1		168.2		101.8		111.1
$\nu_6(\nu_4\ H_2C_2)$	s	745.2	808.0		816.6	782.0	495.3	539.5
	ns	743.6		571.6		783.9		546.1
$\nu_7(\nu_4'\ H_2C_2)$	s	834.5	811.6		821.2	786.4	531.8	543.6
	ns	836.0		576.7		786.5		547.2
$\nu_8(\nu_2\ O_3)$[b]	s	836.8	926.0		854.8	848.9	734.5	734.1
	ns	836.7		806.2		847.8		732.4
$\nu_9(\nu_3\ H_2C_2)$	s	899.5	933.0		895.7	867.3	785.1	738.1
	ns	900.3		1008.2		871.9		750.0
$\nu_{10}(\nu_5'\ H_2C_2)$	s	901.2	938.6		910.4	874.9	834.1	749.0
	ns	901.1		1013.4		876.0		752.9
$\nu_{11}(\nu_5\ O_3)$	s	1594.2	1692.4		1449.7	1434.6	1174.6	1183.8
	ns	1590.6		2111.8		1433.3		1183.1
$\nu_{12}(\nu_1\ O_3)$[c]	s	1597.6	1702.2		1537.5	1544.2	2388.2	2439.1
	ns	1602.9		2359.1		1546.6		2437.7
$\nu_{13}(\nu_2\ H2C2)$[c]	s	2138.2	2181.7		2241.0	2206.3	2000.7	1955.1
	ns	2138.3		2377.9		2205.8		1954.7
$\nu_{14}(\nu_3\ H_2C_2)$	s	3310.3	3411.6		3582.8	3568.2	3497.5	3451.5
	ns	3310.4		3133.0		3566.8		3450.3
$\nu_{15}(\nu_1\ H_2C_2)$	s	3389.3	3469.4		3695.1	3679.9	3588.8	3549.1
	ns	3389.5		3267.8		3678.8		3548.2

[a]s: symmetrical H-bond; ns: non-symmetrical H-bond. [b]Strong coupling with $\nu_6(\nu_4\ H_2C_2)$ at D95++(d,p) level. [c]Reverse trends for ν_{12} and ν_{11} in MP2 calculations.

Table XVIII. Statistic Analyses of Frequency Calculations (Except for O_3)[a]

Method - calculated frequencies are compared to experimental ...		PM3	AM1	SAM1	Hartree-Fock		MP2	
					I	II	I	II
fundamentals (ratio)	average	1.098	1.125	1.079	1.159	1.147	1.017	1.012
	stand. dev.	0.143	0.135	0.184	0.065	0.054	0.093	0.061
fundamentals (abs. error in cm^{-1})	average	110.6	135.9	57.5	256.3	244.6	86.1	70.2
	stand. dev.	132.6	146.1	206.0	109.0	118.3	124.9	117.0
harmonics (ratio)	average	1.069	1.096	1.051	1.128	1.116	0.989	0.984
	standard dev.	0.147	0.142	0.190	0.075	0.064	0.086	0.052
harmonics (abs. error in cm^{-1})	average	42.0	67.3	-11.2	187.7	176.0	17.5	1.6
	standard dev.	172.9	198.2	276.5	75.0	80.5	93.9	90.7

[a]Ratio is calculated/experimental, while the difference is calculated - experimental. Standard deviations correspond to the average values of different types of error.

existence of the BSSE is well recognized, the appropriateness of the CP correction has remained controversial (see Chapter II, part 4 for more discussion). The application of CP on flat surfaces, such as those considered in this study, complicates the evaluation of the vibrational corrections (ZPVE and enthalpy at 298°K) because the potential minimum with and without the CP correction can differ significantly. Bouteillier has recently shown that both potential minima and vibrations are dependant upon BSSE[39]. We have seen this to be an important factor in several of the present calculations: 1) for HCN/H_2O complex where the CP corrected planar complex is lower in energy than the CP corrected minimum; 2) For HCN/O_3 and $HCCH/O_3$, where the symmetric 3-center H-bonding interactions are favored for the ZPVE/CP corrected HF and MP2/D95++(d,p) calculations; and 3) for the fully corrected $HCCH/O_3$ complexes which are repulsive at the uncorrected

minima. These observations do not support a recent suggestion that fully optimized, CP corrected, MP2 calculations are sufficient to properly describe H-bonding.[40]

The MP2/6-31G(d,p) calculations always produced greater bonding interactions than MP2/D95++(d,p) by between 0.6 and 1.8 kcal/mole. However this difference basically vanishes upon CP correction. In fact, after CP correction the MP2/D95++(d,p) calculations often predict a stronger interaction. This is a clear indication that the 6-31G(d,p) basis set leads to larger BSSE's than does D95++(d,p). This observation may be because D95 has more primitive gaussians that better approximate the electron density near the nuclei, where the cusp is difficult to describe. Because of its larger BSSE, the 6-31G(d,p) potential wells become artifactually deeper leading to inappropriately high ZPVE's. In certain cases, notably the complexes involving H_2O and O_3, the BSSE seems to be a determining factor in the optimized geometry. Since the ZPVE must be overestimated due to the neglect of the effect of BSSE upon the surface, the fully corrected interaction energies are probably too weak. If one supposes that the CP correction overcorrects for BSSE, then the calculated interactions will be artifactually weakened still more.

The ZPVE poses another problem. When the symmetric structure has a negative force constant, but is lower in energy than the minimum after CP, it is likely to be a minimum rather than a transition state. The apparent negative force constant should really be positive (after CP correction) causing the true ZPVE to be greater than calculated without correction for BSSE. Thus, the relative energies of such structures (optimized without BSSE correction) are artifactually lowered. On the other hand, the frequency

corresponding to the harmonic approximation associated with the minimum that disappears upon CP correction is surely overestimated, as this frequency should be very anharmonic. This error is in the direction opposite to that due to ignoring the imaginary frequency. (See Figure 4, where (I) and (II) represent a double-well potential and a single-well potential, respectively, with the dashed lines showing the harmonic potentials that correspond to the curvature at the minima.)

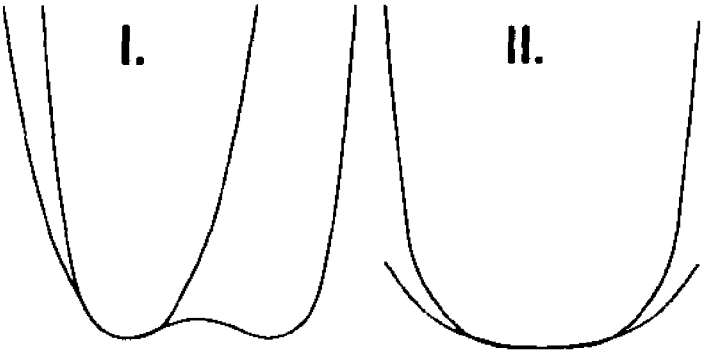

Figure 4. Hypothetical potential curves for the lowest intermolecular vibrations of HCN or H_2C_2/H_2O and HCN or H_2C_2/O_2 complexes.

Comparison of the HF and MP2 vibrations for $HCCH/H_2O$ is informative. While the MP2 vibrations are in better agreement with the experimental values, both for the monomers and the complex, the shift in the asymmetric C-H stretch of HCCH is better described by the HF calculations. That the MP2 calculations predict a greater shift is consistent with the larger BSSE errors found for these calculations, as the attraction of the acetylene hydrogen to the water oxygen is overestimated. This observation agrees with Bouteillier's report.

In most cases, the MP2 intramolecular vibrations are lower than those predicted by the HF calculations. A major exception is the symmetrical stretch of O_3, where the HF vibrations are much lower than the MP2. This is undoubtedly due to the large electron

correlation error, only partially corrected at the MP2 level. For the intermolecular vibrations, the MP2 calculations generally predict higher frequencies than the HF calculations. This is consistent with the stronger binding energies predicted by MP2. A major exception is the HCN/H_2O complex where the MP2/D95++(d,p) are smaller than the HF intermolecular frequencies. It may be significant that both MP2 and HF/D95++(d,p) predict the complex to be planar (before any correction); however, while HF/6-31G(d,p) also predicts a planar complex, MP2/6-31G(d,p) does not.

Comparison of the semiempirical and ab initio results is important as the former will certainly be used in calculations of large systems and biochemical simulations. Of the three methods tested, AM1 is clearly the best for both the structures and energetics of the complexes studied here, although it often predicts H-bonds to be too weak in other systems.[41] SAM1 consistently predicts stronger interactions, with shorter H-bonds, than indicated by the best ab initio results. PM3 is erratic in both energetics and structure, sometimes giving what appear to be physically absurd results. For HCCH/O_3, PM3 predicts a minimum that is 0.70 kcal/mol higher than the separated species. This suggests that a transition state exists between this structure and the separated molecules. If the hydrogen bond be essentially electrostatic in nature, this result is very difficult to reconcile with a reasonable physical model. I have mentioned similar results in Chapter II for ammonia dimer,[42] and for an interaction between two molecules of methane.[43]

The calculations are in good agreement with the observations that carbonyl groups form H-bonds in the plane of the ketone with H...O=C angles near the 120° angle expected if the lone pairs were in sp^2 hybrid orbitals, and that ethers form H-bonds both

in the COC plane, as well as somewhat above and below.[6] Except for AM1 (which predicts a nearly linear H..O=C angle), all methods predict planar interactions of HCN and HCCH with H_2C=O, with H..O=C angles of 117-158°. MP2/D95++(d,p) predicts 128°. The interactions of HCN with H_2O all have the axis of HCN in the HOH plane, while the similar interactions of HCCH with H_2O usually involve some nonplanarity. While these results definitely parallel Glusker's observations,[6] one should note that multiple H-bonds or other interactions are possible in a crystal. Multiple interactions would disfavor symmetrical H-bonds (i.e., linear H..O=C angles and coplanar HCN or HCCH and H_2O). In addition to the striking resemblance of the orientation of the C-H interactions to the geometric patterns of the stronger H-bonded systems,[6] all of the (C)-H...O contacts (with the exception of the H_2C_2/O_3 complex which is very close) were shorter than the sum of the van der Waals radii of the interacting hydrogen and the acceptor oxygen,[44] which serves as one of the most important geometrical characteristics of H-bonds.[45] The usually applied cutoff limit is 2.6 - 2.8 Å depending upon the directionality of the interaction (see the phenomenon of polar flattening[46]). Although, it was repeatedly pointed out that the sum of the van der Waals radii of the interacting atoms is not a useful measure of the C-H hydrogen bonds,[5a] the existence of short contacts is more than reassuring.

4. Conclusions

Fully optimized ab initio and semiempirical molecular orbital calculations on

complexes containing C-H..O interactions were reported in this Chapter, that are prototypes of interactions commonly found in crystals. The ab initio calculations were performed both at the Hartree-Fock (HF) and second order Møller-Plesset (MP2) levels using the 6-31G(d,p) and D95++(d,p) basis sets. The semiempirical calculations used the AM1, PM3 and SAM1 methods. The complexes considered were those of acetylene or hydrogen-cyanide with water, formaldehyde and ozone. The interaction energies, geometries and vibrations are presented with corrections for zero point vibration energy (ZPVE), basis set superposition error (BSSE) and enthalpy at 298 K, where appropriate.

The fully corrected H-bonding interactions (kcal/mol) at the MP2/D95++(d,p) level are -3.79, -2.74, and -1.15 for HCN and -2.19, -1.15 and -0.49 for HCCH for interactions with H_2O, $H_2C{=}O$ and O_3, respectively. The strength of these interactions indicates that the C-H hydrogen-bonds must play a significant role in aggregation processes. The potential surfaces were calculated to be rather flat. In particular, the energetic differences between planar and nonplanar complexes with H_2O and symmetric and unsymmetric 3-center H-bonds in complexes with O_3 are insignificant. The fact that BSSE can influence the shape of the potential surface, and, consequently, the ZPVE is demonstrated. The unscaled MP2 calculated vibrations agree reasonably well with experimentally derived harmonics, while the HF vibrations were about 12% too high.

The striking geometric resemblance of the C-H H-bonded complexes to the orientations of their stronger X-H (X = O, N) counterparts, the short (C)-H...O contacts and the strong interaction energies and enthalpies underline the earlier suggestions, that *there exist* C-H hydrogen-bonds.

Agreement of AM1 and the best ab initio calculations was generally good with respect to both energetics and structure. SAM1 consistently predicted stronger complexes with shorter H-bonding interactions, while PM3 was erratic. The semiempirical vibrations were 5-10% too high, and had much larger standard deviations than the ab initio results.

5. References and Notes

1. This chapter is based upon the following paper: Turi, L.; Dannenberg, J. J. *J. Phys. Chem.*, **1993**, *97*, 7899.

2. Glasstone, S. *Trans. Faraday Soc.*, **1937**, *33*, 200.

3. Taylor, R.; Kennard, O. *J. Am. Chem. Soc.*, **1982**, *104*, 5063.

4. Allen, H. F.; Bellard, S.; Brice, M. D.; Cartwright, B. A.; Doubleday, A.; Higgs, H.; Hummelink, T.; Hummelink-Peters, B. G.; Kennard, O.; Motherwell, W. D. S.; Rodgers, J. R.; Watson, D. G. *Acta Crystallogr. Sect. B.*, **1979**, *B35*, 2331.

5. a) Steiner, T.; Saenger, W. *J. Am. Chem. Soc.*, **1992**, *114*, 10146. b) Desiraju, G. R. *J. Chem. Soc. Chem. Commun.*, **1990**, 454. Desiraju, G. R. *J. Chem. Soc. Chem. Commun.*, **1989**, 179.

6. a) Murray-Rust, P.; Glusker, J. P. *J. Am. Chem. Soc.*, **1984**, *106*, 1018. b) Glusker, J. P. *Mol. Cryst. Liq. Cryst. Sci. Tech., Sect A*, **1992**, *211*, 75.

7. Mielke, Z.; Andrews, A. *J. Phys. Chem.*, **1990**, *94*, 3519.

8. Goodwin, E. J.; Legon, A. C. *J. Chem. Phys.*, **1987**, *87*, 2426.

9. Block, P. A.; Marshall, M. D.; Pedersen, L. G.; Miller, R. E. *J. Chem. Phys.*, **1992**, *96(10)*, 7321.

10. Peterson, K. I.; Klemperer, W. *J. Chem. Phys.*, **1984**, *81*, 3842.

11. Engdahl, A.; Nelander, B. *Chem. Phys. Lett.*, **1983**, *100*, 129.

12. Fillery-Travis, A. J.; Legon, A. C.; Willoughby, L. C. *Proc. R. Soc. London, A.*, **1984**, *396*, 405.

13. Gutowsky, H. S.; Germann, T. S.; Augspurger, J. D.; Dykstra, C. E. *J. Chem. Phys.*, **1992**, *96*, 5808.

14. a) Sreerama, N.; Vishveshwara, S. *J. Mol. Struct. (THEOCHEM)*, **1985**, *133*, 139. b) Frisch, M.; Pople, J. A.; Del Bene, J. E. *J. Chem. Phys.*, **1983**, *78*, 4063. c) Tsuzuki, S.; Uchimaru, T.; Tanabe, K.; Hirano, T. *J. Phys. Chem.*, **1993**, *97*, 1346. d) Reynolds, C. H. *J. Am. Chem. Soc.*, **1990**, *112*, 7903. e) Hinchliffe, A. *J. Mol. Struct. (THEOCHEM)*, **1986**, *136*, 193.

15. See Jeffrey, G. A.;, Saenger, W. In *Hydrogen Bonding in Biological Structures*, Springer-Verlag, Berlin 1991, for numerous examples including many from nonbiological systems.

16. Dykstra, C. E. *J. Am. Chem. Soc.*, **1989**, *111*, 6168.

17. Gutowsky, H. S., personal communication.

18. Bonchev, D. *Croat. Chem. Acta*, **1977**, *49*, 83.

19. Dykstra, C. E. *J. Am. Chem. Soc.*, **1990**, *112*, 7540.

20. After having communicating with Prof. Miller he agreed that their reported geometry is in error and would be corrected in a forthcoming erratum.

21. The dihedral angle H_1-C_1=O..H_3 of -107.1° for AM1 is somewhat misleading as the C_1=O..H_3 valence angle is close to linear (177°). The largest deviation from the plane of the H_2C=O is 0.34 Å (for the N).

22. Suzuki, I.; Pariseau, M., A.; Overend, J. *J. Chem. Phys.*, **1966**, *44*, 3561.

23. Strey, G.; Mills, I. M. *Mol. Phys.*, **1973**, *26*, 129.

24. Smith, A. M.; Coy, S. L.; Klemperer, W.; Lehmann, K. K. *J. Mol. Spectrosc.*, **1989**, *134*, 134 and references therein.

25. Suzuki, I.; Overend, J. *Spectrochim. Acta*, **1969**, *25A*, 977.

26. Strey, G.; Mills, I. M. *J. Mol. Spectrosc.*, **1976**, *59*, 103.

27. Wiggins, T. A.; Plyler, E. K.; Tidwell, E. D. *J. Opt. Soc. Am.*, **1961**, *51*, 1219. Allen, H. C., Jr.; Tidwell, E. D.; Plyler, E. K. *J. Res. Natl. Bur. Stand.*, **1956**, *57*, 213.

28. Herzberg, G. *Infrared and Raman Spectra*, Van Nostrand: Princeton, 1945.

29. Benedict, W. S.; Gailar, N.; Plyler, E. K. *J. Chem. Phys.*, **1956**, *24*, 1139 and references therein.

30. Hoy, A. R.; Mills, I. M.; Strey, G. *Mol. Phys.*, **1972**, *24*, 1265.

31. Duncan , J. L.; Mallinson, P. D. *Chem. Phys. Lett.*, **1973**, *23*, 597.

32. Tanaka, I.; Machida, K. *J. Mol. Spectrosc.*, **1977**, *64*, 429.

33. Reisner, D. E.; Field, R. W.; Kinsey, J. L.; Dai, H.-L. *J. Chem. Phys.*, **1984**, *80*, 5968.

34. Harding, L. B.; Ermler, W. C. *J. Comput. Chem.*, **1985**, *6*, 13.

35. Blau, H. H., Jr.; Nielsen, H. H. *J. Mol. Spectrosc.*, **1957**, *1*, 124.

36. Allegrini, M.; Johns, J. W. C.; McKellar, A. R. W. *J. Mol. Spectrosc.*, **1977**, *67*, 476.

37. Barbe, A.; Secroun, C.; Jouve, P. *J. Mol. Spectrosc.*, **1974**, *49*, 171.

38. See for example: a) Adler-Golden, S. M.; Langhoff, S. R.; Bauschlicher, Jr., C. W. *J. Chem. Phys.*, **1985**, *83*, 255. b) Lee, T. J.; Scuseria, G. E. *J. Chem. Phys.*, **1990**, *93*, 489.

39. Bouteillier, Y.; Behrouz, H. *J. Chem. Phys.*, **1992**, *96*, 6033.

40. van Duijneveldt, F. B.; de Groot-den Hartogh, M.; Van Duijneveldt-Van de Rijdt, J. G. C. M. *Croat. Chem. Acta*, **1992**, *65*, 1.

41. Dannenberg, J. J.; Evleth, E. M. *Int. J. Quant. Chem.*, **1992**, *44*, 869.

42. Jurema, M.W; Shields, G. C. *J. Comput. Chem.*, **1992**, *14*, 89.

43. Messinger, J.; Heuser, N. *QCPE Bulletin*, **1991**, *11(1)*.

44. Bondi, A. *J. Phys. Chem.*, **1964**, *68*, 441.

45. Hamilton, W. C.; Ibers, J. A. *Hydrogen Bonding in Solids*, W. A. Benjamin: New York, 1968.

46. Nyburg, S. C. *Acta Crystallogr.*, **1979**, *A35*, 641.

V. AGGREGATION AND NUCLEATION OF 1,3-DIONES[1]

1. Introduction

The first series of examinations on the hydrogen-bond directed crystal formation includes the investigations on the crystal structure of 1,3-diones, particularly, 1,3-cyclohexanedione (CHD). The crystal formation of this molecule is a subject of both considerable theoretical and experimental interest. Like other beta-dicarbonyl compounds, in addition to the diketo form, 1,3-cyclohexanedione have energetically accessible tautomer enol forms that have been reported to form unusually strong hydrogen bonds. In addition, 1,3-cyclohexanedione is known to crystallize in two different forms, including an unusual 6:1 stoichiometric cocrystal with benzene.[2] The normal crystal is formed from the anti-enol, the least stable of the easily accessible forms. The availability of extensive crystallographic data on the crystals of 1,3-cyclohexanedione provides an excellent opportunity to further test the applicability of the available molecular orbital methods to modelling hydrogen-bonding and crystal structure.

In the case of 1,3-cyclohexanedione, cooperativity of hydrogen-

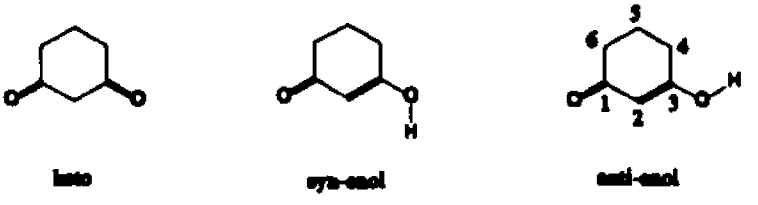

Figure 1. Tautomers and conformers of 1,3-cyclohexanedione. Note the numbering of the carbon atoms.

cooperativity of hydrogen- also might play an important role in the crystal

formation process providing the driving force for overcoming the activation necessary to convert the monomeric keto molecules to the enol forms observed in the crystal structures. The effect of cooperativity can presumably be crucial in two and three-dimensional aggregates, too, by influencing the unit cell dimensions (and other characteristic geometric parameters) of the aggregates.

In this Chapter, I present the results of various MO calculations on different 1,3-dione (1,3-propanedione (PPD), 1,3-cyclohexanedione (CHD) and 5,5-dimethyl-1,3-cyclohexanedione (DMCHD)) aggregates. The purpose of these calculations is to explore the influence of cooperativity on the crystal formation of 1,3-cyclohexanedione and on the structure of the established crystals.

2. Methods

Both the AM1 approximation to molecular orbital theory and various levels of ab initio calculations have been used for these studies. Since ab initio calculations of H-bonding systems are very sensitive to basis set and correction for electron-correlation, calculations of sufficient accuracy on molecular complexes of the size to be considered here are not practical using such costly methods. Nevertheless, ab initio calculations were performed on the monomers and several smaller aggregates for comparison and as an aid in interpreting the semiempirical results. For the ab initio calculations, PPD was often used as a model, in place of CHD to reduce the calculational complexity. In these

calculations, the carbons and oxygens were constrained to be coplanar in the conformation the dione would have if it were part of the 1,3-cyclohexanedione.

The geometries of the aggregates were optimized completely with the constraints that the geometry of all molecules in each aggregate be the same and that the three carbons and two oxygens involved in the enolic fragment be coplanar with the corresponding atoms in the other molecules. These constraints were removed in several test cases including an aggregate of six diones using AM1. The energy did not differ from the constrained geometry by more than 0.2 kcal/mol. Six-fold symmetry was enforced in the models of the 6:1 dione:benzene cocrystals. In addition to the restrictions applied on one-dimensional aggregates, the appropriate translation vectors were kept parallel in two- and three-dimensional structures. These geometric constraints allow one to calculate one or more parameters characteristic of the unit cell and compare them to the experimentally determined values.

The ab initio calculations were performed at both the HF and MP2 levels using 3-21G, 6-31G and 6-31G(d,p), and at the HF level only using 6-311G(d,p) basis sets. The HF/6-31G and HF/6-31G(d,p) calculations on dimer structures were corrected for BSSE and ZPVE differences.

3. Results and Discussion

Calculations were performed on aggregates of 1,3-propanedione (PPD), 1,3-cyclohexanedione (CHD), as well as, several derivatives of 1,3-cyclohexanedione, each

Table I. Relative Energies (kcal/mol) of Keto and Enol Tautomers of Different 1,3-Diones

method/basis set	enol		keto	total energies (hartrees)[a] of the most stable form
	syn	anti		
		1,3-Propanedione		
HF/3-21G	0	3.4	2.3	-264.133422
HF/6-31G	0	2.2	2.4	-265.503381
HF/6-31G(d,p)	1.3	3.5	0	-265.636698
HF/6-311G(d,p)	0.7	2.8	0	-265.699410
MP2/3-21G	4.6	8.0	0	-264.655489
MP2/6-31G	3.8	5.8	0	-266.026963
MP2/6-31G(d,p)	1.4	3.5	0	-266.407996
AM1	2.6	6.4	0	-70.7
		1,3-Cyclohexanedione		
HF/3-21G	2.1	6.6	0	-379.462330
HF/6-31G	0.5	4.1	0	-381.423661
HF/6-31G(d,p)	4.5	7.7	0	-381.613108
AM1	4.5	6.9	0	-86.7
		5,5-Dimethyl-1,3-Cyclohexanedione		
AM1	4.7	7.0	0	-93.7

[a]For AM1 results, heats of formation (kcal/mol) are reported.

in several different geometrical configurations. Calculations were also performed on aggregates of these diones with both one molecule of benzene, fluoro- and perfluorobenzene.

Monomers

Table I collects the relevant data on the different tautomers and conformations of the isolated molecules (Figure 1).

For PPD, AM1, the larger basis set Hartree-Fock (HF) and all the (MP2) calculations favor the keto form, while the smaller basis sets (without polarization functions) favor the syn-enol form at the HF, but not the MP2 level. The syn enol is consistently favored by between 2.0 (MP2/6-31G) and 3.8 (AM1) kcal/mol by all methods.

CHD was studied using Hartree-Fock methods up to 6-31G(d,p) basis set, but is too large to optimize using MP2. All methods are consistent with the keto form having the lowest energy (although, just barely so for 6-31G). The syn form of the enol is again favored over the anti by from 2.4 (AM1) to 4.5 (3-21G) kcal/mol. The relative energies for DMCHD (only calculated using AM1) were very similar to those for the parent 1,3-cyclohexanedione.

Aggregates

Various aggregates of the enol forms of the diones were modeled in these studies. The enols could be syn or anti (Figure 1), and they could hydrogen bond to give either

head to head (hh) or head to tail (ht) junctions depending upon the directionality of the cyclic ring. If we only consider structures where each monomeric unit is alike, there are four possibilities: anti ht (AHT), anti hh (AHH), syn ht (SHT), and syn hh (SHH).[3] Of these two are known from crystal studies: AHT is the normal assemblage found in the crystal structures of the pure diones, while SHH is the assemblage found in the 6:1 cocrystals of 1,3-cyclohexanedione with benzene. Figure 2 illustrates the four possible hydrogen-bonding patterns of the 1,3-cyclohexanedione chains, while Figure 3 shows the structure of the 6:1 CHD:benzene complex.

The hydrogen-bonding energies for the dimers and higher aggregates studied are collected in Tables II and VI.

1,3-Propanedione: Dimers

The dimers were studied at several levels of theory to help interpret the AM1 calculation that were performed on the larger aggregates. AM1 consistently gives the weakest hydrogen bonding interactions, while the smallest basis set HF calculations give the strongest interactions. The best HF calculations (HF/6-31G(d,p)) predict interactions virtually midway between the 6-31G and AM1 values (before correction for zero point vibrational energy, ZPVE). The predicted O...O distances are in the inverse order of the stabilization energies, as expected. These range from 2.67 to 2.98 Å. Corrections for ZPVE and BSSE were performed for the dimers at the HF/6-31G and HF/6-31G(d,p) levels (Table III). These values will be applied to the larger aggregates by assuming the ZPVE and CP corrections for each H-bond to be those calculated for the dimers.

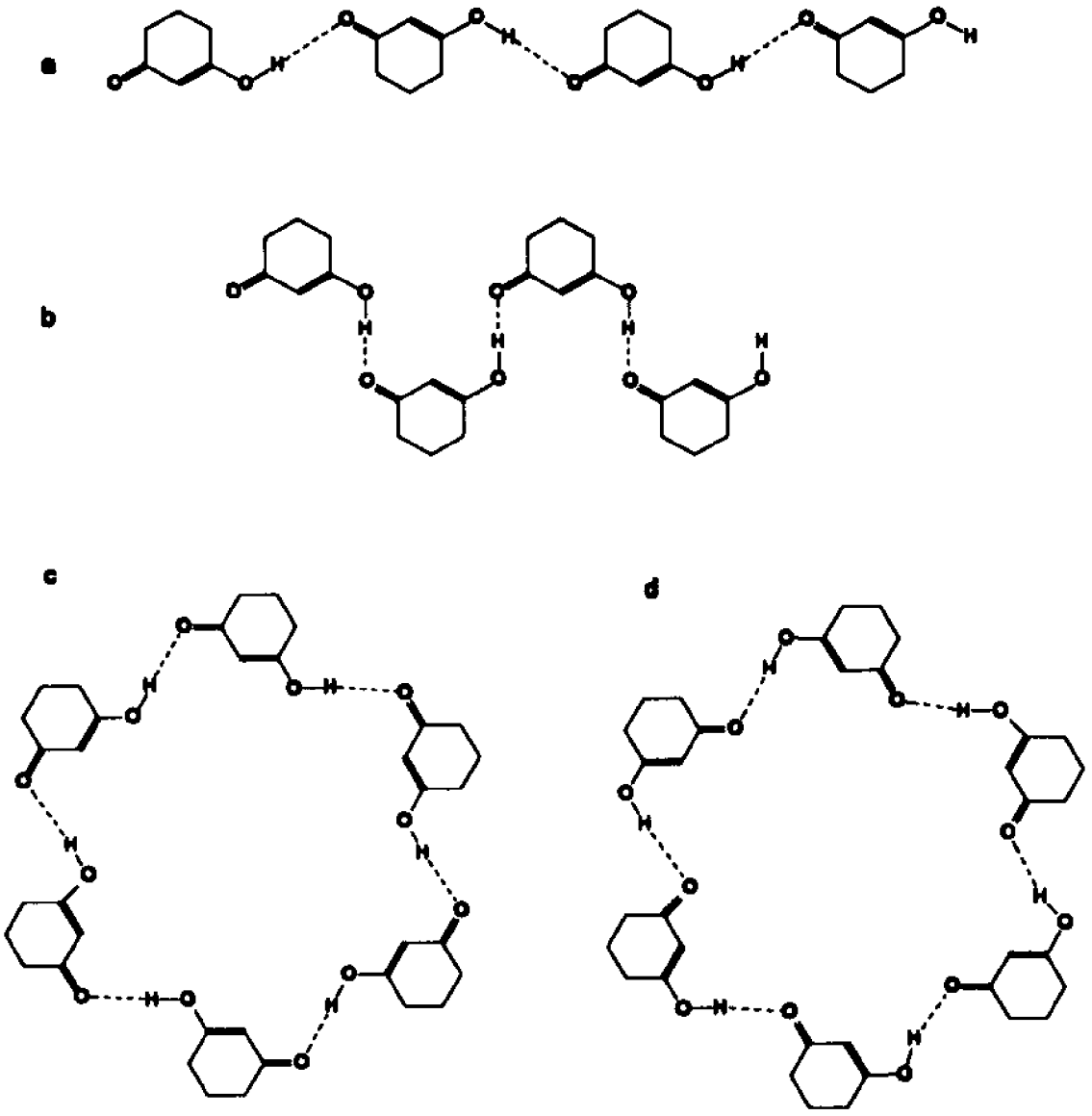

Figure 2. Schematic drawings of the various interactions considered for 1,3-dione aggregates: (a) AHT; (b) SHT; (c) AHH; (d) SHH.

After taking the ZPVE and CP corrections into account, the ab initio H-bonding stabilizations for AHT would be reduced by 2.6 and 2.3 kcal/mol for the HF/6-31G and HF/6-31G(d,p) basis sets, respectively. Considering the tendency of CP to overestimate the correction I shall arbitrarily use a smaller value of 2.3 kcal/mol to correct the interactions.

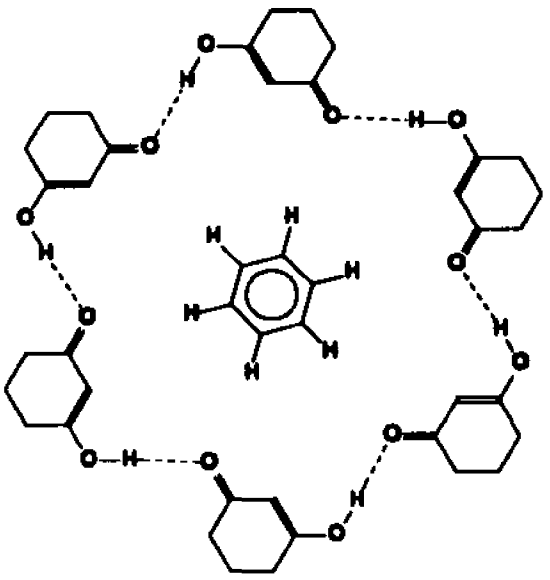

Figure 3. Schematic drawing of the 6:1 CHD:benzene complex in the experimentally observed SHH form.

HF calculations are often insufficient for accurate modelling of H-bonding complexes. For this reason, I performed several calculations at the MP2 level (MP2/6-31G, MP2/6-31G(d,p)//HF/6-31G(d,p), MP2/6-31G(d,p)//MP2/6-31G)[4] to assess the accuracy of the HF calculations. Due to the complexity of the calculations, I only treated the AHT dimer. The results are summarized in Table IV. Except for the HF/6-31G(d,p), all the ab initio methods predict stabilizations between 12.0 and 12.4 kcal/mol. After correction for ZPVE (using the HF/6-31G(d) correction, 1.3 kcal/mol) and BSSE, all methods, except HF/6-31G, give stabilization energies of 8.0-8.6 kcal/mol.

Table II. Incremental Hydrogen-Bonding Energies and Enthalpies (AM1) for the 1,3-Propanedione Aggregates at Different Levels of Theory (kcal/mol)

aggregates	SHT			AHT			SHH	AHH
	AM1	6-31G	6-31G(d,p)	AM1	6-31G	6-31G(d,p)	AM1	AM1
dimer	-4.6	-11.5	-9.3	-5.6	-12.4	-10.3	-3.8	-5.7
trimer	-4.6	-13.6	-10.6	-6.6	-14.8	-12.3	-5.4	-6.8
tetramer	-4.8	-14.1		-6.9	-15.7		-6.2	-4.3
pentamer	-4.8			-7.0			-3.8	-7.7
hexamer	-4.9			-7.1			-3.4	-7.2
heptamer	-4.9			-7.1				
octamer	-4.9			-7.2				

1,3-Propanedione: Trimers and Higher Aggregates

The AM1 method predicts the interaction energies to be weaker than the ab initio methods. However, ab initio calculations for many aggregates considered here is beyond the limits of the practical. For this reason, I shall scale the AM1 results as described in the following paragraph.

All methods predict the second hydrogen bond to be more stabilizing than the first by similar percent increases. From Table II, it is clear that the H-bonding stabilization for the last interaction increases asymptotically to the value expected in the infinite aggregate or crystal. One also can see that the ratio between the HF/6-31G(d,p) (after correction for ZPVE and CP) and AM1 stabilizations is roughly constant between 1.4 and 1.5, and that between AM1 and HF/6-31G between 1.7 and 1.9 (Table III). The best dimer calculations suggest that the HF/6-31G interactions are too strong by 1.5 kcal/mol. Based upon these

Table III. ZPVE and CP Corrections for the Dimers of 1,3-Propanedione (kcal/mol)

	HF/6-31G			HF/6-31G(d,p)		
	AHT	SHT	AHH	AHT	SHT	AHH
H-bonding energy (no correction)	-12.4	-11.5	-12.3	-10.3	-9.3	-10.4
CP correction	1.1	1.5	1.2	1.0	1.3	1.2
ZPVE correction	1.5	1.4	1.6	1.3	1.3	1.4
total correction	2.6	2.9	2.7	2.3	2.6	2.6
H-bonding energy (after correction)	-9.8	-8.6	-9.6	-8.0	-6.7	-7.8
H-bonding enthalpy (AM1)	-5.6	-4.6	-5.7	-5.6	-4.6	-5.7
ratio[a]	1.8	1.9	1.7	1.4	1.5	1.4

[a]Ratio is ab initio H-bonding energy/AM1 H-bonding enthalpy.

data, I scale the AM1 interaction energies of aggregates too large to calculate by the ab initio methods by a factor of 1.7. While this value is rather arbitrary, small changes in it will not affect the qualitative conclusions described below.

Nevertheless, a plot of the interactions obtained by fitting the exponential function of equation V.1,

$$E_n = -8.60 - 3.84\,(1 - e^{-0.90(n-1)}) \qquad \text{(V.1)}$$

where n is the number of H-bonding interactions, to the HF/6-31G H-bonding energies for AHT (after correction for ZPVE and BSSE with 2.3 kcal/mol) in Table II corrected by 1.5 kcal/mol compared with the AM1 values multiplied by 1.7, suggests that the approximation is sound (see Figure 4).

Equation V.1 also indicates that the stabilization of adding another monomer to an infinite chain (at large n) should be 12.4 kcal/mol (after the appropriate corrections),

Table IV. Total Energies (hartrees) and Hydrogen-Bonding Energies (kcal/mol) of AHT Dimers of 1,3-Propanedione at Different Levels of Theory

Method/Basis set	total energy		H-bonding energy		
	dimer	monomer	No correction	CP corrected	CP+ZPVE corrected
HF/6-31G	-531.019452	-265.499848	-12.4	-10.3	-10.0
HF/6-31G(d,p)	-531.278617	-265.631068	-10.3	-9.3	-8.0
MP2/6-31G//HF/6-31G	-532.041466	-266.010870	-12.4	-9.9	-8.6
MP2/6-31G	-532.054608	-266.017733	-12.0	-9.4	-8.1
MP2/6-31G(d,p)//MP2/6-31G	-532.815506	-266.397988	-12.3	-9.9	-8.6
MP2/6-31G(d,p)//HF/6-31G(d,p)	-532.817189	-266.398947	-12.1	-9.8	-8.5

or about 50% more than for the dimer interaction.

Significant geometric changes become apparent as the aggregates grow. These are displayed in Table V. The O...O distances across the H-bond become smaller. Geometric changes also occur within the molecules, themselves, as the longer bonds shorten, while the shorter ones lengthen. With one exception all the geometrical changes are in the direction necessary to convert the geometry calculated for the isolated molecule to that experimentally observed for the crystal. Even for the exception (the C=C distance by AM1), the bond length changes in the same direction as in the ab initio calculations. This tendency continues for all cases where tetramers could be studied, as well as for higher

aggregates studied only by AM1. The calculations clearly predict that the molecular structures in the gas and crystalline phases should be different. The calculated behavior of these H-bonds seems similar to the 'resonance' interaction suggested by Jeffrey for the aggregation of imides.[5]

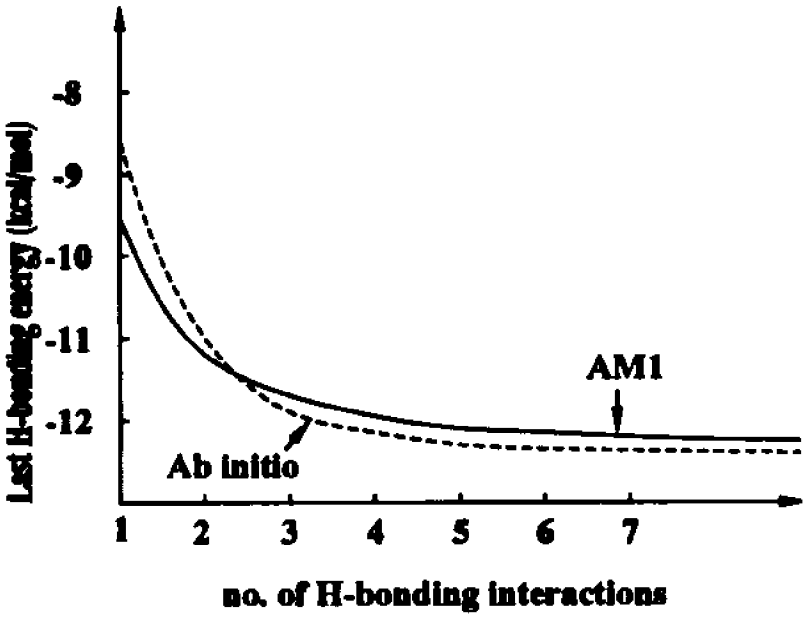

Figure 4. Comparison of ab initio and AM1 H-bonding interactions for the last H-bond as a function of the size of the AHT aggregate. See text for explanation.

1,3-Cyclohexanediones

Table VI collects the data on the enthalpies of interaction of the various aggregates studied. Figure 2 illustrates the geometries of the aggregates that have been considered. Due to the sizes of the aggregates, only AM1 calculations have been considered. Since the enols of the cyclohexanediones are not planar due to ring pucker, the aggregates can assemble with the pucker in the rings aligned or not (see Figure 5). Calculations showed little difference in energy of interaction dependance of the relative direction of the ring puckering. The

Figure 5. AM1 optimized AHT tetramer of CHD illustrating the pucker of the rings.

Table V. Bond Lengths (in Å) in the AHT Form of 1,3-Propanedione and 1,3-Cyclohexanedione Aggregates at Different Levels of Theory

Bond length	no. of monomers								expt[2]
	1	2	3	4	5	6	7	8	
				1,3-Propanedione (AM1)					
C_1-C_2	1.461	1.457	1.455	1.453	1.453	1.452	1.452	1.451	
C=C	1.349	1.349	1.350	1.351	1.351	1.352	1.352	1.352	
C=O	1.234	1.236	1.238	1.238	1.239	1.239	1.239	1.240	
C-O	1.371	1.368	1.366	1.365	1.364	1.364	1.363	1.363	
O..O		2.964	2.946	2.936	2.930	2.926	2.923	2.921	
				1,3-Propanedione (HF/6-31G)					
C_1-C_2	1.455	1.446	1.441	1.438					
C=C	1.325	1.330	1.333	1.335					
C=O	1.218	1.223	1.226	1.228					
C-O	1.360	1.348	1.342	1.339					
O..O		2.747	2.706	2.684					
				1,3-Propanedione (HF/6-31G(d,p))					
C_1-C_2	1.464	1.455	1.450						
C=C	1.325	1.329	1.332						
C=O	1.192	1.198	1.200						
C-O	1.335	1.325	1.320						
O..O		2.816	2.779						
				1,3-Cyclohexanedione (AM1)					
C_1-C_2	1.463	1.460	1.458	1.457	1.456	1.456	1.455		1.410
C=C	1.351	1.353	1.354	1.355	1.355	1.356	1.356		1.346
C=O	1.238	1.241	1.242	1.243	1.243	1.244	1.244		1.243
C-O	1.374	1.371	1.370	1.369	1.368	1.368	1.367		1.323
O..O		3.043	3.033	3.027	3.024	3.022	3.020		2.561

Table VI. Incremental Hydrogen-Bonding Enthalpies (kcal/mol) for 1,3-Cyclohexanedione and 5,5-Dimethyl-1,3-Cyclohexanedione Aggregates Calculated by AM1 Method

aggregates	1,3-cyclohexanedione				5,5-dimethyl-1,3-cyclohexanedione			
	SHT	AHT	SHH	AHH	SHT	AHT	SHH	AHH
dimer	-4.7	-5.7	-4.3	-5.6	-4.7	-5.7	-4.4	-5.6
trimer	-4.6	-6.3	-4.6	-6.4	-4.6	-6.3	-4.6	-6.4
tetramer	-4.8	-6.5	-4.7	-6.7	-4.8	-6.5	-4.7	-6.6
pentamer	-4.8	-6.6	-4.7	-6.9	-4.8	-6.6	-5.5	-6.8
hexamer	-4.9	-6.7	-5.3	-6.9	-4.9	-6.6	-4.7	-6.9
heptamer	-4.9	-6.7			-4.9	-6.7		

crystal structure is reported to be disordered with respect to pucker,[2] which is consistent with this observation. Without any energetic preference, all further calculations are performed on aggregates with alternating pucker.

The trends for the aggregates of the 1,3-cyclohexanedione are similar to those discussed above for 1,3-propanedione.

The known crystal structures suggest that the AHT structure of the enol (predicted to be the least stable monomer) be the most stable in the crystal (however, this is not a requirement since the crystal structure could be determined by kinetics rather than thermodynamics). For the AHT structure to be favored, hydrogen bonding (or other) interactions must overcome both the unfavorable energy difference between the keto and enol forms, as well as, that between the anti and syn enols. Since the stabilization of a H-bond is greater than the difference between the keto and enol forms, the first requirement is easily met.

The second requirement needs more consideration. For it to be met, the H-bonding stabilization of the AHT structure must exceed that of the SHH and SHT structures by at least as much as the syn monomer is favored over the anti. One must use an extrapolated H-bonding stabilization for the AHT and SHT structures for comparison with the average H-bonding energy for the cyclic hexameric structure of SHH. The extrapolated values were obtained by fitting an exponential function to the *cooperative* part of the H-bonding stabilization using equation V.2 where n is the number of H-bonds in the aggregate, E_n is the energy of the last H-bond and the parameters a (which represents the additional stabilization due to cooperativity in an infinite aggregate) and b are determined by a least squares fit.

$$E_n = E_1 - a(1 - e^{-b(n-1)}) \qquad \text{(V.2)}$$

At the AM1 level, these extrapolated values are 6.66 (AHT) and 4.85 (SHH), for 5,5-dimethyl-1,3-cyclohexanedione; 6.67 and 4.96 for 1,3-cyclohexanedione; and 7.27 and 4.94 for 1,3-propanedione, or about 1.7 to 2.3 kcal/mol apart. These values are slightly less than the AM1 calculated difference between the syn and anti 1,3-cyclohexanediones of about 2.4 kcal/mol. However, if one applies the correction factor of 1.7 that allows the AM1 stabilizations to approximate the ab initio stabilization, these energy differences become between 2.9 and 3.9 kcal/mol, enough to overcome the syn/anti energy difference. The H-bond cooperativity is slightly less for CHD than for the 1,3-propanedione model but this will not effect my conclusions.

The H-bond energies obtained by multiplying the AM1 values by 1.7 are consistent with a recent preliminary report that the heat of sublimation of crystals of 1,3-

cyclohexanedione is 26 kcal/mol, several kcal/mol higher than anticipated for an alcohol of this size.[6]

An interesting manner to consider the data is depicted in Figure 6 and Table VII, where the energy per molecule of a growing aggregate is considered relative to the energy of an equivalent number of non-interacting diones, with zero defined as the energy of the lowest energy (keto) form. For this model, I use the AM1 calculated energy differences for the monomeric forms, and 1.7 times the AM1 energies of the H-bonding interactions. The data show that 3-4 molecules must aggregate before the enthalpy of the AHT aggregate dips below the enthalpy of the non-interacting molecules in their keto form. Furthermore, 6-7 molecules must aggregate before the AHT becomes energetically equivalent to the SHT form. At infinite chain length, the enthalpy/molecule relative to the free keto form (kcal/mol) is calculated to be -4.5 for the AHT and -3.9 for the SHT forms.

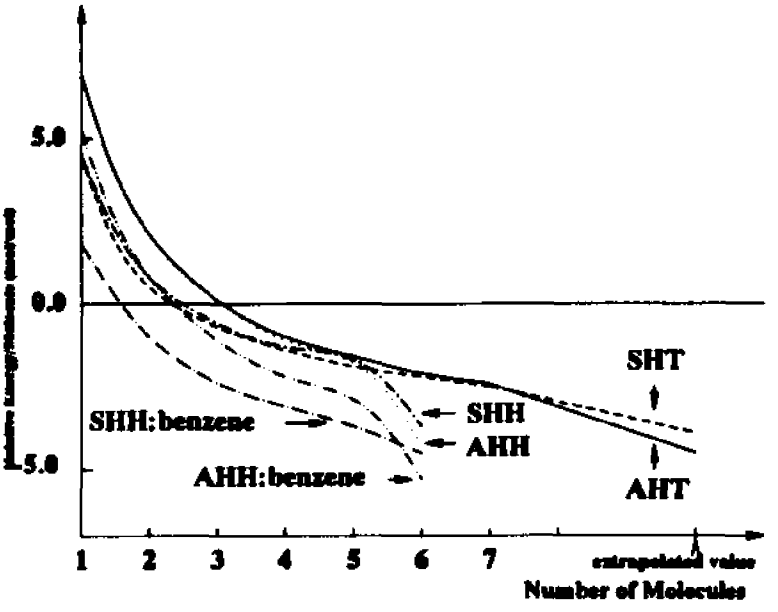

Figure 6. Relative energies per molecule of various CHD aggregates compared to the most stable (keto) monomer.

Table VII. Relative Energy (AM1 Results after Correcting by the Factor of 1.7) of CHD Aggregates Compared to the Energy of an Equivalent Number of Noninteracting Diones (kcal/mol)

no. of monomers	AHT	SHT	AHH	SHH	6:1 AHH:benzene	6:1 SHH:benzene
1	6.9	4.5	6.9	4.5	5.2	1.8
2	2.1	0.5	2.1	0.8	0.8	-1.0
3	0.1	-0.7	0.1	-0.6	-1.1	-2.4
4	-1.0	-1.5	-1.1	-1.3	-2.2	-3.1
5	-1.6	-1.9	-1.8	-1.7	-2.9	-3.7
6	-2.1	-2.2	-4.3	-3.7	-5.3	-4.5
7	-2.4	-2.4				
extrapolated	-4.5	-3.9				

I now consider the SHH and AHH structures. One of these is observed in the remarkable 6:1 stoichiometric cocrystal formed with benzene upon crystallization from that solvent. As is evident from Figure 2, these AHH and SHH structures can be interconverted by moving the six H-bonding H's from one O to another. Both AM1 and HF/6-31G predict the SHH structure to be more stable for 1,3-propanedione (Table VIII). AM1 predicts the SHH form of CHD to be more stable than the AHH, but by less than for 1,3-propanedione. The data in Table VII indicate that the AHH structure for CHD becomes more stable if one multiplies the AM1 H-bonding energies by the factor of 1.7, as the enhanced H-bond cooperativity in the anti form once again overcomes the intrinsic stability of the syn structure. In the 6:1 cocrystal with benzene, the preferred SHH structure, with the H-atoms of the benzene attracted to the carbonyl oxygens of the enols,

forms a second H-bond to the same oxygen. In the corresponding AHH structure, the benzene H's would have a (presumably) weaker interaction with the hydroxyl oxygens. The H-bonding aggregate cannot exceed the size of the cyclic structure of enols that is six. The average hydrogen bond energy of the crystal becomes that of the six molecule cyclic aggregate divided by six, rather than the value extrapolated to infinity used for the linear AHT and SHT structures.

The thermodynamic stabilities of the cyclic structures of six cyclohexyl enols are calculated to be -4.3 (AHH) and -3.7 (SHH) kcal/mol per enol unit (based on 1.7 times the AM1 interaction energy) relative to free keto form, both more stable than six enols in the AHT structure. However, in the absence of benzene, these structures may be severely kinetically disfavored. In forming aggregates of the SHH structure, I encountered problems with the optimization, in that small cyclic H-binding structures would often be most stable, even for dimers. These cyclic structures would have to break at least one of their H-bonds to form larger aggregates. Furthermore, the likelihood of forming populations of different sized cyclic aggregates is very high. It is unlikely that different sized cyclic aggregates could come together to form a stable crystal lattice. Hence, kinetics should disfavor the formation of six membered cyclic aggregates in crystals. Moreover, the extrapolated value for the infinite chain of AHT (-4.5 kcal/mol) is more stable than those for both cyclic structures (and SHT) indicating that AHT chains are more stable thermodynamically than the other three possible H-bonded patterns.

The influence of the benzene can be important. To evaluate this I calculated the optimized structures corresponding to the 6:1 cocrystal (Figure 3) using both AM1 and

Table VIII. Total Energies, Heat of Formations and Hydrogen-Bonding Energies of AHH and SHH Complexes with and without Benzene; Energies in kcal/mol Except Otherwise Noted

method		SHH	6:1 SHH:benzene	AHH	6:1 AHH:benzene
		1,3-Propanedione			
AM1	heat of formation	-436.4	-417.4	-421.7	-403.0
	H-bonding enthalpy	-27.5	-30.5	-31.6	-35.0
	H-bonding enthalpy due to benzene		-3.0		-3.3
6-31G	total energy (hartrees)	-1593.157913	-1823.788868	-1593.142050	-1823.772600
	H-bonding energy	-86.4	-90.4	-89.7	-93.5
	H-bonding energy due to benzene		-4.1		-3.8
		1,3-Cyclohexanedione			
AM1	heat of formation	-521.8	-503.0	-517.7	-499.4
	H-bonding enthalpy	-28.9	-32.0	-39.4	-43.1
	H-bonding enthalpy due to benzene		-3.1		-3.7

HF/6-31G with PPD and using only AM1 with CHD. These are compared to analogous calculations on the cyclic hexamer without a benzene. The structures were independently optimized with and without the benzene. Due to the size of the $C_{24}O_{12}H_{30}$ aggregate, the ab initio calculations were too complex to calculate the ZPVE.[7] AM1 calculations were then performed with a benzene molecule and from one to six molecules of enol to obtain the incremental H-bonding energies.

The values of Table VIII indicate the benzene interaction with the cyclic aggregate of 1,3-propanediones to be 3.03 kcal/mole, or 0.50 kcal/mol/molecule using AM1 and 4.07 kcal/mol and 0.68 kcal/mol/molecule for HF/6-31G. These results are in good agreement, especially if one assumes that the stabilization energy calculated using HF/6-31G should be less when corrected for BSSE and by the difference in ZPVE's for the cyclic hexamer with and without the benzene. The AM1 value for interaction of six 1,3-cyclohexanedione enols with benzene in SHH orientation is 3.14 kcal/mol, similar to the value for 1,3-propanedione. The geometries of the cyclamers are collected in Table IX. The structural features of the HF/6-31G calculation on 1,3-propanedione agree reasonably well with the experimental values for CHD, the AM1 values are in poorer agreement. In all cases, the distance between the two carbonyl oxygens opposite each other contracts upon insertion of the benzene, suggesting a geometric response to an attractive interaction. Table IX also contains the (C-)H...O non-bonding distances. These values (2.5-2.6 Å for AM1 and 3.0-3.1 Å for HF/6-31G) and the intermolecular attraction between the cyclamer and the benzene molecule strongly support the existence of C-H...O hydrogen bonds. Thus, this complex can be viewed as a peculiar example of C-H...O H-bonds with the participation of aromatic hydrogens.

The kinetic effect of the benzene may be even more important. If one imagines the enols aggregating around the benzene molecule, one can easily account for the six membered structure. No smaller ring size could accommodate the benzene in the center. If the benzene were the template around which the aggregate formed, then no H-bonds need be broken as the aggregate grows. Finally, the benzene in the center could serve the

Table IX. Bond Lengths (in Å) in AHH and SHH Cyclic Structures with and without Benzene at AM1 and Ab Initio HF/6-31G Theory.

Bond length	Structure				expti (6:1 CHD:benzene)[2]
	AHH	AHH:benzene	SHH	SHH:benzene	
		1,3-Propanedione (AM1)			
C_1-C_2	1.451	1.451	1.451	1.450	
C=C	1.352	1.352	1.350	1.350	
C=O	1.241	1.241	1.239	1.239	
C-O	1.360	1.361	1.355	1.356	
O..O	3.010	3.006	3.019	3.015	
(C-)H..O[a]		2.523		2.585	
cavity[b]	10.213	10.039	10.890	10.155	
		1,3-Propanedione (HF/6-31G)			
C_1-C_2	1.429	1.429	1.4428	1.427	
C=C	1.341	1.341	1.345	1.345	
C=O	1.238	1.237	1.235	1.236	
C-O	1.323	1.325	1.323	1.323	
O..O	2.635	2.638	2.639	2.642	
(C-)H..O		2.985		3.155	
cavity	10.875	10.895	11.331	11.237	
		1,3-Cyclohexanedione (AM1)			
C_1-C_2	1.453	1.454	1.455	1.454	1.413
C=C	1.357	1.357	1.354	1.354	1.349
C=O	1.246	1.246	1.243	1.244	1.253
C-O	1.363	1.363	1.363	1.363	1.318
O..O	3.020	3.016	3.009	3.009	2.579
(C-)H..O		2.541		2.669	3.00
cavity	10.097	10.001	10.591	10.327	

[a]Distances between the carbonyl oxygens and the benzene protons. [b]Distances between carbonyl oxygens (SHH) or OH oxygens (AHH) on enols opposite to each other.

Table X. Hydrogen-Bonding Enthalpies of *n*:1 SHH:Benzene Complexes (*n*=1-6) for PPD and CHD Calculated by AM1 Method.

n	1,3-Propanedione		1,3-Cyclohexanedione	
	total H-bonding	energy of the last H-bond	total H-bonding	energy of the last H-bond
1	-1.0	-1.0	-1.1	-1.1
2	-6.2	-5.2	-6.5	-5.4
3	-11.6	-5.4	-12.2	-5.7
4	-17.1	-5.5	-17.8	-5.6
5	-24.4	-7.3	-24.1	-6.2
6	-30.5	-6.1	-32.0	-7.9

purpose of creating a uniform size enol aggregate. Included in Figure 6 are the energies of the cyclic structure with and without the benzene. For energetic comparison, a free benzene is assigned a value of zero. The energies of a benzene with from one to six enols arranged around it (to form the 6:1 SHH:benzene ring structure step by step) are presented in Tables VII and X. These values are used in Figure 6 to indicate the relative energies of the aggregates as they form. The energy of the benzene-stabilized cyclic aggregate is lower than the AHT and SHT structure at each step of formation to completion of the ring. Once the ring is formed, no further aggregated H-bonds are possible. However, although the AHT infinite chain of H-bonds leads to a slightly more stable structure than the 6:1 SHH:benzene complex, there does not seem to be an accessible kinetic route from the cyclic structure to AHT. Such a route would require breaking of one H-bond between enols, six weak bonds between the enols and benzene and several rotations about the remaining H-bonds.

The only disturbing fact in the discussion above is the behavior of the 6:1 AHH:benzene complex. It is evident from Figure 6 and Table VII, that although the step by step formation of this complex is less favored than that of the SHH complex, the established AHH:benzene complex becomes more stable (applying the 1.7 factor) after building six enol molecules around the benzene template. Again the kinetics of the crystal formation may offer an explanation for this discrepancy. After five molecules of enol gathered around the benzene molecule in SHH orientation, the interaction energy with the sixth CHD molecule is presumably not sufficient to provide the necessary activation energy for the sextuple hydrogen transfer leading to the AHH:benzene complex.

An interesting extension of the problem is the possibility, as a first step toward designing new cocrystals, to replace the benzene molecule with fluorobenzene (C_6H_5F) or perfluorobenzene (C_6F_6) in the cyclamer cavity. Table XI contains the calculated hydrogen-bonding energies for the complexes of C_6F_6 and C_6H_5F with the diones. These values suggest that C_6F_6 should have a favorable interaction energy with the cyclic six-membered aggregate of PPD, but not

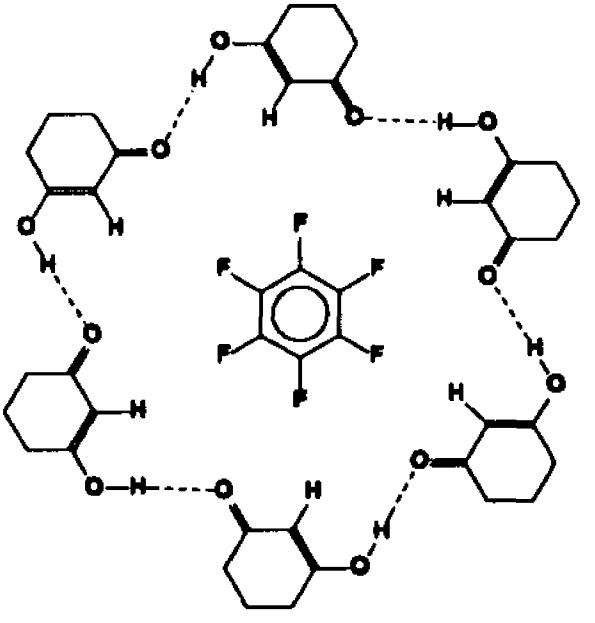

Figure 7. Schematic drawing of 6:1 CHD:C_6F_6 complex in SHH form.

Table XI. Heat of Formations and Hydrogen-Bonding Enthalpies (kcal/mol) of 6:1 SHH:X Complexes, where X = C_6H_6, C_6H_5F and C_6F_6

method		X = C_6H_6	X = C_6H_5F	X= C_6F_6
		1,3-Propanedione		
AM1	heat of formation	-417.4	-462.1	-668.1
	H-bonding enthalpy	-30.5	-29.9	-28.1
	H-bonding enthalpy due to X	-3.0	-2.4	-0.6
		1,3-Cyclohexanedione		
AM1	heat of formation	-503.0	-547.3	-752.4
	H-bonding enthalpy	-32.0	-31.4	-28.3
	H-bonding enthalpy due to X	-3.1	-2.5	+0.6
		5,5-Dimethyl-1,3-Cyclohexanedione		
AM1	heat of formation	-544.6	-589.1	-794.0
	H-bonding enthalpy	-32.3	-31.4	-28.4
	H-bonding enthalpy due to X	-3.2	-2.3	+0.7

that of CHD or DMCHD. The stabilization with the PPD cyclamer is 0.6 kcal/mol, while the destabilization is 0.6 and 0.7 kcal/mol for CHD and DMCHD, respectively. Although the results suggest cocrystallization of CHD with C_6F_6 to be unlikely, the hydrogen-bonding pattern is quite interesting (see Figure 7). Comparison of this structure with the analogous benzene complex indicates the C_6F_6 to be rotated by about 22° relative to the benzene in its complex. Each fluorine atom is directed toward a proton at the 2-position on each of the dione monomers. These hydrogens are appreciably positive (+0.172 au by

Table XII. Characteristic Distances (in Å) in 6:1 SHH:X Complexes at Semiempirical AM1 Level, where X = C_6H_6, C_6H_5F and C_6F_6

Distance	X = C_6H_6	X = C_6H_5F	X = C_6F_6
	1,3-Propanedione		
O...O	3.015	3.013	3.021
cavity[a]	10.155	10.359	11.612
	1,3-Cyclohexanedione		
O...O	3.009	3.007	3.016
cavity	10.327	10.388	11.139
	5,5-Dimethyl-1,3-Cyclohexanedione		
O...O	3.008	3.007	3.017
cavity	10.344	10.387	11.128

[a]Distances between carbonyl oxygens on diones opposite to each other.

AM1). Despite these favorable interactions, C_6F_6 does not interact favorably with the CHD and DMCHD complexes. This may be due to the short F...H contacts, that would push the enols away from each other. The cavities of the cyclamers contract upon insertion of C_6H_6 or C_6H_5F, but expand upon the insertion of C_6F_6. The O...O distances in the perfluorobenzene and benzene aggregates remain similar (Table XII).

The cocrystal of C_6H_5F with PPD is predicted to be stabilized by 2.4 kcal/mol compared to the hexamers. The analogous complexes with CHD and DMCHD are stabilized by 2.5 and 2.3 kcal/mol, respectively. However, these cocrystals must compete with aggregation of C_6H_5F (which has a significant dipole moment) in solution. The fluorine atom in these structures must have an unfavorable interaction with an oxygen for

the five aromatic hydrogens to remain able to H-bond with the adjacent enols. This might create a kinetic problem since the enol facing the fluorine would likely be last to attach.

1,3-Cyclohexanedione: Two- and Three-dimensional Structures

Although the previous sections gave plausible explanation for the preference of the 1,3-cyclohexanedione H-bonded chains to assume AHT (without benzene) or SHH orientation (with benzene) in the crystal structure, due to the complexity of the problem, this treatment could not take other interactions than the strong H-bonds within the chains into account. For completeness, in this section I shall explore two- and three-dimensional structures modeling the organization of the bulk solid phase of 1,3-cyclohexanedione. For this purpose, calculations were performed on aggregates consisting of 2-4 interacting trimers and tetramers in two-dimensions and on structures of two interacting layers from two interacting trimer and tetramer chains. For simplicity I shall use the following notation in this section: *L/C/M* will denote *L* interacting two-dimensional layers where a layer consists of *C* interacting chains from *M* monomeric units. An interesting feature of these aggregates is evident from Figure 8 which shows the largest of all considered two-dimensional structures, 1/4/4 (four tetramers interact in a layer approximately corresponding to the structure found in the crystals of 1,3-cyclohexanedione): the existence of C-H..O interactions between the chains. Every monomer participates in two such interactions: its carbonyl group is the H-bond acceptor to one of two neighboring chains, while its C_5 is the H-donor toward the other chain. The C-H...O interactions are partly responsible for the stability of the AHT network leading to the crystal structure.

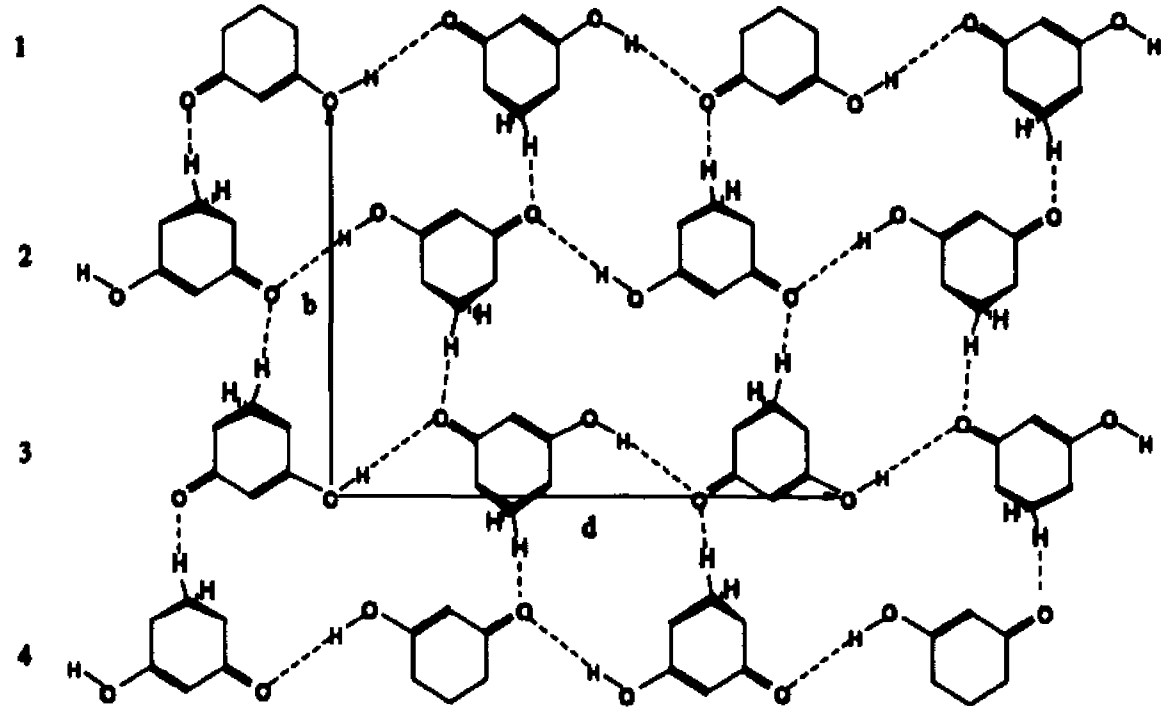

Figure 8. Four interacting tetramers in a single layer.

These interactions cannot be present in 5,5-dimethyl-1,3-cyclohexanedione (DMCHD), which might explain why DMCHD crystallizes in its SHH pattern.[2] Tables XIII and XIV contain the most important energetic and geometric data calculated for two-dimensional structures. The last interaction energies between the chains for two, three and four interacting trimers (M=3 and C=2, 3 or 4 in Table XIII) are -5.76, -5.50 and -5.86 kcal/mol. Thus, the second interaction (C=3, three chains) appears to be weaker than the first one (C=2) indicating repulsion between the first and third chains (1-3 interaction).

Table XIII. AM1 Incremental Interaction Energies (kcal/mol) Between Interacting Trimers and Tetramers (M=3,4 in C/M aggregates)[a]

chains	no. of interacting chains		
	C=2	C=3	C=4
M=3	-5.76	-5.50	-5.86
M=4	-9.34 (-4.93)	-4.56	-9.75

[a]Number in parentheses corresponds to a different H-bonding pattern. See text for more explanation.

In the next step (four chains), we have an additional repulsive 1-3 interaction between the second and fourth chains and a new, attraction between the first and fourth chains (1-4 interaction). Single point calculations on aggregates consisting of the first and second chains, first and third chains; and first and fourth chains in the geometry they assume in the 1/4/3 aggregate illustrate these 1-2, 1-3 and 1-4 pairwise interactions, respectively. The 1-2 (and the equivalent 2-3, 3-4) interactions are stabilized by -5.73 kcal/mol (compared to the completely optimized 1/3 chain). The 1-3 (and 2-4) interactions are repulsive by 0.58 kcal/mol, the 1-4 pairwise interactions are slightly attractive (-0.09 kcal/mol). The sum of the pairwise interactions for the 1/4/3 complex, -16.12 kcal/mol, is 1.00 kcal/mol less than the total interchain stabilization (-17.12 kcal/mol) indicative of the presence of strong non-additive contribution. One, however, must be aware that in this case non-additivity stems from both the electronic and geometric relaxation phenomena. Because of the almost negligible 1-4 interaction, the slight (-0.36 kcal/mol) increase of the last interaction energy between the second (C=3) and third (C=4) interactions can be mostly attributed to cooperativity in the second dimension (Table XIII).

Table XIV. Geometrical Characteristics of AM1 Optimized Two- and Three-dimensional Structures (Distances in Å)

aggregates	O..O	O..H(O)	O..C	O..H(C)	*d*	*a*	*b*	*c*	β
trimers									
1/1/3	3.033	2.066			13.983				
1/2/3	3.025	2.055	3.483	2.362	13.989				
1/3/3	3.023	2.052	3.464	2.342	14.011		12.006		
1/4/3	3.022	2.051	3.457	2.335	14.015		12.010		
2/2/3	3.022	2.049	3.438	2.320	14.046	9.073		8.664	104.70
tetramers									
1/1/4	3.028	2.061			13.973				
1/2/4	3.014	2.044	3.478	2.356	13.976				
$1/2/4_a$	3.022	2.051	3.501	2.380	13.992				
1/3/4	3.019	2.048	3.478	2.356	13.995		12.006		
1/4/4	3.016	2.044	3.461	2.339	13.996		12.001		
2/2/4	3.020	2.048	3.466	2.344	14.006	8.875		8.869	104.25
expt[2]	2.561	1.63			11.007	8.193	11.712	6.128	99.44

The changes in H-bonding geometry (Table XIV) indicate that cooperative effects in the second dimension influence the strength of the H-bonds within the chains significantly. An increase in the number of interacting chains results in shortening in the O...O and O...H(O) distances of the AHT chains suggesting an enhancement of these H-bonds. The C...O and (C)H...O interchain distances are surprisingly short, 3.45-3.48 Å and 2.33-2.36 Å, respectively. These C-H...O H-bonding distances resemble the results of Chapter IV and the previous section about SHH:benzene complex.

The analysis of interactions between tetramer chains is more difficult, as can be seen from Figure 8. Figure 8 shows two different H-bonding interaction networks: (a) between the first and the second chains (and between the third and fourth chains); (b) between the second and third chains. In the first case there are two C-H...O interactions at the end of chains 1 and 2 where the carbonyl groups are not involved in H-bonding within the linear chains and two C-H...O interactions with completely H-bonded carbonyl groups in the middle of the chains. Between the second and third chains one can find four C-H...O interactions with fully H-bonded carbonyl groups. While C-H...O bonds to a non-hydrogen-bonding carbonyl group represent an artificial end effect inherent in finite models, the C-H...O H-bonds between the second and third chains are clearly characteristic of the interactions found in crystals. According to the two different H-bonding networks, two 1/2/4 aggregates can be constructed: 1/2/4 (with interactions between chains 1 and 2 on Figure 8) and $1/2/4_a$ (with interactions between chains 2 and 3 on Figure 8). The interaction energies are listed in Table XIII (in parentheses for $1/2/4_a$). The large deviation in the interaction energies suggests that $1/C/4$ layers are not suitable models for examining cooperative effects because of the alternating H-bonding patterns between the chains. For example, the incremental interaction energies between the chains for the tetramer on Figure 8 are -9.34, -4.56 and -9.75 kcal/mol (for M=4 and C=2, 3 or 4 in Table XIII). As the $1/2/4_a$ aggregate contains all characteristic interactions of a layer structure, the strength of the individual C-H...O bonds can be estimated from the interchain stabilization. As the interaction between two chains of a $1/2/4_a$ is solely due to the four equivalent C-H...O H-bonds, the interchain interaction energy (-4.93 kcal/mol

from Table XIII) divided by four can give a sound estimation for the strength of the C-H...O interactions (neglecting additional cooperative effects). The estimated -1.2 kcal/mol value is in good agreement with the results of Chapter IV and a previous paper.[8]

An interesting geometric feature of these two-dimensional layer structures is also illustrated in Table XIV. As a result of appropriate geometric restrictions and structure definition during the geometry optimization, one can optimize geometric parameters that are characteristic of the bulk solid phase, like the parameters of the traditional unit cell. This procedure can furnish an additional test for the applicability of the AM1 method employed in this study. For 1,3-cyclohexanedione, a translation vector connecting every second monomeric unit within the H-bonded chains correspond to the diagonal (*d*) of a parallelogram defined by *a*, *c* and β of the unit cell, while a translation vector between every second H-bonded chains represent *b* (see Figures 8 and 9). While, vector *b* is in very good agreement with the experimental data indicating good description of the interactions between the chains, the diagonal is too long by about 25%. This large error is mainly due to the underestimation of the strength of the O-H...O H-bond in AM1. As the diagonal is too long, both *a*, *b* and perhaps β are overestimated though to a less extent. It is also worth mentioning that the geometries of the 1/4/4 and $1/4/4_s$ structures are significantly different due to their different H-bonding pattern.

The structure of a three-dimensional microcrystal is shown in Figure 10. The structure depicts a 2/2/4 AM1 optimized aggregate. It must be noted that this aggregate consists of two different layers, 1/2/4 and $1/2/4_s$. There is no such difference between the interacting layers for the other considered two-dimensional aggregate, the 2/2/3 complex

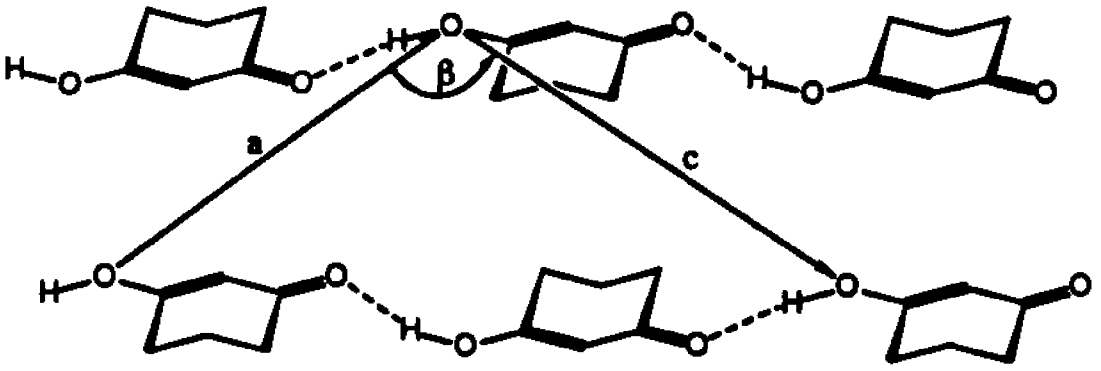

Figure 9. Illustration of the unit cell parameters *a*, *c* and β.

(both layers are equivalent). The results for these two three-dimensional structures (2/2/3 and 2/2/4) underscore my observations of both the energetic and geometric changes from earlier.

As expected, in lack of strong H-bonds, the interaction energy is small between two two-dimensional structures. The layers are shifted relative to each other as on Figure 9. The oxygens of the upper layer are weakly attracted to the axial hydrogens on the rings of the layer beneath. The partial opposite charges on the neighboring layers are in the most energetically favorable alignment in this shifted orientation. The nearest H...O interlayer distances are in the range of 4.0-5.0 Å. These distances are definitely longer than the characteristic C-H...O H-bonding distances. Thus, I conclude, that the interactions between the layers are mainly due to weak electrostatic forces. The stabilizations between two layers are -0.50 and -0.90 kcal/mol for 2/2/3 and 2/2/4 structures, respectively.

The decrease of the appropriate O...O and O...C distances with increasing aggregate size manifests the existence of three-dimensional cooperative effects (Table XIV). The presence of the second layer decreases both the O-H...O and C-H...O H-

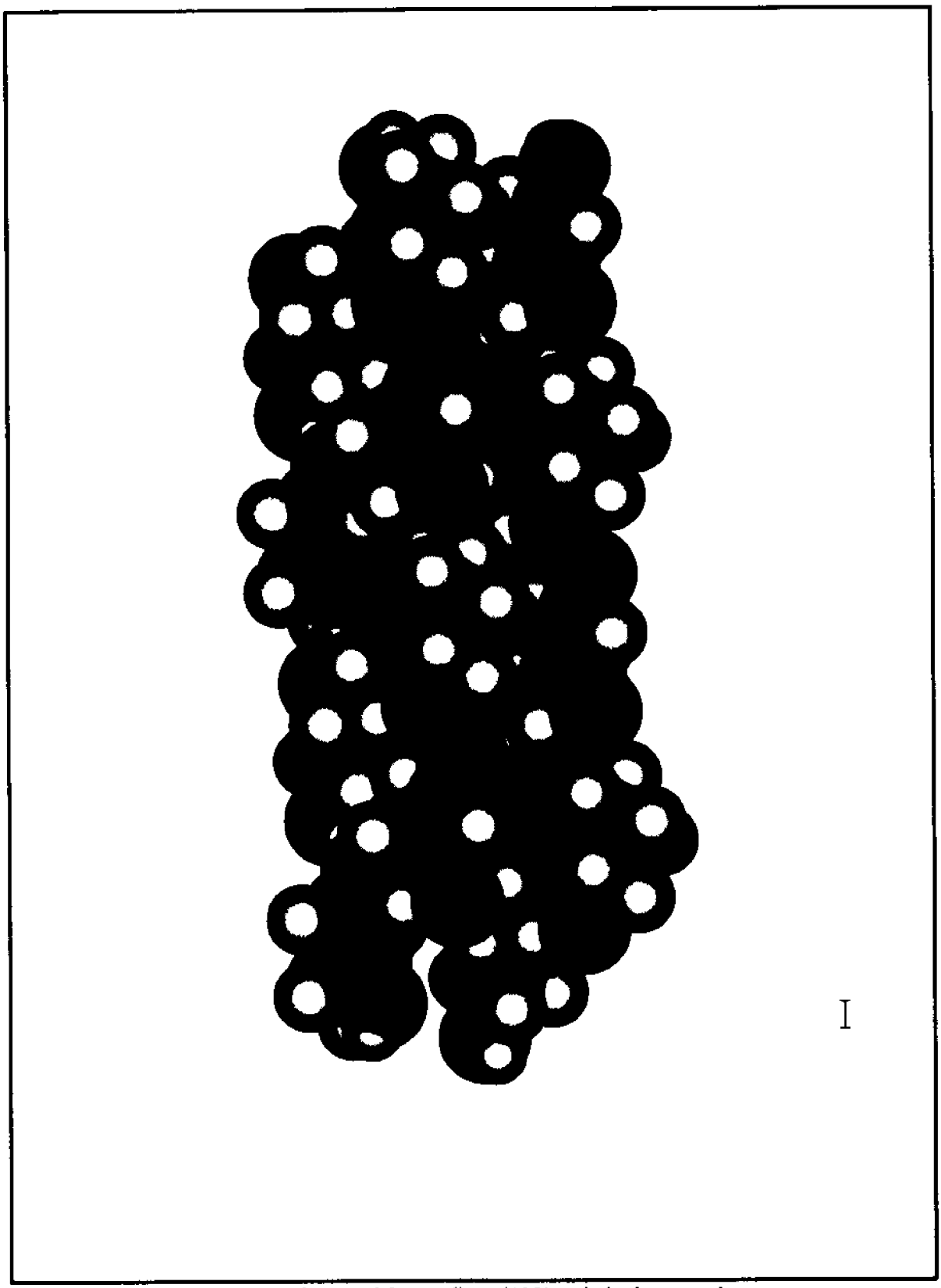

Figure 10. A 2/2/4 microcrystal of 1,3-cyclohexanedione (AM1 optimized structure).

bonding distances within the layers. For example, the C...O distance between the chains (Table XIV) decreased from 3.483 Å (in 1/2/3) to 3.438 Å (in 2/2/3). With this observation my results about the influence of cooperativity on intermolecular geometry are complete. The example of O...O distance can serve as an illustration: the O...O distance decreased from 3.043 Å to 3.033 Å as one goes from single dimer (1/1/2) to trimer (1/1/3). The aggregation of trimers resulted in another decrease to 3.025 Å in 1/2/3 and 3.022 Å in 2/2/3 aggregate. If one accepts that shorter O...O H-bonding distances indicate stronger interactions then the forementioned geometric changes definetely support the presence of interdimensional cooperativity.

Contrary to the expectations from diagonal *d* of the unit cell for single layers, only *c* deviates significantly from the experimental unit cell parameters demonstrating the problems in AM1 method at describing O...H-O H-bonds correctly. Another plausible explanation for overestimating *c* might be the underestimation of the magnitude of the electrostatic attraction. If the layers were closer to each other in the three-dimensional calculated microcrystals, both *a* and *c* could be dramatically shortened (but probably β would increase).

4. Conclusions

Ab initio and semiempirical (AM1) molecular orbital calculations are reported on the relative energies of the tautomers and conformations and energies of association of 1,3-cyclohexanedione and 1,3-propanedione used as a model. Small basis set HF

calculations make predictions of the relative energies of the monomers that differ from the larger basis set HF and MP2 calculations. The AM1 calculations are in general agreement with the better ab initio results for the monomers. H-bonding interactions have been calculated using HF/6-31G, HF/6-31G(d,p) and AM1 for aggregates containing up to sixteen (AM1), four (HF/6-31G) and three (HF/6-31G(d,p) monomeric units. Both the H-bonding interactions and the geometries of the monomeric units are calculated to change due to a significant cooperative interaction ia all three dimensions. The reported 6:1 cocrystal of 1,3-cyclohexanedione with benzene has been calculated using AM1, while a model 6:1 aggregate using 1,3-propanedione has been calculated at the HF/6-31G level, as well. From comparison of the best ab initio and AM1 results with each other and a preliminary experimental report, I conclude that the AM1 H-bonding energies (presumably, the O...H-O energies, too) need to be scaled by a factor of 1.7 for these systems. The crystal structures for 1,3-cyclohexanedione and its 6:1 cocrystal with benzene can be explained using the calculated interaction energies for one-dimensional chains. Molecular orbital calculations on 6:1 complexes of CHD or DMCHD with fluorobenzene or perfluorobenzene suggest that, unlike the case of benzene, cocrystallization of CHD or DMCHD with these molecules is unlikely.

The MO calculations presented here indicate that we can understand the relative energies of several of the possible aggregates of 1,3-diones that can lead to crystal formation or nucleation. The cooperativity of the H-bonding network eventually overcomes the energetic barrier(s) necessary to transform the monomeric units from the most stable (keto) form to the enol forms observed in the two different crystal structures

of CHD. This cooperativity ultimately dictates the form of the crystal. Thus, the effect of cooperativity is central to understanding both the relative energies and structural details, such as O...O distances, in these crystals.

Calculations on three-dimensional crystal-like structures demonstrated the ability of AM1 to predict the trends in geometric and energetic changes caused by crystal growth. AM1 also predicts reasonable unit cell dimensions, unless O...H-O H-bonds are involved.

5. References

1. This Chapter is based on the following papers: Turi, L.; Dannenberg, J. J. *J. Phys. Chem.*, **1992**, *96*, 5819. Turi, L.; Dannenberg, J. J. *Mol. Cryst. Liq. Cryst.*, **1992**, *219*, 63. Note, that the contents of both papers are slightly changed, few corrections are made concerning the CP corrections and the scaling of the AM1 method to ab initio calculations.

2. Etter, M. C.; Urbanczyk-Lipkowska, Z., Jahn, D. A., Frye, J. S. *J. Am. Chem. Soc.*, **1986**, *108*, 5871. Etter, M. C.; Parker, D. L.; Ruberu, S. R.; Panunto, T. W.; Britton, D. *J. Incl. Phenom. and Molec. Rec. in Chem.* **1990**, *8*, 395.

3. This notation is different from that of Etter, who refers to the positions of the lone pairs (which are neither uniquely defined nor experimentally determinable).

4. The *method-1/basis set-1//method-2/basis set-2* notation indicates single-point calculations using *method-1* with *basis set-1* on the *method-2/basis set-2* optimized structure.

5. For a discussion see: Jeffrey, G. A.; Saenger, W. *Hydrogen Bonding in Biological Structures*, Springer-Verlag, Berlin: 1991, p35.

6. Chikos, J. S.; Hesse, D. G. private communication.

7. Geometry optimization on the 6:1 SHH:benzene complex took 25 days on an RS/6000 Model 320H.

8. Turi, L.; Dannenberg, J. J. *J. Phys. Chem.*, **1993**, *97*, 7899.

VI. MO STUDIES ON THE CRYSTAL STRUCTURE OF ACETIC ACID[1]

1.Introduction

In the previous chapters, I indicated the importance of cooperativity in molecular nucleation and aggregation. However, due to the size of the molecules, the previous studies were mostly limited to interactions in one dimension.[2] To critically study these effects in three dimensions, I sought for an example of an unusual crystal structure of a small molecule, preferably one where the crystal structure defies simple intuition. Such a case is that of acetic acid.

Spectroscopic[3] and vapor-density measurements[4] indicate that acetic acid forms hydrogen-bonded cyclic dimers in gas phase. From these studies, statistical calculations,[5] and other experimental techniques[6] (i.e. thermal conductivity measurements), the standard thermodynamic parameters for the dimer formation were determined. The dimer forms to the extent of about 50% at 20 °C. Several previous MO studies on acetic acid monomers and dimer have been reported.[6,7]

Normally carboxylic acids crystallize as dimers similar to those that exist in the gas and liquid phases. For example, the crystal structures of both propionic acid[8] and fluoroacetic acid[9] consist of associated cyclic dimers. However, acetic acid crystallizes in long chains that involve C-H...O as well as O-H...O H-bonds.[10] This peculiar behavior makes the examination of the crystal structure of acetic acid especially interesting.

Another important structural aspect of the acetic acid crystal is the C-H..O

hydrogen bonding network. In a recent study[11] we estimated the strengths of these interactions to vary between -0.5 and -3.8 kcal/mol (see also Chapter IV).

Derissen and Smit have attempted to rationalize the unusual crystal structure of acetic acid using atom-atom potential calculations.[12] Theoretical studies of this type (generally based upon two-body interactions) cannot adequately treat the cooperativity. They neglect the non-additivity or many-body interactions which are inherent in intermolecular interactions of more than two molecules. In contrast, MO theory is an extremely useful tool in treating the cooperative effects correctly as illustrated in the previous chapter on the crystallization of 1,3-diones.[2]

In the first part of this Chapter, I shall concentrate on the dimerization of acetic acid molecules. Both ab initio and semiempirical molecular orbital methods will be used to evaluate the extent to which both O...HO, and O...HC H-bonds contribute to the stability of the dimers. Due to the complexity of the problem, the effects of aggregation (and cooperativity) leading to the three-dimensional crystal structure will be considered separately, in the second half of this Chapter. I shall summarize the results of various MO calculations on aggregates in one, two and three dimensions, containing up to 36 individual molecules.

Although there is a similar approach in the literature for the calculation of the lattice energy of formic acid,[13] to my best knowledge, no MO calculations have been performed on acetic acid aggregates.

2. Computational Methods

As in the previous chapters of my Thesis, I applied both semiempirical (AM1, PM3, and SAM1) and various levels of ab initio molecular orbital methods for acetic acid aggregates. The approach of the problem is similar to that of the 1,3-dione nucleation: the costly ab initio methods performed on smaller aggregates have been used to reinforce the semiempirical results on large, crystal-like structures.

The three semiempirical methods were applied to aggregates consisting of up to 36 acetic acid monomers. While the semiempirical monomer and dimer structures were optimized completely in all internal coordinates, I imposed the following geometric restrictions on larger aggregates to ease computational complexity: a) the four heavy atoms and the acidic hydrogen of every acetic acid monomer are coplanar; b) a C-H bond of the methyl group is eclipsed with the C=O bond of the molecule; c) every monomer has C_s symmetry (i.e. symmetry plane); d) the internal geometric parameters for every monomer were the same. In addition to these constraints, all structures were optimized in a way that the individual monomers be superimposable with each other after performing simple translations. The appropriate translation vectors must be kept parallel to reflect the proper relations within the ordered crystalline phase. This approximation made the optimization of the traditional unit cell dimensions possible.

I performed accurate ab initio calculations at the Hartree-Fock (HF) and second-order Møller-Plesset (MP2) levels using several different basis sets. At both levels I used 6-31G, 6-31G(d), 6-31G(d,p), 6-311G++(d,p) and D95++(d,p) basis sets for acetic acid

monomers. For dimers and larger aggregates I employed the first three basis sets at the HF, but only 6-31G and 6-31G(d) at the MP2 level. The ab initio dimer optimizations were performed with a symmetry plane (containing the heavy atoms and a methyl hydrogen eclipsed with the C=O) enforced. Nevertheless, force calculations confirmed convergence to minima on the potential surface.[14] For larger aggregates, I used the same geometric constraints as for the semiempirical calculations. In all cases the counterpoise (CP) correction for the basis set superposition error (BSSE) was performed in a way described in Chapter II. This procedure has the advantage of being independent of the direction of the extension of the aggregate. Wherever the size of the system under consideration allowed it, I also calculated the zero point vibration energy (ZPVE) corrections. The ab initio enthalpies at 298 K were also computed for comparison with the semiempirical results.

3. Monomers and Dimers

Energies and geometries

Acetic acid can exist in either the cis or trans conformation (Figure 1). The cis form is calculated to be more stable by 2.6 to 8.4 kcal/mol (Table I). The best calculations [MP2/6-311G++(d,p)] predict the difference to be 6.1 kcal/mol. Aside

Trans Cis

Figure 1. The structure of trans and cis acetic acid.

Table I. Total Energies (kcal/mol) of cis Acetic Acid and Relative Energies of trans

Method	total energy of cis (hartrees)[a]	relative energy of trans (kcal/mol)
AM1	-103.0	5.9
SAM1	-102.3	7.9
PM3	-102.0	2.6
HF/6-31G	-227.7011160	8.4
HF/6-31G(d)	-227.8106476	7.2
HF/6-31G(d,p)	-227.8221715	7.1
HF/D95++(d,p)	-227.8760442	6.8
HF/6-311G++(d,p)	-227.8835478	6.8
MP2/6-31G	-228.1355903	7.7
MP2/6-31G(d)	-228.4339791	7.0
MP2/6-31G(d,p)	-228.4692244	6.8
MP2/D95++(d,p)	-228.5670329	6.3
MP2/6-311G++(d,p)	-228.6440324	6.1

[a]Heats of formation for semiempirical methods.

from the calculations using 6-31G, all the ab initio calculations predict differences in the range 6.1 to 7.2 kcal/mol. Among the semiempirical methods, AM1 predicts 5.9 (close to the best ab initio value); SAM1, 7.9 (at the high end of the ab initio values); and PM3, 2.6 kcal/mol (much less than any of the ab initio results). The cis structure probably owes its energetic preference to a combination of a weak internal H-bond, and repulsion between the lone pairs on the hydroxyl and carbonyl oxygens that would occur in the trans conformation.

As the cis form is more stable and the structure experimentally observed in both the gas phase and crystal structures, the trans form is not likely to be important in the

aggregation process. While the most stable conformer might be expected to exist in the crystal structure, this is not always the case. The crystal structures of (4-chlorophenyl)propiolic acid,[15] 1,3-cyclohexanedione[16] and formohydroxamic acid[17] are among experimental examples of cases where the monomeric and crystalline structures differ. The calculated geometrical parameters of cis acetic acid are collected in Table II.

The geometries (Table II) predicted by the HF calculations are usually in poor agreement with experimental microwave[18] and electron-diffraction[19] results.[20] Increasing the size of the basis set does not substantially improve the calculated geometries. On the other hand, the MP2 calculations (except 6-31G) agree reasonably well with the experimental geometries. Undoubtedly, HF calculations are inadequate to describe the geometry of the monomer. The semiempirical methods do moderately well, especially for bond lengths. Oddly, PM3, worst for the relative energies of the conformations, gives the best geometry. All ab initio methods and PM3 predict one of the C-H bonds of the methyl group to be eclipsed with the C=O group at the global minimum. This structure is more stable than staggered by 0.4 kcal/mol using MP2/6-311G++(d,p). Both AM1 and SAM1 predict however, that the staggered (relative to the C=O bond) conformation is slightly preferred by 0.04 and 0.12 kcal/mole, respectively.

There are several possible structures for the dimer of acetic acid (Figure 2). Dimer I, containing two OH..O H-bonds, predominates in both the gas and liquid phases. In dimer II, one of the C=O..H-O interactions is replaced by a C=O..H-C. Unlike dimer I, this dimer can participate in hydrogen-bonded chains and is observed in the crystal structure.

Table II. Optimized Structures of cis Acetic Acid Monomer, Dimers I and II

Methods and Structures		R_{C-O}	R_{C-O}	R_{C-C}	R_{O-H}	R_{C-H}^{a}	R_{C-H}^{b}	$R_{O...O}$	$R_{O...C}$	α_{O-C-O}	α_{C-C-O}	α_{C-O-H}
AM1	monomer	1.364	1.234	1.486	0.971	1.1167	1.1178			116.5	129.3	109.8
	dimer I	1.356	1.238	1.487	0.976	1.1167	1.1176	3.067		117.3	128.2	110.5
	dimer II	1.357	1.237	1.488	0.976	1.1163	1.1176	3.076	3.284	117.3	128.4	110.5
		1.362	1.238	1.484	0.971	1.1211	1.1163			116.1	129.3	109.9
							1.1182					
SAM1	monomer	1.385	1.249	1.521	0.971	1.0959	1.0967			119.8	128.9	107.7
	dimer I	1.368	1.259	1.524	0.988	1.0961	1.0970	2.710		121.3	126.3	109.0
	dimer II	1.372	1.256	1.524	0.986	1.0961	1.0970	2.741	2.975	121.0	127.1	109.2
		1.383	1.255	1.520	0.971	1.1053	1.0959			118.8	129.0	107.9
							1.0980					
PM3	monomer	1.355	1.218	1.497	0.952	1.0973	1.0979			115.7	129.1	109.9
	dimer I	1.339	1.228	1.499	0.967	1.0974	1.0980	2.741		117.5	126.8	112.1
	dimer II	1.341	1.225	1.500	0.967	1.0973	1.0979	2.741	2.934	117.5	127.3	112.4
		1.348	1.226	1.492	0.953	1.1148	1.0973			114.6	128.7	110.0
HF/6-31G	monomer	1.355	1.211	1.489	0.954	1.0775	1.0821			121.7	126.3	113.8
	dimer I	1.326	1.227	1.489	0.973	1.0772	1.0821	2.714		122.6	123.9	115.8
	dimer II	1.336	1.219	1.491	0.967	1.0776	1.0822	2.763	3.402	122.8	124.6	115.9
		1.345	1.220	1.487	0.955	1.0772	1.0825			120.4	126.4	114.2
HF/6-31G(d)	monomer	1.332	1.187	1.502	0.952	1.0793	1.0838			122.4	125.8	108.1
	dimer I	1.308	1.201	1.501	0.966	1.0794	1.0838	2.794		123.6	123.6	110.8
	dimer II	1.318	1.193	1.504	0.961	1.0797	1.0840	2.863	3.479	123.6	124.4	110.5
		1.325	1.195	1.499	0.953	1.0783	1.0841			121.3	126.1	108.5
HF/6-31G(d,p)	monomer	1.331	1.187	1.501	0.948	1.0794	1.0840			122.3	125.7	108.3
	dimer I	1.306	1.201	1.501	0.962	1.0794	1.0839	2.779		123.6	123.5	111.0
	dimer II	1.316	1.193	1.503	0.957	1.0797	1.0841	2.855	3.461	123.6	124.3	110.8
		1.323	1.196	1.498	0.948	1.0786	1.0842			121.2	126.0	108.7
HF/D95++(d,p)	monomer	1.333	1.190	1.505	0.950	1.0798	1.0842			122.2	125.7	108.6

Table II. Cont.

Methods and Structures		R_{C-O}	R_{O-O}	R_{CC}	R_{O-H}	R_{C-H}[a]	R_{C-H}[b]	$R_{O..O}$	$R_{O..C}$	α_{O-C-O}	α_{C-C-O}	α_{C-O-H}
MP2/6-31G	monomer	1.403	1.249	1.508	0.985	1.0934	1.0967			122.1	126.9	109.6
	dimer I	1.368	1.264	1.507	1.004	1.0931	1.0967	2.763		123.4	123.8	112.6
	dimer II	1.381	1.256	1.510	0.995	1.0935	1.0967	2.833	3.393	123.3	125.0	112.3
		1.391	1.256	1.504	0.986	1.0933	1.0971			120.7	126.9	110.8
MP2/6-31G(d)	monomer	1.361	1.217	1.500	0.979	1.0883	1.0921			122.6	126.4	105.5
	dimer I	1.330	1.233	1.499	1.000	1.0883	1.0921	2.742		124.3	123.3	109.1
	dimer II	1.344	1.223	1.503	0.990	1.0884	1.0922	2.828	3.349	124.1	124.6	108.5
		1.352	1.226	1.494	0.980	1.0883	1.0925			121.1	126.7	106.0
MP2/6-31G(d,p)	monomer	1.360	1.216	1.500	0.970	1.0830	1.0868			122.7	126.3	105.4
MP2/D95++(d,p)	monomer	1.365	1.221	1.506	0.973	1.0864	1.0903			122.5	126.3	105.7
MP2/6-311G++(d,p)	monomer	1.358	1.210	1.501	0.967	1.0877	1.0918			122.7	126.3	105.9
Experiment												
microwave[c]	monomer	1.357	1.209	1.494	0.970	1.090				123.8	126.2	105.9
microwave[d]	monomer	1.323	1.243	1.500	0.946	1.086				122.4	123.4[f]	108.4
gas electron diffraction[e]	monomer	1.364	1.214	1.520	0.97[f]	1.102				122.8	126.6	107.0[f]
gas electron diffraction[e]	dimer I	1.334	1.231	1.506	1.03[f]	1.102		2.684		123.4	123.6	110.0[f]
neutron diffraction[g]	solid (III)	1.321	1.206	1.501	1.011	1.078	1.050 1.052	2.631	3.429	121.9	124.9	110.5
X-ray diffraction[h]	solid (III)	1.319	1.226	1.479				2.624		121.3	124.9	

[a]H is in the plane of the heavy atoms. [b]H is out of the plane of the heavy atoms. [c]Reference 18a. [d]Reference 18b. [e]Reference 19. [f]Estimated value. [g]At -140 °C. Reference 10c. [h]The results of reference 10b interpolated to -140 °C by reference 10c.

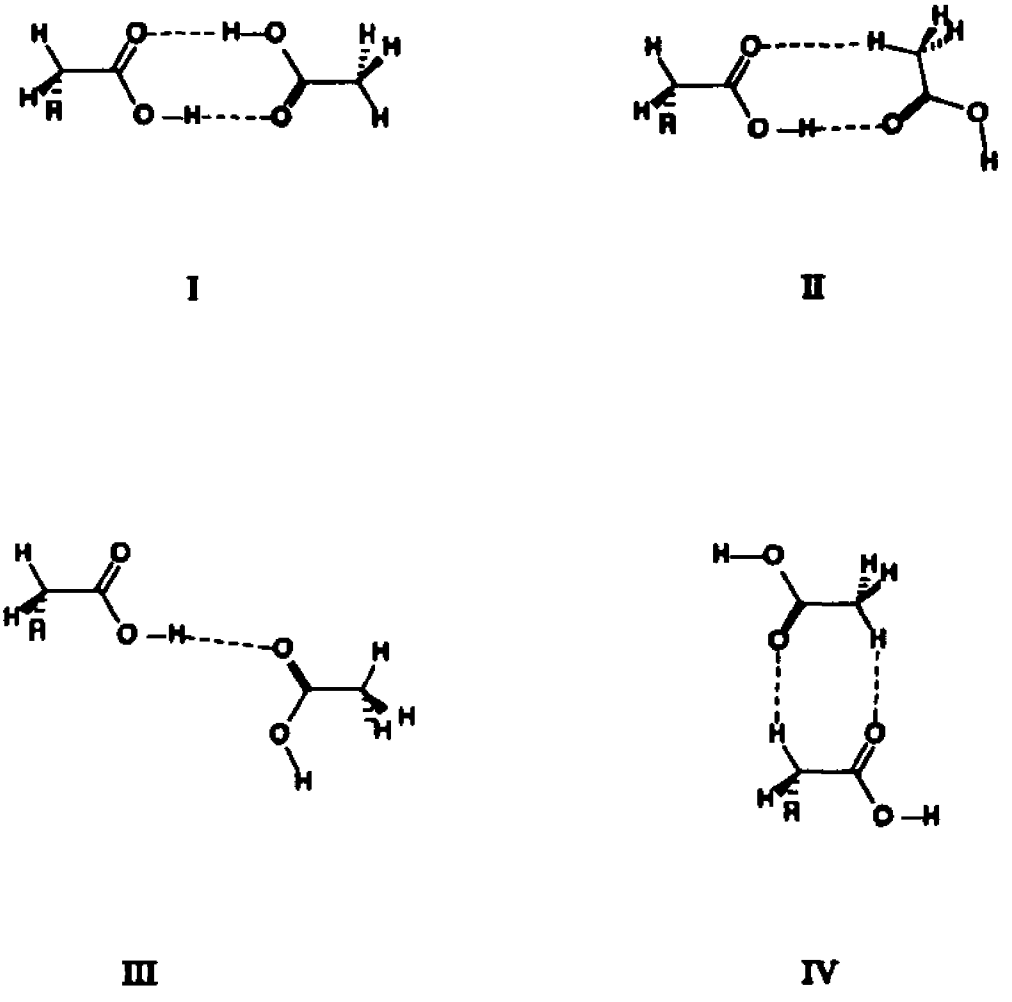

I II III IV

Figure 2. Four possible hydrogen-bonding patterns in acetic acid dimers.

Table III collects the hydrogen-bonding energies of the optimized dimers I and II. Except for HF/6-31G, the ab initio methods all predict ΔH of -11.2 to -11.8 kcal/mol for I. Reported experimental values are -13.8 to -17.0 kcal/mol,[3,4,6] which are greater in magnitude. Among the semiempirical methods, SAM1 predicts -8.1, PM3, -8.9; and AM1, -6.4 kcal/mol. Multiplying the AM1 value by 1.9 as suggested in a previous study[2] (or

Table III. Hydrogen-Bonding Energies (kcal/mol) of Acetic Acid Dimers I and II

Method		Hydrogen bonding energies				Enthalpies at 298.15 K
		without corr.	after CP	after ZPVE	after CP+ZPVE	
HF/6-31G	I	-19.5	-16.7	-17.8	-15.0	-15.0
	II	-11.5	-9.6	-10.2	-8.4	-8.0
HF/6-31G(d)	I	-15.6	-13.1	-14.0	-11.5	-11.3
	II	-8.8	-7.1	-7.6	-6.0	-5.6
HF/6-31G(d,p)	I	-15.5	-13.2	-14.0	-11.7	-11.6
	II	-8.8	-7.2	-7.7	-6.1	-5.7
MP2/6-31G	I	-18.8	-13.2	-16.8	-11.3	-11.2
	II	-11.2	-7.4	-9.8	-5.9	-5.6
MP2/6-31G(d)	I	-19.1	-13.5	-17.4	-11.8	-11.8
	II	-11.2	-7.3	-9.9	-6.0	-5.7
AM1	I					-6.4
	II					-4.9
SAM1	I					-8.1
	II					-5.0
PM3	I					-8.9
	II					-5.4
Experiment[a]	I					-13.8 - -17.0
	I					-14.2[b]

[a]References 3, 4 and 6 for dimer I. [b]Our preferred value from Reference 3b for dimer I.

by 1.7 as in Chapter V), gives -12.2 (-10.9) kcal/mol. One must consider the reasons for the discrepancies between the calculated and experimental enthalpies. I believe they come from overcorrection of the calculations. The uncorrected binding energies are all too large. Correction for BSSE or ZPVE reduces them to the approximate experimental range; however correction for both lowers the values too much. The problem arises from the fact that CP correction reduces the depth of the potential well. Since the vibrational frequencies are calculated for the original potential well, they are too large, leading to an artificially excessive ZPVE. In principle, the ZPVE should be calculated on the BSSE

corrected surface. The effect of CP correction of the potential surface upon the intermolecular vibrations has been illustrated by Bouteillier.[21] This phenomonon has already been discussed in Chapters II and IV. Chapter II also indicated that the validity of the CP correction for BSSE remains controversial. Moreover, the accuracy of the experimental reports has been questioned by Mathews and Sheets,[36] who attributed the larger reported stabilizations to problems involving surface adsorption. Their preferred value (-14.21 kcal/mole), however, is still larger than those calculated here.

Table II also presents the geometrical data for dimers I and II. As for the cis monomer, the HF calculations agree poorly with the experimental gas phase structure. Only MP2/6-31G(d) agrees adequately with experiment. Curiously, all ab initio methods (except HF/6-31G) predict similar association energies (Table III) although the HF methods predict poor geometries for both the monomeric and dimeric acids. Del Bene has suggested that HF/6-31G(d) is a good basis set for H-bond calculations due to a fortuitous cancellation of errors.[22] The present results support that conclusion about the interaction energies, but not for the optimized geometries.

The ab initio methods (again except 6-31G) predict II to have H-bonding enthalpies of -5.6 to -5.7 kcal/mol (Table III). Among the semiempirical methods, PM3 is closest (-5.4), while AM1 and SAM1 predict slightly weaker interactions. A recent study suggested that AM1 is accurate for CH..O interactions, while SAM1 overestimates them and PM3 is erratic (see Chapter IV).[11]

In an infinite one dimensional aggregate similar to the crystalline arrangement, each acetic acid molecule forms two pairs (one OH..O and one CH..O) of H-bonds (see

Figure 3). On the other hand, each carboxylic acid in a crystal constructed from dimers analogous to I can only form one pair (2 OH..O) of H-bonds. If the H-bonding energy of II be more than half that of I, this would be sufficient to suggest that infinite chains of II be enthalpically preferred before cooperativity or interactions in the second and third dimensions are considered. If one assumes that each OH..O interaction energy is the same in both dimers, then the additional stabilization (before cooperativity is considered) is due to the two CH..O

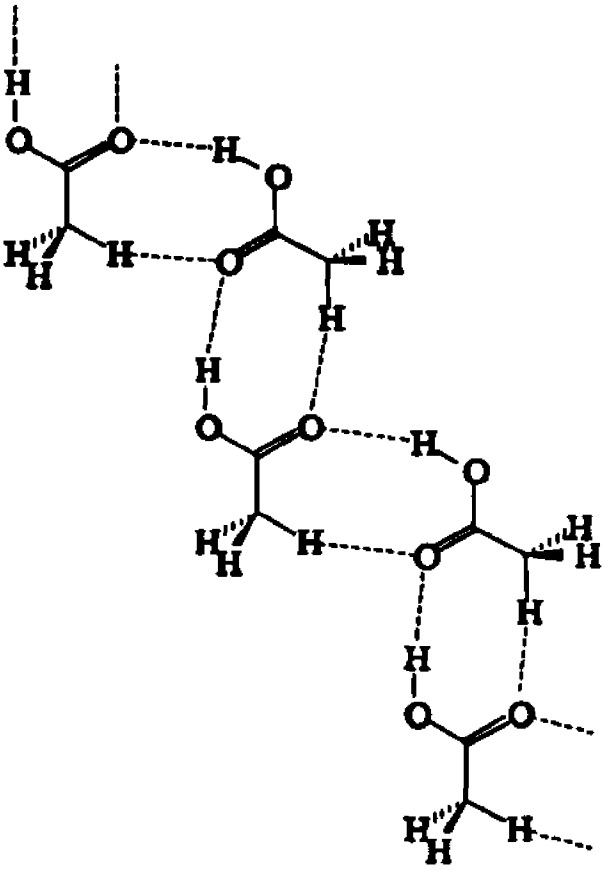

Figure 3. Orientation of acetic acid molecules in the hydrogen-bonded chains of the crystal structure.

(in addition to the 2 OH..O) interactions that occur in infinite chains of dimer II. The data of Table III indicate that this condition is not met for all ab initio calculations, indicating that cooperativity will probably play an important role in determining the crystal structure. This subject will be further pursued in later sections. The semiempirical calculations appear to suggest that the cooperativity is not necessary to achieve the preference of infinite chains with interactions similar to II. This can easily be seen as an artifact due to the underestimation of the stability of I by all three semiempirical methods. From

Table II, one can see that the calculated geometrical parameters for II are significantly different from those taken from the crystal data. This observation is consistent with the assessment that cooperativity is important to determining the crystal structure.

One can estimate the energy of the CH..O interaction in several different ways. First, again assuming that each OH..O interaction is energetically equivalent in both dimers, the CH..O interaction energy should be the difference between the stabilization of II less half that of I. Using the results for the highest level calculation [MP2/6-31G(d)], the CH..O interaction becomes -1.54, -0.56, -1.17, -0.10, and +0.22 kcal/mol respectively for uncorrected, CP corrected, ZPVE corrected, both corrections, and enthalpy at 298 K, respectively. Thus, the stabilization due to the CH..O interaction, apparent in the original calculation, becomes attenuated and eventually disappears upon application of all corrections. While acetic acid is liquid at 298 K, I do not attribute this to an enthalpically repulsive CH..O interaction. Rather, I believe that the calculated enthalpies are too low due to the overcorrection discussed above.

Another method of estimating the strength of the CH..O bond involves comparison of II with III, where the CH..O interaction is absent. In III, a cis monomer hydrogen bonds to a trans acetic acid with one O-H..O H-bond. (Using two cis acids would have resulted in an additional attractive interaction between the acidic hydrogen and the oxygen atom of the OH group.) The hydrogen bonding energies and enthalpies of dimer III are collected in Table IV. The ab initio calculations predict a consistent H-bonding enthalpy of -4.4 to -4.8 kcal/mole. The difference in the stabilizations for III and II (ΔE_{III} - ΔE_{II}) should correspond to the C-H..O stabilization. The MP2/6-31G(d) values are 3.16, 1.75,

2.73, 1.32, and 1.01 kcal/mol depending on the extent of correction.

A third method of estimating the CH..O interactions involves consideration of dimer IV, a cyclic complex with two C-H..O hydrogen bonds. Half the interaction energy should represent the stabilization due to one CH..O H-bond. Its H-bonding energies and enthalpies are presented in Table IV. These data suggest the H-bonding enthalpy of one C-H..O interaction to be in the range of -0.40 to -0.53 kcal/mole. These, presumably underestimated values (see the discussion above about the overcorrection of ZPVE and CP corrections), are smaller than those determined by the semiempirical methods.

Although these approximations give slightly different estimates of the C-H...O interaction energy, they suggest a value of slightly less than 1 kcal/mol (considering the overcorrection when CP and ZPVE corrections are both applied), which is in agreement with previous estimates of other C-H...O interactions.[11]

The H-bonding energy of III plus the half of the interaction energy of IV can be compared to the H-bonding of II. Since II contains one OH..O and one CH..O interaction, this provides a test of the additivity of the individually determined OH..O (from III) and CH..O (from IV) interactions energies. At the best ab initio level, the interaction energy of dimer II is greater than the sum by 0.55, 0.51, 0.55, 0.51 and 0.48 kcal/mole for the uncorrected, CP corrected, ZPVE corrected, CP and ZPVE corrected energies and enthalpy at 298 K, respectively. Thus, the interaction energy of II is consistently 0.5 kcal/mol stronger than the sum of the estimated individual OH..O and CH..O interactions independent of the extent of correction.

In all calculations the interaction energies of III are less than half of that of I. At

Table IV. Hydrogen-Bonding Energies (kcal/mol) of Acetic Acid Dimers III and IV

Method		Hydrogen bonding energies				Enthalpies at 298.15 K
		without corr.	after CP	after ZPVE	after CP+ZPVE	
HF/6-31G[a]	III	-	-	-	-	-
	IV	-4.3	-3.2	-3.6	-2.5	-1.8
HF/6-31G(d)	III	-6.3	-5.3	-5.5	-4.5	-4.4
	IV	-3.3	-2.1	-2.6	-1.5	-0.8
HF/6-31G(d,p)	III	-6.2	-5.3	-5.5	-4.6	-4.5
	IV	-3.4	-2.2	-2.7	-1.6	-0.9
MP2/6-31G	III	-8.1	-5.8	-7.1	-4.8	-4.8
	IV	-5.1	-2.4	-4.2	-1.5	-1.0
MP2/6-31G(d)	III	-8.0	-5.6	-7.1	-4.7	-4.7
	IV	-5.2	-2.5	-4.4	-1.6	-1.1
AM1	III					-2.8
	IV					-3.6
SAM1	III					-1.9
	IV					-2.8
PM3	III					-3.2
	IV					-2.1

[a]No minimum observed at HF/6-31G level.

the MP2/6-31G(d) level the difference (ΔE_t - $2\Delta E_m$) is -3.06, -2.38, -3.14, -2.46 and -2.46 kcal/mol for uncorrected, CP corrected, ZPVE corrected, CP and ZPVE corrected energies and enthalpy at 298 K, respectively. The values for the CP-corrected interactions are about 0.6 kcal/mole lower indicating larger BSSE in I than III. The observations that I is stabilized by 2.4-3.1 kcal/mol more than twice the OH..O stabilization of III, while II is stabilized by 0.5 kcal/mol more than expected from the CH..O and OH..O interactions determined from III and IV suggest that there might be a cooperative interaction inherent in the cyclic H-bonding structures of I and II. This suggestion is reinforced by comparison of the structures of the monomer and the various dimers. The

shortening of the C-O bonds and the O...O distances, and the lengthening of the C=O and O-H bonds are all more pronounced in the structure of dimer I than II.[23] One should note that IV is also cyclic. Therefore, there may already be some cooperativity in the estimate of the CH..O interactions derived from it (we were unable to find a conformationally stable structure with only one CH..O interaction). Thus the 0.5 kcal/mol for the cooperativity in II might be slightly low.

The optimized C-H bond distances have also been included in Table II. The in-plane are consistently shorter than the out-of-plane C-H bond lengths, in accord with previous reports.[20a,24] The difference between the two distinct C-H bond types for acetic acid has been reported to be constant (0.0052-0.0053 Å) for HF/4-21G and HF/5-31G** optimizations.[24] The present data suggest that these values to be 0.0044-0.0046 Å for HF and 0.0033-0.0041 Å for MP2 calculations, in conflict with the earlier findings.

Vibrational analysis

Tables V and VI contain the calculated and the experimental vibrational frequencies of cis acetic acid and dimer I, while Tables VII, presents statistical analyses of comparisons to experimental frequencies. Previous ab initio (4-31G) frequency calculations have been reported for monomeric acetic acid[7c].

In Table V, the calculated frequencies are listed corresponding to the observations of Haurie and Novak,[25] Maréchal,[26] Bertie and Michaelian,[27] and Zelsmann, et al.[28]

All the assignments are straightforward except for δ(O-H), the O-H in-plane bend, and ν(C-O), the C-O stretch, which are strongly coupled. I assign the lower frequency to

Table V. Calculated and Experimental Frequencies of Acetic acid Monomer[a]

vibrations	AM1	PM3	SAM1	Hartree-Fock					MP2					Exp.
				I	II	III	IV	V	I	II	III	IV	V	
$\tau(CH_3)$ A"	23.0	37.5	56.3	110.4	100.8	102.9	98.9	96.3	99.8	90.5	90.7	58.4 (0.6)	43.4	93[b,c]
γ(O-H) A"	521.3	506.4	527.8	588.4	587.2	584.6	579.2	582.3	549.4	557.6	554.7	531.3 (48.8)	542.1	534[b]
δ(C-C-O) A'	418.1	394.7	406.7	452.6	451.1	452.0	454.7	452.2	423.8	427.6	426.6	429.1 (3.9)	426.1	581[b] 448.0[d]
δ(O=C-O) A'	570.1	466.4	556.8	621.6	637.4	638.0	640.4	636.3	568.0	585.9	584.4	589.2 (38.6)	579.8	642[b]
γ(C-C=O) A"	589.1	570.2	597.1	701.1	725.3	721.3	705.6	706.7	652.9	695.3	690.5	640.8 (82.9)	644.9	642[b]
ν(C-C) A'	1100.2	961.5	1027.7	930.8	938.3	937.4	931.7	935.4	845.4	888.3	888.0	880.9 (6.7)	877.8	847[b] 850.9[d]
$\rho_r(CH_3)$ A'	1038.7	977.5	1004.7	1127.8	1113.9	1106.6	1101.3	1104.3	1027.3	1035.4	1032.2	1015.8 (69.7)	1025.4	989[b] 988[e]
$\rho_w(CH_3)$ A"	1073.4	1007.6	1046.8	1205.0	1183.8	1175.5	1170.3	1172.2	1122.9	1103.8	1098.3	1072.3 (5.4)	1081.0	1048[b] 1075[e]
ν(C-O) A'	1549.7	1450.0	1433.9	1298.4	1355.1	1346.3	1339.0	1343.9	1190.7	1239.8	1232.0	1222.9 (218.8)	1224.3	1182[b] 1178[e]
δ(O-H) A'	1430.4	1240.6	1285.3	1483.4	1483.5	1474.0	1453.4	1461.8	1370.8	1388.1	1382.2	1349.6 (43.5)	1356.8	1264[b] 1280[e]
$\delta_s(CH_3)$ A'	1412.8	1355.4	1344.0	1584.4	1574.1	1562.8	1546.6	1555.7	1482.7	1469.3	1465.7	1428.8 (66.2)	1446.7	1382[b] 1395[e]
$\delta_s'(CH_3)$ A'	1364.2	1386.7	1355.6	1624.0	1613.7	1596.3	1586.8	1589.0	1553.9	1537.2	1534.9	1492.3 (14.0)	1509.7	1430[b]
$\delta_a(CH_3)$ A"	1371.7	1385.8	1363.1	1630.0	1619.6	1604.0	1594.9	1597.7	1550.4	1538.9	1539.3	1493.0 (9.9)	1510.4	1430[b]
ν(C=O) A'	2087.7	1981.6	1998.0	1925.4	2040.6	2038.6	2002.2	2014.3	1720.7	1862.0	1862.7	1826.2 (302.9)	1826.0	1788[b] 1788[e]

Table V. Cont.

vibrations	AM1	PM3	SAM1	Hartree-Fock					MP2					exp
				I	II	III	IV	V	I	II	III	IV	V	
$\nu_s(CH_3)$ A'	3153.0	3176.0	2968.7	3223.4	3231.8	3211.4	3193.6	3219.9	3091.2	3132.3	3156.8	3107.3 (1.7)	3140.0	2944[b] 2954.1[d]
$\nu_a(CH_3)$ A"	3058.4	3083.6	2899.3	3294.4	3295.4	3279.0	3256.9	3294.2	3174.8	3218.0	3249.9	3192.8 (2.4)	3241.6	2996[b]
$\nu_a'(CH_3)$ A'	3069.4	3091.1	2906.9	3341.5	3345.1	3327.8	3303.0	3340.9	3207.1	3257.4	3289.1	3232.5 (3.1)	3280.9	3051[b]
ν(O-H) A'	3431.2	3854.1	3397.2	3992.2	4054.3	4129.9	4117.4	4132.4	3596.8	3696.4	3818.7	3812.5 (73.7)	3814.4	3583[b] 3583[e]

[a]For the best ab initio calculation (MP2/6-311G++(d,p)), the calculated IR intensities are in parentheses. Frequencies in cm^{-1}, intensities in km/mol. Basis sets: *I.* 6-31G; *II.* 6-31G(d); *III.* 6-31G(d,p); *IV.* 6-311G++(d,p); *V.* D95++(d,p). [b]Reference 25. [c]Calculated value from Reference 25. [d]Reference 27. [e]Reference 26.

the C-O stretching vibration as it is predicted to have the higher intensity by all ab initio methods in accord with expectations for a C-O stretch and Maréchal's assignment.[26]

All ab initio methods predict the same order with one exception: at the MP2/6-31G level the asymmetric appears at higher frequency than the symmetric methyl deformation. All MO methods (both ab initio and semiempirical) predict the δ(C-C-O) in-plane torsion to appear at lower frequency than γ(O-H), the wagging motion of the O-H hydrogen. Sverdlov[29] assigned a band at 452 cm^{-1} to the δ(C-C-O) vibration, but his proposal was ignored for about 25 years. Raman studies[3a,27] reopened the assignment of the sharp monomer band found at 448 cm^{-1}. As all the calculations agree with Sverdlov and the Raman studies, I assign the δ(C-C-O) vibration to the band at 448 cm^{-1}. The qualitative order of the semiempirical frequencies is different form that of the ab initio calculations. The stretching vibrations are generally overestimated, while the frequencies of methyl distortions (which are approximately correct) are in the wrong order.

Table VI presents the calculated and experimental frequencies for dimer I. In the dimer, each monomer vibration is doubled, resulting in pairs of symmetric (g) and unsymmetric (u) frequencies that are alternatively Raman and IR active. While the frequency shifts and splittings for most pairs are small, several large shifts and splittings are observed. They are particularly apparent for those vibrations that should be most affected by the H-bonding interactions, such as the O-H stretches (which weaken) and out-of-plane deformations (which stiffen substantially).

The statistical analyses of Table VII indicate that the HF ab initio methods tend to overestimate the frequencies. Surprisingly, the semiempirical have smaller errors than

Table VI. Calculated and Experimental Frequencies of Acetic Acid Dimer I[a]

Vibrational modes	AM1	PM3	SAM1	HF			MP2		Experiment
				I	II	III	I	II	
Intermolecular frequencies									
γ(twist) A_u	43.8	53.7	61.5	84.3	72.9	73.2	78.2	72.0 (0.0)	48.5[b]
γ(O-H..O) A_u	21.0	41.3	30.9	55.4	48.9	49.7	51.7	50.7 (4.3)	56.0[b]
γ(O-H..O) B_g	50.9	82.7	82.5	120.8	117.7	118.1	123.0	128.2	98.9[c]
δ(O-H..O) A_g	68.5	135.0	120.1	162.2	154.1	153.9	154.8	157.1	120.0[c]
ν(O-H..O) A_g	141.2	285.5	204.7	180.0	165.2	159.6	172.2	178.4	155.0[c]
δ(O-H..O) B_u	128.3	220.3	182.9	168.2	157.8	153.9	167.6	174.3 (23.1)	171.0[b]
Intramolecular frequencies									
τ(CH_3) B_g	19.6	34.5	40.8	90.9	83.6	84.0	83.3	79.9	
τ(CH_3) A_u	22.2	33.5	35.2	99.5	91.6	91.9	88.9	86.6 (0.4)	
δ(C-C-O) A_g	422.0	421.1	419.1	467.0	467.6	468.6	441.0	446.1	438.7[c]
δ(C-C-O) B_u	447.5	557.5	472.6	499.8	494.4	493.1	475.5	483.3 (34.3)	
γ(C-C=O) B_g	539.8	563.8	542.7	646.0	655.9	654.9	586.5	609.9	616.2[c]
γ(C-C=O) A_u	538.4	562.9	542.4	639.8	646.4	645.3	582.1	601.4 (0.3)	
δ(O-C=O) A_g	582.1	572.5	595.7	655.4	668.1	668.4	607.8	627.1	616.2[c]
δ(O-C=O) B_u	567.6	497.7	584.3	655.7	668.0	670.1	611.6	632.4 (53.5)	623.0[d]
ν(C-C) A_g	1101.1	988.4	1034.0	960.7	967.7	967.6	887.3	925.0	891.7[c]
ν(C-C) B_u	1100.6	974.5	1034.9	959.6	968.2	968.7	882.4	923.8 (3.8)	896.0[d]
γ(O-H) B_g	602.0	647.7	682.2	978.0	909.3	913.3	930.1	941.1	
γ(O-H) A_u	629.7	679.7	703.0	1032.2	963.1	966.9	972.7	987.4 (254.2)	942.0[d]
ρ_s(CH_3) A_g	1041.1	983.5	1009.5	1153.1	1131.3	1123.8	1072.9	1063.8	1007.0[c]
ρ_s(CH_3) B_u	1041.2	987.0	1009.8	1156.8	1133.6	1125.9	1078.6	1066.3 (37.2)	1014.0[d]
ρ_a(CH_3) B_g	1072.7	1007.6	1044.6	1207.4	1185.9	1177.7	1126.9	1106.8	1065.0[c]
ρ_a(CH_3) A_u	1073.2	1008.5	1045.4	1209.0	1187.1	1179.0	1128.3	1107.5 (11.3)	1066.0[d]
ν(C-O) A_g	1569.1	1491.9	1479.2	1405.7	1436.8	1436.9	1280.0	1342.1	1285.0[c]
ν(C-O) B_u	1575.0	1497.1	1482.6	1396.9	1436.4	1436.1	1285.8	1349.9 (365.2)	1290.0[d]

Table VI. Cont.

Vibrational modes	AM1	PM3	SAM1	HF			MP2		Experiment
				I	II	III	I	II	
$\delta_s(CH_3)/\delta(O\text{-}H)$ A_g[f]	1410.6	1361.2	1348.6	1559.1	1539.9	1527.8	1460.1	1447.6	1370.2[c]
$\delta_s(CH_3)/\delta(O\text{-}H)$ B_u[f]	1409.7	1360.4	1348.0	1551.2	1521.7	1510.1	1455.2	1435.9 (1.4)	
$\delta_s(CH_3)/\delta(O\text{-}H)$ A_g[f]	1422.9	1291.0	1295.7	1592.1	1599.2	1586.8	1485.6	1516.2	1428.3[c]
$\delta_s(CH_3)/\delta(O\text{-}H)$ B_u[f]	1424.0	1272.1	1289.2	1596.4	1598.6	1587.6	1488.5	1505.4 (208.6)	1430.0[d]
$\delta_s'(CH_3)$ A_g	1364.6	1389.4	1358.2	1626.6	1620.2	1612.1	1554.2	1540.3	1428.3[c]
$\delta_s'(CH_3)$ B_u	1364.7	1388.8	1358.3	1622.0	1614.6	1603.1	1551.5	1535.5 (52.2)	1430.0[d]
$\delta_s(CH_3)$ B_g	1372.1	1385.5	1364.6	1629.7	1619.6	1604.0	1550.0	1538.1	
$\delta_s(CH_3)$ A_u	1372.1	1385.5	1364.6	1629.7	1619.6	1604.0	1550.0	1538.1 (19.5)	
$\nu(C=O)$ A_g	2062.7	1918.5	1928.9	1852.3	1955.8	1951.1	1687.6	1789.4	1681.5[c]
$\nu(C=O)$ B_u	2077.4	1948.2	1964.3	1871.6	1993.3	1989.5	1694.8	1825.1 (625.2)	1737.0[d]
$\nu_s(CH_3)$ A_g	3153.7	3176.2	2967.5	3223.5	3232.5	3212.2	3091.2	3131.4	2954.1[c]
$\nu_s(CH_3)$ B_u	3153.6	3176.0	2967.4	3223.5	3232.5	3212.1	3091.2	3131.5 (1.3)	
$\nu_s(CH_3)$ B_g	3059.6	3083.0	2896.9	3294.2	3296.8	3280.2	3174.4	3217.4	
$\nu_s(CH_3)$ A_u	3059.7	3083.0	2896.9	3294.2	3296.8	3280.2	3174.4	3217.4 (3.5)	
$\nu_s'(CH_3)$ A_g	3070.0	3091.4	2904.7	3343.9	3344.7	3328.2	3207.8	3256.2	3035.0[e]
$\nu_s'(CH3)$ B_u	3070.0	3091.4	2904.8	3343.9	3344.8	3328.3	3209.1	3257.0 (10.3)	
$\nu(O\text{-}H)$ A_g	3373.9	3735.5	3120.9	3580.9	3766.9	3805.3	3215.0	3275.6	
$\nu(O\text{-}H)$ B_u	3385.6	3771.6	3155.7	3647.4	3813.6	3854.2	3295.2	3357.3 (2338.3)	2965.0[d]

[a]For the best ab initio calculation (MP2/6-31G(d)), the calculated IR intensities are in parentheses. Frequencies in cm^{-1}, IR intensities in km/mol. Basis sets: I. 6-31G; II. 6-31G(d); III. 6-31G(d,p). [b]Reference 28. [c]Reference 27. [d]Reference 26. [e]Calculated value from Reference 28. [f]The methyl and hydroxyl bends are strongly coupled.

the HF calculations, though the standard deviations are similar. The MP2 calculations provide the best results. The corrected assignment of δ(C-C-O) provides an improvement in the error analysis (about 15 cm^{-1} or 2 - 4 % in standard deviation). The analyses for the frequencies of dimer I show larger error. The assignment of the experimental frequencies is complicated by the somewhat broad peaks in the spectra. All MO calculations predict the two lowest intermolecular vibrations to be in the reverse order to the experimental assignments. Since they have the same symmetry (A_u), and the predicted IR intensity of one of them is close to zero, their relative assignment is difficult. I assign the lower frequency to the out-of-plane bend, rather than the twist.

Table VIII compares the calculated frequencies of the monomers (cis and trans) with those of all four dimers for the MP2/6-31G(d) calculations (the highest level used for dimer frequencies). Several comparisons are particularly interesting. The O-H stretches are both considerably weakened in I. For II, only one O-H stretch is weakened as there is but one H-bond. In III, the H-bond involves the O-H of the cis conformation, whose frequency decreases significantly while that of the trans barely changes. Dimer IV, which has no O-H H-bonds, shows little change in O-H stretch. The C=O stretches are weakened in all four dimers, but particularly in I. The frequencies for the C-O stretches and O-H deformations (which are strongly coupled) increase in each dimer, particularly for I. There are apparent weakenings of two C-H stretches (at 3132 and 3218 cm^{-1}) for one vibration in II and both in IV. Similarly, the methyl deformation at 1539 cm^{-1} increases for one vibration for II and both for IV.

The particularly large changes in the O-H, C=O and C-O vibrations for dimer I

Table VII. Statistical Analyses of Frequency Calculations[a]

Method:		AM1	PM3	SAM1	Hartree-Fock					MP2				
					I	II	III	IV	V	I	II	III	IV	V
monomers[b]														
ratio	average	1.037 (1.028)	0.995 (0.986)	0.998 (0.989)	1.099 (1.089)	1.107 (1.097)	1.103 (1.093)	1.095 (1.085)	1.099 (1.089)	1.023 (1.014)	1.043 (1.033)	1.044 (1.035)	1.023 (1.014)	1.030 (1.020)
	stand. dev.	0.119 (0.140)	0.111 (0.130)	0.093 (0.116)	0.046 (0.089)	0.044 (0.088)	0.043 (0.087)	0.038 (0.083)	0.041 (0.085)	0.052 (0.087)	0.044 (0.084)	0.045 (0.085)	0.039 (0.077)	0.044 (0.082)
abs. error	average	57.3 (53.3)	37.1 (32.7)	-8.6 (-12.6)	162.3 (158.3)	175.6 (171.6)	171.8 (167.8)	159.5 (155.5)	169.1 (165.1)	50.8 (46.8)	80.5 (76.5)	90.6 (86.6)	61.9 (57.9)	74.3 (70.3)
	stand. dev.	142.1 (150.7)	129.9 (137.0)	116.1 (122.4)	109.4 (125.2)	117.5 (132.4)	127.3 (140.8)	122.0 (135.1)	130.0 (143.0)	73.6 (89.0)	71.8 (88.4)	89.3 (103.6)	78.5 (91.7)	90.4 (103.3)
dimer I[c]														
ratio	average	0.961	1.033	1.001	1.132	1.116	1.113			1.061	1.077			
	stand. dev.	0.206	0.198	0.132	0.095	0.076	0.079			0.095	0.080			
abs. error	average	56.7	42.8	13.1	129.4	139.3	136.1			47.1	68.7			
	stand. dev.	159.3	184.1	114.4	128.5	158.5	163.1			73.4	78.2			

[a]Ratios are calculated over the experimental frequencies, while the absolute errors are the difference between calculated and experimental frequencies in cm^{-1}. Standard deviations are relative to the average values of different types of error. Basis sets: I. 6-31G; II. 6-31G(d); III. 6-31G(d,p); IV. 6-311G++(d,p); V. D95++(d,p). [b]Comparison made to the most recent values of References 26 and 27 (δ(C-C-O) is assigned to 448 cm^{-1}). The values in parentheses are compared to reference 25, where δ(C-C-O) is assigned to 581 cm^{-1}. [c]Comparison made to references 26-28.

Table VIII. Comparison of MP2/6-31G(d) Frequencies (in cm^{-1}) for Acetic Acid Monomers with the Intramolecular Frequencies of Dimers I, II, III and IV

Approximate vibrational modes	monomers		dimers			
	cis	trans	I	II	III	IV
$\tau(CH_3)$	90.5	128.2	79.9	84.5	98.1	155.2
			86.6	156.3	122.6	165.1
δ(C-C-O)	427.6	437.6	446.1	439.1	437.0	438.2
			483.3	452.6	447.7	441.6
δ(O-C=O)	585.9	597.7	627.1	601.7	595.3	588.8
			632.4	611.8	619.5	591.3
γ(C-C=O)	695.3	606.0	601.4	565.3	594.3	562.7
			609.9	598.0	612.4	563.1
γ(O-H)	557.6	466.2	941.1	707.4	478.4	699.1
			987.4	891.6	893.0	700.2
ν(C-C)	888.3	880.6	923.8	900.4	891.5	890.7
			925.0	908.9	901.6	892.7
$\rho_r(CH_3)$	1035.4	1025.5	1063.8	1053.3	1036.2	1045.2
			1066.3	1060.7	1047.3	1049.1
$\rho_r(CH_3)$	1103.8	1092.9	1106.8	1103.4	1096.3	1110.2
			1107.5	1115.3	1101.8	1112.2
ν(C-O)	1239.8	1245.6	1342.1	1255.8	1249.5	1244.3
			1349.9	1299.5	1286.0	1247.0
δ(O-H)	1388.1	1343.8	1505.4	1408.1	1459.2	1391.2
			1516.2	1427.0	1477.0	1397.8
$\delta_s(CH_3)$	1469.3	1454.4	1435.9	1480.9	1359.3	1478.3
			1447.6	1484.8	1416.7	1479.0
$\delta_a'(CH_3)$	1537.2	1540.4	1535.5	1537.5	1539.4	1539.5
			1540.3	1538.8	1546.9	1544.0
$\delta_a(CH_3)$	1538.9	1549.0	1538.1	1539.7	1537.4	1553.7
			1538.1	1557.4	1540.9	1557.9
ν(C=O)	1862.0	1884.3	1789.4	1825.7	1849.6	1844.9
			1825.1	1843.9	1864.2	1852.6
$\nu_s(CH_3)$	3132.3	3115.4	3131.4	3128.2	3117.6	3127.2
			3131.5	3130.6	3128.8	3127.4
$\nu_a(CH_3)$	3218.0	3196.7	3217.4	3213.4	3199.7	3211.3
			3217.4	3216.0	3214.1	3211.4
$\nu_a'(CH_3)$	3257.4	3252.8	3256.2	3254.7	3251.7	3258.5
			3257.0	3262.5	3256.6	3259.8
ν(O-H)	3696.4	3756.0	3275.6	3501.6	3535.4	3694.0
			3357.3	3689.4	3751.6	3694.2

(in comparison to the other dimers) provide additional evidence for strong cooperativity in the cyclic structure. The smaller changes in dimers II and IV suggest less cooperativity for these cases. On the other hand, the changes in the methyl vibrations of II and IV confirm the presence of CH..O H-bonding interactions.

4. The Crystal Structure of Acetic Acid: Aggregation in One, Two and Three Dimensions.

After summarizing the results for monomeric and dimeric acetic acids, I begin exploring the crystal structure itself whose organization is completely different from the characteristic features of both the gas and liquid phases. Instead of forming cyclic dimers (I) in the crystalline state, acetic acid molecules assemble in different hydrogen-bonding network corresponding to II and Figure 3. The infinite hydrogen-bonded chains contain both O-H...O and C-H...O interactions (Figure 4). The chains stack upon each other in the second direction involving weak C-H...O H-bonds between the chains (Figure 5). The third direction can be characterized by C-H...O interactions between the stacks, with each stack roughly perpendicular to each other (Figure 6).

The main structural features of the acetic acid crystal structure are illustrated on Figures 7 and 8. The structure is viewed along the *a* axis of the unit cell. The *b* and *c* axes translate the acetic acid molecules between stacked hydrogen-bonded 'one-dimensional' chains. The unit cell is orthorhombic, meaning that all angles of the unit cell are right angle. The diagonal (*d*) of the rectangle defined by *b* and *c* vectors translates

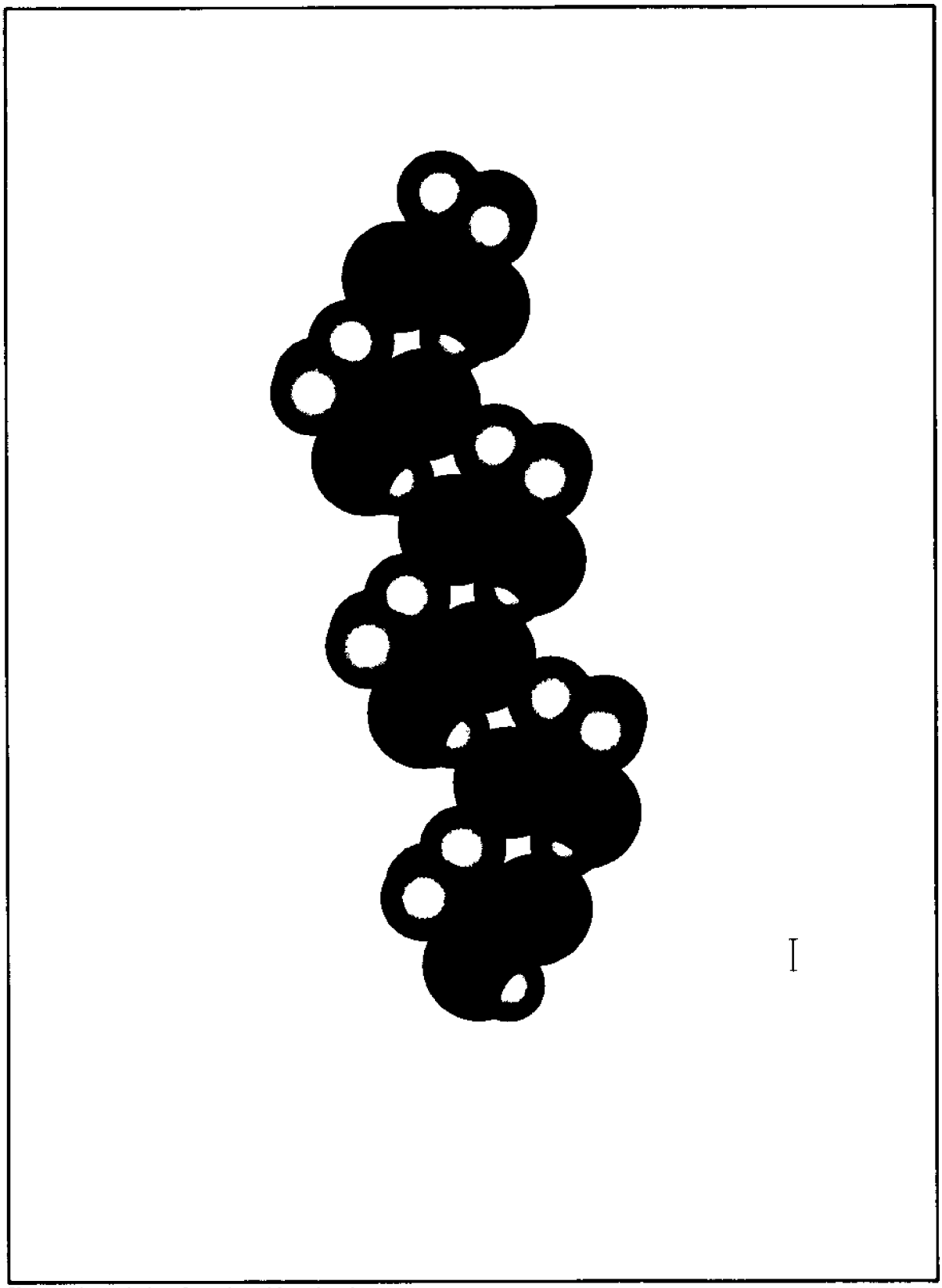

Figure 4. A chain of acetic acid molecules.

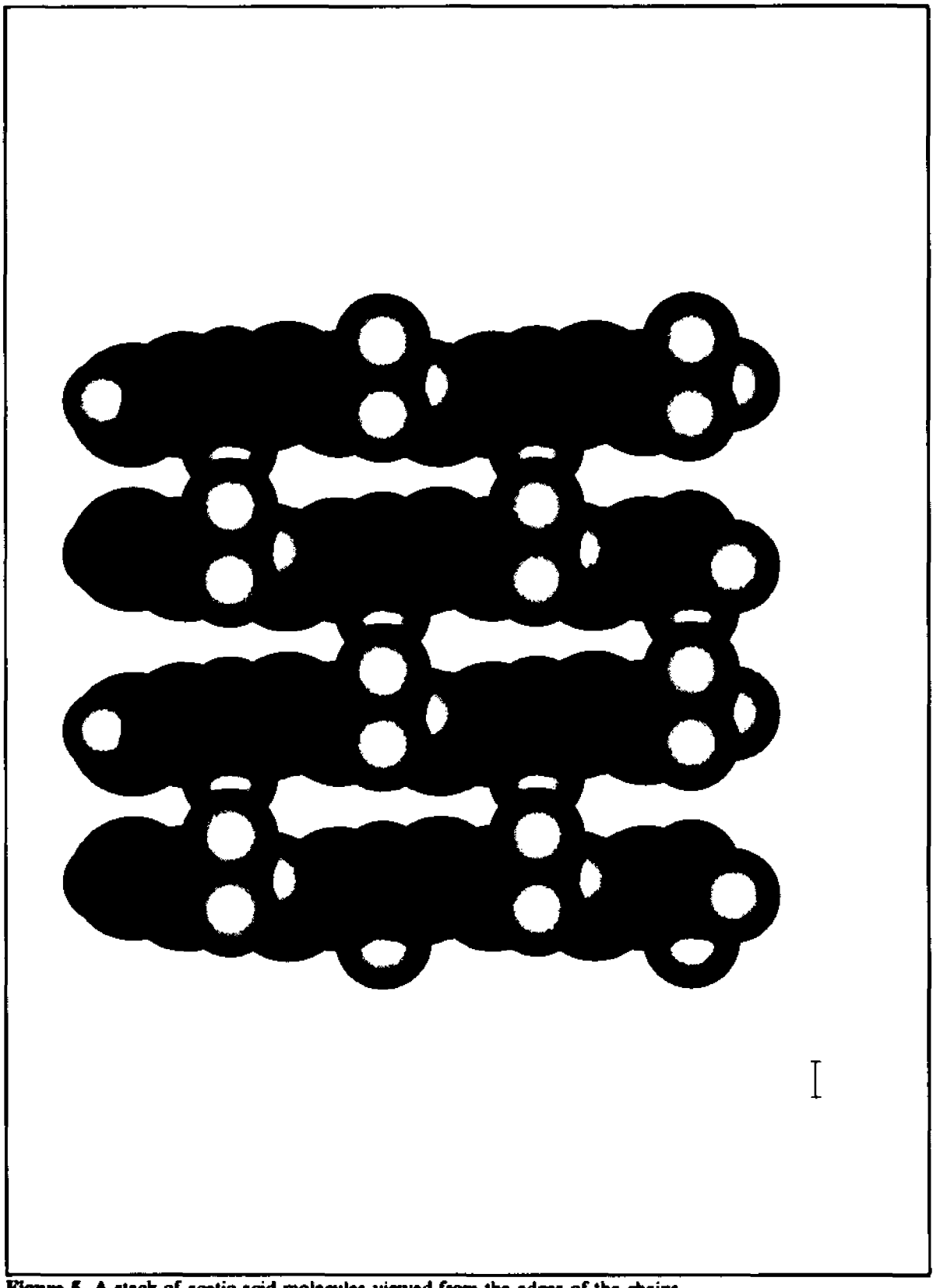

Figure 5. A stack of acetic acid molecules viewed from the edges of the chains.

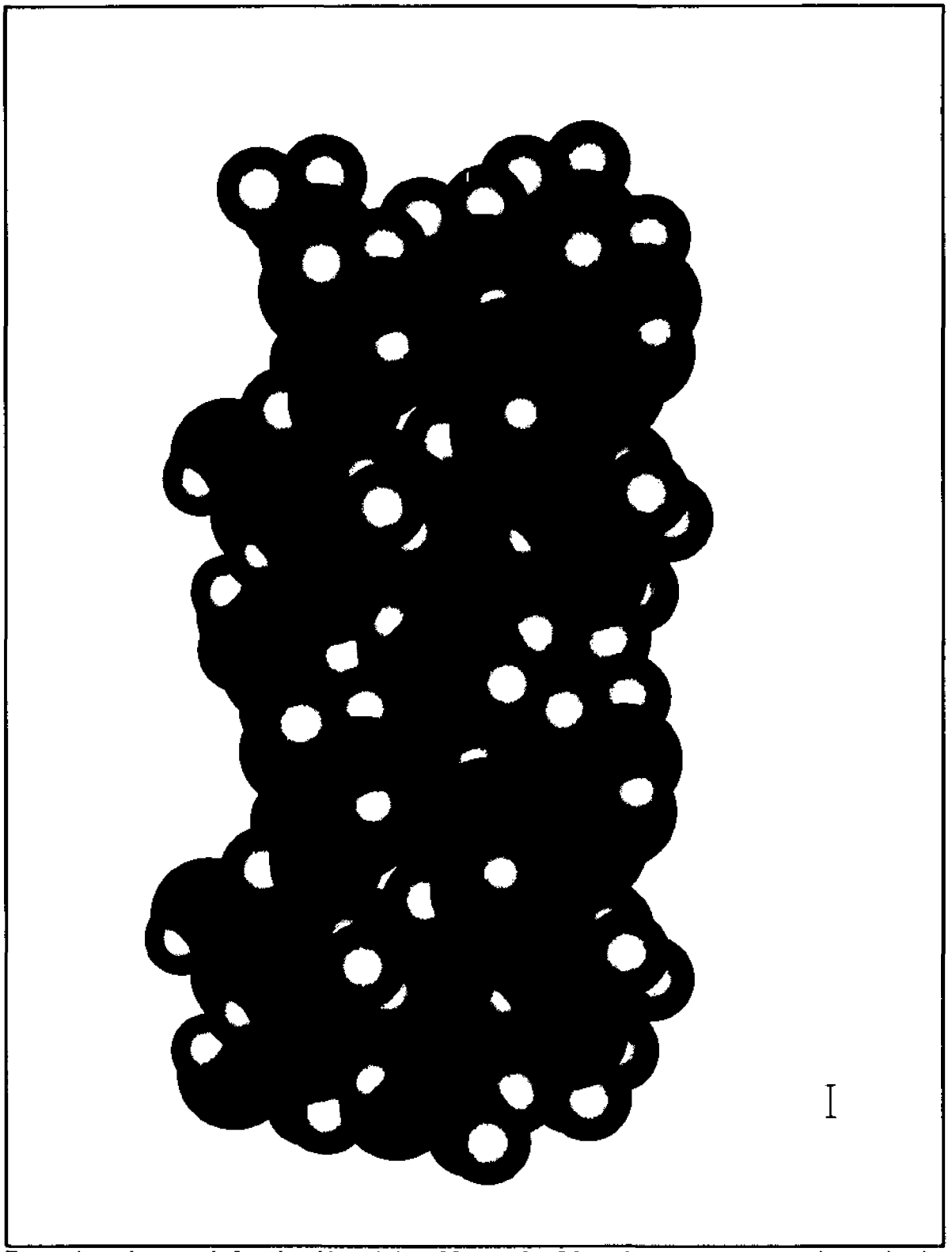

Figure 6. A microcrystal of acetic acid consisting of four stacks of three chains each containing three molecules (4/3/3). Note the C-H...O interactions between the stacks.

every second acetic acid molecule into each other within the hydrogen-bonded catemeric chains. On the top of this 'two-dimensional' structure another similar aggregate packs tightly from along the *a* axis roughly perpendicularly. The vector *a* then translates this structure periodically resulting in the three-dimensional crystal structure (Figures 6 and 8). The notation will be similar to that used in Chapter V for 1,3-diones. Thus, *L/C/M* will denote an aggregate containing *L* stacks of *C* chains, where the chains consist of *M* monomers. Thus the chains will be denoted by 1/1/*M* (or *M*), the stacks by 1/*C*/*M* (or *C*/*M*) and the three-dimensional aggregates by *L*/*C*/*M*.

Aggregation in the first direction: H-bonding chains

Tables IX-XI collect the energetic and geometrical results pertinent to the aggregation of hydrogen-bonding chains in the first direction. As can be seen from Figures 3, 4 and 7, every molecule participates in two pairs of H-bonding (one O-H..O and one C-H..O) interactions. Tables IX and X illustrate the gradual increase in the strength of the incremental H-bonding interactions: each additional acetic acid molecule interacts more strongly with the aggregate than the previous one. All MO methods predict strong cooperativity, except AM1. One can expect the incremental stabilization to asymptotically approach the value expected for an infinite chain. The stabilization between a theoretical infinite one-dimensional chain and an additional acetic acid molecule can be approximated by fitting an exponential function to the calculated interaction energies. Using equation V.2 as in Chapter V and a previous paper,[2] the strengthening is 1.17 kcal/mol or 10.2% (of the dimer interaction), 0.66 kcal/mol (7.7%),

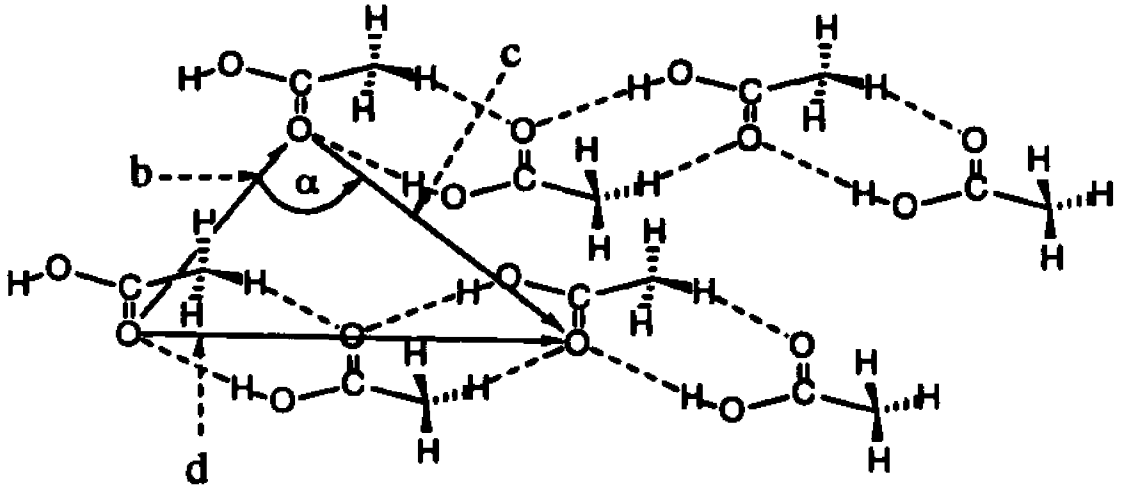

Figure 7. Schematic view of two acetic acid chains illustrating the cell parameters *b*, *c*, *d* and α.

0.22 kcal/mol (4.4%) and 0.29 kcal/mol (5.3%) for completely optimized HF/6-31G, HF/6-31G(d), SAM1 and PM3 methods, all of which have enough points to make reliable extrapolation. The cooperativity is approximately constant within the HF ab initio methods, weaker in semiempirical ones. I tested the validity of the geometrical constraint of keeping each acetic acid molecule in the same geometry by performing complete optimizations in several cases (indicated in parentheses in Tables IX and X). Clearly, the constraint has only a small effect upon the interaction energies, which tends to diminish as the aggregate continues to grow. For example, the difference in the incremental interaction energy at the HF/6-31G(d,p) level decreases from 0.20 to 0.09 kcal/mol upon going from dimer to tetramer.

Table X contains the corrected ab initio stabilizations for the same one-dimensional aggregates. As I emphasized on many occasions, the applications of CP correction for BSSE and ZPVE correction together overestimate the error of the

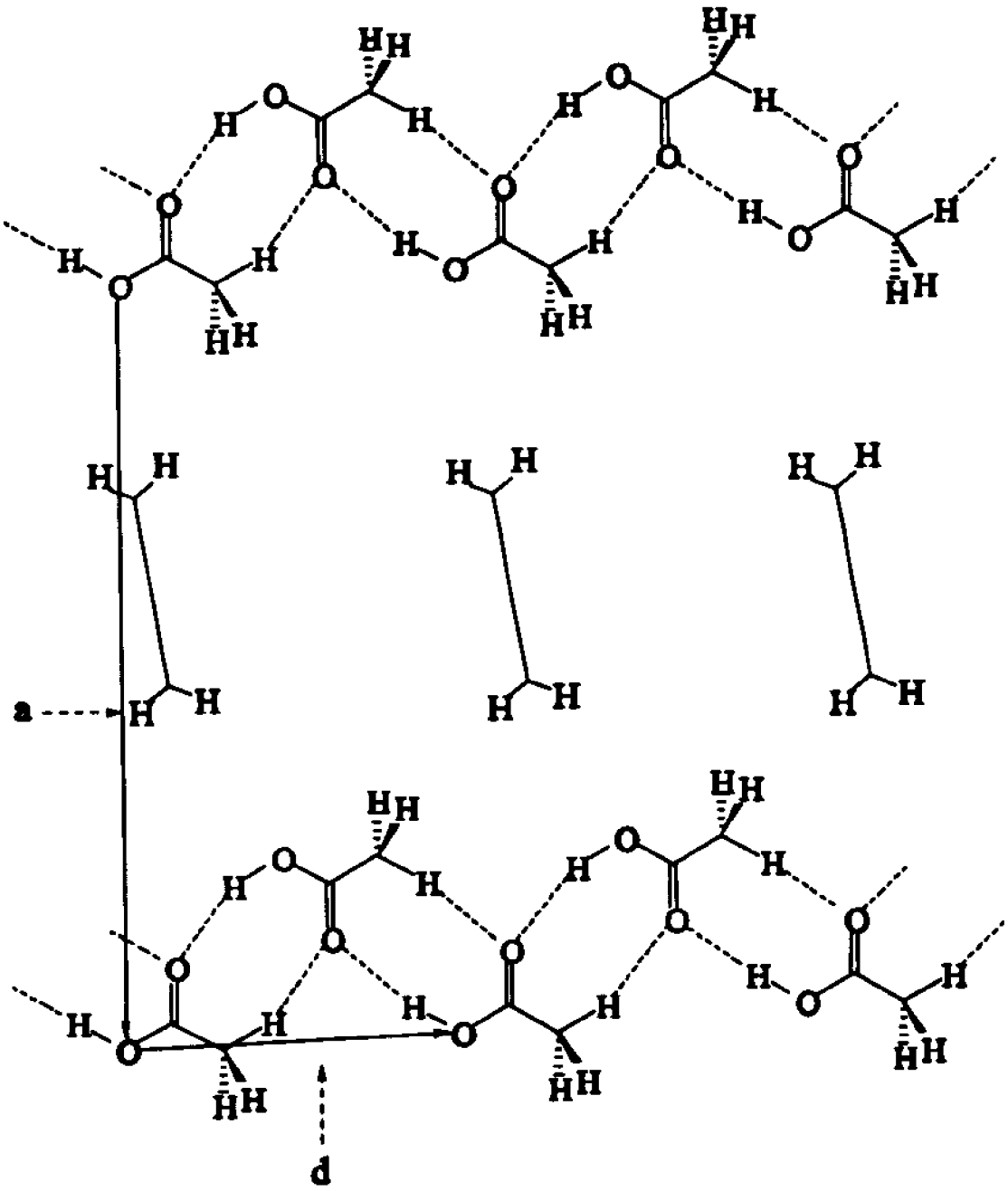

Figure 8. Schematic illustration of an acetic acid microcrystal illustrating the unit cell parameters *a* and *d*.

Table IX. Incremental Hydrogen-bonding Energies (and Enthalpies in AM1, PM3 and SAM1) of Different Acetic Acid Aggregates at Different Levels of Theory Without Corrections[a]

aggregates	Method							
	AM1	SAM1	PM3	HF/6-31G	HF/6-31G(d)	HF/6-31G(d,p)	MP2/6-31G	MP2/6-31G(d)[b]
dimer I	-6.37	-8.05	-8.86	-19.51	-15.54	-15.50	-18.75	-18.82
dimer II	-4.79 (-4.85)	-4.70 (-5.04)	-4.87 (-5.44)	-11.28 (-11.49)	-8.57 (-8.75)	-8.59 (-8.79)	-10.99 (-11.18)	-10.76
trimer II	-4.73 (-4.77)	-5.10 (-5.20)	-5.40 (-5.09)	-11.70 (-11.88)	-8.89 (-9.02)	-8.90 (-9.02)	-11.64	-11.37
tetramer II	-4.79 (-4.80)	-5.19 (-5.26)	-5.51 (-5.55)	-11.99 (-12.14)	-9.10 (-9.18)	-9.11 (-9.20)		
pentamer II	-4.77 (-4.78)	-5.21 (-5.24)	-5.54 (-5.57)	-12.11	-9.16			
hexamer II	-4.79 (-4.79)	-5.22 (-5.25)	-5.57 (-5.59)	-12.17				
infinite chains	-4.77 (-4.78)	-5.23 (-5.26)	-5.57 (-5.73)	-12.24 (-12.66)	-9.21 (-9.41)	-9.55 (-9.85)		

[a]Values in parentheses correspond to completely optimized structures. Energies in kcal/mol. [b]Frozen core calculations.

Table X. Incremental Hydrogen-bonding Energies and Enthalpies of Different Acetic Acid Aggregates at Different Levels of Theory with CP, ZPVE and CP+ZPVE Corrections

aggregates	Method															
	I				II				III				IV				V
	ΔE_{CP}	ΔE_{ZPE}	ΔE_{CP+ZPE}	ΔH_{298K}	ΔE_{CP}	ΔE_{ZPE}	ΔE_{CP+ZPE}	ΔH_{298K}	ΔE_{CP}	ΔE_{ZPE}	ΔE_{CP+ZPE}	ΔH_{298K}	ΔE_{CP}	ΔE_{ZPE}	ΔE_{CP+ZPE}	ΔH_{298K}	ΔE_{CP}
dimer I	-16.7	-17.8	-15.0	-15.0	-13.1	-13.9	-11.5	-11.3	-13.2	-14.0	-11.7	-11.6	-13.2	-16.8	-11.3	-11.2	-13.5
dimer II	-9.4 (-9.6)	-10.0 (-10.2)	-8.2 (-8.4)	-7.8 (-8.0)	-7.0 (-7.1)	-7.5 (-7.6)	-5.8 (-6.0)	-5.4 (-5.6)	-7.1 (-7.2)	-7.5 (-7.7)	-6.0 (-6.1)	-5.5 (-5.7)	-7.2 (7.4)	-9.6 (-9.8)	-5.8 (-5.9)	-5.5 (-5.6)	-7.2
trimer II	-9.8 (-10.0)	-10.6 (-10.8)	-8.7 (-8.9)	-8.8 (-8.5)	-7.2 (-7.3)	-7.9 (-8.0)	-6.2 (-6.3)	-6.3 (-5.8)	-7.3 (-7.4)	(-8.0)	(-6.4)	(-5.9)	-7.8				-7.7
tetramer II	-10.1 (-10.2)	-10.9 (-11.1)	-9.0 (-9.2)	-8.6 (-8.7)	-7.4 (-7.5)	-8.1 (-8.2)	-6.4 (-6.5)	-6.5 (-6.0)	-7.5 (-7.6)	(-8.2)	(-6.6)	(-6.1)					
pentamer II	-10.2				-7.5												
hexamer II	-10.3																
infinite chains	-10.3 (-10.4)	-11.2 (-11.4)	-9.5 (-9.7)	-8.8 (-8.8)	-7.7 (-7.7)	-8.3 (-8.4)	-6.6 (-6.9)	-6.6 (-6.4)	-7.9 (-8.3)	(-8.4)	(-6.9)	(-7.0)					

[a]Methods: I. HF/6-31G; II. HF/6-31G(d); III. HF/6-31G(d,p); IV. MP2/6-31G (full); V. MP2/6-31G(d) (frozen core).

Energies in kcal/mol. Values in parentheses correspond to completely optimized structures.

intermolecular interaction. Consequently, ΔE and ΔH values represent an upper limit of the true stabilization. For this reason, I collected the interaction energies with the individual, as well as, total corrections. Dimer I is also included for comparison.

Both Tables IX and X demonstrate the significance of cooperativity. In the previous section on acetic acid dimers we have seen that the stabilization of dimer II is less than half of that of dimer I. However, due to cooperativity the incremental H-bonding enthalpies (even in the trimers) are larger than the half of the H-bonding enthalpy of I (see HF/6-31G(d) and HF/6-31G(d,p) methods). This indicates that the formation of long chains becomes enthalpically favorable over the formation of dimers of type I. The extent of cooperativity (compared to the extrapolated H-bonding value) is similar to that for the uncorrected results (constrained geometries): 0.9 kcal/mol (9.6%) and 0.7 kcal/mol (10%) for CP corrected HF/6-31G and HF/6-31G(d) energies. The correlated methods (MP2) indicate stronger cooperative effects. While going from dimer to trimer results 5.7% (0.61 kcal/mol) increase in the strength of the uncorrected MP2/6-31G(d) energies, the similar numbers are 3.7% or 0.32 kcal/mole for HF/6-31G(d) method.

The geometries of the aggregates are presented in Table XI. Several trends are immediately evident. The presence of strong C-H...O interactions is especially striking. All methods (except SAM1) predict the C-H...O hydrogen-bonding distance to be the short 2.2 - 2.6 Å. The orientation of the C-H...O interaction (characterized by β in Table XI) is in excellent agreement with Glusker's observation of the general alignment properties of H-bonds (see Chapter IV). The intermolecular O...O and O...H distances across the H-bonds decreases with increasing aggregate size. On the other hand, the

Table XI. Selected Geometrical Parameters Characteristic of H-bonding Interactions in One-dimensional Chains at Different Levels of Theory[a]

Aggregates	Geometrical parameters										
	C=O	C-O	O..O	O..H(O)	O..C	O..H(C)	α(C=O..H)[c]	α(O-H..O)[c]	β(C=O..H)[c]	β(C-H..O)[c]	d
AM1											
dimer	1.237	1.360	3.075	2.104	3.327	2.245	128.2	175.1	139.4	162.3	
trimer	1.238	1.359	3.063	2.093	3.340	2.252	127.0	173.2	137.5	163.5	7.224
tetramer	1.239	1.358	3.059	2.089	3.344	2.254	126.8	172.8	137.1	163.8	7.239
pentamer	1.239	1.357	3.058	2.088	3.346	2.256	126.5	172.4	136.7	164.0	7.255
hexamer	1.239	1.357	3.056	2.086	3.347	2.257	126.4	172.2	136.5	164.1	7.262
PM3											
dimer	1.223	1.347	2.729	1.792	3.519	2.505	131.1	164.6	133.7	153.0	
trimer	1.225	1.344	2.722	1.784	3.533	2.519	131.1	164.3	133.1	153.0	7.043
tetramer	1.226	1.342	2.720	1.780	3.538	2.523	131.1	164.2	132.8	153.1	7.054
pentamer	1.226	1.341	2.718	1.778	3.541	2.525	131.0	164.1	132.6	153.2	7.061
hexamer	1.227	1.340	2.717	1.777	3.543	2.527	131.0	164.0	132.4	153.3	7.067
SAM1											
dimer	1.255	1.379	2.740	1.770	2.987	1.906	125.4	171.2	134.9	166.4	
trimer	1.257	1.376	2.729	1.757	2.998	1.915	124.8	170.1	133.8	167.0	6.856
tetramer	1.259	1.374	2.725	1.752	3.001	1.916	124.6	169.8	133.4	167.2	6.866
pentamer	1.259	1.374	2.722	1.749	3.002	1.916	124.5	169.6	133.2	167.3	6.871
hexamer	1.260	1.373	2.721	1.747	3.003	1.916	124.5	169.5	133.1	167.4	6.874
HF/6-31G											
dimer	1.219	1.341	2.768	1.808	3.407	2.383	138.8	179.2	131.4	158.3	

Table XI. Cont.[a]

Aggregates	Geometrical parameters										
	C=O	C-O	O..O	O..H(O)	O..C	O..H(C)	α(C=O..H)[c]	α(O-H..O)[c]	β(C=O..H)[c]	β(C-H..O)[c]	d
trimer	1.222	1.336	2.738	1.774	3.489	2.468	138.9	178.4	129.0	157.8	7.003
tetramer	1.224	1.332	2.723	1.757	3.516	2.497	139.3	177.9	128.3	157.4	7.018
pentamer	1.225	1.330	2.713	1.746	3.534	2.517	139.4	177.5	127.7	157.2	7.029
hexamer	1.226	1.329	2.706	1.738	3.546	2.529	139.6	177.2	127.4	157.1	7.035
HF/6-31G(d)											
dimer	1.194	1.321	2.868	1.918	3.486	2.455	137.7	171.8	130.2	159.5	
trimer	1.196	1.318	2.841	1.891	3.542	2.515	135.4	170.4	128.7	158.8	7.141
tetramer	1.198	1.315	2.829	1.879	3.560	2.534	135.4	169.9	128.0	158.6	7.159
pentamer	1.198	1.314	2.821	1.870	3.517	2.546	135.7	169.9	127.7	158.4	7.159
HF/6-31G(d,p)											
dimer	1.194	1.320	2.862	1.916	3.470	2.437	134.9	172.1	130.2	159.8	
trimer	1.197	1.316	2.834	1.888	3.524	2.494	135.0	170.5	128.5	159.3	7.139
tetramer	1.198	1.314	2.821	1.874	3.539	2.510	135.2	170.3	127.9	159.1	7.146
MP2/6-31G											
dimer	1.255	1.387	2.840	1.853	3.395	2.334	133.5	174.8	129.7	163.2	
trimer	1.258	1.380	2.806	1.817	3.438	2.379	133.7	173.4	128.3	162.7	7.177
MP2/6-31G(d)[b]											
dimer	1.225	1.350	2.838	1.867	3.367	2.310	130.5	168.0	129.2	163.2	
trimer	1.228	1.344	2.808	1.836	3.396	2.341	130.9	167.3	128.3	162.7	7.131
experiment	1.206	1.321	2.631	1.642		2.409					6.993

[a]Restricted structures. Distances in Å, bond angles in degrees. [b]Frozen core calculations. [c]While α refers to the angles pertaining to the O-H..O H-bond, β corresponds to the C-H..O H-bonding angles.

corresponding O...C and O...H distances for the C-H...O H-bond increase. These observations suggest that the O-H...O interactions become stronger with increasing aggregation, but the C-H...O interactions become weaker. Thus, the total cooperative effect is the sum of two divergent components. It is also interesting to note that the increasing C-H...O H-bonding distances move toward the experimental value only in case of AM1 and SAM1 methods. Table XI clearly show trends for the C-O bond to shorten and the C=O bond to lengthen as the aggregate grows. While not all MO methods are converging towards the experimental (crystal) molecular geometries because they underestimate the C-O and/or overestimate the C=O bond lengths, this tendency is appropriate as the two bond lengths do shorten and lengthen, respectively, upon changing from the gas phase[18,19] to the crystal. The translation vector, *d* (the distance between repeating points in two adjacent units of two molecules), is too long and not converging toward the experimental value (going from 7.003 to 7.035 Å for HF/6-31G). These facts indicate that consideration of the aggregation in the other two directions is necessary.

The geometrical data shed light on the small extent of cooperativity in this direction predicted by the semiempirical methods. I have previously noted that these methods (especially AM1) tend to underestimate O-H...O interactions, however, AM1 is quite good at estimating the C-H...O interactions.[11] Thus, I suggest that the artificially low cooperativity expected for the O-H...O interaction is roughly cancelled by the decrease in the C-H...O interaction at the AM1 level.

Aggregation in the second direction: Stacking

The second direction that I consider involves 'stacking' the chains (Figures 5 and 7). I calculated various 'stacks' containing different numbers of chains and chain lengths. Tables XII to XIV present the energetic and geometrical data. Only AM1 and PM3 among the semiempirical methods are capable of treating the stacking phenomenon. SAM1 is unable to find suitable stacking potential minima. The data of Table XII indicate that adding C molecules to an C/M aggregate to form an $C/M+1$ stack, which would create C new interactions in the first direction, stabilizes the aggregate by increasingly more than C times the interaction energy (for $C=1$) as C grows. Thus, increasing the size of the stack (in the second direction) cooperatively enhances the interaction energy for increasing the chain (in the first direction). This provides support for the concept of interdimensional cooperativity. One should note that AM1, which did not predict cooperativity in the first dimension when individual chains are considered (see above), clearly does predict cooperativity in the same direction when the chains are stacked.

The interactions between chains in a stack are the weakest of the three distinct directional interactions (see Table XIII). The chains appear to be held together by a what may be a very weak C-H...O interaction between a second methyl C-H bond and two OH oxygens in an adjacent chain (see Figure 5). The C-H...O orientation is not ideal as the methyl group conformation optimizes the stronger C-H...O interactions of the other two C-H bonds (one in the chain, the other is used in the third direction). In fact the shortest H...O distance is about 3.6 Å, rather long for a H-bond. The next sections on the structure of microcrystals and the discussion of cooperativity and pairwise interactions will shed

Table XII. Hydrogen-Bonding Energies[a] (kcal/mol) for Adding *C* Acetic Molecules to *C*/*M* Stacks to form *C*/(*M*+1) Aggregates. See explanation in text.

	M=1	*M*=2	*M*=3	*M*=4	*M*=5
AM1					
C=1	-4.79	-4.73	-4.79	-4.77	-4.79
C=2		-9.66	-9.68	-9.71	-9.72
C=3		-14.56	-14.65		
C=4		-19.49	-19.55		
PM3					
C=1	-4.87	-5.40	-5.51	-5.54	-5.57
C=2		-11.03	-11.22	-11.31	-11.42
C=3		-16.60	-16.97		
C=4		-22.24	-22.58		
HF/6-31G[b]					
C=1	-11.28 (-9.44)	-11.70 (-9.85)	-11.99 (-10.12)	-12.11 (-10.23)	-12.17 (-10.29)
C=2		-24.53 (-19.44)			
C=3		-38.12 (-29.71)			
HF/6-31G(d)					
C=1	-8.75 (-7.09)	-9.02 (-7.34)	-9.18 (-7.49)		
C=2		-18.92 (-14.21)			

[a]Enthalpies for AM1 and PM3. [b]Ab initio values in parentheses correspond to CP corrected interaction energies.

Table XIII. Incremental Interaction Energies[a] (kcal/mol) Between Chains of Different Size in Two-dimensional Stacked Aggregates

	C/M aggregates				
	M=2	*M*=3	*M*=4	*M*=5	*M*=6
AM1					
C=2	-0.60	-0.80	-0.90	-1.07	-1.20
C=3	-0.40	-0.57	-0.74		
C=4	-0.51	-0.71	-0.82		
PM3					
C=2	-0.89	-1.12	-1.32	-1.55	-1.83
C=3	-0.57	-0.74	-0.98		
C=4	-0.76	-1.00	-1.10		
HF/6-31G					
C=2	-4.15 (-1.59)	-5.29 (-1.44)			
C=3	-2.04 (+0.06)	-3.94 (-0.28)			
HF/6-31G(d)					
C=2	-3.18 (-0.80)	-4.32 (-0.54)			
HF/6-31G(d,p)					
C=2	-3.19 (-0.77)				

[a]Ab initio values in parentheses correspond to CP corrected interaction energies.

more light on these interactions. Table XIII gives the interaction energies for the incremental addition of chains of varying length to the growing aggregate. These interactions are mildly attractive at best (as they are repulsive with SAM1, the structures could not be optimized). After CP correction, the ab initio values descend to the order of those calculated by AM1. One is even slightly repulsive. ZPVE correction would further reduce the interaction, but this would lead to overcorrection. The interaction of a stack of *C* chains with another chain depends upon the value of *C*. Thus, adding a 1/*M* chain to a 2/*M* stack provides less stabilization than combining two 1/*M* chains or adding a 1/*M* chain to a 3/*M* stack. The analysis of the pairwise and nonadditive contributions below will show that the interaction in the second direction is cooperative.

One can see from Table XIV that the molecular geometries and H-bonding distances continue to converge, but the unit cell dimensions, particularly *b*, do not. While AM1 is primarily in error for the unit cell dimension, *b* and the translation vector, *d*, PM3 and the HF calculations are primarily in error for the cell dimensions, *b* and *c* (see Figure 7). Thus, the two dimensional model remains inadequate to fully understand the crystalline intermolecular interactions for acetic acid.

Aggregation in the third direction: microcrystals

The individual stacks interact essentially through C-H...O H-bonds (involving the third methyl C-H bond) as can be seen from careful inspection of Figure 6. Each stack is roughly perpendicular to its neighbors. Each molecule has two C-H...O interactions (one each as donor an receptor) with two different molecules in different chains of an adjacent

Table XIV. Selected H-bonding Geometries and Unit Cell Dimensions at Different Levels of Theory[a]

	C=O	C-O	O...O	O...HO	O...C	O...HC	*b*	*c*	α	*d*
AM1										
2/2	1.237	1.360	3.061	2.097	3.341	2.246	5.390	5.390		
3/2	1.238	1.360	3.057	2.096	3.342	2.243	5.393	5.398	86.70	
4/2	1.238	1.360	3.054	2.095	3.345	2.245	5.420	5.421	86.52	
2/3	1.238	1.359	3.055	2.090	3.346	2.256	5.436	5.437	84.79	7.332
			3.055	2.090	3.346	2.257				
3/3	1.238	1.359	3.049	2.088	3.348	2.252	5.471	5.480	85.11	7.406
			3.052	2.089	3.353	2.258				
4/3	1.239	1.359	3.049	2.088	3.352	2.254	5.493	5.493	84.98	7.420
			3.049	2.088	3.352	2.254				
2/4	1.239	1.358	3.051	2.087	3.352	2.255	5.484	5.486	84.32	7.364
			3.052	2.087	3.352	2.256				
3/4	1.239	1.358	3.047	2.086	3.353	2.252	5.514	5.516	84.34	7.405
			3.050	2.087	3.355	2.258				
4/4	1.239	1.358	3.047	2.086	3.356	2.256	5.523	5.524	84.43	7.422
			3.047	2.086	3.356	2.256				
2/5	1.239	1.357	3.050	2.086	3.352	2.257	5.498	5.510	84.02	7.367
			3.051	2.086	3.354	2.259				
2/6	1.239	1.357	3.049	2.084	3.354	2.257	5.526	5.533	83.58	7.370
			3.049	2.084	3.355	2.258				
PM3										
2/2	1.223	1.347	2.723	1.792	3.516	2.495	5.190	5.193		
3/2	1.223	1.348	2.721	1.794	3.512	2.487	5.115	5.286	86.41	
4/2	1.223	1.348	2.719	1.793	3.502	2.480	5.129	5.303	86.09	
			2.721	1.794	3.514	2.495				

Table XIV. Cont.[a]

	C=O	C-O	O...O	O...HO	O...C	O...HC	*b*	*c*	α	*d*
PM3										
2/3	1.225	1.344	2.721	1.785	3.514	2.518	5.342	5.345	82.40	7.039
			2.722	1.786	3.521	2.525				
3/3	1.225	1.345	2.716	1.785	3.524	2.500	5.145	5.277	86.10	7.115
			2.719	1.786	3.528	2.506				
4/3	1.225	1.345	2.720	1.786	3.506	2.518	5.351	5.356	82.22	7.040
			2.720	1.786	3.507	2.519				
2/4	1.226	1.343	2.716	1.781	3.535	2.515	5.184	5.222	86.11	7.105
			2.716	1.781	3.536	2.516				
3/4	1.226	1.343	2.714	1.781	3.533	2.510	5.164	5.272	86.05	7.121
			2.714	1.783	3.533	2.511				
4/4	1.226	1.343	2.715	1.782	3.530	2.507	5.175	5.279	85.93	7.125
			2.715	1.782	3.532	2.510				
2/5	1.226	1.342	2.716	1.779	3.534	2.520	5.237	5.281	84.79	7.092
			2.716	1.779	3.538	2.524				
2/6	1.227	1.341	2.714	1.777	3.542	2.521	5.192	5.228	86.13	7.115
			2.714	1.778	3.542	2.521				
HF/6-31G										
2/2	1.220	1.342	2.755	1.795	3.409	2.380	4.818	4.818		
3/2	1.220	1.343	2.763	1.804	3.386	2.343	4.892	4.892	86.44	
2/3	1.223	1.337	2.738	1.775	3.484	2.456	4.909	4.910	87.71	7.080
3/3	1.223	1.338	2.738	1.776	3.454	2.418	4.905	4.911	86.68	7.139
HF/6-31G(d)										
2/2	1.195	1.322	2.858	1.911	3.476	2.439	4.918	4.920		
2/3	1.197	1.319	2.840	1.894	3.539	2.506	5.016	5.017	88.29	7.080
HF/6-31G(d,p)										
2/2	1.195	1.321	2.852	1.909	3.458	2.419	4.914	4.915		
experimental	1.206	1.321	2.631	1.642		2.409	3.963	5.762	90.00	6.993

[a]Distances in Å, bond angles in degrees.

stack. Each successive molecule in a chain interacts with a stack on the opposite side of the chain.

The interaction energies are presented in Table XV. The size of the aggregates precluded use of ab initio calculations for these structures. The microcrystals are minima on all the semiempirical potential surfaces, so AM1, PM3 and SAM1 results are presented. Due to the significantly larger size of AMPAC 4.5 compared to AMPAC 2.1, I could not calculate microcrystals larger than 2/3/3 (18 molecules) for SAM1 and PM3. Only AM1 and PM3 predict attractive interactions in all three directions. The SAM1 2/3/3 microcystal is also a minimum despite the observation that the stacking interaction is repulsive at SAM1 level. This attraction can be attributed to six C-H...O interactions between the interacting 3/3 stacks. Thus, the strength of the individual C-H...O H-bonds can be estimated (from dividing the data of Table XV by six) to be about 1.2 - 1.3 kcal/mol at both AM1 and PM3 levels, very similar to that found for dimer II. The orientation of C-H...O interactions between the chains within the stacks becomes more favorable after considering the third direction. As I mentioned before, one methyl proton participates in C-H...O H-bonding within the H-bonded catemeric chains, while the second proton interacts with a carboxylic oxygen on the neighboring stacks. The distance between the third methyl hydrogen and an OH oxygen within the stacks decreases from 3.6 Å to 2.8 Å when considering the aggregation in the third direction. This change is due partly to the compression of the chains within the stacks and partly to the shift between the neighboring chains, caused by the stacking interactions between the stacks.

The geometrical data of Table XVI indicate that, when all three directions of

Table XV. Incremental Stabilization Energies (kcal/mol) Between Stacked 3/3 Aggregates in *L*/3/3 Aggregates

Method	*L*/3/3 Aggregates		
	L=2	*L*=3	*L*=4
SAM1	+5.46		
PM3	-7.21		
AM1	-7.26	-7.55	-7.67

aggregation are considered, the unit cell dimensions (as well as the molecular dimensions) converge to their experimental values as the size of the aggregate increases. The agreement between the experimental and AM1 unit cell parameters is striking, with the exception of *b*, which is due to the familiar failing of AM1 to accurately predict the H-bonding distances in O-H...O interactions (see also Chapter V). Nevertheless, even in this unit cell direction, the growing microcrystal is converging in the right direction. One should recall (Table XIV) that the HF calculations do not accurately predict the experimental value of *b* in the stacks (although are slightly better than AM1).

Heat of sublimation

I estimated the heat of sublimation by calculating the energy associated with removing a molecule from the interior of a microcrystal using AM1. I calculated the energy of the microcrystal containing the hole with its geometry either fixed as in the original microcrystal or optimized with the normal constraints. As removing each molecule individually would break twice the correct number of intermolecular

Table XVI. Selected H-bonding Distances and Unit Cell Parameters (Å) in Three-Dimensional Orthorhombic *L*/3/3 (*L*=2,3,4) Aggregates[a]

	C=O	C-O	O...O	O...HO	O...C	O...HC	*a*	*b*	*c*	*d*
SAM1										
1/3/3	1.257	1.377	2.735	1.778	3.045	1.950		5.032	5.035	7.118
			2.738	1.781	3.047	1.953				
2/3/3	1.257	1.377	2.736	1.778	3.069	1.977		4.992	5.103	7.139
			2.742	1.790	3.071	1.976				
PM3										
1/3/3	1.225	1.345	2.714	1.788	3.535	2.506		5.027	5.120	7.175
			2.717	1.789	3.540	2.514				
2/3/3	1.225	1.345	2.710	1.786	3.548	2.520		5.084	5.088	7.193
			2.712	1.787	3.552	2.526				
AM1										
1/3/3	1.239	1.359	3.050	2.092	3.353	2.250		5.261	5.291	7.461
			3.052	2.093	3.356	2.254				
2/3/3	1.239	1.359	3.032	2.081	3.365	2.269		5.059	5.487	7.463
			3.037	2.084	3.370	2.274				
3/3/3	1.239	1.359	3.027	2.080	3.372	2.276	13.043	5.042	5.549	7.498
			3.032	2.084	3.376	2.281				
4/3/3	1.239	1.359	3.025	2.078	3.373	2.277	13.042	5.033	5.555	7.496
			3.028	2.079	3.377	2.283				
experimental	1.206	1.321	2.631	1.642		2.409	13.225	3.963	5.762	6.993

[a]For comparison I included the 3/3 orthorhombic aggregates (as 1/3/3) in the Table.

interactions, half this energy difference corresponds to the heat of sublimation. The 6.0 kcal/mol obtained in this manner (the same value was obtained with and without

optimization) is somewhat lower than the experimental[30] value of 10.0 kcal/mol. This is consistent with the previous observations that AM1 tends to underestimate the stabilizations of O-H...O interactions (although it is accurate for C-H...O interactions[11]). If I multiply the AM1 O-H...O stabilization (4.78 kcal/mol, the incremental stabilization energy of an infinite chain from Table IX) by a factor of 1.7 as in Chapter V (or 1.9 as in a previous report$_2$) to obtain agreement with good ab initio calculations, the correction for the heat of vaporization is 3.3 kcal/mol (4.3 using the factor of 1.9). The corrected value, 9.3 kcal/mole (10.3 kcal/mol) is now in good agreement with the experimental heat of sublimation.

Cooperativity

In this section I shall use the results of Chapter III and apply the principles developed in Chapter V in a more quantitative manner. According to Chapter III, cooperativity can be arbitrarily divided into two effects: a) the pairwise interactions between individual units, and b) the remaining 'nonadditive' contribution. In this section I shall use the same notation as in Chapter V for the two-body (or pairwise) interactions of two- and three-dimensional aggregates of 1,3-diones. 1-2 interaction will mean the interaction energy between the first two neighboring chains (or stacks) of an aggregate; 1-3 interaction will denote the interaction between the first and third chains (stacks) and so on.

Table XVII illustrates the pairwise and nonadditive contributions to the interactions in the second and third directions in a 4/4 stack and a 4/3/3 microcrystal.

Within the 4/4 stack there are three attractive (1-2, 2-3, and 3-4) and three repulsive (1-3, 2-4 and 1-4) interactions compared to the optimized tetramer. By symmetry the 1-2 and 3-4; and 1-3 and 2-4 interactions are equivalent. Adding the pairwise interactions predicts a stabilization of 1.88 kcal/mol, 0.59 less than predicted by the calculation on the supermolecule. The apparent reason for the repulsion between the *n*-th and (*n*+2)-th chains lies in the structure of the chain that alternates the orientations of the methyl groups in adjacent chains (see Figure 5). The reason for the 1-4 repulsion is less intuitive. It is probably due to long distance electrostatic repulsions that can be overcome at shorter distances by the weak C-H...O interactions discussed above. In fact, it provides the major argument for considering this a weak C-H...O H-bond, as a similar phenomenon occurs for the pairwise interactions of stacks (discussed below), where the C-H...O H-bond is much more evident.

This analysis helps explain the difference in the incremental stacking interactions (Table XIII). Thus adding a 1/*M* chain to a 1/*M* chain creates one (stabilizing) 1-2 interchain interaction. Adding another 1/*M* chain to the 2/*M* stack creates a second pairwise 1-2 interaction (stabilizing), a pairwise 1-3 interaction (destabilizing) plus a nonadditive component. Adding a fourth 1/*M* to the 3/*M* stack, creates another 1-2, 1-3 and a 1-4 interaction plus a modification in the nonadditive component. The stacking interaction for 1/*M* plus 2/*M* is less than for 1/*M* plus 1/*M* because of the repulsive 1-3 interaction in the former. The greater stabilization shown for 1/*M* plus 3/*M* than for 1/*M* plus 2/*M* indicates cooperativity in the second direction because the new interactions contain both (1-2 and 1-3) those expected for the formation of the 3/*M* plus a slightly

Table XVII. Pairwise Interactions (kcal/mol) Between Stacked Chains in 1/4/4 Aggregate and Between Interacting Stacks in 4/3/3 Aggregate.

Aggregate	Pairwise interaction				Sum of pairwise interactions	Calculated interaction energy	Non-additivity
	1-2	1-3	1-4	2-3			
1/4/4	-0.86	+0.25	+0.14	-0.80	-1.88	-2.47	-0.59
4/3/3	-7.42	+0.88	+0.75	-7.42	-19.75	-22.92	-3.17

repulsive 1-4 interaction. From Tables XIII and XVII one can see that the incremental interaction for 1/4 plus 3/4 is 0.82 kcal/mol, while the individual pairwise interactions are -0.86, +0.25, and +0.14 (for a total of -0.47) kcal/mol, respectively, for 1-2, 1-3, and 1-4 pairwise interactions. Thus, if we assume that the small differences in the optimized geometries between the 1/4, 3/4 and 4/4 stacks are unimportant, the 0.35 kcal/mol difference (0.82 - 0.47) can be attributed to a change in the nonadditive contribution. This value is almost half the incremental stabilization of adding the fourth chain. In fact, the pairwise contributions alone would predict an anticooperative interaction, as 0.47 would be less than the stabilizations for the incremental additions of a 1/4 chain to form a 2/4 or 3/4 stack.

In the third direction, one can make a similar examination. Table XVII presents the pairwise and nonadditive interactions for a 4/3/3 microcrystal. Again, the interactions between adjacent units are stabilizing, while those between nonadjacent units are

repulsive. The major difference is that the stabilizations between adjacent units is much greater (due to the better orientation of the C-H...O interactions, see Figure 6) than in the second direction. Although the nonadditive effect in the third direction of the 4/3/3 microcrystal is much greater than for the second direction of the 4/4 stack (3.17 vs. 0.59 kcal/mol), it is a smaller fraction of the total interaction. Following the reasoning used above, Tables XV and XVII indicate the incremental stabilization upon adding a 1/3/3 stack to a 3/3/3 microcrystal is 7.67 kcal/mol, while the sum of the three pairwise interactions created would predict 5.79, leaving 1.88 kcal/mol (roughly a quarter) to be accounted for in the nonadditive contribution.

The analysis presented above clearly indicates the dangers inherent in any attempt to explain the intermolecular interactions with a theory dependant strictly upon pairwise potential functions. Pairwise functions would have to be different for different sized aggregates and (presumably) for different orientations of the monomeric units in the aggregate.

It is also very important to realize the effects of geometric relaxation phenomena. Although, I have not performed analysis about the influence of geometry changes on the non-additive components, preliminary results indicate that relaxation can contribute significantly to the observed non-additivity. We also have seen that the non-additive energy component is a sum of very small numbers. Thus, changes in these small numbers originating from the relaxation phenomena can change the non-additive energy component (and the previous qualitative argument, as well).

The process of self-assembly

The acetic acid crystal provides insight into the mechanism of molecular recognition in crystal formation. The strongest intermolecular interactions are the pair of H-bonds (one O-H...O and one C-H...O) that form the chains. However, bimolecular interactions involving two O-H...O H-bonds (as in I) are more stabilizing. Thus, if the crystal were to grow from an original dimer, I, it might break one of the O-H...O bonds and add a third molecule. Enthalpically, this is not too unfavorable as the resulting trimer has two of each (O-H...O and C-H...O) interaction, while the equivalent dimer, I, plus a monomer have only the H-bonds in I. If one considers the formation of a tetramer from two dimers, I, the situation is less favorable, as there are four O-H...O interactions in the two dimers vs only three (plus three C-H...O) in the tetramer. Continuing this reasoning, one can see that any even quantity of monomers will lose one O-H...O interaction, but gain n-1 C-H...O interactions (where n=number of monomers) upon transformation from n/2 dimers, I, to a single oligomeric chain. Ultimately, the single chain must become enthalpically favorable since: a) the n-l C-H...O interactions will more than compensate for the single lost O-H...O interaction as the chain grows, and b) the O-H...O interactions increase in strength as the chain grows due to the cooperativity. In solution, the entropic component of ΔG dominates, so the dimeric structure prevails. In a crystal, however, the intermolecular degrees of freedom are all essentially lost, so the entropic differences become much less important, allowing the enthalpic component to dominate.

The two ends of a growing chain are different. One end has an uncomplexed carboxyl group, the other the carbonyl of the carboxyl and a methyl group (see figure 1).

Thus, the first (carboxyl) end can bind another monomer either to continue the chain, or to form a local 2 O-H...O H-bond interaction similar to that of I. The other (methyl) end can only accommodate a monomer in the chain-like manner. Thus, growth rates of the chains should be different at each end. Another mechanism for the original nucleation might be maintaining the initial dimer, I, while growing the chain in two equivalent directions (each chain end would have methyl and a C=O available for attaching another monomer). Eventually, the H-bonds in the original dimer could break, creating two growing chains, or the original dimer could remain as a flaw in the crystal.

Growth in the second and third directions are more difficult to imagine. The weaker interactions between the chains in the second direction, suggest that the greater stabilizing interactions in the third direction might initially be more important. However, it is difficult to visualize a mechanism for the interactions between the stacks unless stacks already exist. Probably, growth in the second and third directions are coupled. Initially, these processes probably have a relatively unfavorable balance between ΔH and ΔS, as many degrees of freedom are lost in the aggregation process, but the resulting enthalpic stabilization/molecule is small (compared to chain growth). Thus, forming the initial microcrystal from the chains is probably the slow step in the nucleation process.

5. Conclusions

The calculations for monomeric and dimeric acetic acid show that HF wavefunctions (while they often give reasonable energies of interaction) are insufficient

to correctly describe the geometries of acetic acid and its gas phase dimer, I. Optimization at least at the MP2 level is necessary. I expect these conclusions to apply to the other dimers, as well. Comparisons of the stabilization energies of the various dimers suggest that there are cooperative contributions to the stabilizations of the cyclic dimers, especially for I, where it is about 2.4 - 3.1 kcal/mol. Comparison of the vibrations of the dimers with those of the monomers confirms this cooperativity. I estimate the C-H..O contribution to the stability of II to be about 0.5 - 1.0 kcal/mol. This is not sufficient to explain the preference for II in the crystal structure, which must involve additional cooperative effects associated with further aggregation.

The vibrational frequencies of acetic acid and dimer I are in the same qualitative order for all levels of ab initio calculation. Based upon the calculated vibrations, we suggest that Sverdlov's original assignment of δ(C-C-O) is correct and that the assignments of the two lowest intermolecular vibrations for I be reversed. The MP2/6-31G(d) calculated frequencies are reasonably accurate, while the HF frequencies are generally too high.

The methods used in this chapter, ab initio and semiempirical molecular orbital calculations as well, are also clearly capable of predicting the crystal structure of acetic acid, despite its unusual nature. Calculations on large aggregates reproduce experimental data surprisingly well. Especially, the agreements between the calculated and experimental unit cell parameters and heat of sublimation are striking. The calculations indicated, however, that all three crystal directions must be considered to receive reliable predictions. Furthermore, the results of the calculations allow us to evaluate and

understand the contributions of the various factors to establishing the crystal structure. Thus, these methods ought to be useful for studying other molecular recognition and self-assembly phenomenon as well as additional crystal structures. The importance of the cooperative effects, particularly the 'nonadditive' part, show that pairwise potentials are not likely to be applicable in different phases where the extent of aggregations will significantly differ. Thus, in the gas phase, acetic acid will be monomeric or dimeric, in the liquid primarily dimeric, but entirely different in the solid phase.

6. References

1. This Chapter is based on the following papers: Turi, L.; Dannenberg, J. J. *J. Phys. Chem.*, **1993**, *97*, 12197. Turi, L.; Dannenberg, J. J. submitted for publication.

2. Turi, L.; Dannenberg, J. J. *J. Phys. Chem.*, **1992**, *96*, 5819. Turi, L.; Dannenberg, J. J. *Mol. Cryst. Liq. Cryst.*, **1992**, *219*, 63.

3. a) Gautres, R.; Maillols, J.; Tabacik, V. *J. Raman Spectrosc.*, **1981**, *11*, 442. b) Mathews, D. M.; Sheets, R. W. *J. Chem. Soc. A*, **1969**, 2203. c) Pross, A. W.; van Zeggeren, F. *Spectrochim. Acta*, **1960**, *16*, 563. d) Miyazawa, T.; Pitzer, K. S. *J. Am. Chem. Soc.*, **1959**, *81*, 74.

4. Bes, R. *Actual. Chim.*, **1978**, *10*, 25. Tabor, W. J. *J. Chem. Phys.*, **1957**, *27*, 974. Taylor, M. D. *J. Am. Chem. Soc.*, **1951**, *73*, 315. Karle, J.; Brockway, L. O. *J. Am. Chem. Soc.*, **1944**, *66*, 574.

5. Jentschura, U.; Lippert E. *Z. Phys. Ch. (Frankfurt)*, **1972**, *77* (1-6), 64.

6. Frurip, D. J.; Curtiss, L. A.; Blander, M. J. *J. Am. Chem. Soc.*, **1980**, *102*, 2610.

7. a) Hartz, N.; Rasul, G.; Olah, G. A., *J. Am. Chem. Soc.*, **1993**, *115*, 1277. b) Allinger, N. L.; Schmitz, L. R.; Motoc, I.; Bender, C.; Labanowski, J. K., *J. Comput. Chem.*, **1992**, *13*, 838. c) Williams, R. W.; Lowrey, A. H., *J. Comput. Chem.*, **1991**, *12*, 761. d) Marcoccia, J. F.; Csizmadia, I. G.; Peterson, M. R. *Gaz. Chim. Ital.*, **1990**, *120*, 77. e) Nagy-Felsobuki, E. I.; Kimura, K. *J. Phys. Chem.*, **1990**, *94*, 8041. f) Ruelle, P. *Chem.*

Phys., **1986**, *110*, 263. g) Bock, C. W. *J. Mol. Struct. (THEOCHEM)*, **1983**, *13*, 383. h) Nagaoka, S.; Hirota, N. *Chem. Phys. Lett.*, **1982**, *92*, 498.

8. Strieter, F. J.; Templeton, D. H.; Scheuerman, R. F.; Sass, R. L. *Acta Crystallogr.*, **1962**, *15*, 1233.

9. Kanters, J. A.; Kroon, J. *Acta Crystallogr.*, **1972**, *B28*, 1946.

10. a) X-ray: Jones, R. E.; Templeton, D. H. *Acta Crystallogr.*, **1958**, *11*, 484. b) X-ray: Nahringbauer, I. *Acta Chem. Scand.*, **1970**, *24*, 453. c) neutron-diffraction: Jönsson, P. G. *Acta Crystallogr.*, **1971**, *B27*, 893.

11. Turi, L.; Dannenberg, J. J.; *J. Phys. Chem.*, **1993**, *97*, 7899.

12. Derissen, J. L.; Smit, P. H. *Acta Crystallogr.*, **1977**, *A33*, 230.

13. Smit, P. H.; Derissen, J. L.; van Duijneveldt, F. B. *Molec. Phys.* **1979**, *37*, 501.

14. Except for dimer **III**, which had one slightly negative force constant (-19 cm^{-1}) corresponding to a deformation out of plane.

15. Desiraju, G. R.; Murty, B. N.; Kishan, K. V. R., *Materials* **1990**, *2*, 447.

16. Etter, M. C.; Urbanczyk-Lipowska, Z.; Jahn, D. A.; Frye, J. *J. Am. Chem. Soc.*, **1986**, *108*, 5872.

17. Larsen, I. K. *Acta Crystallogr.*, **1988**, *B44*, 527.

18. a) van Eijck, B. P.; van Opheusden, J.; van Schaik, M. M. M.; van Zoeren, E. *J. Mol. Spectrosc.*, **1981**, *86*, 465. b) Caminati, W.; Scappini, F.; Corbelli, G. *J. Mol. Spectrosc.*, **1979**, *75*, 327.

19. Derissen, J. L. *J. Mol. Struct.*, **1971**, *7*, 67.

20. For a useful discussion of errors in the comparison of calculated and measured geometries see a) Schäfer, L.; Ewbank, J. D.; Siam, K.; Chiu, N.-S.; Sellers, H. L. In *Stereochemical Applications of Gas-Phase Electron Diffraction*, Hargittai, I.; Hargittai, M., Eds., VCH, New York, 1988; Part A, p 301; b) Boggs, J. E., *Ibid.*, part B, p 455.

21. Bouteillier, Y.; Behrouz, H, *J. Chem. Phys.*, **1992**, *96*, 6033.

22. Del Bene, J., *Int. Quantum Chem Biol. Symp.*, **1988**, *15*, 119.

23. Note that the experimental geometrical parameters for **II** refer to the crystal (not the dimer) where extensive cooperativity occurs.

24. Klimkowski, V. J.; Pulay, P.; Ewbank, J. D.; McKean, D. C.; Schäfer, L. *J. Comput. Chem.*, **1984**, *5*, 517.

25. Haurie, M.; Novak, A. *J. Chim. Phys.*, **1965**, *62*, 137.

26. Maréchal. Y., *J. Chem. Phys.*, **1987**, *87*, 6344.

27. Bertie, J. E.; Michaelian, K. H. *J. Chem. Phys.*, **1982**, *77*, 5267.

28. Zeismann, H. R.; Mielke, Z.; Maréchal, Y., *J. Mol. Struct.*, **1990**, *237*, 273.

29. Sverdlov, L. M. *Izv. Akad. Nauk. SSSR Ser. Khim.*, **1953**, *17*, 567.

30. CRC Handbook of Chemistry and Physics, 67th Ed., 1986-87, C-664.

VII. CRYSTAL STRUCTURE AND NONLINEAR OPTICS: MO STUDIES OF THE AGGREGATION OF NITROANILINES

1. Introduction: Nonlinear Optics and Nitroanilines

In the previous two Chapters we have seen examples how crystal structures can be rationalized through thorough inveatigations of molecular interactions. In this Chapter I go further and apply similar principles to that used in the preceding to a more complicated problem: How can nucleation and crystal formation influence certain macroscopic properties of chemical compounds?

A very interesting example involves nonlinear optics.[1] Nonlinear optical properties depend not only on the molecular properties but on the macroscopic environment (for example, crystal structure), as well. The nonlinear optical phenomenon arises when an intense electric field such as the electric component of an intense laser pulse interacts with a medium. In this case, the well-known approximation describing linear relationship between the polarization and the electric field strength is no longer true. Equations VII.1 and VII.2 illustrate the Taylor series expansion of the molecular (ρ) and the macroscopic (*P*) polarization of a medium in terms of the electric field strength (*E*).

$$\rho = \alpha E + \beta EE + \gamma EEE + \ldots \qquad \text{(VII.1)}$$

$$P = \chi^{(1)}E + \chi^{(2)}EE + \chi^{(3)}EEE + \ldots \qquad \text{(VII.2)}$$

where ρ, *P* and *E* are vector quantities, α and $\chi^{(1)}$ (the molecular polarizability and the

macroscopic susceptibility) are second rank tensors, β and $\chi^{(2)}$ (the molecular second-order hyperpolarizability and the macroscopic second-order nonlinear susceptibility) are third rank tensors and so on.[1]

At small electric fields, ignoring the second and higher order terms can be a valid approximation giving rise to linear optics. However, the influence of intense electric fields on a medium can be explained only by the inclusion of higher order terms. The peculiar properties stemming from the second and higher order expressions are called nonlinear optical properties. Substituting a sinusoidal field equation [$E=E_0(\cos(\omega t-kz)$] into equation VII.2 and using trigonometric identities we obtain equation VII.3 for the polarization that illustrates some of the numerous nonlinear optical effects.

$$P = \chi^{(1)}E_0\cos(\omega t - kz) + \frac{1}{2}\chi^{(2)}E_0^2[1 + \cos(2\omega t - 2kz)] + \chi^{(3)}E_0^3[\frac{3}{4}\cos(\omega t - kz) + \frac{1}{4}\cos(3\omega t - 3kz)] + \ldots \quad \text{(VII.3)}$$

The quadratic polarization term leads to a frequency independent static field and a term oscillating at twice the applied frequency. The former (the static polarization) results in a d.c. electric field, that is, optical rectification takes place. The oscillating term leads to the so-called second harmonic generation. Other interesting effects arise when we apply two frequencies. The result is always a mixing phenomenon generating sum and difference frequencies of various forms. The cubic polarization gives rise to the third harmonic generation (see VII.2 for the term containing 3ω) and related mixing phenomena.[1]

There are fundamental differences in the behavior of the even- and odd-order

expansion terms of VII.3 depending upon the symmetry of the medium. The even-order nonlinear susceptibilities (and, thus, for example, the second-harmonic generation) vanish in centrosymmetric media. Consequently, even-order terms (and second-order nonlinear effects) can originate only from non-centrosymmetric media. It was pointed out by Zyss and Oudar that in such media the maximum efficiency of the second harmonic generation can be as high as 38% depending on the orientation of the average molecular polarizabilities.[2] The odd-order nonlinear susceptibilities, on the other hand, can come from any medium regardless of symmetry.

The different behavior of the even-order terms in centrosymmetric and non-centrosymmetric media offers a very interesting problem for my investigations. Examining centrosymmetric and non-centrosymmetric crystal structures of chemically similar compounds can provide valuable information about the factors influencing the nucleation process. These factors (energetic and geometric patterns) may be used to predict the manner molecules aggregate and (ultimately) design non-centrosymmetric crystal structures with nonlinear optical properties.

Nitroanilines provide an excellent case for investigating the connection between non-linear optical properties and crystal structure. Etter et al. investigated the crystal structures of various nitroanilines and related compounds[3] and found that the primary structure determinants of these crystals are intermolecular hydrogen bonds. Vinson and Dannenberg performed AM1 calculations on various dimers of six different nitroanilines and analyzed the interactions leading to the observed crystal structures.[4] Although the geometric differences between the calculated gas and experimental solid phase geometries

were largely manifest in the dimer structures, this study also showed that dimer calculations are not fully sufficient to explain the energetic and geometric changes of the crystal structures.

A somewhat peculiar problem involves the different nonlinear optical properties of *p*-nitroaniline and *m*-nitroaniline. Although *p*-nitroaniline is expected to have larger second-order hyperpolarizability (β),[1] its centrosymmetric crystal structure[5] does not exhibit any second-order nonlinear properties. On the other hand, *m*-nitroaniline with its smaller hyperpolarizability crystallizes in a non-centrosymmetric manner[6] thereby leading to significant second-order nonlinear effects such as the appearance of the second harmonic generation.

In this chapter my goal will be the complete investigation and comparison of the crystal structures of *para*- and *meta*-nitroaniline. I shall explore the characteristic interactions, H-bonding patterns and other factors that are responsible for the different nucleation of these crystals. Due to the size of a nitroaniline molecule (ten heavy and six hydrogen atoms), only semiempirical calculations will be performed on nitroaniline aggregates containing up to 10 individual molecules.

2. Computational Methods

As in the previous parts of my Thesis, I performed semiempirical AM1, SAM1 and PM3 (see references in Chapter II) calculations on various aggregates of *para*- and *meta*-nitroaniline. The optimization procedure was similar to that employed for 1,3-diones

or acetic acid. The aggregates were optimized completely with the geometric constraints seen in Chapters V and VI: a) the individual molecules were kept superimposable; b) the appropriate translational vectors characterizing the ordered crystal structure were kept parallel. In addition to these two constraints, all ten heavy atoms and the aromatic hydrogens of the nitroaniline molecule were constrained in a common plane. Due to the large size of the nitroaniline molecules, the largest aggregate contained only 10 individual monomers (still enough to model the three-dimensional crystal structures).

3a. Results and Discussion: *para*-Nitroaniline

Four possible orientations for the interaction of two *p*-nitroaniline molecules are shown on Figure 1. These orientations will be the models for H-bonding interactions found in crystals and considered in this work. According to Vinson and Dannenberg[4] the H-bonding pattern at the AM1 global minimum corresponds to I characterized with two equivalent N-O...H interactions between each of the amino hydrogens and a corresponding nitro oxygen. II has an almost symmetric three-centered H-bond between an amino hydrogen and two nitro oxygens. This pattern is different from both the orientation found in the crystal structure (III and Figure 2) and the most stable arrangement (I), nonetheless represents a local minimum on the AM1 potential surface. III (not a local minimum), the interaction of the crystal structure, has a rather asymmetric, three-centered H-bond with an additional C-H...O interaction between a nitro oxygen and an aromatic proton *meta* to the nitro group. Dimer IV with its weakest interaction will have a crucial role in

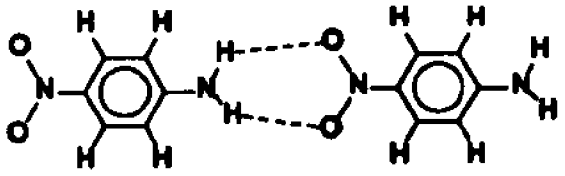

I

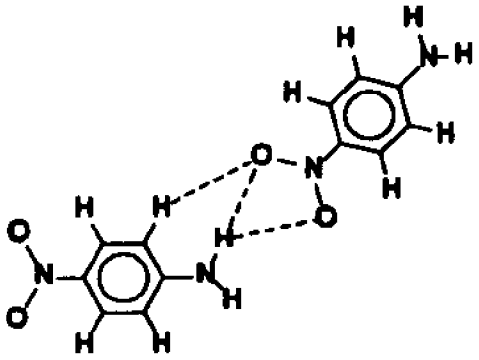

II

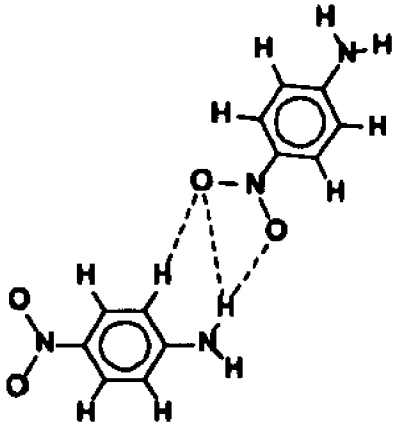

III

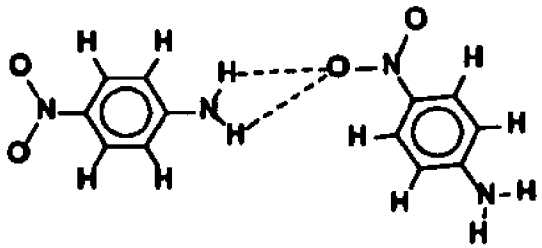

IV

Figure 1. Four possible H-bonding orientations (I-IV) of *p*-nitroaniline dimers.

determining the two-dimensional layer structure (Figure 3).

In the first part of this section the aggregation of *p*-nitroaniline is considered in all three crystallographic directions. The first direction contains the strongest H-bonding interaction between the nitro and the amino groups of two *p*-nitroaniline molecules (Figure 2). The H-bonded chains can form two-dimensional layers involving additional N-H...O interactions (Figure 3). The three-dimensional crystal structure forms from

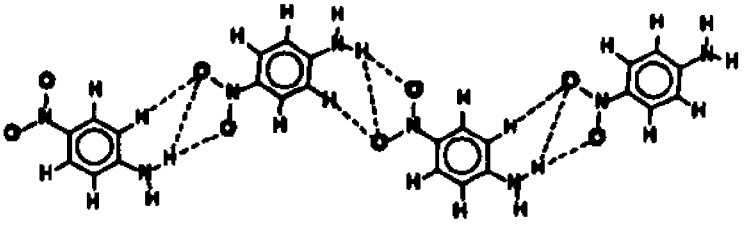

Figure 2. H-bonding patterns in *p*-nitroaniline chains.

stacked layers with opposite (head-to-tail, or *ht*) directionality of the neighboring layers (Figure 4). The unit cell contains four nitroaniline molecules. The cell parameters *a* and *c* translate every second layers into each other. The angle between theses two vectors is β=91.45°.[5] Figure 3 illustrates the relation between the other two parameters, *b* and *d*. The diagonal (*d*) of the parallelogram determined by *a* and *c* superimposes every second molecule in the first H-bonded direction defined above. The second direction (perpendicular to *d*) corresponds to *b*. The notation (*L/C/M*) of the aggregates will follow the definition of Chapter V, where *L*, *C* and *M* mean the number of layers, chains and monomers in each of the three main directions.

The hydrogen bonded network: chains and layers

Figure 2 illustrates the geometric relations within the H-bonded chains of the crystal structure, while Tables I and II collect the energetic and geometric data.

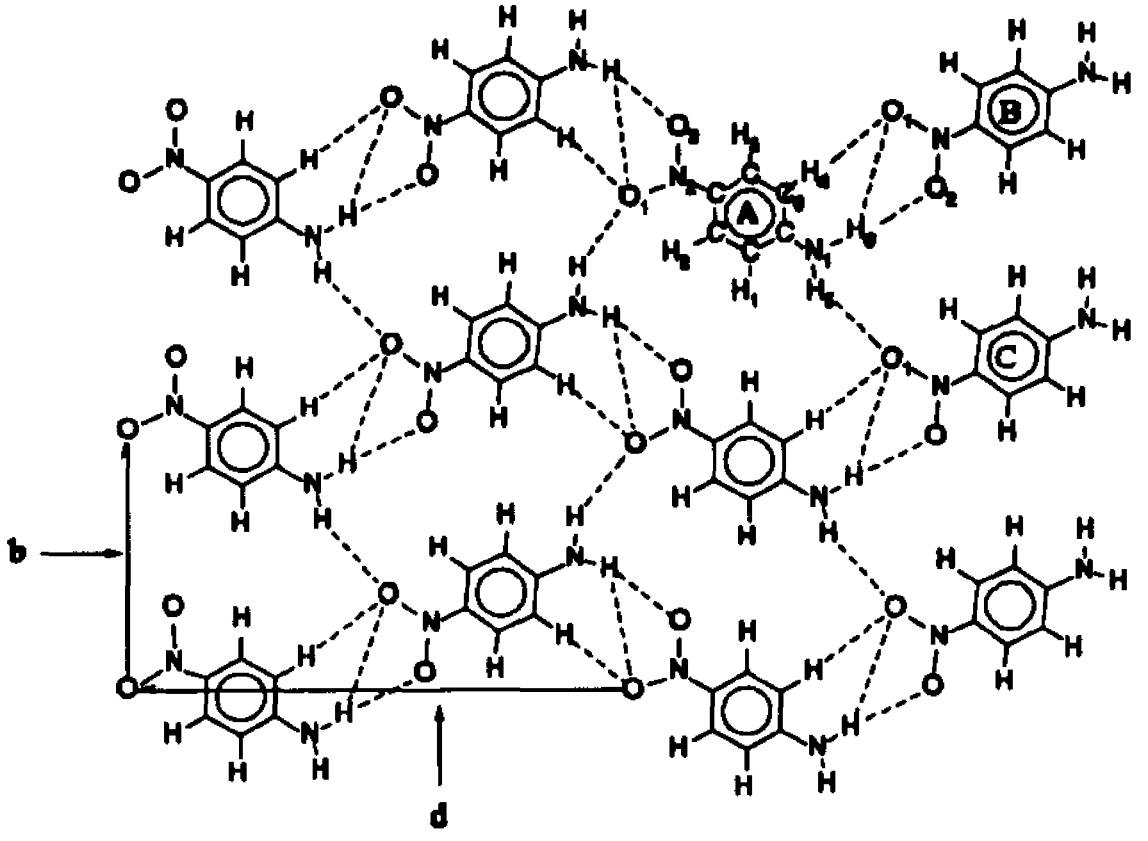

Figure 3. Schematic illustration of the layer structure of *p*-nitroaniline crystals. Note the numbering of the atoms and the unit cell parameters.

All three methods predict two distinct minima. At the global minimum the H-bonding orientation of the chains resembles the H-bonded pattern of I, while in the other that of II (Figure 1). The only exception involves the dimer structure. At PM3 level II is not a minimum, but collapses to I (Figure 1). First I turn my attention to the chains closest to the experimentally observed crystal structure (II).

All three methods indicate cooperativity (Table I). The strongest H-bond is predicted by AM1, the weakest by PM3. PM3 also shows cooperativity after three molecules aggregated. The H-bonding strength in an infinite chain is estimated by fitting

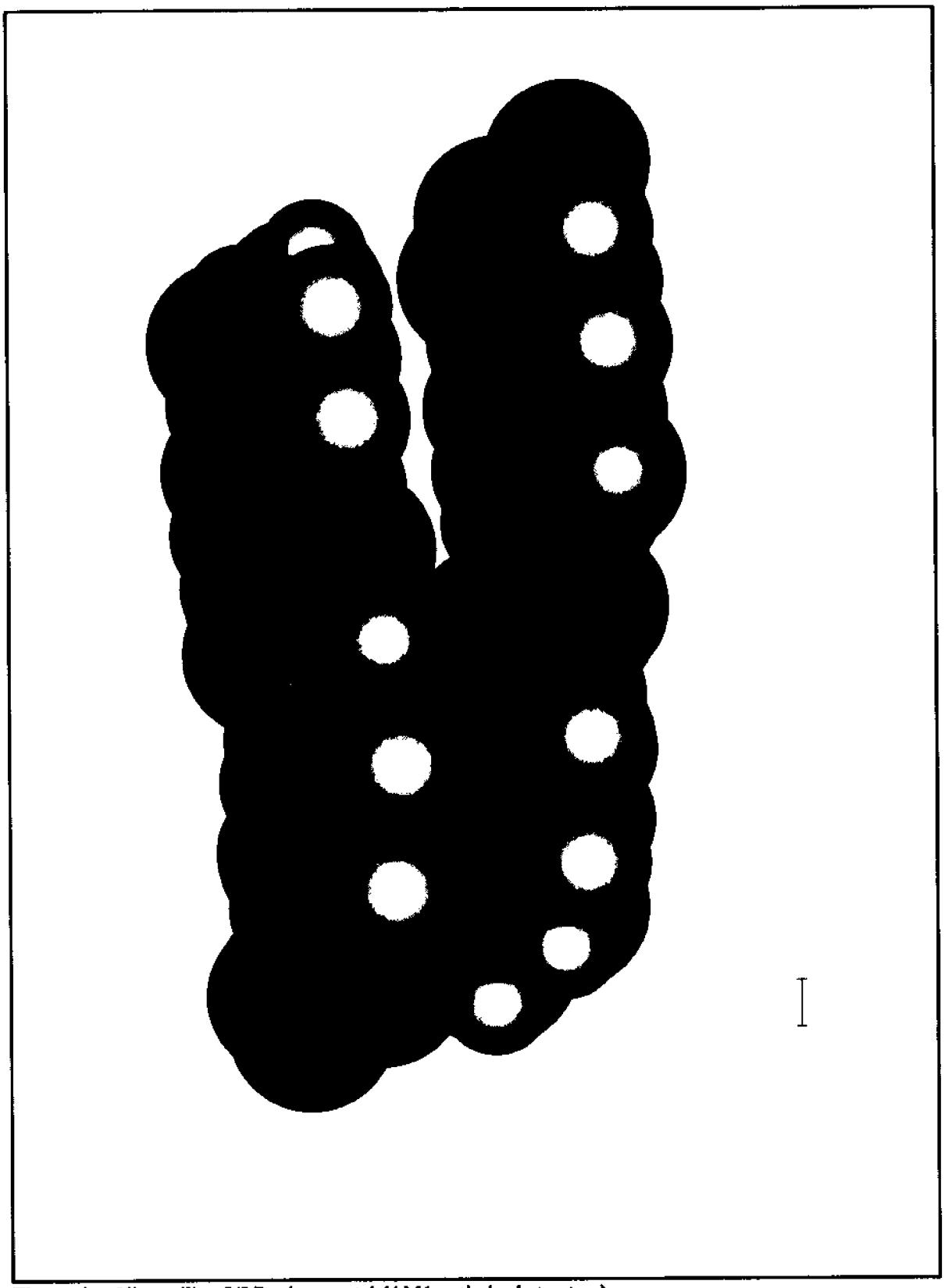

Figure 4. *p*-Nitroaniline 2/2/2 microcrystal (AM1 optimized structure).

Table I. Incremental Hydrogen-bonding Energies (kcal/mol) for *para*-Nitroaniline Chains[a]

aggregate[b]	AM1	PM3[c]	SAM1
dimer	-5.81 (-6.84)	-2.97 (-3.01)	-4.11 (-4.61)
trimer	-6.75 (-7.88)	-2.69 (-2.67)	-5.14 (-4.80)
tetramer	-7.06 (-8.18)	-3.45 (-3.15)	-5.45 (-5.57)
pentamer	-7.16 (-8.30)	-3.40 (-3.60)	-5.59 (-5.43)
hexamer	-7.23 (-8.33)	-3.56 (-3.35)	-5.66 (-5.72)
extrapolated	-7.29 (-8.34)	-3.85 (-)	-5.72 (-5.75)

[a]Heats of formation of the monomer: 21.55 kcal/mol (AM1), 10.69 kcal/mol (PM3) and 11.83 kcal/mol (SAM1). [b]Numbers in parenthesis correspond to H-bonding chains with two equivalent N-H...O H-bonds (I). [c]No PM3 extrapolation for chains I, due to non-cooperative trends.

an exponential function (see equation V.2) for the incremental part of the H-bonding interaction. According to the extrapolated values the cooperativity is 25% and 39% (compared to the dimer interactions) in AM1 and SAM1 methods, 36% in PM3 compared to the half of the total trimeric interaction (see the different dimer interactions in PM3) PM3).

The geometries predicted by three different methods differ only in slight details (Table II). Of the four possible H-bonding patterns (Figure 1) of a previous study,[4] AM1 and PM3 prefer an almost symmetric three-centered H-bond between an amino hydrogen and two nitro oxygens, similar to II. SAM1 gives a very nonsymmetric three-centered H-

Table II. Calculated and Experimental Geometries for *p*-Nitroaniline Chains[a]

aggregates	N_2-O_2	N_2-O_1	N_2-C_4	C_1-N_1	N_1-H_6	N_1-H_5	τ^b	N_1..O_2[c]	N_1..O_1[c]	H_6..O_2[c]	H_6..O_1[c]	α^b	β^b	H_6..O_1[c]	d
AM1															
monomer	1.206	1.204	1.474	1.370	0.990	0.989	7.9								
dimer	1.206	1.206	1.471	1.366	0.989	0.987	0.3	3.180	3.257	2.271	2.341	139.8	19.5	2.434	
trimer	1.207	1.207	1.469	1.364	0.990	0.987	0.3	3.163	3.239	2.259	2.317	140.5	20.1	2.443	16.187
								3.157	3.263	2.246	2.347	139.6	19.3	2.424	
tetramer	1.207	1.207	1.468	1.363	0.991	0.987	0.1	3.154	3.247	2.247	2.328	140.2	19.8	2.435	16.180
								3.144	3.243	2.237	2.325	140.1	19.8	2.424	
pentamer	1.208	1.208	1.468	1.363	0.991	0.988	0.1	3.147	3.238	2.241	2.317	140.4	20.1	2.434	16.179
								3.144	3.250	2.235	2.331	140.0	19.6	2.425	
hexamer	1.208	1.208	1.466	1.362	0.992	0.988	0.3	3.145	3.244	2.237	2.324	140.2	19.8	2.427	16.169
								3.138	3.239	2.230	2.320	140.2	19.8	2.420	
PM3															
monomer	1.216	1.216	1.490	1.416	0.994	0.994	27.7								
dimer	1.218	1.218	1.483	1.412	0.994	0.994	24.6	3.398	3.466	3.267	2.762	112.4	74.0	4.295	
trimer	1.219	1.219	1.481	1.410	0.994	0.994	22.7	3.578	3.707	2.655	2.769	132.4	18.6	2.750	16.586
								3.555	3.831	2.621	2.887	130.5	17.1	2.868	
tetramer	1.219	1.219	1.479	1.409	0.994	0.994	22.4	3.556	3.785	2.610	2.865	128.9	15.3	2.729	16.728
								3.527	3.651	2.695	2.699	137.2	28.5	3.243	
pentamer	1.219	1.220	1.478	1.408	0.994	0.994	22.0	3.546	3.734	2.611	2.807	130.8	16.9	2.724	16.701
								3.528	3.698	2.650	2.737	135.5	23.9	3.078	
hexamer	1.220	1.220	1.477	1.407	0.994	0.994	21.9	3.541	3.760	2.599	2.837	129.7	15.9	2.727	16.720
								3.508	3.662	2.661	2.708	136.8	27.1	3.190	

Table II. Cont.

aggregate	N_2-O_2	N_2-O_1	N_2-C_4	C_1-N_1	N_1-H_6	N_1-H_5	τ^b	N_1..O_2^c	N_1..O_1^c	H_6..O_2^c	H_6..O_1^c	α^b	β^b	H_6..O_1^c	d
SAM1															
monomer	1.231	1.231	1.484	1.379	0.991	0.991	11.6								
dimer	1.234	1.231	1.480	1.371	0.994	0.989	0.0	2.898	4.059	1.946	3.125	135.6	13.6	3.114	
trimer	1.235	1.231	1.478	1.369	0.996	0.990	0.0	2.875	4.015	1.922	3.082	135.9	13.7	3.066	16.556
								2.890	4.043	1.933	3.112	135.3	13.1	3.075	
tetramer	1.235	1.231	1.477	1.368	0.997	0.990	0.0	2.879	4.012	1.922	3.082	135.5	13.2	3.041	16.518
								2.868	4.005	1.910	3.075	135.4	13.1	3.029	
pentamer	1.236	1.231	1.476	1.367	0.998	0.990	0.0	2.868	3.990	1.910	3.061	135.6	13.2	3.015	16.501
								2.875	4.006	1.915	3.078	135.2	12.9	3.019	
hexamer	1.236	1.231	1.476	1.366	0.999	0.990	0.0	2.872	3.992	1.912	3.064	135.3	13.0	3.005	16.483
								2.863	3.986	1.903	3.059	135.3	12.9	2.995	
expt.[5]	1.247	1.246	1.460	1.371				3.07	3.76			120.6	12		15.211

[a]Distances in Å, angles in degrees. [b]α: C_1-N_1...O_2^B angle; β: H_6-N_1...O_2^B angle; τ: H_6-N_1-C_1-C_4 torsional angle. [c]H-bond is between molecules A and B (Figure 3).

bond with too short $N_1...O_2$ and too long $N_1...O_1$ distances between the H-bonded nitro and amino groups.

The individual geometric parameters provide additional information of the structural changes upon aggregation (Table II). All methods predict, for example, the C_4-N_2 distance to be within 0.02 Å to the experimental value. The other C-N distance (C_1-N_1) involving the amino group is very well reproduced in AM1 and SAM1, while PM3 overestimates it significantly. Generally all three methods reproduce the intramolecular parameters reasonably well. Although AM1 and PM3 give too short N-O bond lengths, they move toward the experimental value. An interesting point involves the nonplanarity of the amino group. Similarly to the observation of Vinson and Dannenberg[4] for the dimer formation at AM1 level, the aggregation results in complete planarization of the amino group at both AM1 and SAM1 levels. Although the H-bonded chain formation slightly decreases the nonplanarity in PM3, the 21.9° out-of-plane torsional angle (or 0.34 Å deviation from the plane of the aromatic ring) of the H-bonded hydrogen in the hexamer is still significant. Despite the fact that the experimentally determined hydrogen atom positions are not very reliable,[5] the observed 0.2 Å deviation from the plane of the aromatic ring also suggests some nonplanarity. The intramolecular geometries are also worth attention. Interestingly enough, while AM1 reproduces the shorter O...N contact ($N_1...O_2$) better, PM3 gives better estimate for the longer one ($N_1...O_1$). As I mentioned earlier, SAM1 fails to predict both. The aggregation decreases the N...O distances indicating cooperative effects. The unit cell dimension, *d*, is too long in all three methods mainly because of the improper H-bonding patterns. While, the AM1 (closest to

experiment) and SAM1 distances converge toward the experimentally observed distance upon aggregation, the PM3 values are oscillating.

The H-bonding energies of the most stable H-bonding chains (I) are collected in Table I in parentheses. The AM1 hydrogen-bonding energies for the chains corresponding to I are about 1 kcal/mol stronger than for the chains of II. For the other two methods the difference is much smaller.

Both the geometries of the H-bonded chains (the large deviations from the experimental data) and the energetic preference of chains with interaction I over that of II (and of course III, the crystal structure) suggest that interactions between neighboring chains will have a crucial role in determining the final structure. One can see from Figures 2 and 3 that an amino hydrogen, not participating in H-bonding within the chains, is capable of forming an extra H-bond to a nitro oxygen on the neighboring chain in a fashion similar to IV. In one-dimensional chains this interaction is missing which explains why the global minimum corresponds to chains of I.

The layer structure of three tetramer chains (a 1/3/4 aggregate) is depicted on Figure 3. In the layer structure, a nitro oxygen (O_2) participates in a strong N-H...O interaction with an amino hydrogen (H_6) and a weaker C-H...O H-bond with an aromatic *meta* hydrogen, H_4 (see molecules A and B on Figure 3). The other oxygen (O_1) H-bonds to the same amino (H_6) and aromatic (H_4) hydrogens within the chain and to another amino hydrogen on a neighboring chain in an interaction resembling IV (see Figure 1 and molecules A and C on Figure 3).

The energetic and geometrical data for the layer structures are collected in Tables

III and IV. The formation of the two-dimensional H-bonding network manifests itself in the smallest two-dimensional aggregate where two dimers interact (2/2). The structures in all three methods bear no resemblance to the one dimensional hydrogen-bonded chains and II. The additional N-H...O interaction between the chains leads to a two-dimensional H-bonding network that is characteristic of the crystal structure (III and Figure 3). Table III indicates that adding two units of *p*-nitroaniline to the end of a 2/*M* aggregate results increasing incremental H-bonding energies: -12.87, -14.51 and -14.85 kcal/mol for AM1; -10.75, -11.81 and -12.45 kcal/mol for SAM1; and -9.13, -10.01 and -10.20 kcal/mol for PM3 are the interactions from 2/3 to 2/5, respectively. As it can be seen from Figure 3, addition of two monomers to the end of a 2/*M* aggregate creates two H-bonding intrachain interactions and an extra N-H...O H-bond between the chains in every step. Thus, the incremental H-bonding energies are indeed comparable and cooperative.

Table IV collects the geometrical data pertinent to the layer structures. The data reveal excellent agreement between the observed and the calculated geometries. The AM1 and SAM1 non-bonding distances (O...N) are especially striking. These methods predict two of the three H-bonding N...O distances with very good accuracy. PM3 predicts all three O...N distances to be too long by about a consistent 0.4-0.6 Å. This might indicate that PM3 underestimates the strength of the N-H...O interactions (see also the weak PM3 interaction energies of Table I). The non-bonding H-bonding angle distribution is less good (approximately within 10° deviation), though still reliable to qualitatively describe the proper H-bonding orientations. The unit cell parameters reflect the slightest imperfections in the geometry description. For example, AM1 gives a little short *d*, and

Table III. H-bonding Enthalpies (kcal/mol) of *p*-Nitroaniline Layers and 2/2/2 Nonplanar and Planar Microcrystals[a]

aggregate	AM1		PM3		SAM1	
	Total	Incremental	Total	Incremental	Total	Incremental
2/2	-10.17 (-14.06)		-9.29 (-9.63)		-6.77 (-6.76)	
2/3	-23.04 (-30.54)	-12.87 (-16.48)	-18.42 (-18.56)	-9.13 (-8.93)	-17.52 (-19.94)	-10.75 (-13.18)
2/4	-37.55 (-48.06)	-14.51 (-17.52)	-28.43 (-28.26)	-10.01 (-9.70)	-29.33 (-27.02)	-11.81 (-7.08)
2/5	-52.40 (-66.02)	-14.85 (-17.96)	-38.63 (-38.80)	-10.20 (-10.54)	-41.78 (-43.02)	-12.45 (-16.00)
3/2	-14.73		-15.89		-9.42	
3/3	-34.35	-19.62	-31.09	-15.20	-25.53	-16.09
2+1[b]	-6.82		-5.73		-5.06	
3+2	-11.57		-12.22		-7.93	
3+2+1	-20.29		-17.23		-15.05	
4+3+2	-31.77		-30.05		-23.68	
4+3+2+1	-42.13		-35.72		-31.90	
2/2/2p[c]	-31.77	-11.43	-21.52	-2.94	-33.70	-20.16
2/2/2np[c]	-30.98	-10.64	-26.02	-7.44	-33.10	-19.56

[a]Numbers in parenthesis correspond to interaction energies for the layers constructed from chains I. [b]See text for explanation. [c]Total enthalpies and enthalpies between layers are listed for 2/2/2 planar (p) and nonplanar (np) aggregates.

long *b* mainly because of deviations from the observed non-bonding angles. Similar conclusions apply to the other two methods. Aside from the small inconsistencies of the geometrical data, the prediction of the H-bonded network is excellent in all three methods. Generally, the N...O and H...O H-bonding distances are decreasing with increasing *M* in

Table IV. Calculated and Experimental Geometries of *p*-Nitroaniline Layers and 2/2/2 Nonplanar and Planar Microcrystals[a]

aggregates	N_2-O_2	N_2-O_1	N_2-C_4	C_1-N_1	τ^b	N_1..O_2[c]	N_1..O_1[c]	H_6..O_2[c]	H_6..O_1[c]	α_1[b]	β_1[b]	H_4..O_1[c]	d	N_1..O_1[d]	H_5..O_1[d]	α_2[b]	β_2[b]	b
AM1																		
2/2	1.205	1.205	1.472	1.368	5.0	3.091	3.804	2.168	2.980	125.9	17.6	2.401		3.224	2.304	126.6	18.0	6.554
2/3	1.207	1.204	1.472	1.366	0.0	3.158	4.349	2.190	3.607	110.1	9.9	2.369	14.888	3.208	2.298	139.4	19.2	7.053
						3.164	4.356	2.196	3.613	110.1	10.0	2.374		3.193	2.280	139.1	18.8	
2/4	1.207	1.205	1.470	1.365	0.1	3.147	4.291	2.171	3.532	112.2	7.8	2.375	14.895	3.208	2.278	136.9	16.6	7.025
						3.155	4.391	2.194	3.660	108.5	11.5	2.363		3.166	2.275	141.7	21.4	
2/5	1.208	1.205	1.469	1.364	0.1	3.143	4.339	2.172	3.593	110.4	9.7	2.368	14.882	3.180	2.265	138.9	18.5	7.026
						3.147	4.351	2.178	3.607	110.1	10.0	2.370		3.171	2.257	139.2	18.8	
3/2	1.206	1.204	1.475	1.373	10.3	3.123	4.098	2.206	3.331	116.7	18.6	2.355		3.203	2.291	131.0	19.2	6.879
3/3	1.207	1.204	1.472	1.366	0.1	3.176	4.394	2.213	3.660	108.9	11.1	2.377	14.844	3.188	2.280	139.7	19.4	7.089
						3.176	4.372	2.209	3.631	109.8	10.2	2.382		3.189	2.269	138.3	17.9	
2+1	1.206	1.204	1.474	1.368	3.6	3.377	4.827	2.491	4.172	97.8	22.2	2.537		3.047	2.407	162.1	42.1	6.910
3+2+1	1.206	1.205	1.473	1.366	1.3	3.186	4.416	2.226	3.685	108.4	11.6	2.393	14.835	3.148	2.246	140.4	20.1	7.060
						3.171	4.377	2.206	3.637	109.6	10.5	2.385		3.146	2.225	138.0	17.7	
4+3+2+1	1.206	1.205	1.471	1.366	0.5	3.178	4.419	2.218	3.686	108.4	11.6	2.395	14.839	3.143	2.238	140.1	19.8	7.064
						3.166	4.375	2.199	3.632	109.8	10.2	2.391		3.151	2.227	137.8	17.4	
2/2/2p	1.207	1.205	1.471	1.367	7.8	3.146	4.348	2.185	3.609	109.9	11.9	2.362		3.198	2.282	136.8	18.5	7.107
2/2/2np	1.207	1.205	1.471	1.365	1.3	3.145	4.327	2.177	3.581	110.5	10.0	2.366		3.214	2.286	136.7	16.7	7.093
expt.[5]	1.247	1.246	1.460	1.371		3.07	3.76			120.6	12		15.211	3.14		146.1	29	6.07

Table IV. Cont.

aggregates	N_2-O_2	N_2-O_1	N_2-C_4	C_1-N_1	τ^b	N_1.O_2[c]	N_1.O_1[c]	H_8.O_2[c]	H_6.O_1[c]	α_1[b]	β_1[b]	H_4.O_1[c]	d	N_1.O_1[d]	H_3.O_1[d]	α_2[b]	β_2[b]	b
PM3																		
2/2	1.219	1.216	1.485	1.414	24.7	3.705	4.334	2.736	3.495	109.3	11.0	2.670		3.610	2.776	139.8	28.4	6.689
2/3	1.220	1.217	1.482	1.412	23.6	3.628	4.409	2.641	3.575	114.6	6.2	2.670	15.727	3.510	2.758	148.2	35.2	6.688
						3.641	4.428	2.650	3.588	114.2	4.1	2.710		3.468	2.684	145.3	32.6	
2/4	1.220	1.218	1.480	1.410	23.2	3.620	4.391	2.632	3.557	115.0	5.6	2.664	15.678	3.469	2.696	146.4	33.5	6.680
						3.602	4.446	2.608	3.610	112.9	1.6	1.722		3.470	2.678	144.3	31.9	
2/5	1.220	1.218	1.479	1.409	22.9	3.594	4.410	2.607	3.579	114.5	6.0	2.662	15.705	3.455	2.691	147.3	34.2	6.677
						3.600	4.427	2.607	3.587	114.0	2.5	2.716		3.459	2.661	144.0	31.4	
3/2	1.219	1.216	1.485	1.415	25.3	3.796	4.463	2.803	3.643	111.0	2.5	2.668		3.486	2.716	145.0	33.8	6.695
3/3	1.220	1.217	1.482	1.412	24.2	3.680	4.470	2.695	3.649	112.9	6.8	2.673	15.653	3.458	2.715	148.3	35.9	6.692
						3.692	4.467	2.704	3.638	113.2	5.8	2.698		3.438	2.671	146.3	33.9	
2+1	1.218	1.217	1.485	1.413	24.9	3.662	5.243	2.730	4.444	96.7	17.6	3.339		3.390	2.699	137.5	39.6	6.690
3+2+1	1.219	1.217	1.483	1.412	25.2	3.737	4.566	2.756	3.763	110.5	8.2	2.689	15.511	3.383	2.653	147.7	36.7	6.685
						3.700	4.534	2.714	3.698	111.4	6.6	2.690		3.370	2.596	144.8	33.3	
4+3+2+1	1.219	1.218	1.481	1.411	25.0	3.717	4.561	2.736	3.760	110.6	8.1	2.686	15.535	3.374	2.642	147.7	36.6	6.683
						3.687	4.498	2.699	3.679	112.0	5.8	2.703		3.388	2.606	144.2	32.6	
2/2/2p	1.220	1.218	1.481	1.407	21.2	3.674	4.329	2.755	3.536	117.8	19.3	2.616		3.460	2.793	153.2	41.4	6.692
2/2/2np	1.220	1.218	1.480	1.412	23.4	3.605	4.269	2.647	3.431	118.6	13.3	2.621		3.538	2.827	151.0	38.4	6.685
expt.[3]	1.247	1.246	1.460	1.371		3.07	3.76			120.6	12		15.211	3.14		146.1	29	6.07

Table IV. Cont.

aggregates	N_2-O_2	N_2-O_1	N_2-C_4	C_1-N_1	τ[b]	N_1..O_2[c]	N_1..O_1[c]	H_6..O_2[c]	H_6..O_1[c]	α_1[b]	β_1[b]	H_6..O_1[c]	d	N_1..O_1[d]	H_5..O_1[d]	α_2[b]	β_2[b]	b
SAM1																		
2/2	1.233	1.231	1.480	1.373	0.0	3.005	3.847	2.020	3.007	127.9	6.1	2.440		3.851	2.940	141.2	19.9	6.831
2/3	1.234	1.231	1.478	1.370	0.0	2.942	3.876	1.958	3.017	129.2	7.3	2.542	15.989	3.887	2.982	142.0	20.7	6.805
						2.971	3.898	1.988	3.037	129.3	7.3	2.572		3.710	2.772	137.3	16.0	
2/4	1.235	1.232	1.477	1.369	0.0	1.946	3.880	1.961	3.019	129.3	7.3	2.548	15.946	3.765	2.843	139.7	18.4	6.772
						2.929	3.879	1.943	3.023	128.8	6.8	2.528		3.745	2.822	139.5	18.2	
2/5	1.236	1.232	1.476	1.368	0.0	2.921	3.878	1.936	3.016	129.3	7.3	2.552	15.968	3.797	2.881	140.5	19.3	6.768
						2.936	3.891	1.950	3.028	129.3	7.3	2.566		3.700	2.767	138.1	16.8	
3/2	1.233	1.231	1.481	1.374	0.0	3.039	3.829	2.052	3.004	126.8	5.0	2.363		3.884	2.981	142.2	20.8	6.856
3/3	1.234	1.231	1.479	1.371	0.0	2.962	3.861	1.976	3.016	128.1	6.2	2.467	15.902	3.869	2.965	142.1	20.8	6.817
						3.001	3.886	2.015	3.036	128.3	6.4	2.507		3.746	2.818	138.8	17.5	
2+1	1.233	1.231	1.481	1.373	0.0	2.944	4.101	1.961	3.225	127.7	6.1	2.785		4.189	3.364	151.1	29.6	6.869
3+2+1	1.234	1.231	1.480	1.371	0.0	2.988	3.905	1.999	3.070	126.5	4.8	2.451	15.795	3.797	2.897	142.7	21.3	6.808
						2.987	3.908	1.999	3.074	126.4	4.7	2.450		3.651	2.721	138.5	17.1	
4+3+2+1	1.234	1.231	1.479	1.370	0.0	2.978	3.915	1.988	3.078	126.5	4.8	2.464	15.748	3.773	2.871	142.4	21.0	6.799
						2.979	3.901	1.991	3.060	127.0	5.3	2.471		3.662	2.730	138.4	17.0	
2/2/2p	1.234	1.233	1.477	1.371	5.0	2.928	3.735	1.938	2.954	123.7	4.9	2.101		3.842	2.943	141.8	21.5	6.866
2/2/2np	1.234	1.233	1.477	1.369	1.5	2.928	3.732	1.935	2.946	124.3	2.8	2.127		3.863	2.955	141.8	30.3	6.866
expt.[5]	1.247	1.246	1.460	1.371		3.07	3.76			120.6	12		15.211	3.14		146.1	29	6.07

[a]Distances in Å, angles in degrees. [b]α_1: C_1-N_1..O_2^B angle; β_1: H_6-N_1...O_2^B angle; α_2: C_1-N_1...O_1^C angle; β_2: H_5-N_1...O_1^C angle. [c]H-bond is between molecules A and B (Figure 3). [d]H-bond is between molecules A and C (Figure 3).

2/*M* aggregates as an indication of two-dimensional cooperative effects.

Table III also shows the interaction energies of some *C/M* aggregates from chains exhibiting H-bonding orientation I (in parenthesis). The data seem to indicate that both PM3 and SAM1 layers I and III are similar in energy. At AM1 level layers of I are preferred enthalpically over those of III. A closer look at the *C/M* aggregates (Figure 3) reveals, however, that only every second molecule of the H-bonded chains at the edges of a two-dimensional aggregate has both nitro oxygens completely H-bonded (not counting the nitro groups at the end of the chain). The unsatisfied hydrogen-bonding potential of those molecules not participating in all of their possible H-bonds assures the growth of the associates and their energetic preference over the chains of I. This observation explains why the *C/M* layers cannot fully account for the energetic preference of pattern III over I. Consideration of complexes with completely H-bonded nitro groups would be necessary. Such structures are shown in Figure 5. In these triangle shaped aggregates all the H-bonding potentials of the nitro groups are satisfied except those at the end of the chains. Tables III and IV contain the data for three such aggregates denoted by 2+1, 3+2+1 and 4+3+2+1. Removal of a molecule from the top of the triangle leads to complexes such as 3+2 and 4+3+2. The total interaction energy of a 2+1 aggregate represents the interaction energy of a fully H-bonded nitro group only approximately because of the interaction (presumably repulsion) between the two molecules that do not H-bond together (at the bottom of the triangle). Adding a monomer to 3+2 aggregate results -8.72, -5.01 and -7.12 kcal/mol for AM1, PM3 and SAM1, all of them are already larger than the extrapolated incremental H-bonding energies for chains I. The difference

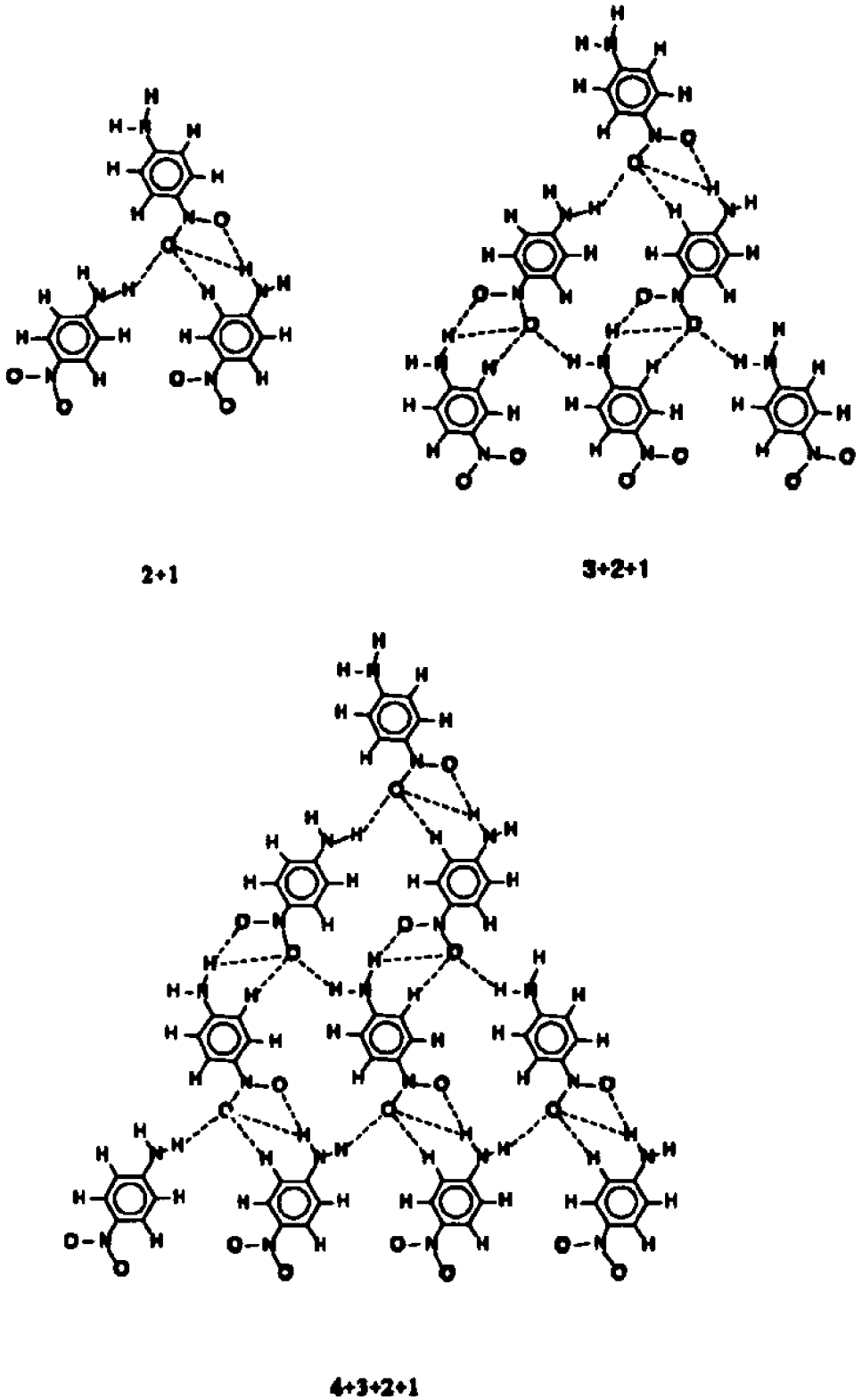

Figure 5. 2+1, 3+2+1 and 4+3+2+1 aggregates of *p*-nitroaniline.

is more striking for adding a monomer to the 4+3+2 aggregate forming 4+3+2+1. The interaction energies are -10.36, -5.67 and -8.22 kcal/mol for AM1, PM3 and SAM1. In the following I attempt to compare the average stabilizations of an individual molecule within layers I and III. For layer I, the stabilization will be approximated as the sum of the extrapolated incremental H-bonding energy of chain I and an estimated extra stabilization between the chains. The extrapolated incremental energies for chain I are -8.3, -3.6 and -5.8 kcal/mol for AM1, PM3 and SAM1, respectively (Table I). (Note that for PM3 where the extrapolation failed, the largest incremental energy is used.) My estimation of the interchain interactions is -1.5, -3.0 and -1.5 kcal/mol for AM1, PM3 and SAM1 from the interchain stabilization of 2/*M* aggregates of I (Table IV, in parentheses) divided by *M*. Thus, the interaction energy per molecule of an infinite two-dimensional layer with interaction I is approximately -9.9, -6.6 and -7.3 kcal/mol. Even without taking further cooperative effects and other weaker interactions between the chains (for example, repulsions originating from the proximity of aromatic hydrogens on neighboring chains) into account, the last stabilization energies for the 4+3+2+1 aggregate (H-bonding pattern III) in AM1 and SAM1 (-10.4 and -8.2 kcal/mol) are greater than those estimated for layers I above. Thus, AM1 and SAM1 predict that the two-dimensional H-bonding network of III (combined with IV) will be enthalpically preferred over that of I. The fact that the PM3 values are also very close (-6.6 kcal/mol for I, -5.7 kcal/mol for III) might suggest that inclusion of cooperativity would be necessary to reverse the unfavorable energetic trends.

The geometries of the aggregates 2+1, 3+2+1 and 4+3+2+1 are collected in Table

IV. The trends are very similar to those experienced for *C/M* aggregates. The changes in the unit cell parameters reflecting the influence of the fully H-bonded nitro groups are small and do not change my previous conclusions.

Aggregation in the third direction

The crystal growth in the third direction can be characterized (similarly to the acetic acid case) by stacking of the infinite two-dimensional layers (Figure 4). The layers are held together by weak electrostatic interactions. The size of the simplest meaningful three-dimensional structures largely limited my calculations. The largest structure considered in this part was a 2/2/2 microcrystal. The results for these structures are shown in Tables III and IV.

The simplest model of the three-dimensional structures consists of two stacked monomers (2/1/1). All three methods predict the inverse (head-to-tail, *ht*) orientation of the molecules to be preferred over the other alignment where the nitro groups point to the same direction (head-to-head, *hh*). In fact, the *hh* complex is repulsive in all calculations. On the other hand, the *ht* orientation is not only stabilized by -2.80, -2.36 and -3.70 kcal/mol in AM1, PM3 and SAM1, respectively, but the molecules assemble in a roughly centrosymmetric manner. This orientation corresponds to the strongest electrostatic attraction between the electron rich nitro group and the positively charged amino protons. Adding two more monomers step by step to the 2/1/1 complex in a similar manner results in the 4/1/1 and 6/1/1 aggregates (four and six stacked molecules, respectively). (The repeating unit, similarly to H-bonded chains, consists of two *p*-nitroaniline molecules.)

The interaction between two 2/1/1 aggregates is greatly reduced by two new 1-3 pairwise repulsions between every second *hh* nitroaniline molecules and the slight repulsion between the nitrogen lone pair of the amino group and the nitro oxygens at the place of the new contact. The interaction energies of this step are -0.50, -0.32 kcal/mol for AM1 and PM3, while no suitable minimum was found in SAM1. The addition of another 2/1/1 aggregate to 4/1/1 lowers the enthalpy by -0.52 and -0.34 kcal/mol (AM1 and PM3), slightly more than in the previous step. The translational vectors connecting every second stacked monomers can be related to the unit cell parameter *c*. The AM1 translations are 9.129 and 9.106 Å for 4/1/1 and 6/1/1, while PM3 predicts 9.305 and 9.306 Å. Despite the simplicity of the model, these values are surprisingly close to the experimental 8.592 Å indicating that both PM3 and AM1 describe the mostly electrostatic interlayer interactions reasonably well.

In a somewhat better model for stacking, a H-bonded dimer interacts with a stacked monomer parallel with one of the two *p*-nitroaniline molecules of the dimer (2+1). Although, we have seen in the previous section that the H-bonding interactions within the H-bonded single chains (II) differ from those of the crystal (III), consideration of this complex is instructive. The results of these calculations were similar to that of 2/1/1. The *hh* orientation is predicted to be repulsive and not a minimum on the potential surface whereas *ht* is stabilized by -2.64, -1.89 and -5.88 kcal/mol in AM1, PM3 and SAM1. The smaller (except for SAM1) stabilization compared to the 2/1/1 molecule is certainly due to the proximity of similarly charged groups of the stacked monomer and the second molecule of the dimer.

In the best model of the crystal structure all relevant interactions must be present. Such aggregate is a 2/2/2 model of the crystal structure containing all H-bonding interactions and shorter range electrostatic forces (Figure 4). The 2/2/2 microcrystal contains two stacked layers from two dimers. Both *ht* and *hh* orientations have been examined in this aggregate. Calculations have been performed with and without a constraint that all heavy atoms of a layer be in a common plane. Neither of the three MO methods was able to locate a suitable minimum with *hh* chain orientation. On the other hand, all methods give stable and almost centrosymmetric crystals with head-to-tail chain direction. AM1 and SAM1 predict the structure consisting of planar layers to be more stable, while PM3 favored nonplanar layers. Both AM1 and SAM1 stabilizations are very strong, -11.43 kcal/mol (or -2.86 kcal/mol/stacked molecule pair) and -20.16 kcal/mole (or -5.04 kcal/mol/stacked molecule pair). For PM3 this value is slightly less, -7.44 kcal/mol (-1.86 kcal/mol/stacked molecule pair). The average stabilization of a molecule within the crystal lattice would then be the sum of the estimated intralayer stabilization (from 4+3+2+1 aggregate: -10.36, -5.67 and -8.22 kcal/mol in AM1, PM3 and SAM1) and the interlayer interaction for a molecule pair. This value would give an estimation for the heat of sublimation of the *p*-nitroaniline crystal. The appropriate heat of sublimation estimates are -13.3, -7.6 and -13.2 kcal/mol for AM1, PM3 and SAM1 respectively. The AM1 and SAM1 values compare favorably with the experimental value (26.1 kcal/mol)[7] especially knowing that, due to the limited size of the largest examined aggregates, the semiempirical values do not contain significant contributions from interdimensional cooperative effects.

The deviation from being centrosymmetric (in centrosymmetric material the appropriate bonds are parallel and opposite in directionality) is within few degrees of the required 180° torsional angle. The geometry of the H-bonding aggregates is not significantly different from that of the individually optimized layers (Table IV). It is also worth mentioning that all methods predict longer *d* than in the appropriate 2/2 layer, so the difference between the observed and the calculated unit cell parameters becomes somewhat larger.

3b. Results and Discussion: *meta*-Nitroaniline.

The crystal structure of *m*-nitroaniline is significantly different from that of *p*-nitroaniline.[5,6] The H-bonded chains of *m*-nitroaniline follow H-bonding pattern II on Figure 1 (see also Figure 6). Instead of forming infinite layers, two H-bonded chains form a strand (Figure 6) via strong H-bonding interactions. The strands then stack in a parallel manner, where all the nitro groups point in the same direction (*hh*) as illustrated on Figure 7. The stacked strands are superimposable by the translation vectors *a* and *c*. The third edge (*d*) of the right triangle with edges *a* and *c* translates every nitroaniline molecule within the H-bonded chains (see Figures 6 and 8). The resulting stacked structure interacts with two other stacks almost perpendicularly (104°) via aromatic C-H...O H-bonds (Figures 8 and 9). These latter interactions will be significant in determining the final crystal structure and the nonlinear optical properties. The longest of all three unit cell parameters (*b*) translates (perpendicular to the plane of *a*, *c* and *d*) this three-dimensional

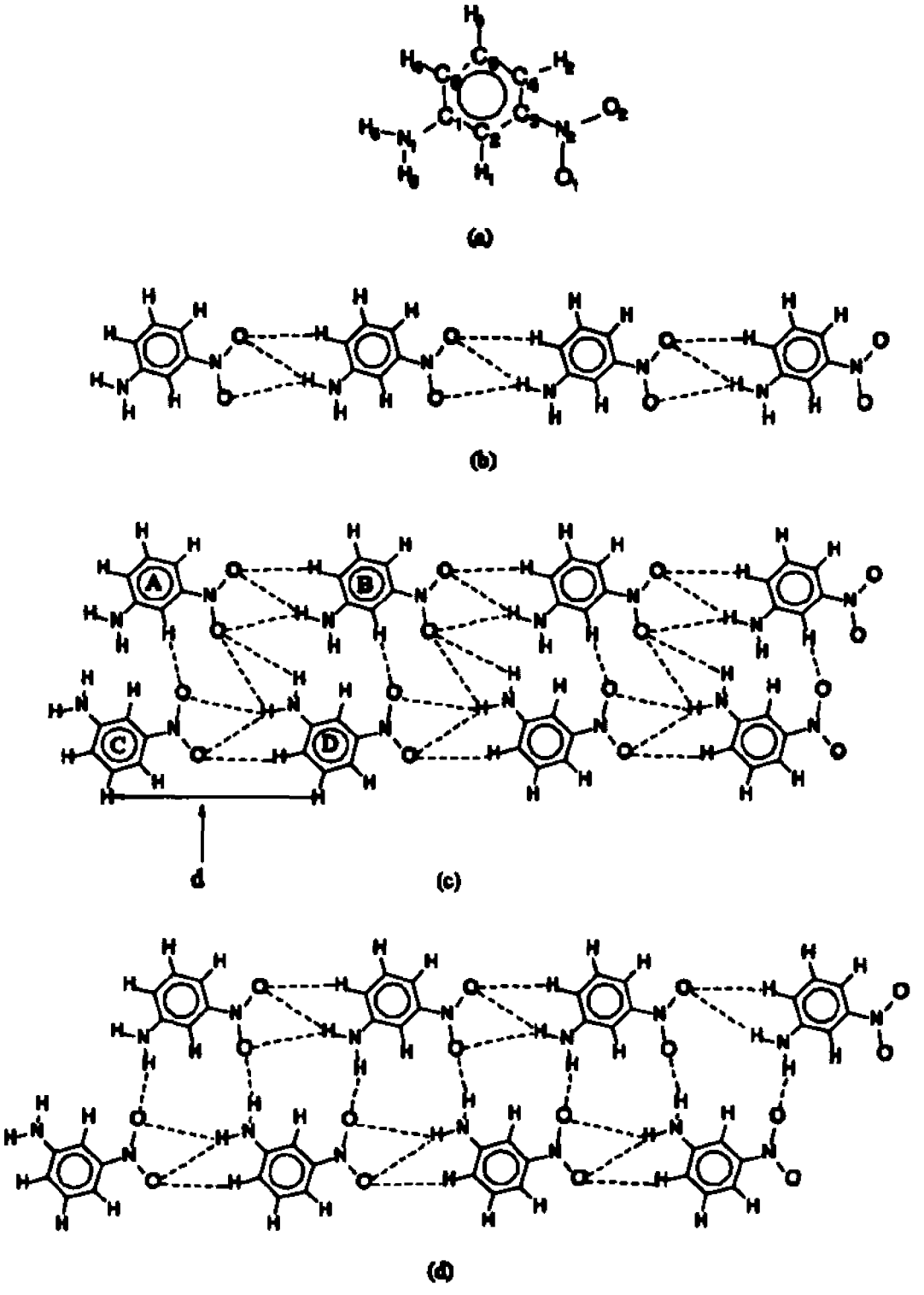

Figure 6. H-bonded chains (b) and strands (c) of *m*-nitroaniline crystal structure. The calculated structure is shown at the bottom (d). Note the numbering (a) and the unit cell parameter *d* (c).

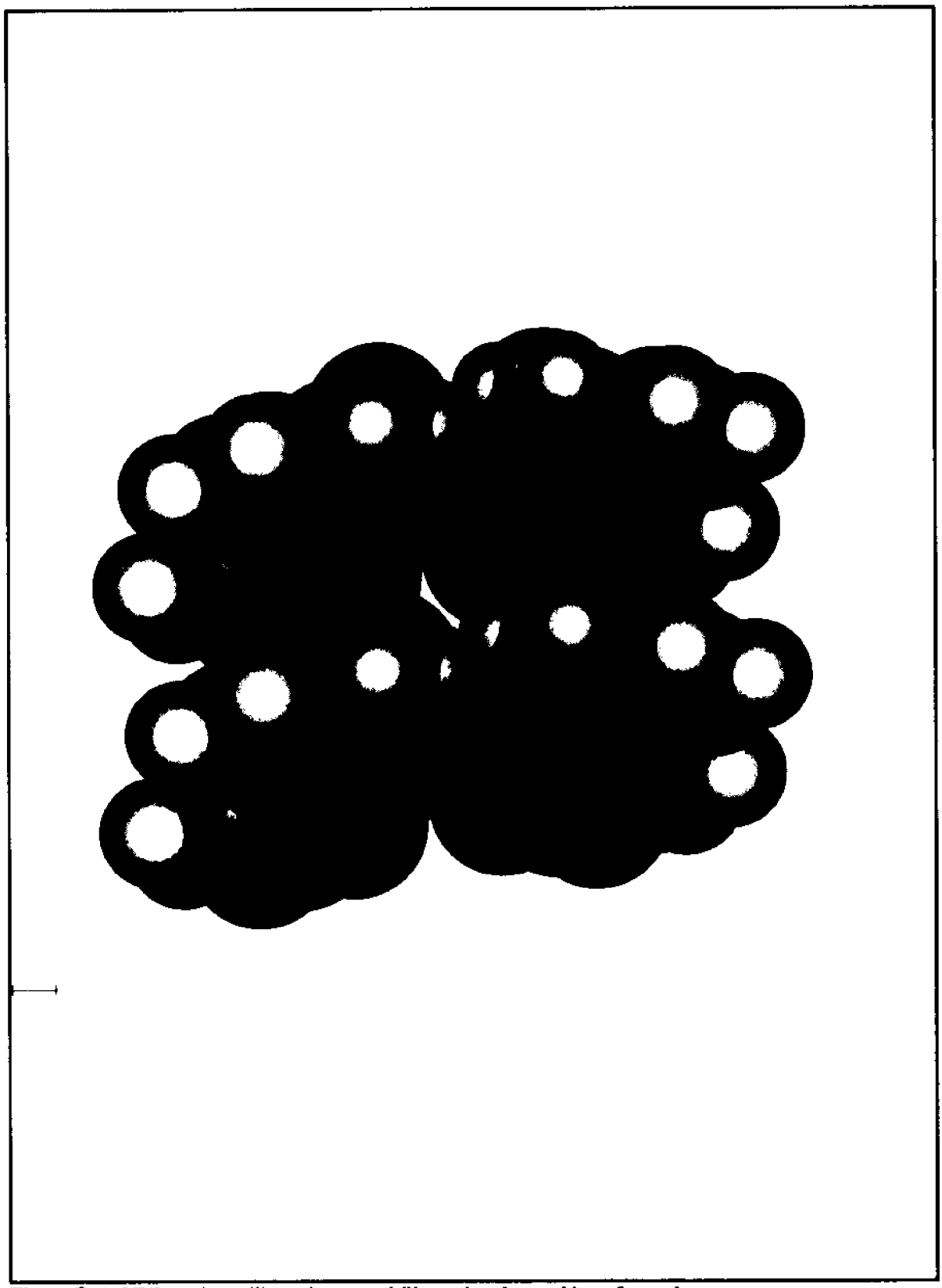

Figure 7. A 2/2/2 *m*-nitroaniline microcrystal illustrating the stacking of strands.

microcrystal periodically giving the final order of the crystal.

Due to the complexity of the crystal structure, four types of interactions will be examined separately. The first and second will include H-bonding interactions within the H-bonded chains and strands of *m*-nitroaniline. The notation of these structures is similar to the one defined earlier; 1/*M* will denote single H-bonded chains, while 2/*M* stands for the H-bonded strands containing 2 chains from *M* monomers. *L*/1/*M* and *L*/2/*M* will be used to denote the stacks of *L* chains and strands, respectively, during the examination of the first stacking direction. The fourth part of the investigation will concentrate on the stacking phenomenon in the *b* direction, that is, the interactions between *L*/2/*M* aggregates that result in forming three-dimensional microcrystals.

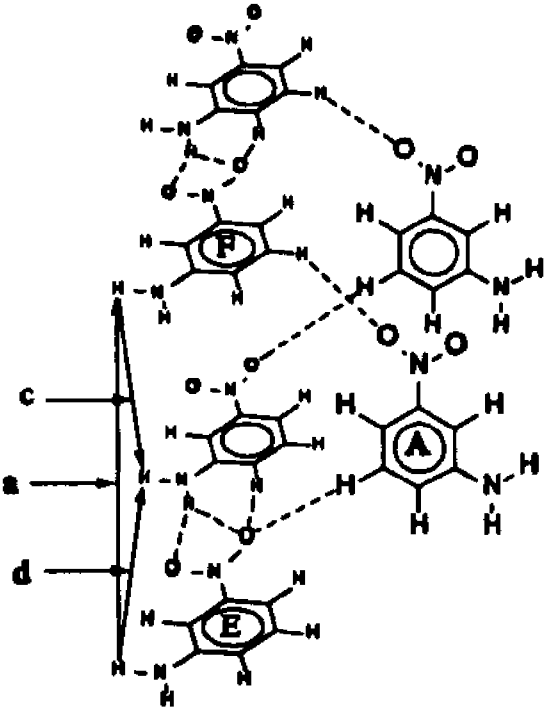

Figure 6. Interactions between stacked strands in the direction of the unit cell parameter *b*.

Hydrogen-bonded chains and strands

Figure 6 illustrates the hydrogen bonding orientation within and between the H-bonded *m*-nitroaniline chains. Tables V and VI contain the energetic and geometric information for the appropriate aggregates.

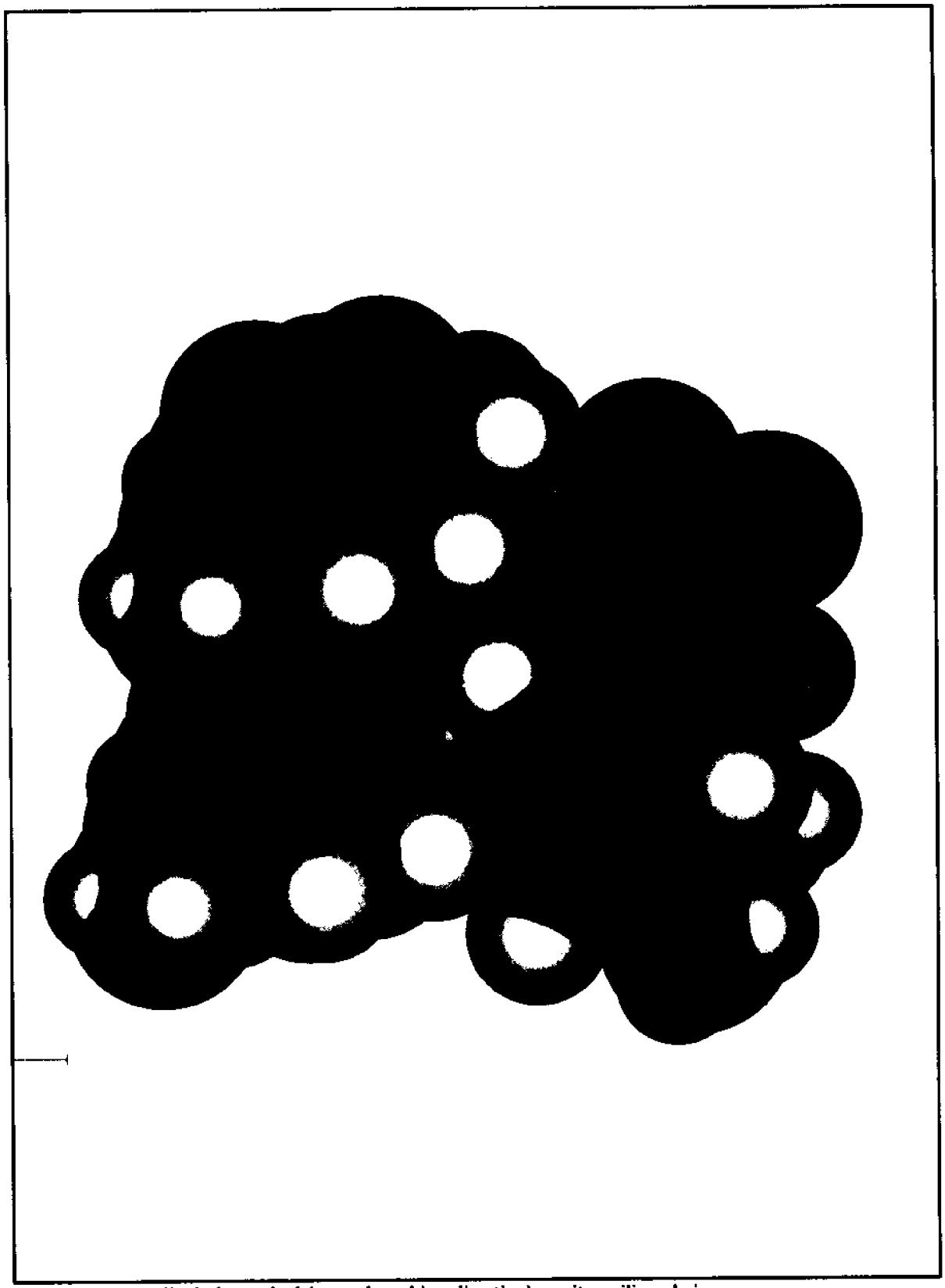

Figure 9. Perpendicularly stacked (second stacking direction) *m*-nitroaniline chains.

Table V. Incremental Hydrogen-bonding Energies (kcal/mol) for *meta*-Nitroaniline Chains.[a]

aggregate	AM1	PM3	SAM1
dimer	-4.77	-2.46	-3.18
trimer	-5.42	-2.89	-3.81
tetramer	-5.62	-3.02	-4.02
pentamer	-5.70	-3.07	-4.09
hexamer	-5.74	-3.10	-4.14
extrapolated	-5.76	-3.12	-4.18

[a]Heats of formation of the monomer: 24.02 kcal/mol (AM1), 12.55 kcal/mol (PM3) and 14.46 kcal/mol (SAM1).

One can see from Figure 6, that the H-bonds within the chains resemble pattern II of Figure 1. The characteristic interaction is an almost symmetrical three-centered H-bond between an amino hydrogen (H_5) and two nitro oxygens (O_1 and O_2). One of the nitro oxygens (O_2) participates in an additional weak C-H hydrogen bond with an aromatic hydrogen (H_2) *para* to the nitro group. The energies for the aggregation in this first direction are collected in Table V. The trends bear similarity to those observed in the *p*-nitroaniline case. The strongest interactions are predicted by AM1, the weakest by PM3. The H-bonds appear to be weaker than for *p*-nitroaniline aggregates. The extent of cooperativity (using the extrapolated values of Table V) is also smaller, 21%, 27% and 31% (compared to the dimer interactions) in AM1, PM3 and SAM1. The smaller cooperative interactions are indicative of the less favorable conjugative effects (thereby smaller polarizability) of the *m*-nitroaniline molecules.

Table VI. Calculated and Experimental Geometries for *m*-Nitroaniline Chains[a]

aggregates	N_2-O_2	N_2-O_1	N_2-C_3	C_1-N_1	N_1-H_5	N_1-H_6	τ[b]	N_1..O_2[c]	N_1..O_1[c]	H_5..O_2[c]	H_5..O_1[c]	C_6..O_2[c]	H_6..O_2[c]	*d*
AM1														
monomer	1.202	1.202	1.490	1.394	0.995	0.995	25.4							
dimer	1.204	1.203	1.487	1.395	0.995	0.994	22.9	3.316	3.227	2.401	2.306	3.334	2.386	8.235
trimer	1.204	1.204	1.486	1.389	0.995	0.994	21.9	3.308	3.217	2.392	2.295	3.326	2.375	8.230
tetramer	1.205	1.204	1.481	1.388	0.996	0.993	21.2	3.306	3.212	2.390	2.289	3.322	2.369	8.228
pentamer	1.205	1.204	1.484	1.387	0.996	0.993	20.9	3.303	3.208	2.387	2.285	3.319	2.366	8.226
hexamer	1.205	1.204	1.484	1.387	0.996	0.993	20.6	3.300	3.206	2.383	2.284	3.318	2.364	8.225
PM3														
monomer	1.215	1.216	1.499	1.427	0.995	0.995	30.9							
dimer	1.217	1.217	1.494	1.426	0.995	0.995	28.2	4.116	3.883	3.226	2.703	3.706	2.687	8.629
trimer	1.217	1.217	1.492	1.426	0.996	0.995	27.3	4.108	3.663	3.218	2.681	3.685	2.665	8.609
tetramer	1.218	1.218	1.495	1.425	0.996	0.995	26.8	4.096	3.654	3.205	2.672	3.677	2.655	8.603
pentamer	1.218	1.218	1.490	1.425	0.996	0.995	26.5	4.090	3.648	3.199	2.667	3.672	2.651	8.598
hexamer	1.218	1.218	1.490	1.425	0.996	0.995	26.3	4.088	3.645	3.196	2.663	3.668	2.648	8.594
SAM1														
monomer	1.228	1.229	1.498	1.391	0.994	0.994	21.5							
dimer	1.230	1.228	1.497	1.385	0.996	0.993	18.7	2.964	3.890	1.979	3.196	4.054	3.400	8.656
trimer	1.231	1.228	1.497	1.382	0.997	0.993	17.2	2.952	3.861	1.964	3.160	4.027	3.363	8.646
tetramer	1.231	1.228	1.497	1.381	0.998	0.992	16.1	2.975	3.843	1.955	3.137	4.009	3.339	8.641
pentamer	1.232	1.228	1.497	1.380	0.998	0.992	15.3	2.941	3.832	1.949	3.125	4.000	3.325	8.638
hexamer	1.232	1.228	1.497	1.379	0.998	0.992	14.8	2.938	3.825	1.946	3.116	3.994	3.316	8.636
expt.[d,e]	1.223	1.222	1.467	1.391				3.459	3.270			3.372		8.251

[a]Distances in Å, angles in degrees. [b]τ: H_5-N_1-C_1-C_6 torsional angle. [c]H-bond is between molecules A and B (Figure 6).

The geometrical data of Table VI demonstrate that AM1 predicts the H-bonding pattern extremely well, while PM3 and SAM1 deviate from the crystal structure seriously. PM3 would prefer a structure similar to III of Figure 1 (with a rather asymmetric three-centered H-bond between the nitro and the amino group) and overestimate the H-bonding distances. SAM1 predicts a structure with only one H-bond between O_2 and H_5. It also overestimates the C-H...O distances. In addition to the excellent prediction of the H-bonding orientation, AM1 is also very good at estimating the translation vector *d*, while the other two methods predict *d* to be too long. The geometrical data also reflect the strong influence of aggregation and cooperativity. The H-bonding distances (and the translational vectors) are becoming shorter with increasing aggregate size suggesting stronger interactions.

The energetic and geometric data of selected *m*-nitroaniline strands (2/*M* aggregates, *M*=2,3,4) can be found in Tables VII and VIII. One of the nitro oxygens, O_1, is capable of forming additional H-bonds with a neighboring chain. In the crystal structure O_1 H-bonds to an amino group on the neighboring chain with an almost symmetric three-centered interaction (see the interaction between molecules A and D on Figure 6). The aromatic *ortho* hydrogen (H_1) forms a C-H...O H-bond to the nitro group on a molecule of the other chain (interaction between molecules A and C). In this orientation those sides of the chains interact which contain both the more available H-donor and acceptor groups (the substituents on neighboring chains are directed toward each other). It is remarkable that only the nitro groups of one chain of a strand (upper chain on Figure 6) form two three-centered H-bonding interactions (one within the chain, the other with the

Table VII. H-bonding Enthalpies (kcal/mol) of *m*-Nitroaniline 2/*M* Strands (*M*=2,3,4), *L*/1/*M* Stacks (*L*,*M*=2,3) and a 2/2/2 *hh* Microcrystal (see text for explanation)

aggregate	AM1		PM3		SAM1	
	Total	Between Chains	Total	Between Chains	Total	Between Chains
2/2	-14.08	-4.54	-7.68	-2.76	-6.43	-0.07
2/3	-28.23	-7.85	-14.02	-3.32	-14.38	-0.40
2/4	-43.14	-11.52	-21.34	-4.60	-23.41	-1.39
2/1/2[a]	-8.03	1.51	-4.51	0.41	-3.78	2.58
2/1/3	-17.79	2.59	-9.85	0.85	-9.30	4.68
2/1/4	-28.19	3.43	-15.65	1.09	-15.61	6.41
3/1/2	-11.67	2.64	-7.09	0.29	-4.68	4.86
3/1/3	-25.35	5.22	-14.59	1.46	-11.31	9.66
2/2/2	-21.77	6.39				

[a]Total enthalpies and enthalpies between layers are listed for *L*/*C*/*M* aggregates.

neighboring chain), while the nitro groups of the other chain (lower chain on Figure 6) participate in one three-centered H-bond within the chain and a C-H...O interaction to the *ortho* H_1 of the first chain. The predicted H-bonding energies between the chains are distinct for the three methods (Table VII). AM1 interaction is very strong (-11.52 kcal for 2/4), PM3 is less than half of the AM1 stabilization (-4.60 kcal/mol for 2/4), while SAM1 barely gives attractive energies (-1.39 kcal/mole for 2/4). AM1 and SAM1 exhibit two-dimensional cooperative effects, that is, the interchain interaction for every molecule pair (interchain interaction divided by *M* in a 2/*M* aggregate) is becoming stronger with increasing *M*.

Table VIII. Calculated and Experimental Geometries of *m*-Nitroaniline Layers[a]

aggregates	N_2-O_2	N_2-O_1	N_2-C_3	C_1-N_1	τ[b]	N_1..O_2[c]	N_1..O_1[c]	H_5..O_2[c]	H_5..O_1[c]	C_6..O_2[c]	H_4..O_2[c]	d	N_1..O_1[d]	H_6..O_1[d]	H_7..O_1[d]	C_2..O_1[d]	H_1..O_1[d]	O_1..O_1[d]
AM1																		
2/2	1.202	1.205	1.487	1.390	23.0	3.251	3.241	2.365	2.381	3.380	2.426	8.301	3.156	2.169	3.669	3.847	3.110	5.115
													3.186	2.226	3.832	3.803	2.963	4.990
2/3	1.203	1.205	1.486	1.387	20.9	3.250	3.231	2.353	2.357	3.371	2.414	8.293	3.157	2.171	3.697	3.825	3.076	5.121
													3.170	2.208	3.811	3.807	2.974	5.015
2/4	1.203	1.206	1.485	1.385	19.6	3.243	3.226	2.341	2.347	3.367	2.412	8.289	3.159	2.172	3.719	3.815	3.052	5.099
													3.166	2.195	3.805	3.807	2.078	5.027
PM3																		
2/2	1.216	1.218	1.494	1.425	28.7	4.035	3.756	3.200	2.885	3.835	2.784	8.836	3.386	2.658	3.270	4.989	4.617	6.896
													3.831	2.942	4.886	3.808	2.785	4.380
2/3	1.216	1.218	1.492	1.424	28.1	3.978	3.772	3.116	2.867	3.833	2.790	8.834	3.451	2.636	3.492	4.571	4.151	6.251
													3.584	2.678	4.248	4.093	3.179	5.067
2/4	1.216	1.219	1.491	1.424	27.6	4.032	3.713	3.179	2.810	3.779	2.721	8.783	3.483	2.620	3.586	4.587	4.108	6.209
													3.588	2.654	4.206	4.186	3.296	5.222
SAM1																		
2/2	1.229	1.229	1.498	1.381	14.4	3.115	4.020	2.140	3.310	4.183	3.477	8.860	3.049	2.068	3.506	4.019	3.346	5.406
													3.285	2.352	3.997	3.458	2.574	4.416
2/3	1.230	1.229	1.498	1.376	8.2	3.026	3.931	2.042	3.215	4.096	3.400	8.768	3.071	2.080	3.651	3.834	3.067	5.133
													3.174	2.217	3.873	3.541	2.676	4.615
2/4	1.230	1.229	1.497	1.373	3.5	3.002	3.902	2.013	3.181	4.068	3.373	8.741	3.074	2.086	3.690	3.767	2.793	5.025
													3.146	2.180	3.841	3.579	2.718	4.686
expt.[e]	1.223	1.222	1.467	1.391		3.459	3.270			3.372		8.251	4.539			3.393		3.337
													3.336			5.355		7.306

[a]Distances in Å, angles in degrees. [b]τ: H_5-N_1-C_1-C_6 torsional angle. [c]H-bond is between molecules A and B (Figure 6). [d]H-bond is between molecules A and C for the first number, between molecules D and A for the second (Figure 6).

All three methods predict the same orientation for H-bonded strands, though it is slightly different from the experimental (Figure 6d and Table VIII). They favor a structure where one oxygen (O_1) of a nitro group H-bonds to only one amino hydrogen (H_6) and an aromatic hydrogen, H_1, on the same molecule of the neighboring chain. This means, that the second chain is strongly shifted relative to the first one in the direction of *d* by about 2 Å (Figure 6), the molecules of the first chain approximately facing the H-bonded part of the second, and vice versa. In this geometry, every molecule participates in two almost equivalent H-bonds: its nitro group H-bonds to an amino hydrogen and an aromatic proton on the neighboring chain, while its amino group and *ortho* hydrogen are H-bond donors to the nearest nitro group of another molecule of the other chain. Thus, both O...N interchain distances in which a molecule takes part are approximately the same (instead of one short 3.336 Å and one long 5.355 Å contact, as in the experiment[6a]). Fortunately, we shall see in the following that the deviation from the experimental H-bonding pattern will not affect my conclusions concerning the stacking phenomena and the origin of nonlinear optical properties.

The trends for the calculated unit cell parameters follow those for single chains. The gradual strengthening of H-bonding interactions results shorter *d* and shorter H-bonding distances, as well. The unit cell parameter *d* is slightly longer in strands than in chains with same *M*, providing an even better agreement between AM1 calculations and experiment. It is also interesting to notice the planarization of the amino hydrogens upon aggregation. The larger out-of-plane torsional angle (τ in Tables VI and VIII) compared to the *p*-nitroaniline case is due to the fact that the amino nitrogens in *m*-nitroaniline

optimizations were *not* confined into the aromatic plane. Despite this technical difference, the out-of-plane torsional angles steadily decrease with increasing aggregate size.

Stacking of the strands: inverse or parallel?

Stacking of the strands can occur in two different ways. In the first one (crystal structure) the nitro groups are pointing in the same direction (*hh* orientation), while in the second one the directionality of the stacked strands is opposite (*ht*). The *ht* arrangement, even in the case of non-centrosymmetric orientation, would reduce the potential non-linear optical properties of the crystals in large extent.[2] Thus, the following questions arise: Which is the energetically more favorable orientation? Does the more favorable orientation coincide with the observed nonlinear optical properties? The studies for *p*-nitroaniline foreshadow the answer: the *ht* direction proved to be attractive, while none of the applied methods could predict stabilized stacks of *hh* directionality. From the results for *m*-nitroaniline stacks one can expect analogous behavior. Stacks of 2/1/2, 2/1/3, 2/1/4, 3/1/2, 3/1/3 (two or three stacked chains) and 2/2/2 (two stacked strands) have been examined in *hh* orientation with both forced orthogonality between translation vectors *a* and *c* (β=90°) and with optimized β. Tables VII and IX summarize the results of these calculations. The structures with optimized β do not result in stable minima for the stacked structures in any of the three semiempirical methods. The angle constraint keeps the chains (or strands, except for 2/2/2 aggregates in PM3 and SAM1) stacked but the interaction energy is repulsive relative to two non-interacting chains (Table VII). Nonetheless these structures are minima on the constrained potential surface. These results

Table IX. Calculated and Experimental Geometries of *m*-Nitroaniline *L/C/M* Stacked Layers[a]

aggregates	N_2-O_2	N_2-O_1	N_2-C_3	C_1-N_1	τ[b]	N_1..O_2[c]	N_1..O_1[c]	H_5..O_2[c]	H_5..O_1[c]	C_6..O_2[c]	H_6..O_2[c]	*d*	*a*	*c*
AM1														
2/1/2	1.203	1.203	1.488	1.392	22.3	3.308	3.264	2.431	2.363	3.386	2.431	8.301	6.400	5.286
2/1/3	1.204	1.204	1.487	1.391	22.0	3.295	3.251	2.371	2.345	3.371	2.420	8.282	6.043	5.663
2/1/4	1.205	1.204	1.486	1.390	21.8	3.288	3.243	2.363	2.335	3.365	2.416	8.273	5.888	5.812
3/1/2	1.203	1.203	1.488	1.394	22.9	3.299	3.278	2.378	2.387	3.403	2.449	8.319	6.409	6.240
3/1/3	1.204	1.204	1.487	1.392	22.4	3.288	3.266	2.362	2.367	3.389	2.439	8.300	6.064	5.667
2/2/2	1.202	1.204	1.488	1.391	24.1	3.250	3.311	2.366	2.475	3.459	2.520	8.368	6.367	5.429
PM3														
2/1/2	1.216	1.217	1.495	1.427	28.0	4.149	3.775	3.269	2.829	3.821	2.763	8.809	6.875	5.507
2/1/3	1.217	1.217	1.493	1.427	27.2	4.069	3.722	3.174	2.768	3.771	2.726	8.751	6.599	5.747
2/1/4	1.218	1.217	1.492	1.426	26.7	4.043	3.700	3.144	2.744	3.751	2.708	8.729	6.519	5.804
3/1/2	1.216	1.217	1.494	1.427	27.5	4.351	3.934	3.516	3.035	3.984	2.906	8.982	7.454	5.011
3/1/3	1.217	1.217	1.493	1.427	27.1	4.106	3.761	3.217	2.817	3.814	2.759	8.804	6.743	5.660
SAM1														
2/1/2	1.229	1.228	1.498	1.386	18.1	3.004	3.985	2.028	3.306	4.158	3.495	8.771	6.813	5.524
2/1/3	1.230	1.228	1.497	1.383	16.0	2.978	3.940	1.995	3.251	4.112	3.447	8.733	6.518	5.813
2/1/4	1.231	1.228	1.497	1.381	14.5	2.966	3.915	1.980	3.221	4.088	3.418	8.717	6.387	5.932
3/1/2	1.229	1.228	1.498	1.387	17.9	3.031	4.027	2.065	3.357	4.204	3.537	8.822	7.018	5.346
3/1/3	1.230	1.228	1.498	1.384	16.1	2.993	3.972	2.015	3.289	4.147	3.480	8.767	6.635	5.731
expl.[4a]	1.223	1.222	1.467	1.391		3.459	3.270			3.372		8.251	6.499	5.084

[a]Distances in Å, angles in degrees. [b]τ: H_5-N_1-C_1-C_6 torsional angle. [c]H-bond is between molecules A and B (Figure 6).

parallel those for *p*-nitroaniline and indicate that the dipole-dipole interaction of the individual molecules in neighboring strands is an important factor in determining the relative orientations. Although, these structures are clearly unstable in *hh* directionality, the unit cell dimensions, *a* and *c* are reasonably reproduced in all three methods (Table IX). Similarly to what we have seen for H-bonded chains, AM1 geometrical parameters are clearly superior over those for the other two methods. I obtained the best agreement for a 2/1/2 aggregate at AM1 level, where the largest difference between the calculated and experimental parameters is 0.2 Å (for *c*) or less. The forementioned problems in the H-bonding orientation between the chains within a strand do not seem to affect the unit cell parameters significantly: the 2/2/2 AM1 aggregate also gives excellent predictions for the unit cell parameters. The only calculation for an aggregate with inverse (*ht*) orientation (a 2/2/2 aggregate) results in strong stabilization between the strands: -7.39, -7.62 and -13.37 kcal/mol for AM1, PM3 and SAM1. Additional potential surface calculations for different aggregates all underscore these observations: the *hh* orientation is repulsive in all single cases, while the *ht* direction is always stabilized. Thus, the evident contradiction between the observed *hh* directionality and the stabilized *ht* orientation suggests that interactions between the stacked strands might be of great importance in determining the crystal structure.

<u>The secret of stable *hh* orientation: C-H...O interactions.</u>

The extra stabilization necessary to overcome the unfavorable energetic relations between the *hh* and *ht* orientations of the stacked layers comes from the interactions

between the stacked strands. The angle between the directions of the H-bonded chains (that is, the angle between two diagonals, *d*, of a rectangle with sides *a* and *c*) of this second stacking interaction is approximately 104°. The only atom which can be H-bond acceptor in this interaction (O_2) is hindered by the aromatic rings. The planar benzene rings (especially its C_5 and H_5 atoms) if rotated appropriately, however, can make close contact with these O_2 atoms. The structures illustrating this kind of interaction are shown on Figures 8 and 9. Of the three methods only AM1 predicted minimum for the simplest case for the interaction of only two molecules (1+1, molecules A and E on Figure 8). The interaction energy (Table X) is surprisingly strong, -2.17 kcal/mol. The aromatic H_5 hydrogen of one molecule forms a C-H...O H-bond to the nitro group of the second nitroaniline. The interaction distance between C_5 and O_2 is 3.350 Å, in good agreement with the experimental 3.456 Å. The next complex (2+1), two stacked *hh* monomers (molecules E and F on Figure 8) interacting with an additional monomer in the second stacking direction (molecule A on Figure 8), considers the effect of *hh* orientation of parallel molecules (molecules E and F) in the first stacking direction. The interaction energy that contains the contribution of two C-H...O H-bonds (between molecules A and E and between molecules A and F) and a repulsion between the unfavorably oriented, stacked nitroaniline molecules is stabilizing by -3.24, -1.55 and -2.65 kcal/mol in AM1, PM3 and SAM1 respectively. The largest aggregate (2/1/2 interacting with two monomers from the second stacking direction: 4+2, see also Figures 8 and 9) is stabilized by -13.44 and -9.90 kcal/mol in AM1 and PM3 (SAM1 did not predict minimum). These values indicate that the stabilizing C-H...O interaction overcomes the *hh* repulsion by 3.90 and

Table X. Stacking Interaction Energies (kcal/mol) and H-bonding Distances (Å)

Aggregate	Interaction Energy		Geometry					
	Total	Stacking[a]	$O_2 \cdots C_5$[b]	$O_2 \cdots H_5$[b]	$O_2 \cdots C_4$[b]	*a*	*c*	*d*
AM1								
1+1	-2.17	-2.17	3.350	2.346				
2+1	-3.24	-3.24	3.362 3.385	2.324 2.322	4.174 4.171	5.927		
4+2	-13.44	-3.90	3.353 3.350	2.339 2.334	4.032 4.022	6.040	5.753	8.341
PM3								
2+1	-1.55	-1.55	2.967 2.966	1.879 1.878	3.771 3.769	6.154		
4+2	-9.90	-4.98	3.600 3.605	2.604 2.613	4.445 4.455	6.850	6.022	9.120
SAM1								
2+1	-2.65	-2.65	3.296 3.100	2.302 2.057	4.259 4.026	7.759		
exptl.[6a]			3.456		3.375	6.499	5.084	8.251

[a]Interactions not including H-bonding energies within chains. [b]The first number corresponds to the interaction for molecules A and F (Figure 8), the second for A and E.

4.98 kcal/mol. Thus, the extra stabilization is the result of the unfavorable *hh* repulsion between the dimers and the strong attraction of the two stacked monomers with four C-H...O interactions. In the crystal structure every molecule participates in two such C-H...O H-bonds. On Figure 8, the nitro oxygen (O_2) of molecule A is the H-bond acceptor (to F), while C_5 of the same molecule is a H-bond donor (to E).

Table X also collects the relevant geometrical parameters. Again, AM1 is especially good at predicting the H-bonding geometries between C_5 and O_2 (3.35-3.38 Å calculated vs. 3.456 Å experimental C...O distance), while all methods overestimate the

$C_4...O_2$ distance.

My attempts to find a stable 2+1 *ht* aggregate (2/1/1 in *ht* orientation plus a stacked monomer) failed. This, of course, does not necessarily mean that 2+1 *hh* aggregate would be more stable. However, this fact indicates, that the *hh* orientation is probably not able to accommodate a monomer from the second stacking direction with two C-H...O H-bonds. In the 2+1 *hh* aggregate the appropriate shift (stemming from the head-to-head repulsion) between the parallel 'chains' insures that the almost perpendicularly stacking monomer can H-bond to a nitro oxygen of one chain *and* an aromatic hydrogen of the next. In *ht* alignment either the favorable orientation of the parallel chains should be distorted or the stacking C-H...O interactions would not be so favorable as in the *hh* case.

From the calculated interaction energies one can attempt to estimate the heat of sublimation of the *m*-nitroaniline crystal, as well. The extrapolated incremental H-bonds in H-bonded chains are -5.8, -3.1 and -4.2 kcal/mol in AM1, PM3 and SAM1. The interchain stabilization within the strands can be estimated from Table VII (values for 2/4 aggregate). The average stabilization per molecule values are (interchain stabilization of a 2/4 aggregate divided by eight) about -1.5, -0.6 and -0.2 kcal/mol for the three MO methods. The interstrand repulsions are approximately 0.8 kcal/mol, 0.2 kcal/mol and 1.6 kcal/mol from Table VII using the repulsions for every molecule pair in the 2/1/4 stacks. The effect of C-H...O H-bonds contributes to the stabilization by an estimated value of -2.0, -1.2 and -1.7 kcal/mol (slightly more than half the value of the 2+1 stabilization). Summing up the appropriate numbers results -8.5, -4.7 and -4.5 kcal/mol as the average

stabilization per molecule within the crystal structure. Although, these values are rather far from the experimental 23.3 kcal/mol heat of sublimation,[7] it is important that all methods reproduce the tendency between the heats of sublimation of the two examined nitroanilines. This example also indicates the importance of interdimensional cooperativity that was completely neglected in my estimation procedure.

4. Concluding Remarks

Semiempirical AM1, PM3 and SAM1 calculations have been performed for *para*- and *meta*-nitroaniline aggregates. The results of these calculations give sound reasons to understand the different crystal structure of these two compounds. *para*-Nitroaniline forms infinite two-dimensional layers from interconnected H-bonded chains. The presence of H-bonds (the combination of patterns III and IV of Figure 1) between the chains suggest the stability and preference of the observed H-bonded network over the structure (I) that would have been expected to be most stable by considering only H-bonded chains. The two-dimensional layer structures then stack with *ht* orientation that is stabilized by dipole-dipole interactions giving rise to the crystal structure. The most important difference in the nucleation of *m*-nitroaniline is the formation of H-bonded strands consisting of two chains. The H-bonded pattern (three-centered H-bonds) is similar to that of *p*-nitroaniline, but due to the different relative orientation of the substituents, this pattern leads to the association of only two chains to form linear strands. Stacking of the strands takes place in *hh* manner (nitro groups pointing to the same direction). Although this orientation in

itself would be destabilized by the forementioned dipole-dipole interactions, additional C-H...O H-bonds between the almost perpendicularly interacting stacks reverse this tendency, overcome the weak repulsion between the strands and ultimately dictate the final arrangement of the crystal structure. The *ht* orientation in *p*-nitroaniline results in centrosymmetric crystal structure, while *m*-nitroaniline owing to the *hh* orientation of the stacked strands crystallizes in non-centrosymmetric manner. As a very important consequence, *m*-nitroaniline crystals exhibit second-order nonlinear optical properties, while *p*-nitroaniline do not.

These studies also illustrated the significance of both the cooperative effects (for example, geometry changes upon aggregation) and the C-H...O interactions (*m*-nitroaniline crystallization). In fact, these crystal structures also exemplify the existence of aromatic C-H...O H-bonds.

Among the applied methods, AM1 performed very well at predicting both relative energies and geometries. Especially its H-bonding geometries and unit cell parameters are impressive. In addition, its heat of sublimation estimates were closest to the experimental data. PM3 and SAM1 methods could reproduce the main trends, their predictions of smaller details, however, are less good. PM3 tends to underestimate the strength of N-O...H interaction, thus overestimates their bondlengths. Its H-bonding energies are always lower than those of the other two methods. The greatest problem with SAM1 is its difficulties to find suitable minima on the potential surface, even in such regions where the other two methods clearly suggest stable alignments. It also appears to overestimate the significance of electrostatic interactions such as the dipole-dipole interactions in the

stacking phenomenon.

5. References

1. For more discussion see for example: Zernike, F.; Midwinter, J. E. *Applied Nonlinear Optics.* New York: Wiley and Sons, 1973. Butcher, P. N.; Cotter, D. *The Elements of Nonlinear Optics.* Cambridge: Cambridge University Press, 1990.

2. Zyss, J.; Oudar, J. L. *Phys. Rev. A*, **1982**, *26*, 2028.

3. Panunto, T. W.; Urbanczyk-Lipkowska, Z.; Johnson, R.; Etter, M. C. *J. Am. Chem. Soc.*, **1987**, *109*, 7786.

4. Vinson, L. K.; Dannenberg, J. J. *J. Am. Chem. Soc.*, **1989**, *111*, 2777.

5. Trueblood, K. N.; Goldish, E.; Donohue, J. *Acta Cryst.*, **1961**, *14*, 1009.

6. a) Dhaneshwar, N. N.; Tavale, S. S.; Pant, L. M. *Acta Cryst.*, **1978**, *B34*, 2507. b) Skapski, A. C.; Stevenson, J. L. *J. C. S. Perkin II*, **1973**, 1197.

7. Hoyer, H.; Peperle, W. *Z. Electrochem.*, **1958**, *62*, 61. Cox, J. D.; Pilcher, G. *Thermochemistry of Organic and Organometallic Compounds*, London: Academic Press, 1970, p 334.

VIII. GENERAL CONCLUSIONS

1. Semiempirical and ab initio MO studies illustrated the significance of cooperative effects in crystal formation. One, two and three-dimensional cooperative effects have been shown to play an important role in determining the structure of solid phases. Cooperativity influences not only the geometrical parameters of the constituent molecules within the crystals but can dictate the way molecules, for example, 1,3-cyclohexanedione, would crystallize. Cooperativity is a crucial factor in the crystal formation of acetic acid and *para*-nitroaniline, as well. The empirical parameters of the equation for the extrapolated H-bonding energies (equation V.2) in infinite chains can be related to the H-bonding energy of the first aggregate (E_1), the strengthening of the H-bonding interactions relative to that of the dimer (*a*) and the rate H-bonds approach the H-bonding strength characteristic of the infinite chains (*b*).

2. Cooperative effects have been demonstrated to arise in simpler models, such as acetic acid H-bonded cyclic dimers. The extra stabilization of the gas (and liquid) phase cyclic dimer is predicted to be 2.4-3.1 kcal/mol compared to single O-H...O bonded species. The appropriate changes in vibrational frequencies underscored this observation.

3. The participation of C-H...O hydrogen-bonds in the crystal formation is remarkable in all the examined crystal structures. In acetic acid, C-H...O interactions take part not only in the stacking interactions (in all three crystallographic directions) but in determining the structure of the primary H-bonded chains, as well. After the possibility of forming primary O-H...O H-bonding networks comes to an end, the weaker C-H...O

bonds dominate the crystal structure. This is the case in 1,3-cyclohexanedione layers, acetic acid and *meta*-nitroaniline microcrystals. In this latter case, C-H...O interactions dictate the head-to-head (*hh*) chain orientation within the stacks leading to the well-known nonlinear optical properties of *meta*-nitroaniline crystals.

4. High level ab initio calculations have been performed to smaller C-H...O H-bonded complexes to model these interactions in crystals. Both the striking geometric resemblance of the C-H...O H-bonded complexes to the orientations of their stronger X-H...O (X=O,N, etc.) counterparts, the short C-H...O contacts and the strong interaction energies and enthalpies (-1.15 - -3.79 kcal/mol for HCN complexes, -0.49 - -2.19 kcal/mol for H_2C_2 complexes) strongly suggest the existence of C-H...O H-bonds. The corresponding shifts in the H-bonded stretching vibrations correlate well with this observation.

5. Macroscopic properties of the examined crystal structures have been reproduced with very good accuracy. The crystallographic unit cell parameters are reasonably good, especially in AM1. AM1 heats of formation also give good agreement with available experimental data.

6. The differences in optical behavior of *para*- and *meta*-nitroanilines have been explained in terms of intermolecular interactions. The small difference in the molecular symmetry of these two compounds leads to strikingly different hydrogen-bonding networks. The infinite layers of *para*-nitroaniline stack in the electrostatically most favorable head-to-tail (*ht*) orientation leading to centrosymmetric crystal structure. On the other hand, the H-bonded strands of *m*-nitroaniline crystallize in the destabilizing *hh*

orientation. The aromatic C-H...O interactions between the stacks, however, overcome the destabilization and give rise to the final, non-centrosymmetric crystal structure. Thus, *m*-nitroaniline crystals exhibit nonlinear optical properties, while those of *p*-nitroaniline do not.

7. It is concluded that, of the three examined semiempirical methods, AM1 is the most applicable for crystal formation processes. Its only evident drawback is to underestimate the strength of the O-H...O H-bonds. It gives C-H...O H-bonding enthalpies, geometries and unit cell parameters superior over those of the other two semiempirical methods. PM3 tends to give physically absurd results, although its predictions are sometimes very similar (or even better) to those of AM1. It is hard to give a general judgement about the capabilities of SAM1, but from these studies my overall impression is that its older sibling (AM1) is more reliable.

8. It has been repeatedly pointed out that theoretical models not considering the cooperative phenomenon (based on pairwise potentials) are not likely to be very successful in statistical simulations of H-bonded systems, biological processes or in any problem where strong non-additivity can occur.

9. At this point of the Thesis I should like to summarize the limitations of the approach I followed in this work. The most evident problem stems from the fact that I considered only the thermodynamical side of the crystal formation. The dynamical features (kinetics) that can be extremely important have been omitted mainly because of the MO treatment. MO methods are not (yet) able to treat the kinetical aspects of such a complex problem as crystal formation. Other problems include those mentioned in

Chapter II in calculating thermodynamical properties (for example, ideal gas behavior in approximating ΔH in equation II.13, etc.). The assumption of thermodynamical equilibrium systems for the nucleation process is not always a valid approximation, either.

IX. BIBLIOGRAPHY

The following references have been used in this work:

Adler-Golden, S. M.; Langhoff, S. R.; Bauschlicher, Jr., C. W. *J. Chem. Phys.*, **1985**, *83*, 255.

Allegrini, M.; Johns, J. W. C.; McKellar, A. R. W. *J. Mol. Spectrosc.*, **1977**, *67*, 476.

Allen, H. C., Jr.; Tidwell, E. D.; Plyler, E. K. *J. Res. Natl. Bur. Stand.*, **1956**, *57*, 213.

Allen, H. F.; Bellard, S.; Brice, M. D.; Cartwright, B. A.; Doubleday, A.; Higgs, H.; Hummelink, T.; Hummelink-Peters, B. G.; Kennard, O.; Motherwell, W. D. S.; Rodgers, J. R.; Watson, D. G. *Acta Crystallogr. Sect. B.*, **1979**, *B35*, 2331.

Allinger, N. L.; Schmitz, L. R.; Motoc, I.; Bender, C.; Labanowski, J. K., *J. Comput. Chem.*, **1992**, *13*, 838.

Andrews; F. C. *Equilibrium Statistical Mechanics*, Wiley and Sons: New York, 1975.

Atoji, M.; Lipscomb, W. N. *Acta Crystallogr.*, **1954**, *7*, 173.

Axilrod, B. M.; Teller E. *J. Chem. Phys.*, **1943**, *11*, 299.

Barbe, A.; Secroun, C.; Jouve, P. *J. Mol. Spectrosc.*, **1974**, *49*, 171.

Bauer, S. H.; Beach, J. Y.; Simons, J. H. *J. Am. Chem. Soc.*, **1939**, *61*, 19.

Belford, D.; Campbell, E. S. *J. Chem. Phys.*, **1983**, *80*, 3288.

Benedict, W. S.; Gailar, N.; Plyler, E. K. *J. Chem. Phys.*, **1956**, *24*, 1139.

Benson, S. W. *Thermochemical Kinetics*, Wiley and Sons: New York, 1968.

Bertie, J. E.; Michaelian, K. H. *J. Chem. Phys.*, **1982**, *77*, 5267.

Bes, R. *Actual. Chim.*, **1978**, *10*, 25.

Bingham, R. C.; Dewar, M. J. S.; Lo, D. H. *J. Am. Chem. Soc.*, **1975**, *97*, 1285.

Binkley, J. S.; Pople, J. A.; Hehre, W. J. *J. Am. Chem. Soc.*, **1980**, *102*, 939.

Blau, H. H., Jr.; Nielsen, H. H. *J. Mol. Spectrosc.*, **1957**, *1*, 124.

Block, P. A.; Marshall, M. D.; Pedersen, L. G.; Miller, R. E. *J. Chem. Phys.*, **1992**, *96(10)*, 7321.

Bock, C. W. *J. Mol. Struct. (THEOCHEM)*, **1983**, *13*, 383.

Boggs, J. E. In *Stereochemical Applications of Gas-Phase Electron Diffraction*, Hargittai, I.; Hargittai, M., Eds., VCH, New York, 1988; Part A, p 301. , part B, p 455.

Bonchev, D. *Croat. Chem. Acta*, **1977**, *49*, 83.

Bondi, A. *J. Phys. Chem.*, **1964**, *68*, 441.

Boutellier, Y.; Behrouz, H. *J. Chem. Phys.*, **1992**, *96*, 6033.

Boys, S. F. *Proc. R. Soc. London A*, **1950**, *200*, 542.

Boys, S. F.; Bernardi, F., *Mol. Phys.*, **1970**, *19*, 553.

Butcher, P. N.; Cotter, D. *The Elements of Nonlinear Optics*. Cambridge: Cambridge University Press, 1990.

Caminati, W.; Scappini, F.; Corbelli, G. *J. Mol. Spectrosc.*, **1979**, *75*, 327.

Campbell, E. S.; Mezei, M. *J. Chem. Phys.*, **1977**, *67*, 2338.

Campbell, E. S.; Mezei, M. *Mol. Phys.*, **1980**, *41*, 883.

Chakravorty, S. J.; Davidson, E. R. *J. Phys. Chem.*, **1993**, *97*, 6373.

Clark, T.; Chandrasekhar, J.; Spitznagel, G. W.; Schleyer, P. v. R. *J. Comput. Chem.*, **1983**, *4*, 294.

Clementi, E. *IBM J. Res. and Dev.*, **1965**, *9*, 2.

Clementi, E.; Raimondi, D. L. *J. Chem. Phys.*, **1963**, *38*, 2686.

Cox, J. D.; Pilcher, G. *Thermochemistry of Organic and Organometallic Compounds*, London: Academic Press, 1970, p 334.

Dahlquist, F. W. *Methods in Enzymology*, **1978**, *48*, 270.

Dannenberg, J. J. *J. Phys. Chem.*, **1988**, *92*, 6869.

Dannenberg, J. J. *Materials*, **1990**, *2*, 635.

Dannenberg, J. J.; Baer, B. *J. Am. Chem. Soc.*, **1987**, *109*, 292.

Dannenberg, J. J.; Evleth, E. M. *Int. J. Quant. Chem.*, **1992**, *44*, 869.

Dannenberg, J. J.; Mezei, M. *J. Phys. Chem.*, **1991**, *95*, 6396.

Dannenberg, J. J.; Vinson, L. K. *J. Phys. Chem.*, **1988**, *92*, 5635.

Daudey, J., P.; Claverie, P.; Malrieu P. *Int. J. Quantum Chem.*, **1974**, *8*, 1.

Davidson, E. R.; Feller, D. *Chem. Rev.*, **1986**, *86*, 681.

Del Bene, J. E. *J. Chem. Phys.*, **1980**, *72*, 3423.

Del Bene, J., *Int. Quantum Chem Biol. Symp.*, **1988**, *15*, 119.

Derissen, J. L. *J. Mol. Struct.*, **1971**, *7*, 67.

Derissen, J. L.; Smit, P. H. *Acta Crystallogr.*, **1977**, *A33*, 230.

Desiraju, G. R. *J. Chem. Soc. Chem. Commun.*, **1989**, 179.

Desiraju, G. R. *J. Chem. Soc. Chem. Commun.*, **1990**, 454.

Desiraju, G. R.; Murty, B. N.; Kishan, K. V. R., *Materials* **1990**, *2*, 447.

Dewar, M. J. S. *Int. J. Quant. Chem. Symp.*, **1988**, *22*, 557.

Dewar, M. J. S.; Ford, G. P. *J. Am. Chem. Soc.*, **1979**, *101*, 5558.

Dewar M. J. S.; Jie, C. *Acc. Chem. Res.*, **1992**, *25*, 537.

Dewar, M. J. S.; Jie, C.; Yu, J. *Tetrahedron*, **1993**, *49*, 5003.

Dewar, M. J. S.; Storch, D. M. *J. Am. Chem. Soc.*, **1985**, *107*, 3898.

Dewar, M. J. S.; Thiel, W. *J. Am. Chem. Soc.*, **1977**, *99*, 4899.

Dewar, M. J. S.; Zoebisch, E. G.; Healy, E. F.; Stewart, J. J. P. *J. Am. Chem. Soc.*, **1985**, *107*, 3902.

Dhaneshwar, N. N.; Tavale, S. S.; Pant, L. M. *Acta Cryst.*, **1978**, *B34*, 2507.

van Duijneveldt, F. B.; de Groot-den Hartogh, M.; van Duijneveldt-van de Rijdt, J. G. C. M. *Croat. Chem. Acta*, **1992**, *65*, 1.

van Duijneveldt-van de Rijdt, J. G. C. M.; van Duijneveldt, F. B. *J. Chem. Phys.*, **1992**, *97*, 5019.

Duncan , J. L.; Mallinson, P. D. *Chem. Phys. Lett.*, **1973**, *23*, 597.

Dunning, T. H.; Hay, P. J. *Modern Theoretical Chemistry*, Plenum: New York, 1976.

Dykstra, C. E. *J. Am. Chem. Soc.*, **1989**, *111*, 6168.

Dykstra, C. E. *J. Am. Chem. Soc.*, **1990**, *112*, 7540.

van Eijck, B. P.; van Opheusden, J.; van Schaik, M. M. M.; van Zoeren, E. *J. Mol. Spectrosc.*, **1981**, *86*, 465.

Eisenshitz, R.; London, F. *Zeits. f. Physik*, **1930**, *60*, 491.

Emsley, J.; Hoyte, O. P. A.; Overill, R. E. *J. Am. Chem. Soc.*, **1978**, *100*, 3303.

Engdahl, A.; Nelander, B. *Chem. Phys. Lett.*, **1983**, *100*, 129.

Etter, M. C.; Parker, D. L.; Ruberu, S. R.; Panunto, T. W.; Britton, D. *J. Incl. Phenom. and Molec. Rec. in Chem.* **1990**, *8*, 395.

Etter, M. C.; Urbanczyk-Lipkowska, Z., Jahn, D. A., Frye, J. S. *J. Am. Chem. Soc.*, **1986**, *108*, 5871.

Fillery-Travis, A. J.; Legon, A. C.; Willoughby, L. C. *Proc. R. Soc. London, A.*, **1984**, *396*, 405.

Foresman, J. B.; Head-Gordon, M.; Pople, J. A.; Frisch, M. J. *J. Phys. Chem.*, **1992**, *96*, 135.

Frank, H. S.; Wen, W.-Y. *Discuss. Faraday Soc.*, **1957**, *24*, 133.

Frisch, M. J.; Del Bene, J. E.; Binkley, J. S.; Schaefer, H. F. III *J. Chem. Phys.*, **1986**, *84*, 2279.

Frisch, M. J.; Pople, J. A.; Del Bene, J. E. *J. Chem. Phys.*, **1983**, *78*, 4063.

Frurip, D. J.; Curtiss, L. A.; Blander, M. J. *J. Am. Chem. Soc.*, **1980**, *102*, 2610.

Gautres, R.; Maillols, J.; Tabacik, V. *J. Raman Spectrosc.*, **1981**, *11*, 442.

Glasstone, S. *Trans. Faraday Soc.*, **1937**, *33*, 200.

Glusker, J. P. *Mol. Cryst. Liq. Cryst. Sci. Tech., Sect A*, **1992**, *211*, 75.

Goodwin, E. J.; Legon, A. C. *J. Chem. Phys.*, **1987**, *87*, 2426.

Gordon, M. S. *Chem. Phys. Lett.*, **1980**, *76*, 163.

Guo, H.; Karplus, H. *J. Phys. Chem.*, **1992**, *96*, 7273.

Gutowski, M.; van Duijneveldt, F. B.; Chalasinski, G.; Piela, L. *Mol. Phys.*, **1987**, *61*, 233.

Gutowski, M.; van Duijneveldt-van de Rijdt, J. G. C. M.; van Lenthe, J. H.; van Duijneveldt, F. B. *J. Chem. Phys.*, **1993**, *98*, 4728.

Gutowsky, H. S.; Germann, T. S.; Augspurger, J. D.; Dykstra, C. E. *J. Chem. Phys.*, **1992**, *96*, 5808.

Hamilton, W. C.; Ibers, J. A. *Hydrogen Bonding in Solids*, W. A. Benjamin: New York, 1968.

Hankins, D.; Moskowitz, J. W.; Stillinger, F. H. *J. Chem. Phys.*, **1970**, *53*, 4544.

Harding, L. B.; Ermler, W. C. *J. Comput. Chem.*, **1985**, *6*, 13.

Hariharan, P. C.; Pople, J. A. *Theor. Chim. Acta*, **1973**, *28*, 213.

Hartz, N.; Rasul, G.; Olah, G. A., *J. Am. Chem. Soc.*, **1993**, *115*, 1277.

Haurie, M.; Novak, A. *J. Chim. Phys.*, **1965**, *62*, 137.

Hehre, W. J.; Ditchfield, R.; Pople, J. A. *J. Chem. Phys.*, **1972**, *56*, 2257.

Herzberg, G. *Infrared and Raman Spectra*, Van Nostrand: Princeton, 1945.

Hess, B. A.; Schaad, L. J.; Carsky, P.; Zahradnik, R. *Chem. Rev.*, **1986**, *86*, 709.

Hill, A. V. *J. Physiol. (London)*, **1910**, *90*, iv-vii.

Hinchliffe, A. *J. Mol. Struct. (THEOCHEM)*, **1986**, *136*, 193.

Hodoscek, M.; Kocjan, D.; Hadzi, D. *J. Mol. Struct. (THEOCHEM)*, **1988**, *42*, 115.

Hoy, A. R.; Mills, I. M.; Strey, G. *Mol. Phys.*, **1972**, *24*, 1265.

Hoyer, H.; Peperle, W. *Z. Electrochem.*, **1958**, *62*, 61.

Huang, X. L.; Dannenberg, J. J. *J. Org. Chem.*, **1991**, *56*, 6367.

Imai, K. *J. Biol. Chem.*, **1974**, *249*, 7606.

Jeffrey, G. A.; Gress, M. E.; Takagi, S. *J. Am. Chem. Soc.*, **1977**, *99*, 609.

Jeffrey, G. A.;, Saenger, W. In *Hydrogen Bonding in Biological Structures*, Springer-Verlag, Berlin 1991.

Jentschura, U.; Lippert E. *Z. Phys. Ch. (Frankfurt)*, **1972**, *77* (1-6), 64.

Jones, R. E.; Templeton, D. H. *Acta Crystallogr.*, **1958**, *11*, 484.

Jönsson, P. G. *Acta Crystallogr.*, **1971**, *B27*, 893.

Jurema, M. W.; Shields, G. C. *J. Comput. Chem.*, **1993**, *14*, 89.

Kaila, N.; Franck, R. W.; Dannenberg, J. J. *J. Org. Chem.*, **1989**, *54*, 4206.

Kanters, J. A.; Kroon, J. *Acta Crystallogr.*, **1972**, *B28*, 1946.

Karle, J.; Brockway, L. O. *J. Am. Chem. Soc.*, **1944**, *66*, 574.

Karpfen, A.; Ladik, J.; Russegger, P.; Schuster, P.; Suhai, S. *Theor. Chim. Acta*, **1974**, *34*, 115.

Kim, K. S.; Mhin, B. J.; Choi, U-S.; Lee, K. *J. Chem. Phys.*, **1992**, *97*, 6649.

Kleeberg, H.; Klein, D.; Luck, W. A. *J. Phys. Chem.*, **1987**, *91*, 3200.

Klimkowski, V. J.; Pulay, P.; Ewbank, J. D.; McKean, D. C.; Schäfer, L. *J. Comput. Chem.*, **1984**, *5*, 517.

Koehler, J. E. H.; Saenger, W.; Lesyng, B. *J. Comput. Chem.*, **1987**, *8*, 1090.

Larsen, I. K. *Acta Crystallogr.*, **1988**, *B44*, 527.

Leclercq, J. M.; Allavena, M.; Bouteiller, Y. *J. Chem. Phys.*, **1983**, *78*, 4606.

Lee, T. J.; Scuseria, G. E. *J. Chem. Phys.*, **1990**, *93*, 489.

Lentz, B. R.; Scheraga, H. A. *J. Chem. Phys.*, **1973**, *58*, 5296.

Levine, I. N. *Molecular Spectroscopy*, Wiley and Sons: New York, 1975.

Levine, I. N. *Quantum Chemistry, 3d ed.*; Allen and Bacon: Boston, 1983.

London, F. *Zeits. f. Physik*, **1930**, *63*, 245.

London, F. *Z. Phys. Chem.(B)*, **1930**, *11*, 222.

London, F. *Trans. Faraday Soc.*, **1937**, *33*, 8.

Maes, G.; Smets, J. *J. Phys. Chem.*, **1993**, *97*, 1818.

Marcoccia, J. F.; Csizmadia, I. G.; Peterson, M. R. *Gaz. Chim. Ital.*, **1990**, *120*, 77.

Maréchal Y., *J. Chem. Phys.*, **1987**, *87*, 6344.

Margenau, H. *Rev. Mod. Phys.*, **1936**, *11*, 1.

Mathews, D. M.; Sheets, R. W. *J. Chem. Soc. A*, **1969**, 2203.

Mayer I. *J. Chem. Phys.*, **1992**, *97*, 5257.

Mayer, I., Surján, P. R. *Int. J. Quant. Chem.*, **1989**, *36*, 225.

Mayer, I.; Surján, P. R. *Chem. Phys. Lett.*, **1992**, *191*, 497.

Mayer, I.; Turi, L. *J. Mol. Str. (THEOCHEM)*, **1991**, *227*, 43.

Messinger, J.; Heuser, N. *QCPE Bull.*, **1991**, *11(1)*.

Mielke, Z.; Andrews, A. *J. Phys. Chem.*, **1990**, *94*, 3519.

Miyazawa, T.; Pitzer, K. S. *J. Am. Chem. Soc.*, **1959**, *81*, 74.

Mo, O.; Yanez, M.; Elguero, J. *J. Chem. Phys.*, **1992**, *97*, 6628.

Møller, C.; Plesset, M. S. *Phys. Rev.*, **1934**, *46*, 618.

Muguet, F. F.; Robinson, G. W.; Bassez-Muguet, M. P. *Int. J. Quantum Chem.*, **1991**, *39*, 449.

Murray-Rust, P.; Glusker, J. P. *J. Am. Chem. Soc.*, **1984**, *106*, 1018.
Murrell, J. N.; Randić, M.; Williams, D. R. *Proc. Roy. Soc. (London)*, **1965**, *284*, 566.

Murrell, J. N.; Shaw, G. *J. Chem. Phys.*, **1967**, *46*, 1768.

Nagaoka, S.; Hirota, N. *Chem. Phys. Lett.*, **1982**, *92*, 498.

Nagy-Felsobuki, E. I.; Kimura, K. *J. Phys. Chem.*, **1990**, *94*, 8041.

Nahringbauer, I. *Acta Chem. Scand.*, **1970**, *24*, 453.

Nyburg, S. C. *Acta Crystallogr.*, **1979**, *A35*, 641.Pariser, R. D.;

Panunto, T. W.; Urbanczyk-Lipkowska, Z.; Johnson, R.; Etter, M. C. *J. Am. Chem. Soc.*, **1987**, *109*, 7786.

Parr, R. G. *J. Chem. Phys.*, **1953**, *21*, 466 and 767.

Pauling, L.; Wilson, E. B. *Introduction to Quantum Mechanics*, McGrew-Hill: New York, 1935.

Peterson, K. I.; Klemperer, W. *J. Chem. Phys.*, **1984**, *81*, 3842.

Pople, J. A. *Trans. Faraday Soc.*, **1953**, *49*, 1375.

Pople, J. A.; Beveridge, D. L.; Dobosh, P. A. *J. Chem. Phys.*, **1967**, *47*, 2026.

Pople, J. A.; Binkley, J. S.; Seeger, R. *Int. J. Quant. Chem. Symp.*, **1976**, *10*, 1.

Pople, J. A.; Nesbet, R. K. *J. Chem. Phys.*, **1959**, *22*, 571.

Pople, J. A.; Santry, D. P.; Segal, G. A. *J. Chem. Phys.*, **1965**, *43*, S129.

Pople, J. A.; Segal, G. A. *J. Chem. Phys.*, **1965**, *43*, S136.

Pople, J. A.; Segal, G. A. *J. Chem. Phys.*, **1966**, *44*, 3289.

Preuss, H. *Z. Naturforsch.*, **1956**, *11*, 823.

Pross, A. W.; van Zeggeren, F. *Spectrochim. Acta*, **1960**, *16*, 563.

Pulay, P. *Mol. Phys.*, **1969**, *17*, 197.

Pulay, P. In *Modern Theoretical Chemistry*, Schaefer, H. F., III, Ed.; Vol. 4, Plenum: New York, 1977.

Racine, S. C.; Davidson, E. R. *J. Phys. Chem.*, **1993**, *97*, 6367.

Reisner, D. E.; Field, R. W.; Kinsey, J. L.; Dai, H.-L. *J. Chem. Phys.*, **1984**, *80*, 5968.

Remko, M. *Z. Phys. Chem. (Munich)*, **1983**, *138*, 223.

Reynolds, C. H. *J. Am. Chem. Soc.*, **1990**, *112*, 7903.

Roothaan, C. C. J. *Rev. Mod. Phys.*, **1951**, *23*, 69.

Rothenberg, S.; Schaefer III, H. F. *J. Chem. Phys.*, **1971**, *54*, 2765.

Ruelle, P. *Chem. Phys.*, **1986**, *110*, 263.

Sadlej, A. J. *J. Chem. Phys.*, **1991**, *95*, 6705.

Sadlej, A. J. *J. Chem. Phys.*, **1992**, *97*, 5259.

Scatchard, G. *Ann. N. Y. Acad. Sci.*, **1949**, *51*, 660.

Schäfer, L.; Ewbank, J. D.; Siam, K.; Chiu, N.-S.; Sellers, H. L. In *Stereochemical Applications of Gas-Phase Electron Diffraction*, Hargittai, I.; Hargittai, M., Eds., VCH, New York, 1988; Part A, p 301.

Schwenke, D. W.; Truhlar, D. G. *J. Chem. Phys.*, **1984**, *82*, 2418.

Skapski, A. C.; Stevenson, J. L. *J. C. S. Perkin II*, **1973**, 1197.

Smit, P. H.; Derissen, J. L.; van Duijneveldt, F. B. *Molec. Phys.*, **1979**, *37*, 501.

Smith, A. M.; Coy, S. L.; Klemperer, W.; Lehmann, K. K. *J. Mol. Spectrosc.*, **1989**, *134*, 134.

Sodupe, M.; Oliva, A.; Bertran, J.; Dannenberg, J. J. *J. Org. Chem.*, **1989**, *54*, 2488.

Sreerama, N.; Vishveshwara, S. *J. Mol. Struct. (THEOCHEM)*, **1985**, *133*, 139.

Steiner, T.; Mason, S. A.; Saenger, W. *J. Am. Chem. Soc.*, **1990**, *112*, 6184.

Steiner, T.; Saenger, W. *J. Am. Chem. Soc.*, **1992**, *114*, 7123.

Steiner, T.; Saenger, W. *J. Am. Chem. Soc.*, **1992**, *114*, 10146.

Stewart, J. J. P. *J. Comput. Chem.*, **1989**, *10*, 209.

Strey, G.; Mills, I. M. *Mol. Phys.*, **1973**, *26*, 129.

Strey, G.; Mills, I. M. *J. Mol. Spectrosc.*, **1976**, *59*, 103.

Strieter, F. J.; Templeton, D. H.; Scheuerman, R. F.; Sass, R. L. *Acta Crystallogr.*, **1962**, *15*, 1233.

Sutcliffe, B. T., Fundamentals of computational quantum chemistry in *Computational Techniques in Quantum Chemistry*; Diercksen, G. H. F.; Sutcliffe, B. T.; Veillard, A., editors; Reidel: Boston, 1975.

Suzuki, I.; Overend, J. *Spectrochim. Acta*, **1969**, *25A*, 977.

Suzuki, I.; Pariseau, M., A.; Overend, J. *J. Chem. Phys.*, **1966**, *44*, 3561.

Sverdlov, L. M. *Izv. Akad. Nauk. SSSR Ser. Khim.*, **1953**, *17*, 567.

Szabo, A.; Ostlund, N. S.; *Modern Quantum Chemistry*; McGraw-Hill: New York, 1989.

Szalewicz, K.; Cole, S. J.; Kolos, W.; Bartlett, R. J. *J. Chem. Phys.*, **1988**, *89*, 3662.

Tabor, W. J. *J. Chem. Phys.*, **1957**, *27*, 974.

Tanaka, I.; Machida, K. *J. Mol. Spectrosc.*, **1977**, *64*, 429.

Taylor, M. D. *J. Am. Chem. Soc.*, **1951**, *73*, 315.

Taylor, R.; Kennard, O. *J. Am. Chem. Soc.*, **1982**, *104*, 5063.

Trueblood, K. N.; Goldish, E.; Donohue, J. *Acta Cryst.*, **1961**, *14*, 1009.

Tsuzuki, S.; Uchimaru, T.; Tanabe, K.; Hirano, T. *J. Phys. Chem.*, **1993**, *97*, 1346.

Turi, L.; Dannenberg, J. J. *J. Phys. Chem.*, **1992**, *96*, 5819.

Turi, L.; Dannenberg, J. J. *Mol. Cryst. Liq. Cryst.*, **1992**, *219*, 63.

Turi, L.; Dannenberg, J. J. *J. Phys. Chem.*, **1993**, *97*, 2488.

Turi, L.; Dannenberg, J. J. *J. Phys. Chem.*, **1993**, *97*, 7899.

Turi, L.; Dannenberg, J. J. *J. Phys. Chem.*, **1993**, *97*, 12197.

Turi, L.; Dannenberg, J. J. submitted for publication.

Turi, L.; Dannenberg, J. J.; Rama, J. B.; Ventura, O. N. *J. Phys. Chem.*, **1992**, *96*, 3709.

Ventura, O. N.; Rama, J. B.; Turi, L.; Dannenberg, J. J. *J. Am. Chem. Soc.*, **1993**, *115*, 5754.

Vinson, L. K.; Dannenberg, J. J. *J. Am. Chem. Soc.*, **1989**, *111*, 2777.

Wells, B. H.; Wilson, S. *Chem. Phys. Lett.*, **1983**, *101*, 429.

Whitten, J. L. *J. Chem. Phys.*, **1966**, *44*, 359.

Wiggins, T. A.; Plyler, E. K.; Tidwell, E. D. *J. Opt. Soc. Am.*, **1961**, *51*, 1219.

Williams, R. W.; Lowrey, A. H., *J. Comput. Chem.*, **1991**, *12*, 761.

Yusukawa, T.; Kimura, T. *Chem. Phys. Lett.*, **1990**, *169*, 259.

Zelsmann, H. R.; Mielke, Z.; Maréchal, Y., *J. Mol. Struct.*, **1990**, *237*, 273.

Zernike, F.; Midwinter, J. E. *Applied Nonlinear Optics*. New York: Wiley and Sons, 1973.

Zyss, J.; Oudar, J. L. *Phys. Rev. A*, **1982**, *26*, 2028.